ARISTOTLE UNIVERSITY OF THESSALONIKI
FACULTY OF SCIENCES
DEPARTMENT OF GEOLOGY
MINERALOGY- PETROLOGY- ECONOMIC GEOLOGY

STYLIANI T. BRAGOU
Geologist

HYDROCARBON GENERATION AND EXPULSION SENSITIVITY ANALYSIS BY APPLYING 1D/2D/3D BASIN MODELING, PATRAIKOS GULF, WESTERN GREECE

MASTER THESIS

POSTGRADUATE STUDIES PROGRAMME "HYDROCARBON EXPLORATION AND EXPLOITATION"

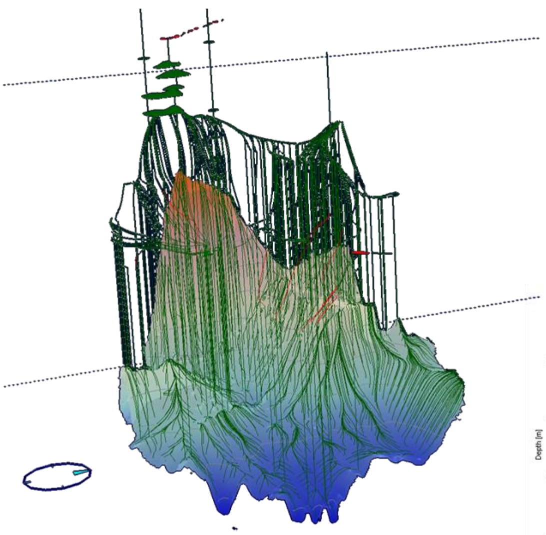

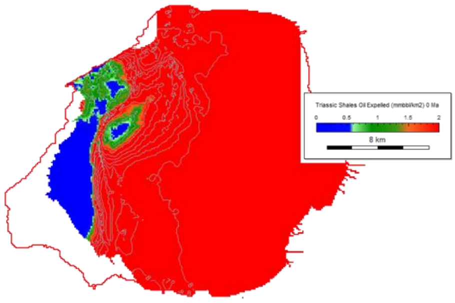

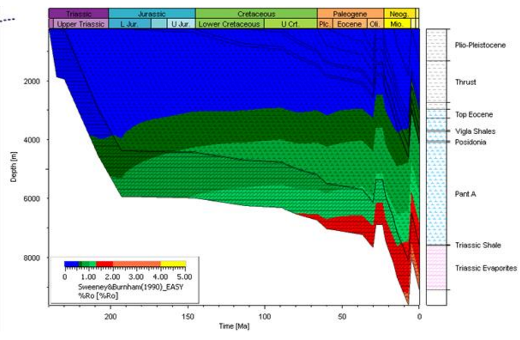

THESSALONIKI 2020

STYLIANI T. BRAGOU
ΣΤΥΛΙΑΝΗ Τ. ΜΠΡΑΓΟΥ
Πτυχιούχος Γεωλόγος

HYDROCARBONS GENERATION AND EXPULSION SENSITIVITY ANALYSIS BY APPLYING 1D/2D/3D BASIN MODELING, PATRAIKOS GULF, WESTERN GREECE

ΑΝΑΛΥΣΗ ΕΥΑΙΣΘΗΣΙΑΣ ΣΤΗΝ ΓΕΝΕΣΗ ΚΑΙ ΑΠΟΜΑΚΡΥΝΣΗ ΥΔΡΟΓΟΝΑΘΡΑΚΩΝ, ΠΑΤΡΑΙΚΟΣ ΚΟΛΠΟΣ, ΔΥΤΙΚΗ ΕΛΛΑΔΑ

Υποβλήθηκε στο Τμήμα Γεωλογίας στα πλαίσια του Διατμηματικού Προγράμματος Μεταπτυχιακών Σπουδών ‘Έρευνα και εκμετάλλευση υδρογονανθράκων,

Ημερομηνία Προφορικής Εξέτασης: 29/10/2020
Oral Examination Date: 29/10/2020

Three-member Examining Board

Professor Kimon Christanis, Supervisor
Professor Andreas Georgakopoulos, Member
Professor Vasilios Karakitsios, Member

Τριμελής Εξεταστική Επιτροπή

Καθηγητής Κίμων Χρηστάνης, Επιβλέπων
Καθηγητής Ανδρέας Γεωργακόπουλος, Μέλος Τριμελούς Εξεταστικής Επιτροπής
Καθηγητής Βασίλειος Καρακίτσιος, Μέλος Τριμελούς Εξεταστικής Επιτροπής

HYDROCARBONS GENERATION AND EXPULSION SENSITIVITY ANALYSIS BY APPLYING 1D/2D/3D BASIN MODELING, PATRAIKOS GULF, WESTERN GREECE – Master Thesis

ΑΝΑΛΥΣΗ ΕΥΑΙΣΘΗΣΙΑΣ ΣΤΗΝ ΓΕΝΕΣΗ ΚΑΙ ΑΠΟΜΑΚΡΥΝΣΗ ΥΔΡΟΓΟΝΑΘΡΑΚΩΝ, ΠΑΤΡΑΙΚΟΣ ΚΟΛΠΟΣ, ΔΥΤΙΚΗ ΕΛΛΑΔΑ – Μεταπτυχιακή Διπλωματική Εργασία

Citation:

Bragou S. T., 2020. – Hydrocarbons generation and expulsion sensitivity analysis by applying 1D/2D/3D basin modeling, Patraikos Gulf, Western Greece. Master Thesis, Department of Geology, Aristotle University of Thessaloniki, pp.149

Μπράγου Σ. Τ., 2020. – Ανάλυση ευαισθησίας στη γένεση και απομάκρυνση υδρογονανθράκων, Πατραϊκός κόλπος, Δυτική Ελλάδα. Μεταπτυχιακή Διπλωματική Εργασία, Τμήμα Γεωλογίας Α.Π.Θ., σελ.149

Cover Figure: ………………………………

Contents

ABSTRACT

The current dissertation shed new scientific light on the critical impact of specific parameters of the modeled thermal regime and the generated/expelled hydrocarbons at the Patraikos modeled area. Patraikos Gulf is located in Western Greece, which is a proven petroleum system area.

A thermal and maturity modelling was applied at the Patraikos Gulf area using 32 pseudowells. The stratigraphy and the formations thicknesses of the 32 pseudowells derived from generalized lithological columns and interpreted seismic data, which were provided from Hellenic Petroleum S.A under confidentiality agreement. The modelling results of the intermediate case (scenario of parameters' combination) in terms of burial history, thermal maturity and timing of petroleum generation/expulsion are presented. The accumulation of hydrocarbons, as modeled, are described in brief since this issue is beyond the purpose of the present dissertation. The results of the two extreme scenarios are presented in the chapter entitled "Sensitivity analysis".

The sensitivity analysis was applied for those parameters that affect both the thermal regime of the modelled area and the generated/expelled volumes of hydrocarbons. Various values of the parameters crustal thickness (CT), beta factor (BF), radioactive heat (RH) and rifting age (RA) were used for the two end-member scenarios of the thermal regime in the area. All used values are based on published literature and the two extremes still meet possible scenarios.

The same reasoning was applied for the parameters of the Total Organic Carbon (TOC), the Hydrogen Index (HI) and the source rock thickness (SRT) which have a great impact on source rock quality and thus on the generated/expelled volumes of hydrocarbons.

The resulted models suggest that the timing of hydrocarbons' generation/expulsion, at the modeled area of Patraikos Gulf, is controlled by the Early Miocene thrusting event. The timing of hydrocarbons' generation/expulsion is also strongly dependent, as modeled, on the crustal thickness and the beta factor (β) parameters. Both parameters are considered as the most critical variables during the applied sensitivity analysis, which significantly affect the thermal regime of the area, thus the maturation of the potential source rocks. The generated volumes of hydrocarbons are affected by the total organic carbon (TOC), the hydrogen index (HI) and the thickness of the modeled source rocks.

The total results of the present dissertation are expected to be the basis for the next step of sensitivity analysis, which will include: a) the variation of the thickness and timing of missing sections; b) the variation of the timing of the major rifting event in the area of Patraikos Gulf.

ΠΕΡΙΛΗΨΗ

Η παρούσα διπλωματική εργασία επικεντρώνεται στην κατανόηση της επίδρασης που έχει η μεταβολή της τιμής συγκεκριμένων παραγόντων, στο θερμικό καθεστώς της περιοχής του Πατραϊκού Κόλπου και συνεπώς στον όγκο και την ποιότητα των παραγόμενων υδρογονανθράκων. Ο Πατραϊκός Κόλπος βρίσκεται στη Δυτική Ελλάδα, περιοχή η οποία συνιστά ένα αποδεδειγμένο πετρελαϊκό σύστημα.

Χρησιμοποιώντας 32 ψευδογεωτρήσεις πραγματοποιήθηκε μοντελοποίηση του θερμικού καθεστώτος της περιοχής και της ωριμότητας των πιθανών μητρικών πετρωμάτων. Τα στρωματογραφικά δεδομένα και το πάχος των σχηματισμών των 32 αυτών ψευδογεωτρήσεων προέρχονται από το συνδυασμό γενικευμένων στρωματογραφικών ακολουθιών (δημοσιευμένο υλικό) και σεισμικών δεδομένων, τα οποία παραχώρησε η εταιρεία Ελληνικά Πετρέλαια με όρους εμπιστευτικότητας. Τα αποτελέσματα από το σενάριο με τις ενδιάμεσες, και ως εκ τούτου περισσότερο αντιπροσωπευτικές, τιμές παραμέτρων (ενδιάμεσο σενάριο) περιγράφονται αναλυτικά. Τα αποτελέσματα που παρουσιάζονται αφορούν στη διαδικασία ταφής των ιζημάτων, την ωριμότητα και τους κρίσιμους χρόνους της γένεσης των υδρογονανθράκων και της εξαγωγής αυτών από τους ορίζοντες των μητρικών. Η συγκέντρωση των υδρογονανθράκων που τελικά παράγονται και μεταναστεύουν προς την παγίδα (σύμφωνα με τα μοντέλα που κατασκευάστηκαν) περιγράφεται εν συντομία, καθώς το αντικείμενο αυτό δεν αποτελεί βασικό στόχο της παρούσας εργασίας. Τα αποτελέσματα από δύο επιπρόσθετα με ακραίες τιμές σενάρια παρουσιάζονται στο κεφάλαιο με τίτλο Sensitivity Analysis.

Η μελέτη με όρους “Sensitivity Analysis” πραγματοποιήθηκε για αυτές τις παραμέτρους που είναι ικανές να επηρεάσουν το θερμικό καθεστώς της περιοχής και τον όγκο των παραγόμενων υδρογονανθράκων. Διάφορες τιμές των παραμέτρων όπως το πάχος του φλοιού (crustal thickness), ο παράγοντας β (beta factor), η θερμότητα από τη ραδιενεργή μεταστοιχείωση (radioactive heat) και η ηλικία των τεκτονικών γεγονότων (rifting age), χρησιμοποιήθηκαν για την κατασκευή μοντέλων για τα δύο ακραία σενάρια του θερμικού καθεστώτος της περιοχής. Όλες οι τιμές που εφαρμόστηκαν βασίζονται σε δημοσιευμένη βιβλιογραφία, ενώ ταυτόχρονα οι δύο ακραίες περιπτώσεις πληρούν τις προϋποθέσεις για πιθανά σενάρια στην περιοχή μελέτης.

Η ίδια λογική χρησιμοποιήθηκε και για τις τιμές των παραμέτρων που επηρεάζουν τα ποιοτικά χαρακτηριστικά των πιθανών μητρικών πετρωμάτων και ως εκ τούτου τον όγκο των παραγόμενων υδρογονανθράκων. Τέτοιες παράμετροι είναι ο συνολικός οργανικός άνθρακας (TOC), ο δείκτης υδρογόνου (HI) και το πάχος του μητρικού πετρώματος (SRT).

Τα μοντέλα τα οποία προέκυψαν δείχνουν ότι η χρονική στιγμή της γένεσης/ αποβολής των υδρογονανθράκων επηρεάζεται κυρίως από τη δράση τού κύριου ανάστροφου ρήγματος (thrust), στην περιοχή που μελετήθηκε, κατά την περίοδο του Μειοκαίνου. Επιπλέον, η χρονική στιγμή της γένεσης/ αποβολής των υδρογονανθράκων στην περιοχή του Πατραϊκού Κόλπου, προκύπτει, με βάση τα μοντέλα, ότι επηρεάζεται έντονα από το πάχος του φλοιού και τον παράγοντα β. Οι δύο

αυτές παράμετροι μπορούν να χαρακτηριστούν ως οι πιο κρίσιμες στην συγκεκριμένη μελέτη, καθώς επιδρούν σημαντικά στο θερμικό καθεστώς της περιοχής και ως εκ τούτου στην ωριμότητα των πιθανών μητρικών πετρωμάτων. Ο όγκος των παραγόμενων υδρογονανθράκων επηρεάζεται από το συνολικό οργανικό άνθρακα (TOC), το δείκτη υδρογόνου (HI) και το πάχος των μητρικών πετρωμάτων (SRT).

Το σύνολο των αποτελεσμάτων της παρούσας εργασίας θα μπορούσε να αποτελέσει τη βάση για περαιτέρω έρευνα (μοντελοποίηση) η οποία να περιλαμβάνει: α) την μελέτη της επίπτωσης της μεταβολής του πάχους των διαβρωμένων οριζόντων και του χρόνου διάβρωσης (διάρκεια και απόλυτη ηλικία), β) την μελέτη της επίπτωσης της μεταβολής του χρόνου δράσης (διάρκεια και απόλυτη ηλικία) των τεκτονικών γεγονότων στην περιοχή του Πατραϊκού Κόλπου.

PREFACE

Although the scientific knowledge and past research in Greece was very limited, the existence of petroleum in western Greece was widely known due to the numerous surface oil shows. For example, Herodotus (484–430 B.C.) has first mentioned the Keri oil seep in Zakynthos island. Systematic research was carried out by exceptional scientists (Monopolis, 1977; Karakitsios, 1992, 1995, 2013; Roussos and Marnelis, 1995; Karakitsios and Rigakis, 1996; Rigakis and Karakitsios, 1998; Karakitsios et al., 2001; Zelilidis et al., 2003; Rigakis et al., 2004; Karakitsios and Rigakis, 2007; Marnelis et al., 2007) and has proven that Western Greece constitutes potential petroleum systems. Western Greece is characterized by rich source rocks of significant thickness and great quality characteristics, located in the Ionian zone.

This dissertation was conducted in Aristotle University of Thessaloniki, within the postgraduate studies program ‘Hydrocarbon exploration and exploitation’, in cooperation with the Hellenic Petroleum S.A. (HELPE). I would like to gratefully acknowledge Dr. Ioannis Oikonomopoulos, Senior Geochemist of HELPE Upstream for his valuable help and guidance to this effort. His patience, motivation and guidance were crucial in completing the research and writing of this thesis. Furthermore, I would like to express my gratitude to HELPE S.A. for the conferral of the geological data.

Special thanks should be addressed to supervisor Professor Kimon Christanis, Professor Andreas Georgakopoulos and Professor Vasilios Karakitsios for providing their insight and expertise that greatly assisted the research and their constructive comments.

The dissertation focuses on potential hydrocarbon field in Patraikos Gulf area. A basin analysis was undertaken to describe the geological setting, the thermal regime, the critical times and the accumulated hydrocarbons of the area. Afterwards, a detailed sensitivity analysis based on crustal thickness, beta factor, radioactive heat, rifting age and source rock properties was carried out.

Geochemical models and basin analysis have accomplished using two software. Schlumberger’s PetroMod software was used for the 1D modeling as Schlumberger sponsorship with a full academic license to postgraduate program ‘Hydrocarbon Exploration and Exploitation’. Genesis and Trinity 3D software by Zetaware were used for the 1D/2D/3D modeling as additional software provided by HELPE Upstream.

Thessaloniki, October 2020

Styliani T. Bragou

INTRODUCTION

Western Greece is characterized by rich source rocks of significant thickness, located in the Ionian and Paxoi zones. Many researches since 1960 (IGRS-IFP, 1966; BP, 1971; Monopolis, 1977; Chiotis, 1983; Palakas et al., 1986; Karakitsios, 1992, 1995, 2013; Roussos and Marnelis, 1995; Karakitsios and Rigakis, 1996; Rigakis and Karakitsios, 1998; Karakitsios et al., 2001; Zelilidis et al., 2003; Rigakis et al., 2004; Karakitsios and Rigakis, 2007; Marnelis et al., 2007) have proven the existence of petroleum in Western Greece. Even when the scientific knowledge and research in Greece was very limited, the existence of petroleum in western Greece was widely known because of the great number of surface oil shows, for example, in the Epirus region, the Keri oil seep on Zakynthos Island, first mentioned by Herodotus (484–430 B.C.), the oil shows in Kyllini (northwestern Peloponnesus), and others (Karakitsios, 2003).

As Karakitsios (2003) described limited early exploration focused on the abundant oil shows (Monopolis, 1977), and more recent exploration did not give encouraging results (Xenopoulos, 2000), although both Albania and Italy host substantial oil and gas fields(Mattavelli and Novelli, 1990; Van Greet et al., 2002; Mavromatidis et al., 2004; Roure et al., 2004;GrahamWall et al., 2006; Vilasi et al., 2009; Maravelis et al., 2012).

However, hydrocarbon exploration in Greece, which was interrupted for more than 10 years, is now commencing again. Western Greece has important petroleum systems as indicated by surface geology. The discovery of hydrocarbon fields results from the identification of the reservoirs, the seals, and the traps where petroleum accumulated.

This study focuses on sensitivity analysis of several parameters which have impact on the thermal behavior of the area and specifically on generated/ expelled volumes of hydrocarbons.

Chapter 1: Geological Setting

The Hellenides geotectonic zone is subdivided into the internal and external Hellenides. The internal Hellenides are characterized by Mesozoic, Paleozoic and older metamorphic rocks, initially affected by the Jurassic-Cretaceous tectonic event during the Alpine orogeny. The external Hellenides are mainly built up by Mesozoic and Cenozoic carbonate rocks, characterized by continuous sedimentation that was terminated with a Tertiary to Neogene flysch deposition (Kilias et al., 2016).

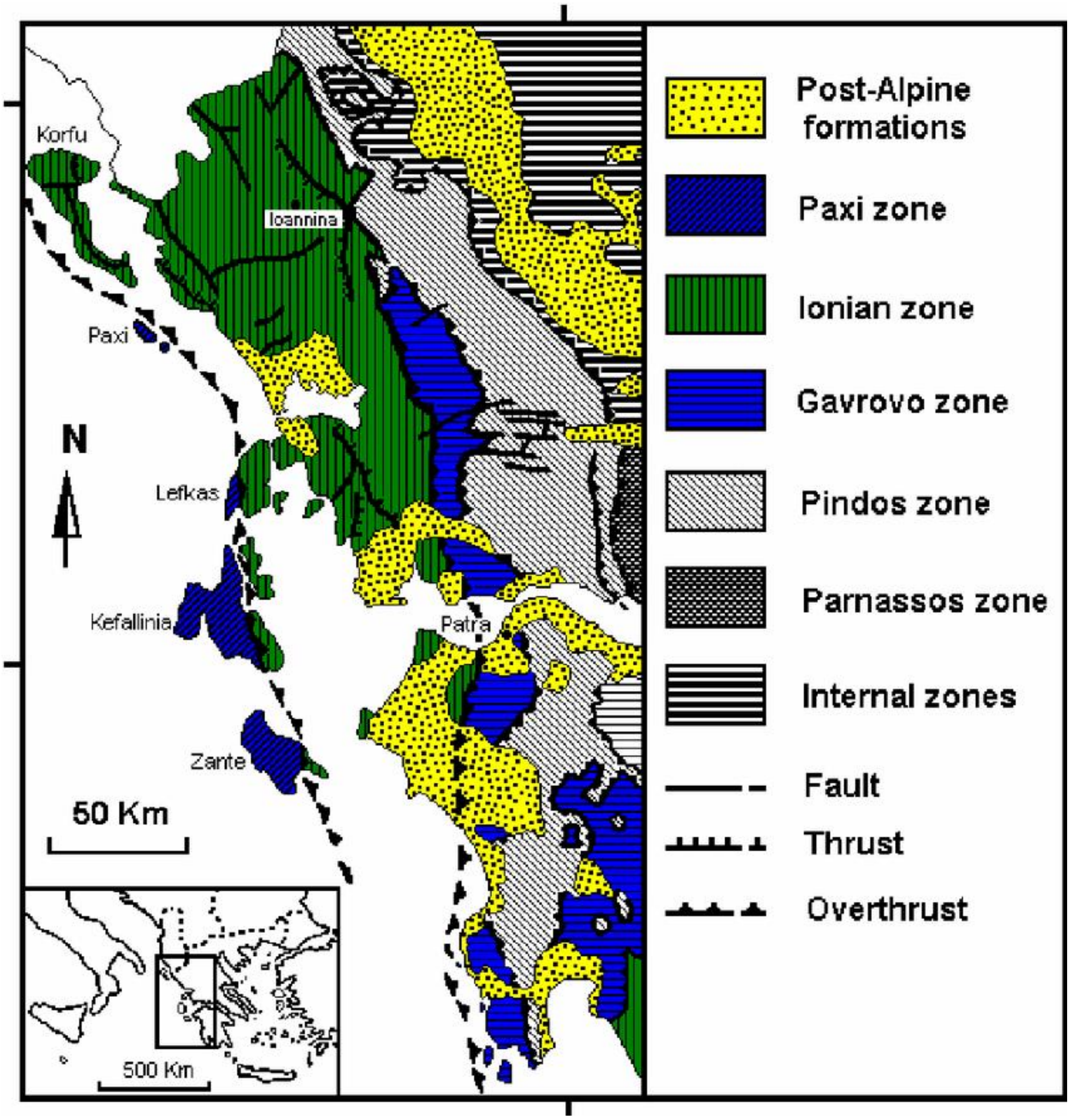

Figure 1: Geological map of the external Hellenides in NW Greece (from Karakitsios, 2007).

The study area belongs to the external zones of the Hellenide fold-and-thrust belt, namely the Ionian zone, Gavrovo-Tripolis zone and the Pre-Apulian zone (known as Paxoi zone). These units have been formed during Lower Jurassic when crustal extension differentiated the southern Tethyan passive margin creating the Ionian basin and the shallow water platforms, Gavrovo to the east and Paxi to the west. In this area the siliceous facies are widely associated with organic carbon-rich deposits (Karakitsios, 2013). The Ionian and the pre-Apulian zones represent, the basin and the transitional zone (slope) to the Apulian platform. The Apulian platform constitutes the deformed foreland of the external Hellenides (Karakitsios, 2013).

The Ionian zone consists of sedimentary rocks. Triassic evaporites, Jurassic- Upper Eocene carbonates, shales minor cherts and Oligocene flysch are the main formations in the Ionian zone. The most important organic-rich intervals within the Mesozoic section of the Ionian zone are the Triassic shales, the Middle- Upper Jurassic Posidonia beds and the Lower Cretaceous Vigla shales (Karakitsios, 2013). On the other hand, no organic -rich interval (source rock) has been identified yet within the Gavrovo zone, which was a shallow water platform from Triassic to Upper Eocene. The pre-Apulian zone consists of Triassic to Miocene deposits, mostly mixed neritic-pelagic carbonates. Pelagic deposits rich in marine organic matter and siliciclastic sediments rich in terrigenous organic matter could also be described as hydrocarbon source rocks (Rigakis et al., 2004; Karakitsios and Rigakis, 2007; Karakitsios, 2013).

1.1 Gavrovo-Tripolis zone

The Gavrovo zone represents a shallow water platform environment were neritic carbonate sediments were deposited from Upper Triassic to Middle Eocene. In western Greece is exposed the Gavrovo sub-zone carbonate succession (Cretaceous to Eocene), followed by Oligocene turbidite deposits (flysch), (Fig. 2).

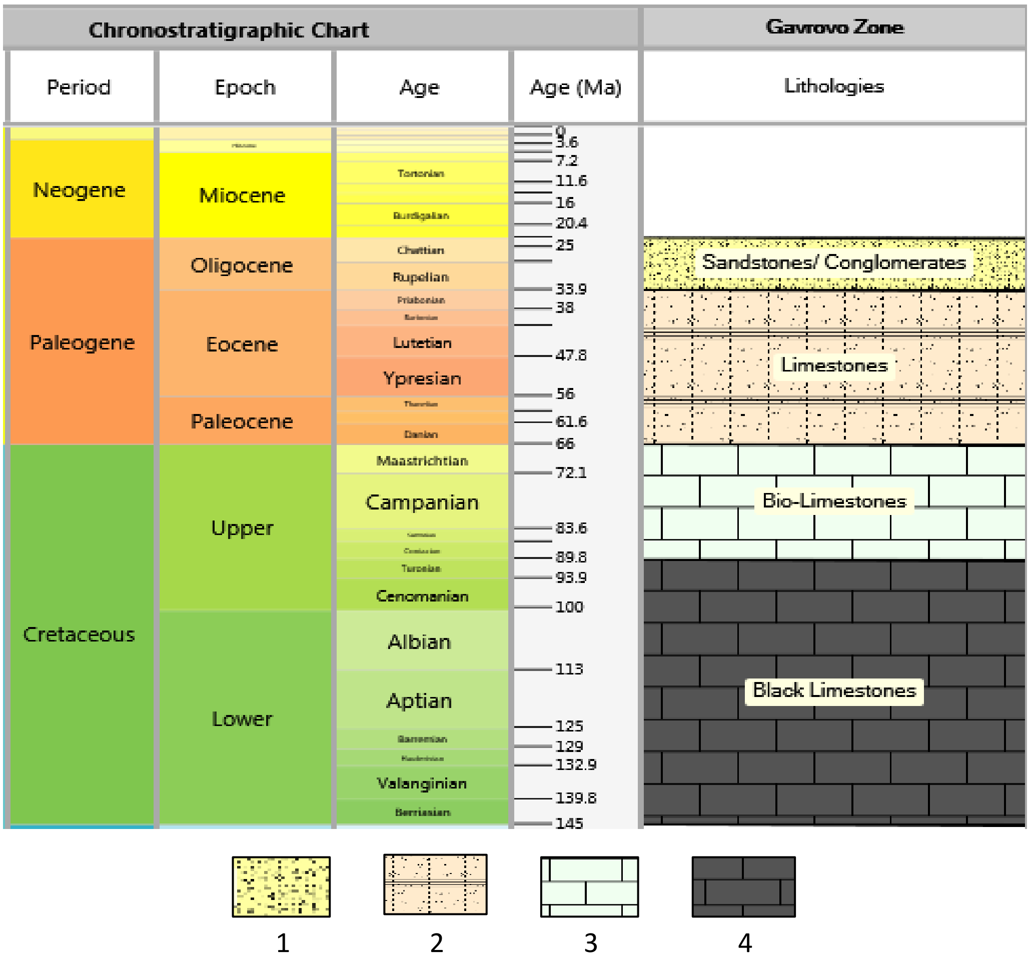

Figure 2: Simplified lithostratigraphic column (Rigakis, 1999) of the Gavrovo zone. (1) Flysch consists of silt, sandstones and conglomerates (limestone conglomerates in particular) (2) Limestones (3) Bio-Limestones with rudist fragments. (4) Black Limestones.

Based on the studies of IGRS-IFP (1966), BP (1971), Fleury (1980), Mavrikas (1993), the lack of Jurassic fossils, put the older horizons within the Lower Cretaceous. In the Senonian-Campanian boundary erosion took place, which is more intense in the west. Bio-limestones with the rudists and reefal carbonates have been identified at the eastern and western part of the Gavrovo zone, respectively.

During the Paleocene-Eocene period, the conditions of the sedimentation become that of deep environment at the western side and that of external platform at the east part. Flysch deposition occurs at the beginning of the Oligocene (IGRS-IFP, 1966; Rigakis, 1999) including the deposition of silt, sandstones and conglomerates (limestone conglomerates in particular).

1.2 Ionian Zone

Ionian zone is made up of three stratigraphic sequences: the prerift, synrift and postrift sequence (Karakitsios 1992; 1995). The prerift sequence consists mainly of carbonates and evaporites. The first Alpine sediments are evaporites. The age of the evaporites (~2000 m thick), derived from stratigraphic data, is Lower-Middle Triassic (Pomoni Papaioannou and Tsaila-Monopolis, 1983; Dragastan et al., 1985; Karakitsios and Tsaila-Monopolis, 1990), however deposition during Permian age is also possible (IGRS-IFP, 1966). The injected evaporites during the orogenesis of Ionian zone were transformed in evaporite dissolution-collapse breccias which are currently exposed as gypsum and associated breccias (Karakitsios and Pomoni-Papaioannou, 1998; Pomoni-Papaioannou et al., 2004; Karakitsios, 2013). Triassic evaporites and breccias are mainly exposed in the central and external Ionian zone (Karakitsios, 2013). The Foustapidima limestones of the Ladinian-Rhaetian age (Dragastan et al., 1985; Karakitsios and Tsaila-Monopolis, 1990) overlie the evaporites and breccias, without distinct contact. This formation occurs only in the external Ionian zone. The Lower Jurassic (Hettangian to Sinemurian) shallow-water limestones known as Pantokrator overlie the Foustapidima limestones and evaporites. The total thickness of Pantokrator formation could be more than 1000 m (IGRS-IFP, 1966, Karakitsios, 1995).

Extensional tectonic movements, faults and deepening of the Ionian zone during lower Jurassic mark the beginning of the synrift period (Karakitsios, 1992, 1995; Karakitsios and Rigakis, 1999). Thus, the synrift sequence begins with the pelagic Siniais limestones and their lateral equivalent semi-pelagic Louros limestones. These Pliensbachian formations correspond to the general deepening of the Ionian domain with the formation of the Ionian basin (Karakitsios, 2013). Siniais limestones (< 150 m thick) occupy the central Ionian Basin, while Louros limestones (approximately 150 m thick) occupy the marginal sides of the Ionian Basin (Karakitsios, 1990; 1992). The first deepening was followed by the internal differentiation of the Ionian Basin: the initial basin separated into smaller paleogeographic units with a half-graben geometry, due to the combination of the extension related to the opening of the Neotethys Ocean and the halokinesis of the Ionian evaporitic base. In the deeper parts of the half-grabens continuous sedimentation comprises the Toarcian Ammonitico Rosso sequences or their lateral equivalent Lower Posidonia beds. Important lateral changes in thickness of the synrift formations, in each half-graben, are observed reaching in the elevated parts of the half-grabens to the unconformity of the Vigla limestones over the Siniais or even the Pantokrator limestones (Karakitsios, 1992, 1995). Limestones with filaments (Callovian) overlying the Lower Posidonia beds, when the stratigraphic sequence is not interrupted. Upper Posidonia shales deposited at the end of Tithonian over the limestones with Filaments. The synrift stratigraphic sequence, which includes Ammonitico Rosso, Lower Posidonia beds, limestones with filaments and Upper Posidonia beds, are not observed in the entire basin. In many areas the limestone horizon with Filaments covers a very short stratigraphic period or is lacking, so the Lower Posidonia beds come in contact with the Upper ones. The two formations are not separated in many cases, and then they are referred to as undifferentiated Posidonia shales (IGRS-IFP, 1966; Karakitsios, 1992, 1995).

The postrift sequence begins with the pelagic Vigla limestones, whose deposition was synchronous throughout the Ionian basin, beginning in the early Berriasian (Karakitsios, 1992; Karakitsios and Koletti, 1992). Vigla limestones extend over the synrift sequence, and in some cases, they directly blanket the prerift units (e.g., the Pantokrator limestones). Variations in Vigla's thickness in the Ionian zone were noticed. These marked variations in the thickness of the Vigla limestones established the longstanding subsidence during the deposition of this formation (Karakitsios, 2013). In the central Ionian zone Vigla formation appears much thinner than its border areas due to the transition to the adjacent neritic platforms (Gavrovo to the East and Apulia to the West respectively). The front of dolomitization reached the Lower Jurassic in the central Ionian zone whereas in the the internal and external Ionian zone it reached the lower layers of the Vigla limestones (IGRS-IFP, 1966).

The Upper Cretaceous limestones, known as Upper Senonian limestones, rest on the Vigla limestones. Upper Senonian formations are limestones with rudist fragments, within calcareous cement containing pelagic fauna (Aubouin, 1959; IGRS-IFP, 1966).

Paleocene and Eocene sediments were deposited without significant facies changes. It is essential to be noticed that the Paleocene is not represented from specific features in the Ionian zone. During the Paleocene, the Ionian basin is provided brecciated rock fragments, due to the erosion of Cretaceous carbonates on the Gavrovo and Apulian platforms. However, during the Eocene the supply of clastic material is diminished, especially in the central Ionian basin. Greatest thicknesses units (Eocene) could be found in the marginal parts of the Ionian zone, where the microbreccias are more frequent (Karakitsios, 2013).

The turbidite sediment deposition which conformably overlies the upper Eocene limestones, occurred at the Eocene- Oligocene boundary (Aubouin, 1959; IGRS-IFP, 1966; Bellas, 1977). There are variations in flysch thicknesses and lithofacies in individual areas of the Ionian basin. Thus, in the eastern part of the basin, the flysch is thicker and coarser. In the central area of the Ionian basin the flysch consists of clay-siltstone-sandstone alternations and occasionally marls. In the western area, the flysch is marl-dominated (IGRS- IFP, 1966).

Focusing on petroleum geology and hydrocarbons' exploration it is noteworthy that the influence of the Triassic evaporites in the evolution of the Ionian basin is of the utmost importance. The Jurassic extensional phase triggered halokinesis of the basement evaporites. This affected the synrift mechanism by enhancing the extensional fault throws, resulting in the formation of small, structurally controlled subbasins with half-graben geometry (Karakitsios, 1992; 1995). During the compressional orogenetic phase, preexisting extensional structures (Pliensbachian to Tithonian) were reactivated. As a result, the Ionian series are duplicated. This tectonic event favors hydrocarbon trapping within the lower carbonate series (subthrust plays).

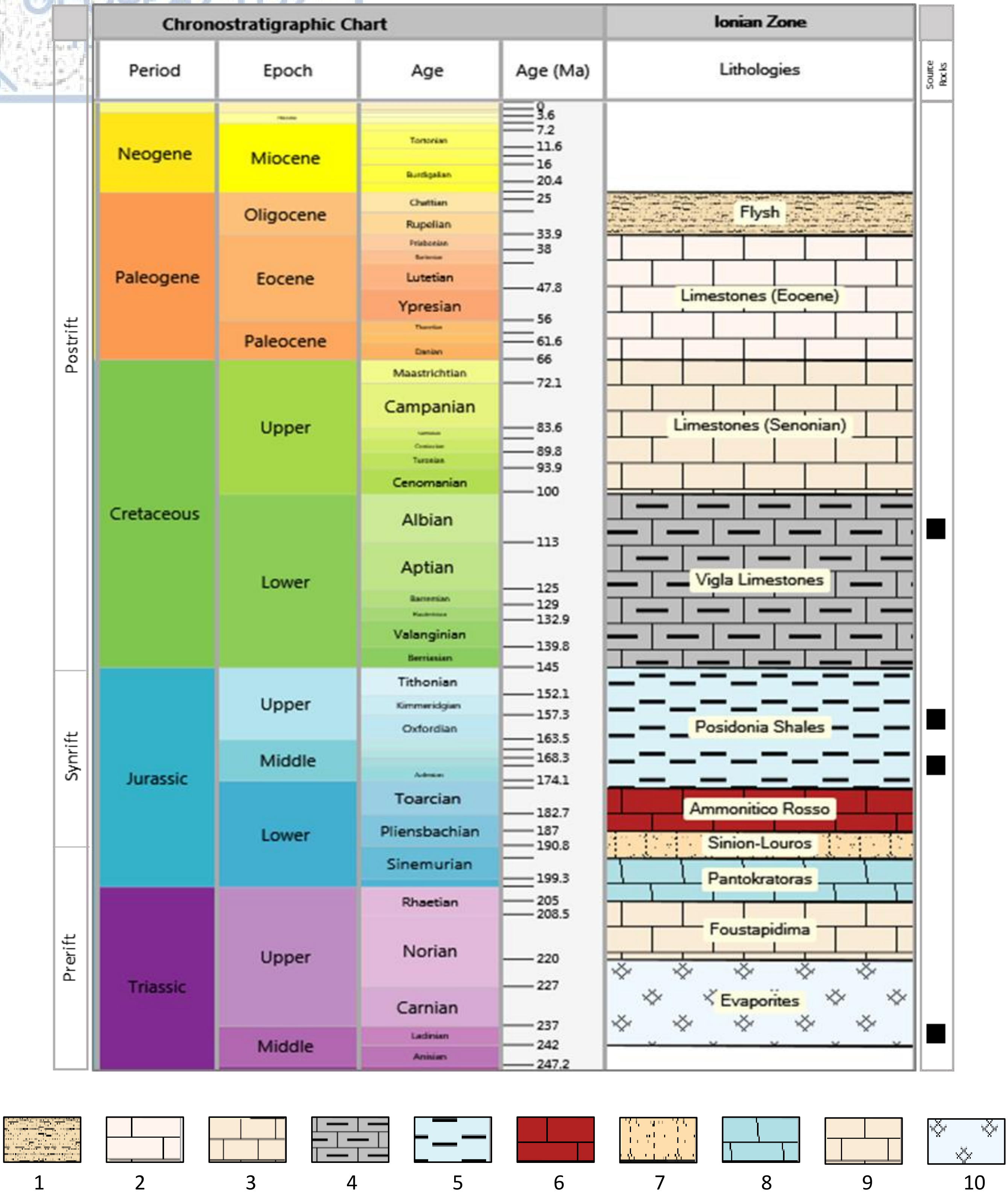

Figure 3: Simplified lithostratigraphic column (Rigakis, 1999) of the Ionian zone. (1) Flysch (2) Eocene Limestones (3) Senonian Limestones (4) Vigla Limestones (5) Posidonia shales (undivided) (6) Ammonitico Rosso (7) Siniais limestones and their lateral equivalent Louros limestones (8) Pantokrator Limestones (9) Foustapidima Limestones (10) Evaporites.

These thrusts are covered by the evaporite intrusions. The flysch remnants are covered of the lower tectonic unit. These traps may contain significant hydrocarbon accumulations (Karakitsios 2013).

1.3 Pre-Apulian (Paxoi Zone)

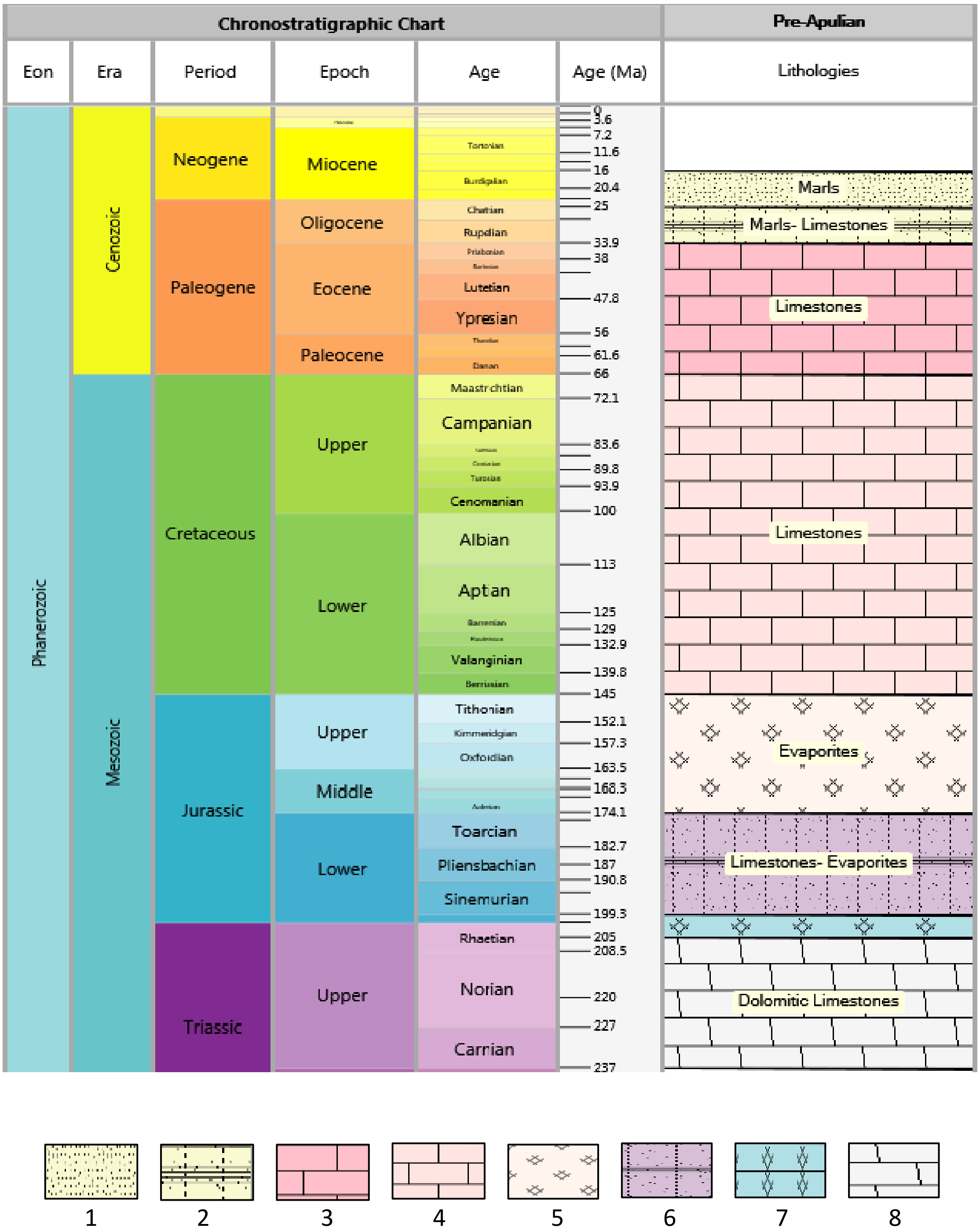

Figure 4: Simplified lithostratigraphic column of the pre-Apulian (Paxos) zone. (1) Marls and marly limestones (2) Marly limestones with brecciated intercalations (3) Organogenic brecciated limestones, neritic Paleocene limestones, Eocene massive limestones (4) Mixed limestones, thick-layered limestones (5) Limestones, evaporites and argillaceous layers (6) and (7) Evaporites, limestones and mudstone or packstone (8) Grey to black color dolomitic limestones with anhydrite fragments.

The pre-Apulian zone represents the transitional zone (slope) between the Apulian platform and the Ionian zone. This zone appears in Ionian islands Paxi, Antipaxi, Lefkada, Kefallonia and Zakynthos. In these islands only the latest formations outcrop. Its general setting is complex as a result of intense tectonic deformation, including phases of extension, collision, and flexural subsidence, with undetermined amounts of shortening and block rotation. Furthermore, the pre-Apulian zone corresponds to the most external domain of the fold-and-thrust belt of the Hellenides (Karakitsios, 2013).

The depositional sequence begins with the Triassic grey to black colored dolomites with anhydrite fragments. Lower Jurassic horizons consist of evaporites and mudstone or packstone. The Middle-Upper Jurassic successions are dominated by limestones, and shaly layers.

Upwards in the Lower Cretaceous limestones showing less pelagic facies than the age-equivalent Ionian facies (Vigla Limestones).

Thick-layered limestones of Upper Cretaceous age are overlain by neritic Paleocene limestones, Eocene massive limestones and Oligocene marly limestones and brecciated intercalations (Rigakis, 1999).

The Oligocene pre-Apulian sediments represent the progressive passage from the Ionian flysch to more calcareous age-equivalent facies in the pre-Apulian zone, indicating that they correspond to an informal distal flysch unit. Calciturbidites replace these facies in the lower part of the pre-Apulian slope. This unit has been partially or completely eroded in the area corresponding to the most external part of the forebulge in the Hellenide foreland basin (Karakitsios and Rigakis, 2007; Karakitsios, 2013).

The depositional sequence continues with the Lower Miocene marly limestones and marls, whereas during the late-early Miocene, progressive deepening occurred, flooding the former carbonate slope (Karakitsios, 2013; Accordi et al., 1998).

Chapter 2: Petroleum system elements

Based on numerous Exploration & Production and research studies a working petroleum system has been proved at western Greece. The majority of the studies have been accomplished by oil and gas companies from Greece and abroad, whereas universities and institutes have also contributed to this knowledge (Karakitsios, 2003). The petroleum system elements in western Greece have been studied through a great number of onshore and offshore E&P wells and also from outcrops. The presence of oil and gas shows in wells throughout western Greece, the oil seeps in the field (mainly in Epirus and Peloponnese) and the oil accumulation with gas cup at offshore Katakolo area (NW Peloponnese) directly suggest the effective petroleum system elements.

As general rule, the success story for the accumulation of hydrocarbons needs to meet the appropriate combination of timing of i) oil generation and expulsion, ii) effective migration, iii) trap formation and iv) seal deposition. In the following paragraphs each of the petroleum system elements is described separately.

2.1 Source rocks

The Ionian zone, which includes the western Patraikos Gulf area, consist of three main source rocks. The Triassic shales, the Middle- Upper Jurassic Posidonia beds and the Lower Cretaceous Vigla shales. The three source rocks differ in their litholgy, thickness and geochemical characteristics such as Kerogen type, Total Organic Carbon (TOC)- and- Hydrogen Index (HI).

The maturation level of the organic matter is considered as the most critical parameter for the hydrocarbons' generation. The maturity of source rocks depends on the burial depth, thus the temperature range, which is geothermal gradient dependent, and the kerogen kinetics, which is organofacies dependent. Maturity could be delayed, or even completely interrupted, when erosion and exhumation of geological formations takes place.

2.1.1 Triassic shales

The Triassic shales, as hydrocarbon source rock, has a particular significance in the context of the Ionian zone. The Triassic shales are commonly associated with Triassic evaporites and breccias, whereas initially were deposited as stratigraphic layers in relatively shallow- water and restricted subbasins (Rigakis and Karakitsios, 1998; Karakitsios, 2013).

According to the Rock-Eval data (Rigakis,1999), which have been accomplished for well and outcrop samples of the Triassic potential source rocks within the Ionian zone, the total organic carbon (TOC) content varies from 0.49% to 16.12%. The organic matter is dominantly type I oil-prone kerogen having hydrogen index (HI) 400 - 600 mg HC/ g rock and petroleum potential (PP) higher than 20 mg HC/ g rock. The Vitrinite reflectance values (VRo %) range from imatumre to 1.01% depending on the location.

Thermal and maturity models suggest that Triassic shales are thermally mature. This particular source rock has entered the gas window in the external and central Ionian zone, whereas in the internal Ionian zone, the Triassic shales have entered the oil window (Karakitsios and Rigakis, 2007).

2.1.2 Posidonia beds

Posidonia beds could be separated in two different units, the lower and the upper Posidonia beds. The lower Posidonia beds are composed of siliceous argillites, well-bedded pelagic laminated marls, and marly limestones. The Posidonia beds are characterized from their thickness variation, which depends on the position of the shales within the half graben (Karakitsios, 1990; 1992; 1995; 2013).

Rock-Eval data (Rigakis,1999), which have been accomplished for the Ionian zone, show that the total organic carbon of Posidonia beds ranges from 1.05% to 19.12%. A good petroleum potential (PP) with values between 4 and 126 mg HC/ g rock has been also noticed. In addition, the hydrogen index (HI), with 460- 565 mg HC/ g rock and type I-II oil-prone organic matter, indicate deep marine depositional environment. The thickness of the Posidonia beds ranges between 10 and 150m (Rigakis, 1999).

Vitrinite reflectance (VRo %) measuments suggest that the lower Posidonia beds are mature showing values from 0.6% to 1.01% (Karakitsios and Rigakis, 2007). As a result, the lower Posidonia beds constitute the most important source rock of the Ionian zone (Karakitsios and Rigakis, 2007; Karakitsios, 2013).

The Upper Posidonia beds of the Ionian zone include jasper beds with cherty clays. These cherty clays are commonly bituminous. Similarly to the lower Posidonia beds the thickness variation is typical also for the upper Posidonia beds and depends on the position of the shales within the half graben (Karakitsios, 1990; 1992; 1995; 2013).

The total organic carbon (TOC) content of the upper Posidonia beds indicates a range from 1.05% to 3.34%. Type II oil-prone organic matter is dominantly observed. The thickness of the upper Posidonia beds ranges between 10 and 140m (Rigakis, 1999).

The Posidonia beds have been only found in the central and external Ionian zone. In many cases the differentiation between the lower and the upper Posidonia beds is very difficult and thus, it is named as ‘undifferentiated’ Posidonia beds. Hence, in the above cases, only cumulative oil potential characteristics can be considered.

2.1.3 Vigla shales

Vigla formation consists of Lower Cretaceous marly limestones and cherty beds with shale interbedding (Karakitsios, 2013). The shale interbedding, usually named as Vigla shales constitutes one of the main source rocks in the Ionian zone.

Vigla shales are rich in total organic carbon based on Rock-Eval data (Rigakis, 1999). The TOC values range between 0.94 to 5.00%; however, higher values have been noticed (Rigakis, 1999). A high petroleum potential (PP) with values between 5 and 25 mg HC/g rock and locally 178.6-182.6 mg HC/g rock have been also observed. The hydrogen index (HI) ranges from 475-600 mg HC/g rock, whereas the organic matter is dominantly oil-prone Kerogen types I – II, suggesting a marine depositional environment. The thickness of the Vigla shales ranges between 10 and 65 m (Rigakis, 1999).

Thermal and maturity models indicate that the Vigla shales are immature to marginally mature in the central and external Ionian zone and mature in the internal Ionian zone (Karakitsios and Rigakis, 2007). Vitrinite reflectance (VRo%) measurements show values from 0.42% to 0.72%. They are marginally mature in terms of oil generation.

According to Karakitsios and Rigakis; (2007), the Triassic shales entered the oil window during the Late Jurassic, the lower Posidonia beds during the Serravalian and the Vigla shales of the internal Ionian zone entered the oil window after Serravalian.

2.2 Reservoirs

The reservoir as one of the petroleum system elements is briefly described in this paragraph because it is beyond the focus of the present study.

In Ionian zone there are several levels of formations, such as Pantokrator limestones, Senonian and Eocene limestones, which could act as reservoirs.

The lower Jurassic Pantokrator limestones consist of thick-layered limestones, which are commonly dolomitized at their lower part. The most important reservoir formations within western Greece are considered the Senonian and the Paleocene-Eocene limestones. The Senonian limestones were deposited during Upper Cretaceous. They are neritic, thick-layered limestones with some rudist fragments. Especially, this formation corresponds to calciturbidites of various lithologies grading from fine- to coarse-grained sequences intercalated with debris- flow deposits and thick slumped levels (Karakitsios, 2013). The Paleocene-Eocene limestones are organogenic pelagic limestones with argillaceous layers, whereas marls are the dominant lithological feature at the upper part of the formation. The upper part of this formation includes marls.

2.3 Seal

Similarly, to the reservoir element (above), the seal element is briefly described here since it is beyond the aims of the present study.

In the Ionian zone, the Oligocene flysch is considered as the main seal formation (Rigakis 1999,). In addition, the upper Miocene and Pliocene marls also act as excellent seal in western Greece, e.g. – the case of Katakolo-. However, the best cap-rock formation for the traps existing beneath the thrust units (subthrust plays)- is the Triassic evaporites (Karakitsios, 2013).

Furthermore, the source rocks themselves may sometimes act as seals under specific conditions, due to the organic matter content. Therefore, the organic rich shaly intervals of the Mesozoic section of the Ionian Zone such as Vigla Posidonia shales may act seal under certain conditions.

2.4 Trap

In brief, major synclines in the Ionian realm (such as the Botsara syncline;) include a series of minor anticlines, which, in themselves, form hydrocarbon traps (Karakitsios, 2013).

The presented cases are also considered promising because trap formation occurred prior to or during the organic matter maturity in most Ionian source rocks. The degree of participation of the subevaporitic base in the deformation of the sedimentary cover, in Ionian zone, determines the position and magnitude of the traps in the unknown (deeper than the evaporites) Paleozoic formations, for which less information is available regarding the petroleum reservoir or source rocks (Karakitsios, 2013).

Chapter 3: Basin analysis

3.1 Introduction

Basin Analysis was conducted with special focus on an assigned model, with specific parameters, such as crustal thickness, beta-factor, rifting time, radioactive heat and source rock parameters. Hence, a sensitivity analysis was undertaken based on changes to these specific parameters. Sensitivity analysis notices differences in generation and expulsion critical times and masses, thermal regime and maturity evolution.

3.2 Modeling methods and parameters

One- dimensional (1D) basin modeling was applied using the specialized software PetroMode by Schlumberger and Genesis by Zetaware, whereas for 2D/3D basin modeling the Trinity 3D software by Zetaware was used.

For the purposes of this dissertation, Hellenic Petroleum (HELPE) company provided data for 32 selected points, known as “Pseudo-Wells” derived from seismic data. The pseudo-wells A and B (PW-A & PW-B) were used for the completion of the sensitivity analysis.

The input data that were used for the purposes of the modeling issued from internal HELPE reports and published data and are the following:

- Formation tops derived from the seismic interpretation.
- Thicknesses as were interpreted and calibrated by onshore well data.
- Lithologies based on onshore equivalents and according to the published work (Getsos et al., 2007; Rigakis,1999; Rigakis and Karakitsios 1998; Rigakis et al., 2013).
- Tectono-stratigraphic history of the area, ages and additional tectonic events such as thrusting and equivalent erosion derived from internal reports and published studies.
- Source rock parameters such as kerogen type, total organic carbon (TOC), hydrogen index (HI) shown in Table 1 based on geochemical analysis data.
- Paleo-bathymetry was estimated based on paleodepositional environments and known lithologies from onshore equivalents.
- Sediment surface interface temperature based on equations of Beardsmore and Cull, (2001).

For the wells PW-A and PW-B the following charts were created:

- Burial History VS Vitrinite Reflectance (%).
- Burial History VS Transformation Ratio (%).
- Vitrinite Reflectance Curve VS Time, according to Burnham and Sweeney, (1989).
- Generation Mass VS Time, for each of the source rocks.
- Expulsion Mass VS Time, for each of the source rocks.

According to the published work (maps are presented in Appendix I) for the western Patraikos Gulf area, adjusted input values were used for the simulation of the scenario 1. Table 2 presents the syn-rift and the post-rift period, the radioactive heat flow, the beta factor and the crustal thickness values.

Table 1:Values of the source rock parameters that were used for the creation of the thermal and maturity model of the western Patraikos Gulf area.

Formation	Age	Kerogen Type	Organo-facies	Average TOC (%)	Average HI	Average Thickness (m)
Vigla	Albian-Cenomanian	II	B	1.8	500	60
Posidonia	Callovian-Tithonian	IIS	B	2.0	600	60
Triassic Shales	Norian	I	C	3.0	650	30

Table 2: Adjusted input parameters for the scenario 1 in pseudo-wells A and B.

Parameter	Value	Literature
Syn-Rift (Ma)	**190-145**	**Karakitsios, 2013**
Post- Rift (Ma)	**145-0**	**Karakitsios, 2013**
Radioactive heat (mW/m^3)	**2.8**	**Based on crust composition in Ionian zone**
Beta factor (crust)	**1.3**	**Pasquale, et al., 1997**
Crustal Thickness (km)	**35**	**Cavazza et al., 2004**

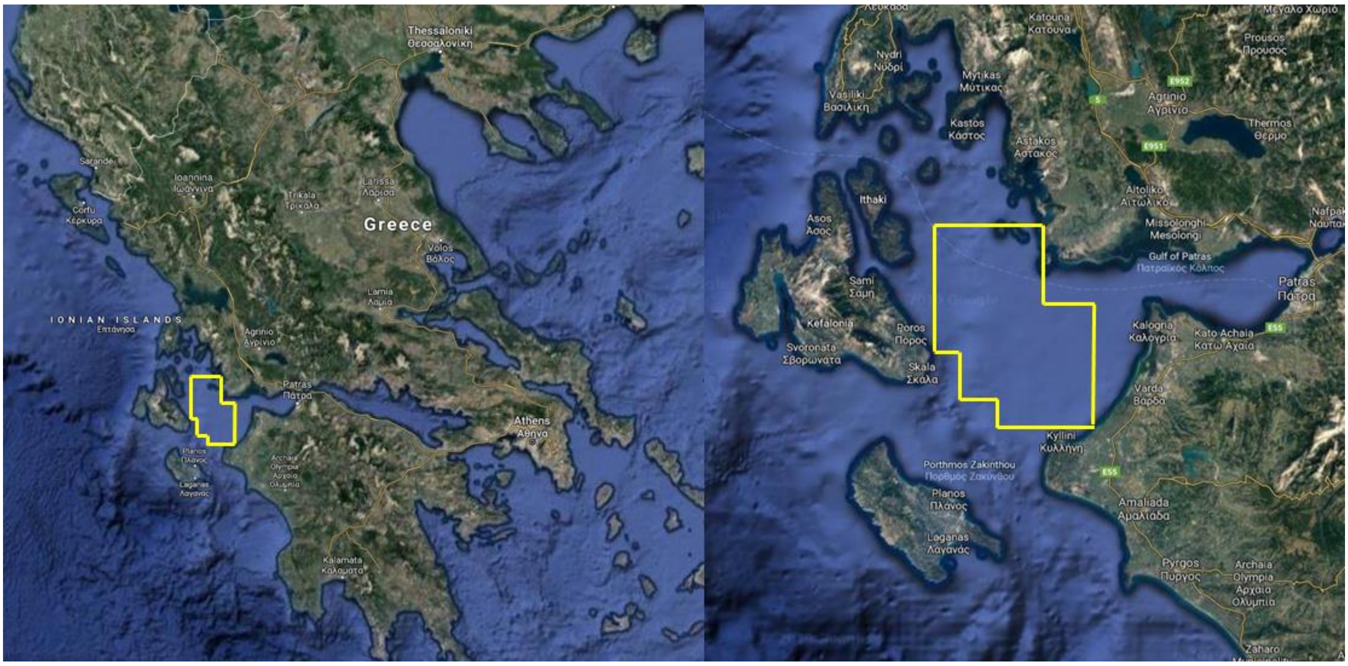

Figure 5:Geomorphological map (Google Maps) of the broader Patraikos Gulf showing the study area.

3.3 Results of Pseudo-well A (PW-A)

One-dimensional (1D) modeling of burial history and thermal maturity sensitivity analysis was performed using pseudo-well A. The pseudo-well location is very close to the kitchen.
In this chapter burial history, transformation ratio, vitrinite reflectance, generation and expulsion masses for the PW-A are discussed. Moreover, 2D maps for vitrinite reflectance and generation/ expulsion masses for the three modeled Mesozoic source rocks are also presented.
Thrust emplacement and erosional events are critical and could affect maturity evolution. Thrusting took place during the end of Oligocene- early Miocene. This event increases the sediment accumulation and buried deeper the formations. There are two modeled erosional events. The first erosional event took place in Oligocene and the second event in Pliocene. The two erosional events correspond to 700 m and 1600 m of missing section respectively. The volume of the deposited and then eroded sediments result in the increase of maturity.

3.3.1 Burial History

According to burial history curves (Figure 6) during Middle to Upper Triassic (240-230 Ma) the sediment accumulation is more than 3000 m thick (Rigakis, 1999); however, in the pseudo-well A almost 1550-m-thick sediments are hosted. The Triassic sequence includes evaporites and the first potential source rock of the area, known as Triassic shales. From Upper Triassic to Lower Jurassic (230-193 Ma) the Pantokrator platform limestones were deposited. The formation thickness amounts to 3464 meters. During the syn-rift period (190-145 Ma) and more specifically during Middle to Upper Jurassic (193-146 Ma) the second potential source rock of the area, known as Posidonia Beds, was deposited. Posidonia beds appear as an undifferentiated formation in this pseudo-well. Later, from 146 to 89 Ma (Berriasian-Coniacian) the pelagic carbonates of Vigla Formation along with the third potential source rock of the area, known as Vigla Shales, were deposited. Between 89 to 36.6 Ma (Coniacian-Oligocene) the deposition continued with the Senonian Carbonates, the Paleocene-Eocene Limestones, and the Ionian Flysch, with approximately 940 meters of thickness. The first erosional event lasted about 2 m.y. and ended with the beginning of thrusting. There is a removal of about 700 meters of the section. After that, the burial history curve drops steeply, representing the rapid increase in sediment accumulation rate during thrusting between 23.7 to 16.6 Ma. Maximum burial occurred around 7 Ma when the second erosional event lasted about 2 Ma. The erosional event started with the end of thrusting and ended with the deposition of the Plio-Pleistocene sediments. About 1600-m-thick sediments were removed. In the last 5 Ma almost 1100 meters of sediment have been deposited in the area of western Patraikos Gulf. Table 3 lists information of the current depth and the calculated maximum depth of the potential source rocks on the western Patraikos Gulf area. The maximum calculated depth as mentioned in Table 3 is equivalent to the maximum burial at 7 Ma.

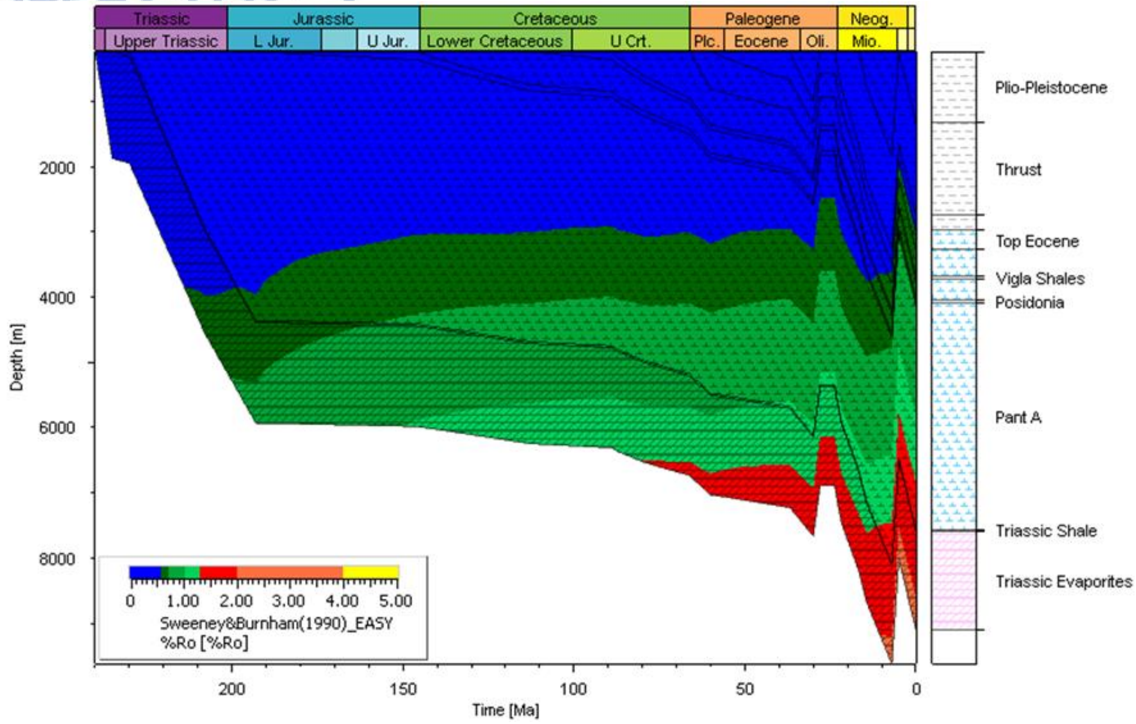

Figure 6: Burial history plot (240 Ma to Present) of the pseudo-well A at Patraikos Gulf. Location shown in Figure 5.

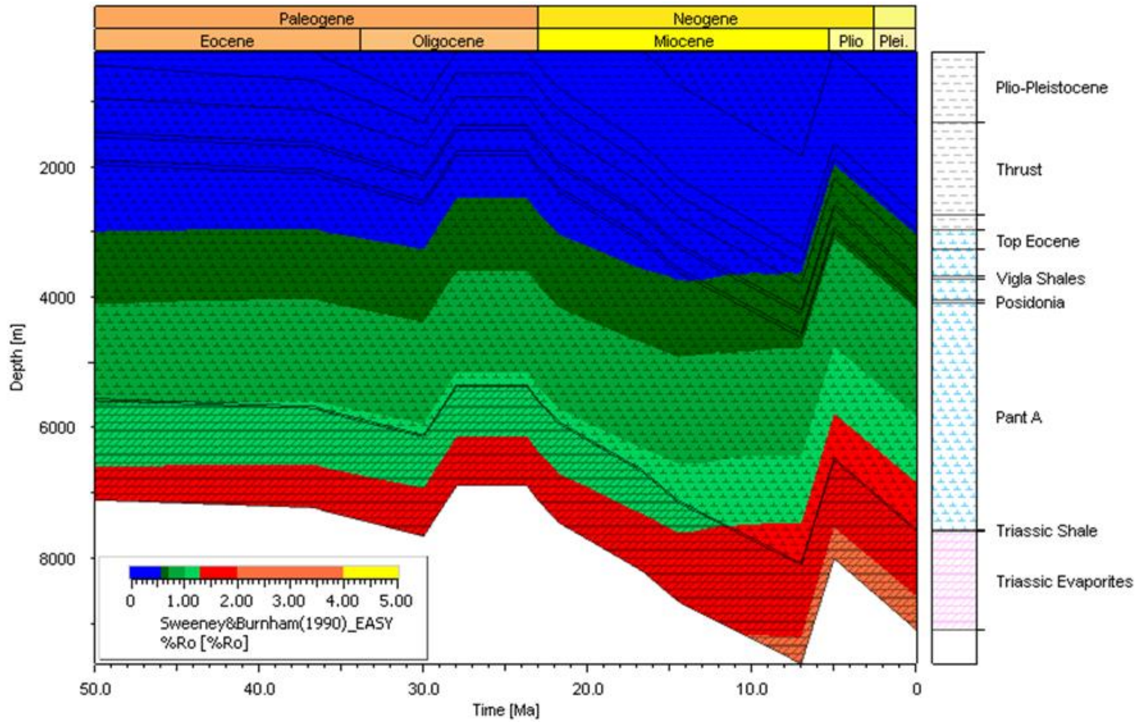

Figure 7: Burial history plot (50 Ma to Present) of the pseudo-well A at Patraikos Gulf. Location shown in Figure 5.

Table 3: Current depth, calculated maximum depth of burial.

Burial history location	Source rock		
Pseudo-well A	**Vigla shales**	**Posidonia Shales**	**Triassic shales**
Current depth	3570 m	3930 m	7454 m
Maximum depth	4100 m	4550 m	8100 m

3.3.2 Maturation History

The maturation history performed for the pseudo-well A is based on calculated equivalent vitrinite reflectance values (%Ro). As illustrated from equivalent vitrinite reflectance maturity graphs in Figures 6-7, the blue-colored area represents the immature to marginally mature organic matter (< 0.55 %Ro). The dark green-colored area introduces the early window of oil generation (0.55 – 0.7 %Ro). The green-colored area presents the main window of oil generation (0.7- 1.0 %Ro). The light-green colored area displays the late oil window (1.0- 1.3 %Ro). The red-colored area represents the wet to dry gas window (1.3- 2.0 %Ro). The orange-colored area introduces the dry gas to post dry gas window (2.0- 4.0 %Ro).

The Triassic source rock is considered as oil-prone and composed of Type I Kerogen. At the present time (0 Ma) Triassic shales are in dry gas window as it shows Figure 8. Posidonia beds and Vigla shales are also considered oil-prone and are mostly composed of Type II Kerogen. Both source rocks at present time are in early oil window as illustrates Figure 8.

Triassic shales are entered in oil window approximately at 197 Ma. The peak oil window for this source rock appears in 48 Ma (0.90- 1.00 Ro%). At 12 Ma Triassic shales are entered the gas window. On the other hand, Posidonia and Vigla shales are appeared only in early oil window, at 14 Ma and 11 Ma, respectively.

The maturation could also be observed from the two-dimensional (2D) maps in Figure 9. These maps show the maturity evolution for the three potential source rocks described in Table 4.

Table 4: Timing of oil and gas generation for Type II (Posidonia and Vigla shales) and Type I (Triassic shales) source rock horizons and the burial history location. Age values are in Ma. Depth values (in meters) are calculated at depth at which %Ro value is reached.

Burial History Location	Source Rock					
	Vigla Shales		**Posidonia Shales**		**Triassic Shales**	
Pseudo-well A	**Age**	**Depth**	**Age**	**Depth**	**Age**	**Depth**
0.55 %Ro – Start Oil	11	3750	14	3850	197	3850
1.0 %Ro – Peak Oil	-	-	-	-	48	5500
1.30 %Ro – Start Gas	-	-	-	-	12	7500

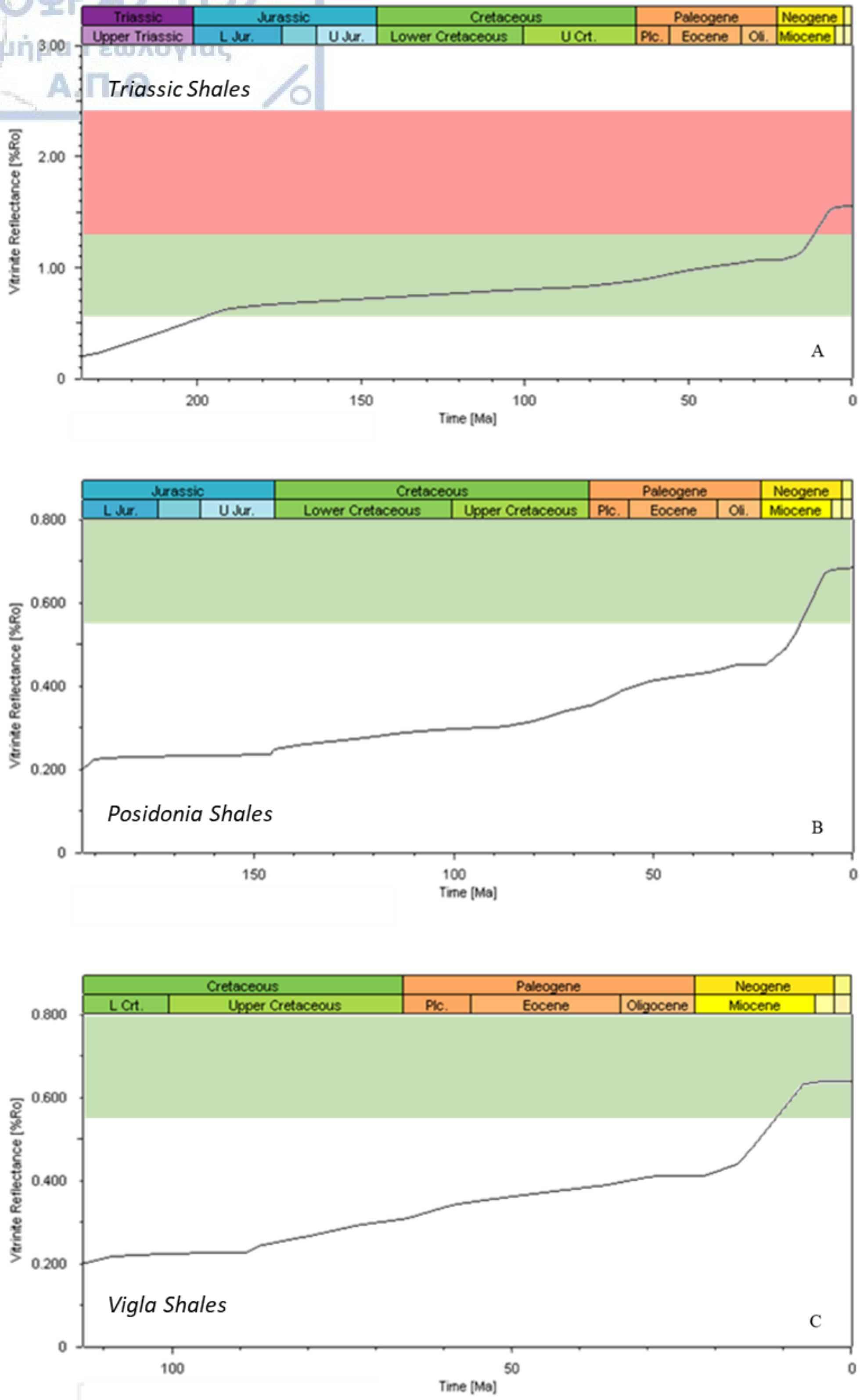

Figure 8: Vitrinite reflectance curves (VRo) through time based on Burnham and Sweeney, 1990. The plots illustrate the evolution of maturity for the three source rocks. Plot A represents the maturity evolution of Triassic shales, plot B of Posidonia and plot C of Vigla shales. The green colored corresponds to 0.55- 1.3% VRo and the red colored area corresponds to 1.3- 2.4% VRo.

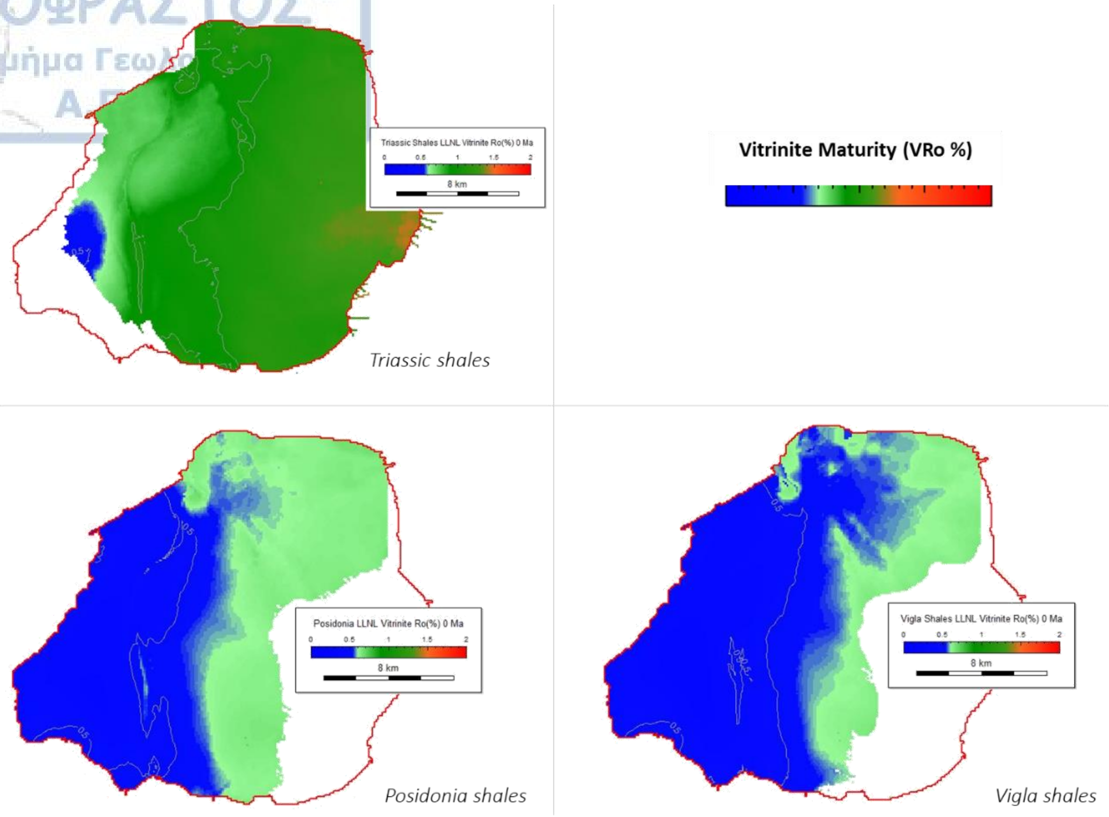

Figure 9: Two-dimensional (2D) maturity maps of the three potential source rocks in western Patraikos Gulf area at present day.

3.3.3 Petroleum Generation History

The timing and extent of petroleum generation from the three potential source rocks at the burial history location of the PW-A are listed in Table 5 and summarized in Figures 10-11 by the transformation ratio evolution through time.

As expected for the oil-prone source rocks, the most extensive petroleum generation occurs at Posidonia beds which experienced deeper burial depths comparing to the Vigla shale source rock horizons. The Vigla shales experienced the shallowest burial depths, thus resulting in the least extensive petroleum generation. Conversely, the Triassic shale horizons generated oil earlier than the Posidonia beds (190 Ma and 14 Ma respectively). However, thrusting buried those horizons, thus cracking the oil to gas.

Table 5*:* Timing of oil generation for the three modeled source rocks and depth of oil generation based on transformation ratio curves. Age values are in Ma. Depth values are in meters. Transformation ratio percentages are in %.

Source Rock	Generation		
	Age	**Depth**	**Transformation ratio**
Triassic Shales	190	4300	1.75
Posidonia Shales	14	3850	3.71
Vigla shales	11	3550	6.13

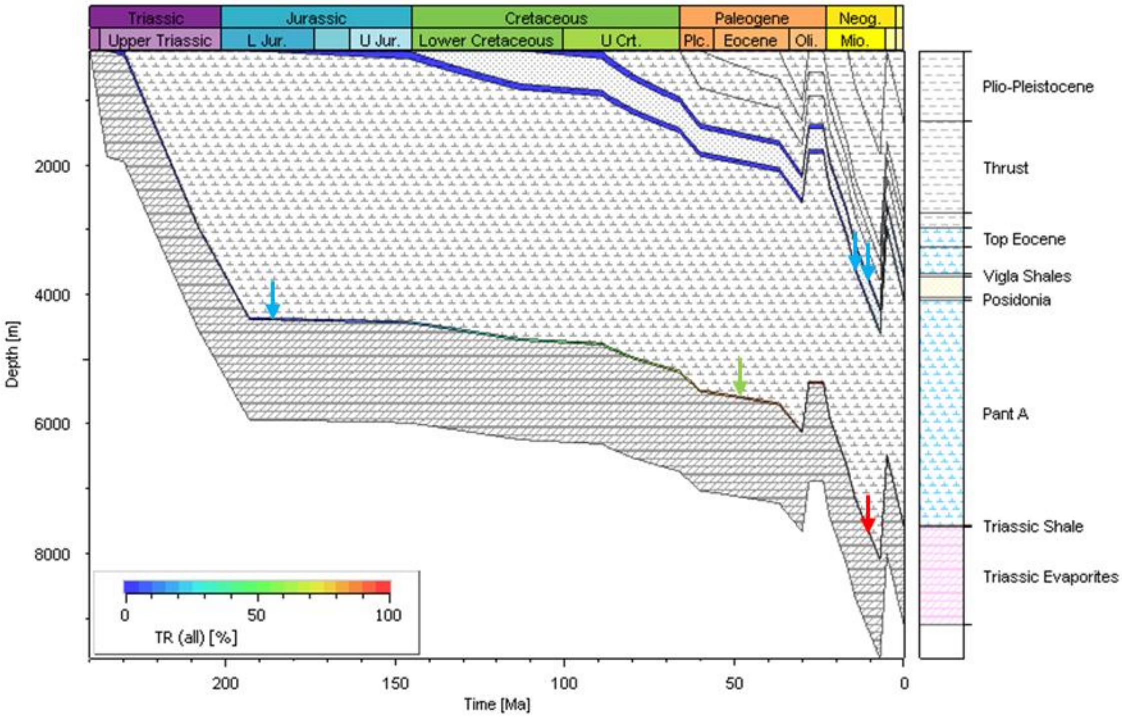

Figure 10: Transformation ratio of organic matter (240 Ma to present) including the three modeled source rocks (Triassic Shales, Posidonia Beds and Vigla Shales) through geological time. Blue, green and red arrows illustrate the start, peak and end of oil generation for all three modeled source rock intervals.

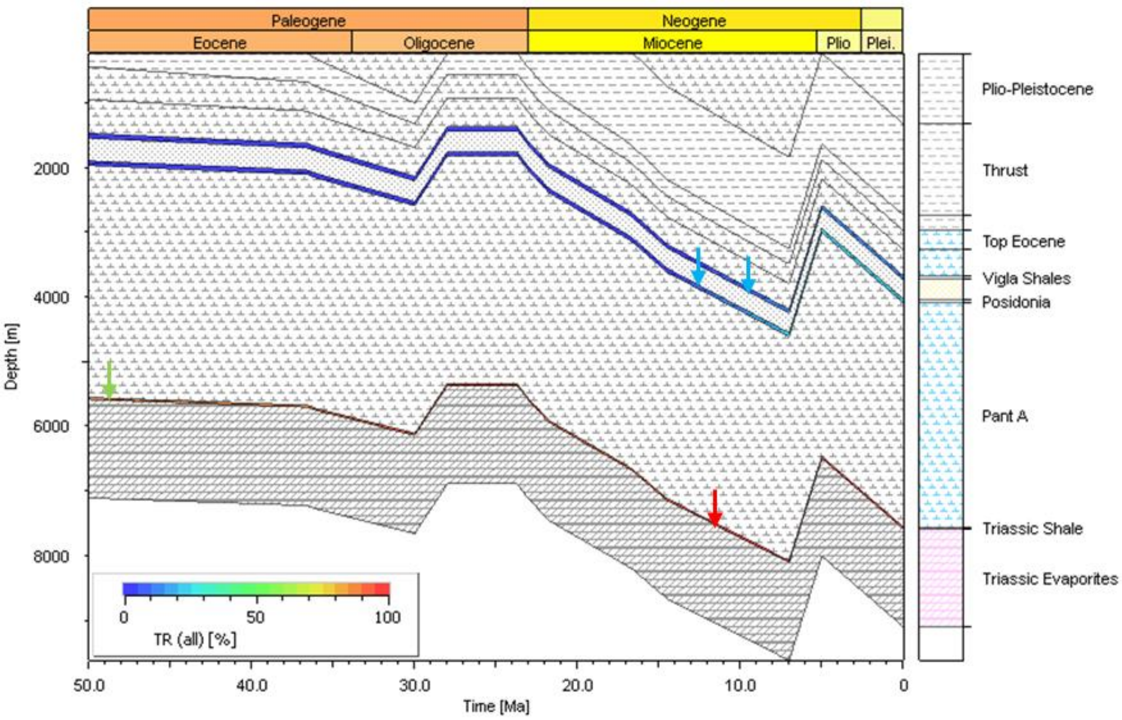

Figure 11: Transformation ratio of organic matter (50 Ma to present) including the three modeled source rocks (Triassic Shales, Posidonia Beds and Vigla Shales) through geological time. Blue, green and red arrows illustrate the start, peak and end of oil generation for all three modeled source rock intervals.

Oil generation in Triassic shales followed the normal process and starts approximately at 190 Ma. The timing of oil cracking to gas took place at the end of the late oil window at about 12 Ma and was maybe controlled by the thrusting due to the deeper burial depths. Oil generation in the Posidonia beds and Vigla shales began at about 20 Ma and 17 Ma respectively. The ages suggest that the thrust emplacement significantly affected the generation of these oils.

Triassic shales generate 19.43 mg HC/g Rock in total, Posidonia shales 2.9 mg HC/g Rock and Vigla shales 1.28 mg HC/g Rock. Hence, Triassic source rock could be considered as the most important in terms of hydrocarbons generation volumes in the Patraikos Gulf. Generation critical times, generation masses and generation value at expulsion starting time, are summarized in the Table 6.

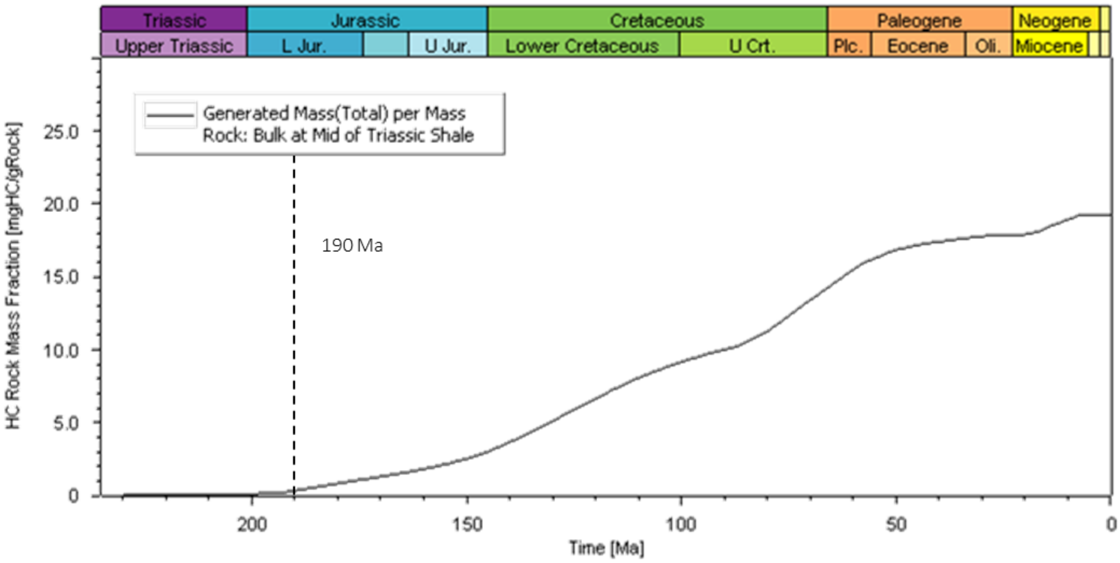

Figure 12: Generation mass curve through geological time for the Triassic shales. Generation mass values are in mg HC/g Rock and time values are in Ma.

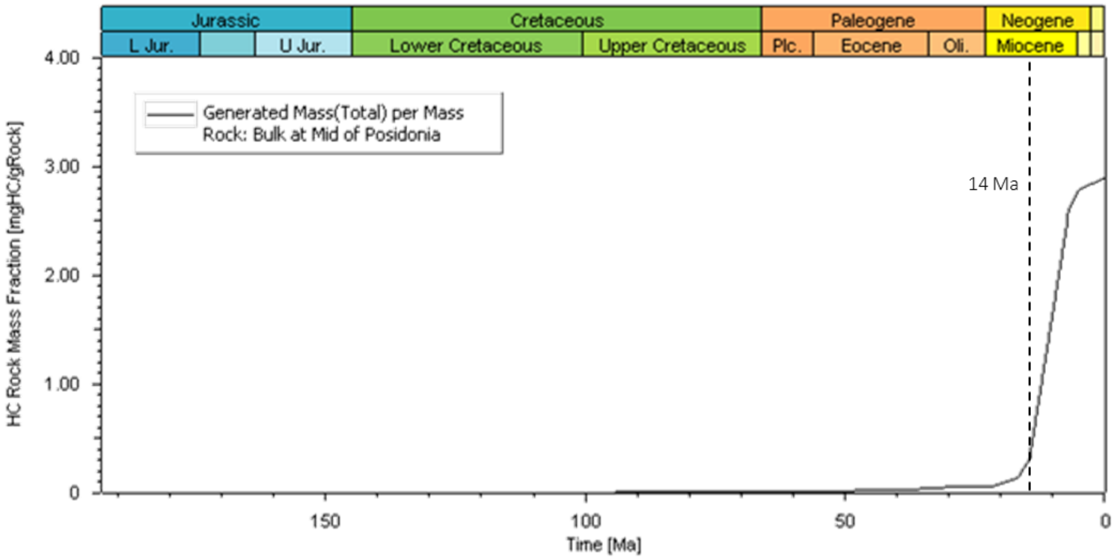

Figure 13: Generation mass curve through geological time for the Posidonia beds. Generation mass values are in mg HC/g Rock and time values are in Ma.

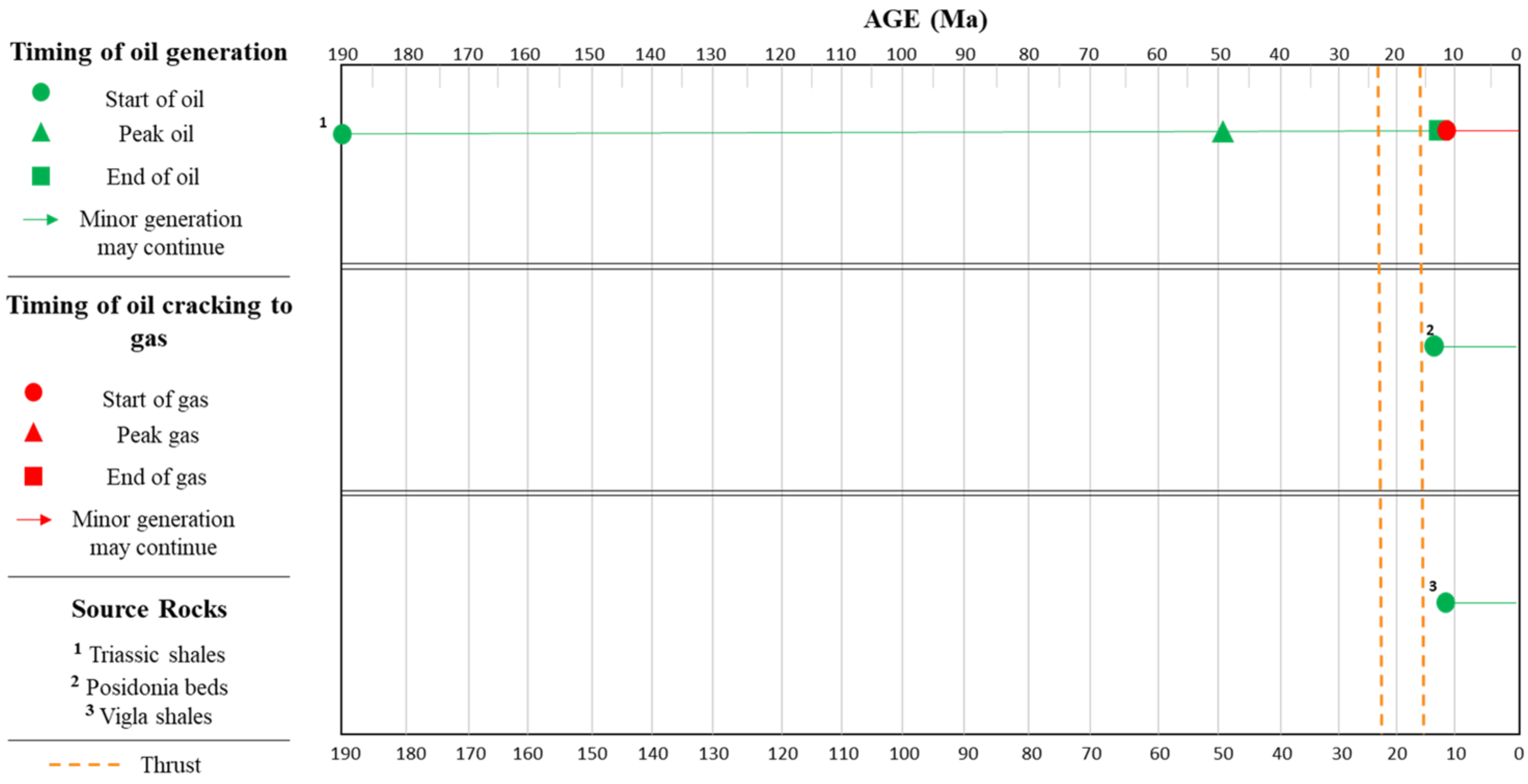

Figure 14: Timing of oil and gas generation for the three modeled source rocks. Dashed line at 23 Ma and at 16.6 Ma represents the thrusting period.

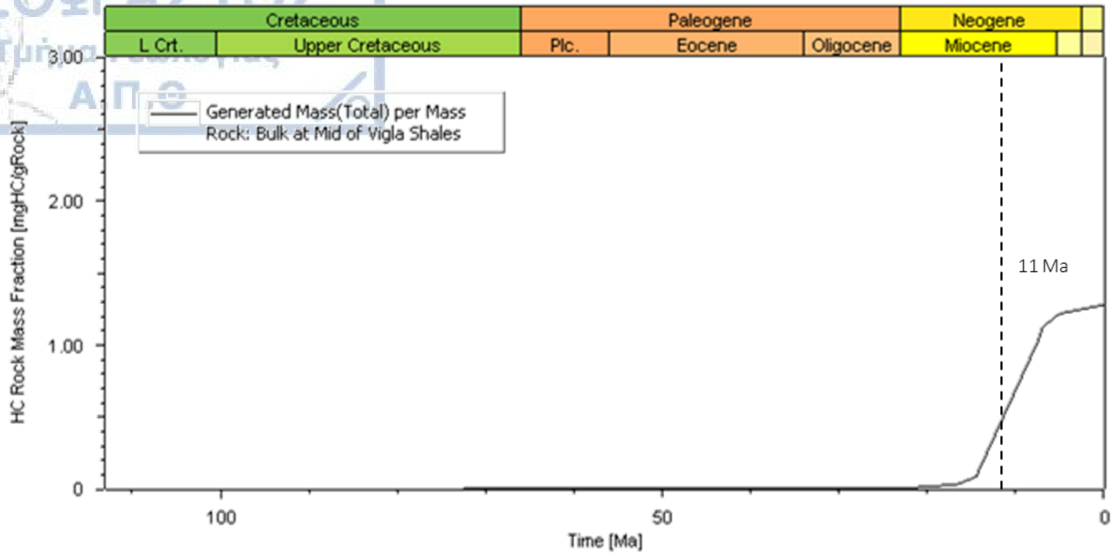

Figure 15: Generation mass curve through geological time for the Vigla shales. Generation mass values are in mg HC/g Rock and time values are in Ma.

3.3.4 Petroleum Expulsion History

Between the starting time of petroleum generation and petroleum expulsion, there is a lag, which is reasonable since certain minimum petroleum saturation (probably about 4%) in the source rock is required before efficient expulsion (internal report from HELPE Upstream). The main expulsion for the Triassic shales occurred at 140 Ma following the normal process. Expulsion for Posidonia shales comes after thrust emplacement at about 7 Ma. No expulsion is observed for the Vigla shales. There is a possibility that the petroleum mass which has generated from Vigla shales to be not competent to expel hydrocarbons

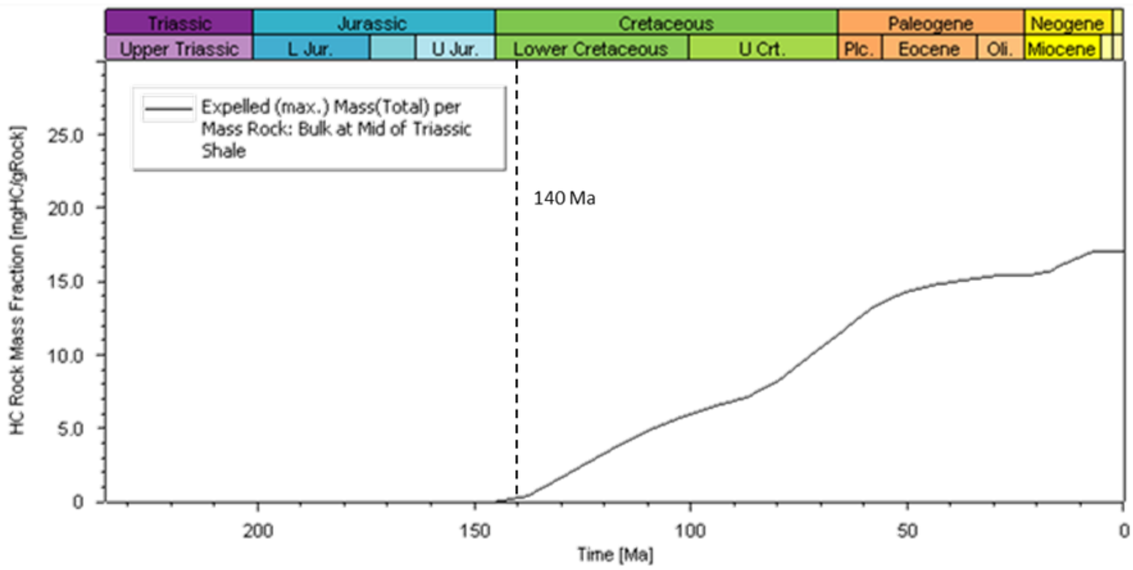

Figure 16: Expulsion mass curve through geological time for the Triassic shales. Expulsion mass values are in mg HC/g Rock and time values are in Ma.

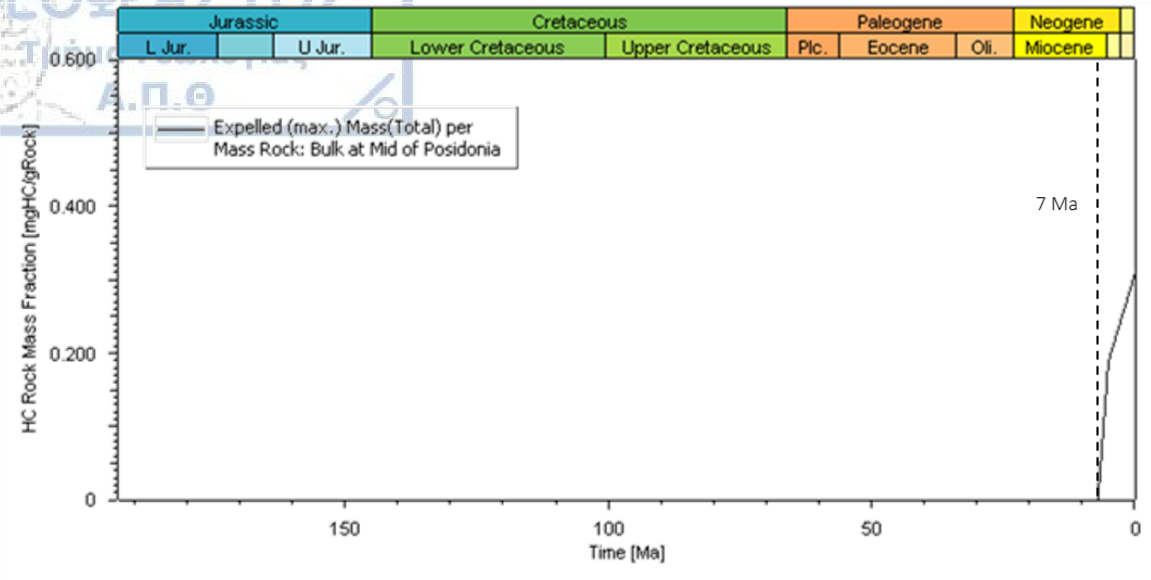

Figure 17: Expulsion mass curve through geological time for the Posidonia beds. Expulsion mass values are in mg HC/g Rock and time values are in Ma.

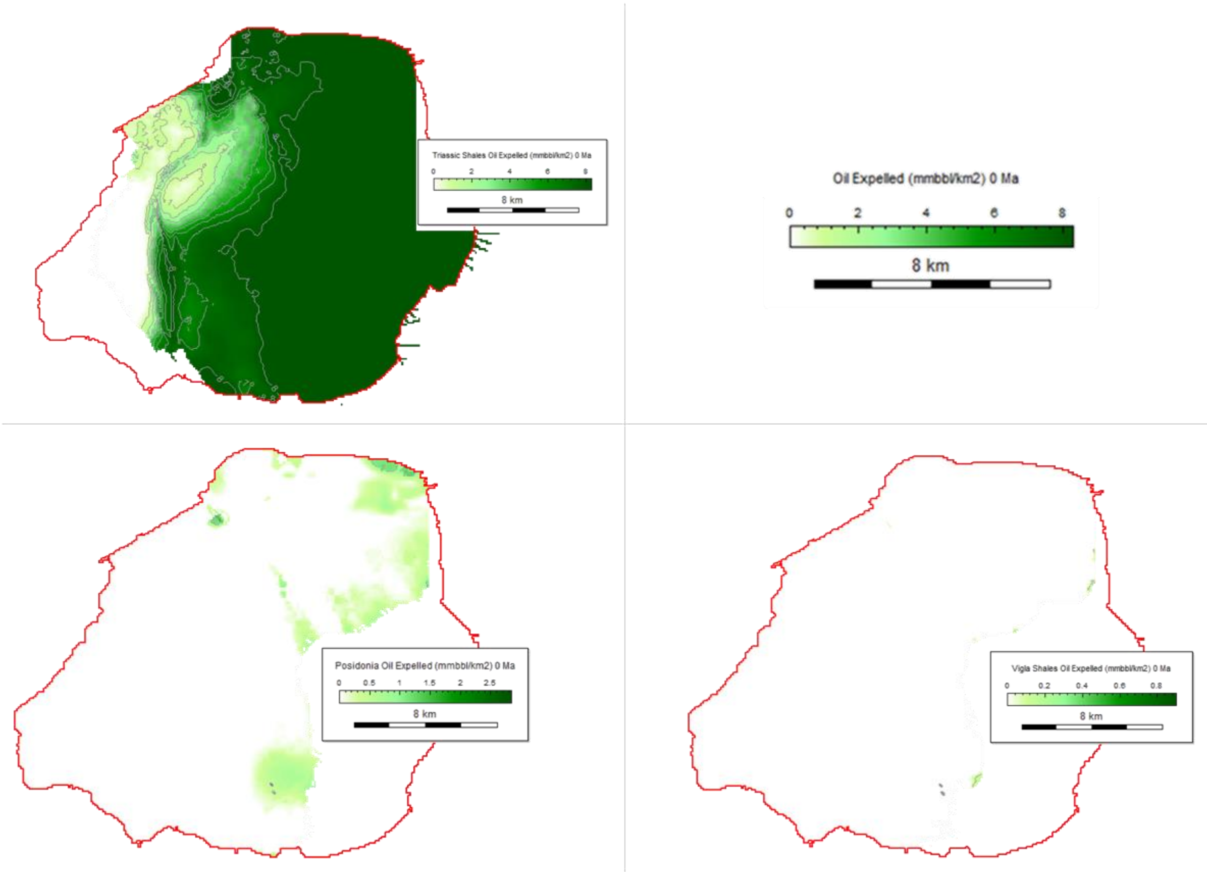

Figure 18: Expulsion maps for the Triassic, Posidonia and Vigla shales, respectively. The oil expelled is in mmbbl/ km^2.

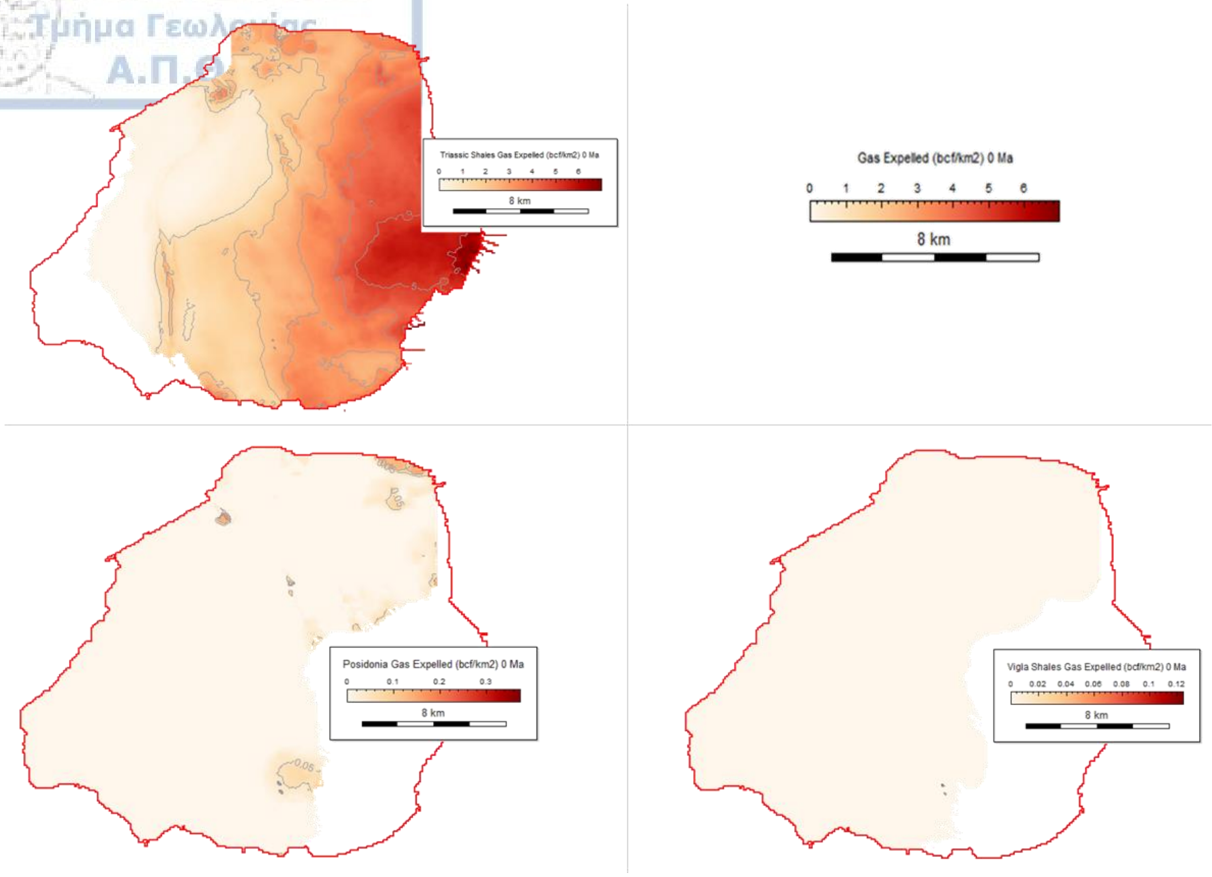

Figure 19: Expulsion maps for the Triassic, Posidonia and Vigla shales, respectively. The gas expelled is in bcf/ km^2.

Triassic shales finally expel 17.08 mg HC/g Rock. However, Posidonia shales expel 0.31 mg HC/g Rock. On the other hand, no expulsion is observed for the Vigla shales. In addition, the oil and gas expelled maps of the three source rocks for the Patraikos Gulf area are presented in Figure 19. Expulsion critical times and expulsion masses are summarized in Table 6.

Table 6: Generation and Expulsion critical times, generation and expulsion mass values and generation mass value at expulsion starting time. Time values are in Ma. Mass values are in mg HC/ g Rock.

Source Rock	Generation (Start Ma)	Generation Mass at present-day (mg HC/g Rock)	Expulsion (Start Ma)	Generation Mass at Expulsion Starting Time (mg HC/g Rock)	Expulsion Mass at present-day (mg HC/g Rock)
Triassic Shales	190	19.43	140	3	17.08
Posidonia Shales	14	2.9	7	2.36	0.31
Vigla	11	1.28	-	-	-

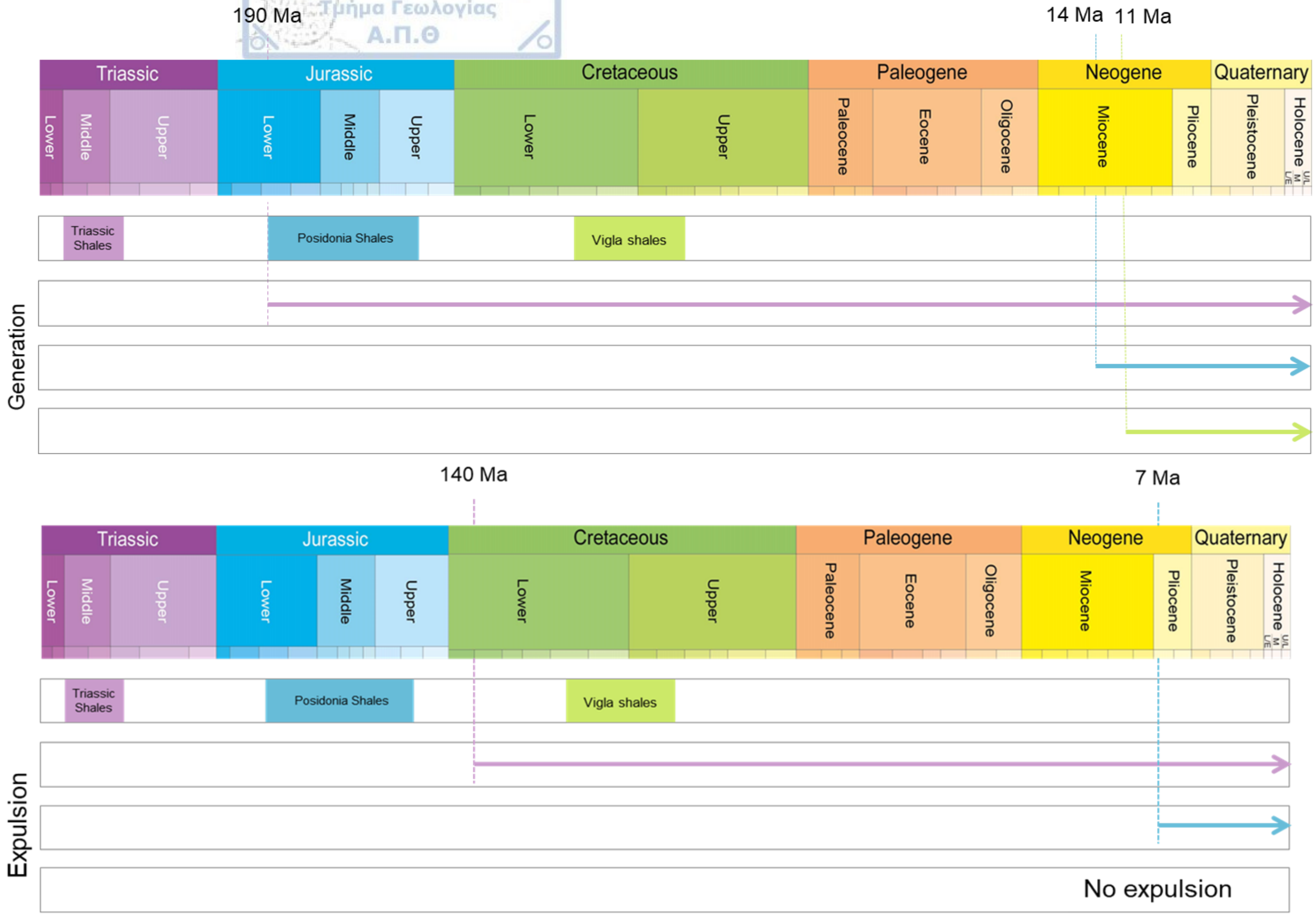

Figure 20: Generation and expulsion of the three source rocks through geological time in pseudo-well A. The geological time scale is in Ma.

3.4 Results of Pseudo-well B (PW-B)

One-dimensional (1D) modeling of burial history and thermal maturity sensitivity analysis was performed using pseudo-well B. The pseudo-well location is very close to the kitchen.

In this chapter burial history, transformation ratio, vitrinite reflectance, generation and expulsion masses for the PW-B are discussed. Moreover, 2D maps for vitrinite reflectance and generation – expulsion masses for the three source rocks are presented too.

Thrust emplacement and erosional events could affect maturity evolution. Thrusting took place during the end of Oligocene- early Miocene. This event increases the sediment accumulation and buried deeper the formations. There are two modeled erosional events. The first erosional event occurs in Oligocene and the second event occurs in Pliocene. These two erosional events characterized by the removal of 1300 meters and 3000 meters of sediment, respectively. The volumes of sediment which deposited and then eroded result in the increase of maturity.

3.4.1 Burial History

According to burial history curves (Figure 21) during Middle to Upper Triassic (240-230 Ma) the sediment accumulation rate is more than 3000 m (Rigakis, 1999) however in the pseudo-well B appear almost 470 meters of sediment. The Triassic sequence includes Triassic evaporites and the first potential source rock of the area, known as Triassic shales. From Upper Triassic to Lower Jurassic (230-193 Ma) were deposited the Pantokrator platform carbonates. The formation thickness amounts to 2885 meters. During the syn-rift period (190-145 Ma) and more specifically during Middle to Upper Jurassic (193-146 Ma) the second potential source rock of the area, known as Posidonia Beds, were deposited. Later, from 146 to 113 Ma the pelagic carbonates of Vigla Formation were deposited. The first erosional event lasted about 7 m.y. and ended with the beginning of thrusting. There is a removal of about 1300 meters of the section. After that, the burial history curve drops steeply, representing the rapid increase in sediment accumulation rate during thrusting between 23.0 to 16.6 Ma. Maximum burial occurred around 7 Ma when the second erosional event lasted about 2 m.y. The erosional event started with the end of thrusting and ended with the deposition of the Plio-Pleistocene sediments. Removal of 3000 meters of sediment was observed. In the last 5 Ma almost 1150 meters of sediment have been deposited in the area of western Patraikos Gulf.

Table 7 lists information of the current depth and the calculated maximum depth of the potential source rocks on the Patraikos Gulf area. The maximum calculated depth as mentioned in Table 7 is equivalent to the maximum burial at 7 Ma.

Table 7*:* Current depth, calculated maximum depth of burial.

Burial history location	**Source rock**	
Pseudo-well B	**Posidonia shales**	**Triassic shales**
Current depth	4585 m	7530 m
Maximum depth	6300 m	9400 m

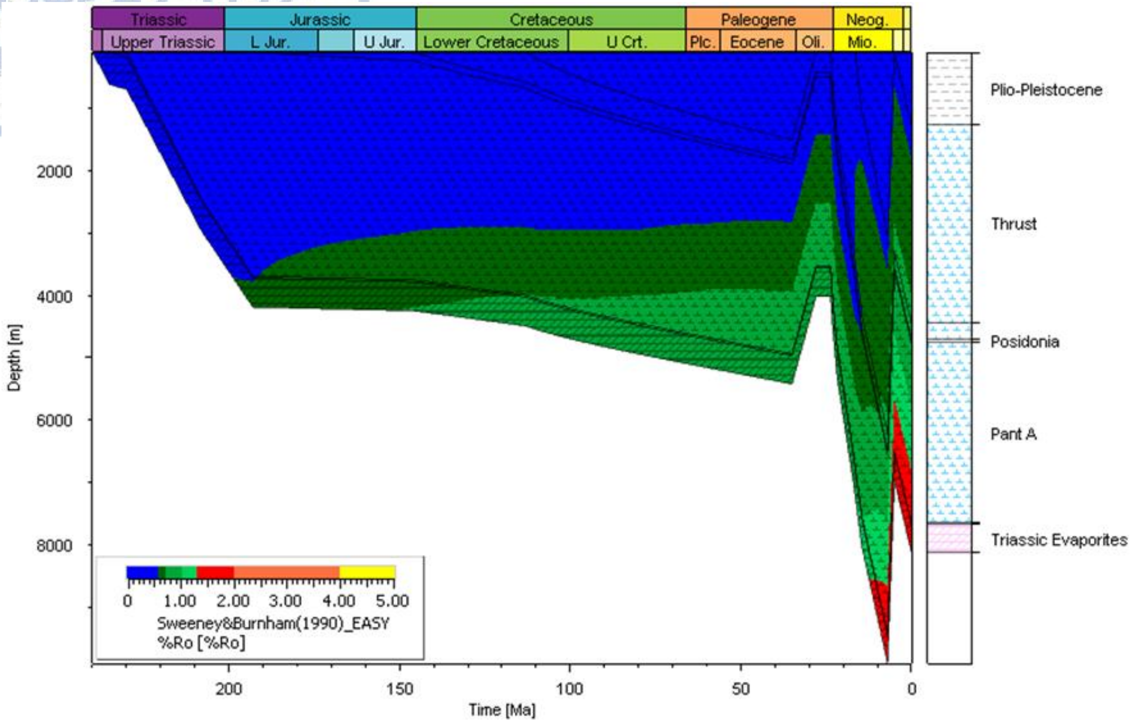

Figure 21: Burial history plot (240 Ma to Present) of the pseudo-well B at western Patraikos Gulf. Location shown in Figure 5.

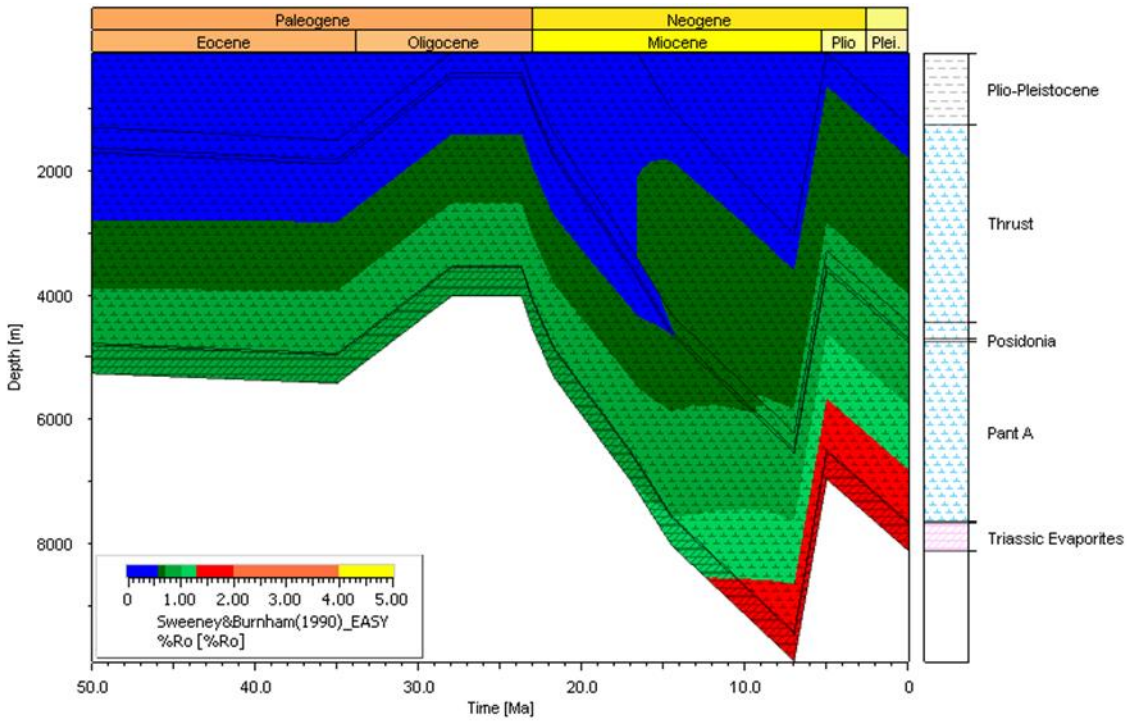

Figure 22: Burial history plot (50 Ma to Present) of the pseudo-well B at western Patraikos Gulf. Location shown in Figure 5.

3.4.2 Maturation History

The maturation history performed for pseudo-well B is based on calculated vitrinite reflectance values (%VRo). As illustrated from the vitrinite reflectance maturity graphs in Figures 21-22, the blue-colored area represents the immature to marginally mature organic matter (< 0.55 %Ro). The dark green-colored area introduces the early window of oil generation (0.55 – 0.7 %Ro). The green-colored area presents the main window of oil generation (0.7- 1.0 %Ro). The light-green colored area displays the late oil window (1.0- 1.3 %Ro). The red-colored area represents the wet to dry gas window (1.3-2.0 %Ro). The orange-colored area introduces the dry gas to post dry gas window (2.0-4.0 %Ro).

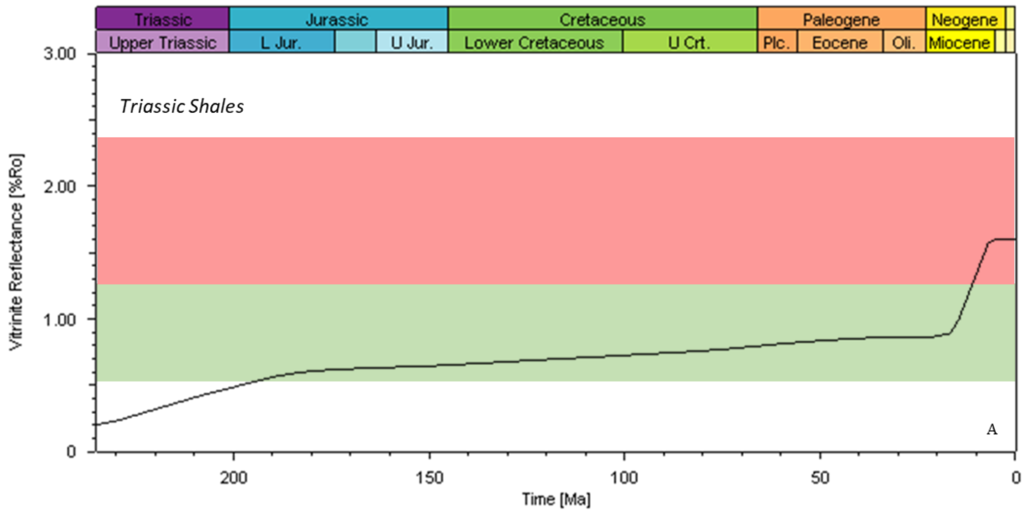

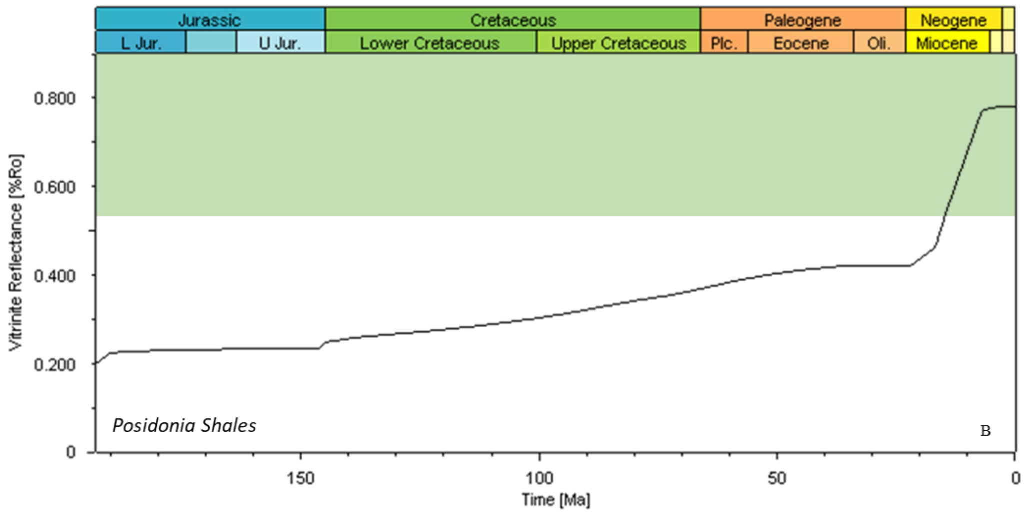

Figure 23: Vitrinite reflectance curves (VRo) through time based on Burnham and Sweeney, 1990. The plots illustrate the evolution of maturity for the three source rocks. Plot A represents the maturity evolution of Triassic shales, plot B of Posidonia. The green- colored area corresponds to 0.55 – 1.3% VRo and the red- colored area corresponds to 1.3 – 2.4% VRo.

The Triassic source rock is considered as oil-prone and composed of Type I Kerogen. At the present time (0 Ma) Triassic shales are in the dry gas window as it shows Figure 23. Posidonia beds are also considered oil-prone and are mostly composed of Type II

Kerogen. Posidonia source rock at present time is in the early oil window as illustrates Figure 23. Vigla shales do not appear in the PW-B. Hence, plots have accomplished only for the Triassic shales and Posidonia beds source rocks.

The maturity evolution for the two potential source rocks are described in Table 8.

Table 8*:* Timing of oil and gas generation for Type II (Posidonia Formation) and Type I (Triassic shales) source rocks and the burial history location. Age values are in Ma. Depth values (in meters) are calculated at depth at which %Ro value is reached.

Burial History Location	Source Rock			
	Posidonia Beds		Triassic Shales	
Pseudo-well B	Age	Depth	Age	Depth
0.55 %Ro – Start Oil	14	4900	192	3800
1.0 %Ro – Peak Oil	-	-	14.5	7400
1.30 %Ro – Start Gas	-	-	10.5	8300

Triassic shales are entered the oil window approximately at 192 Ma. The peak oil window for this source rock appears in 14.5 Ma (0.90- 1.00% Ro). At 10.5 Ma Triassic shales are entered the gas window. On the other hand, Posidonia shales appear only in early oil window at 14 Ma.

3.4.3 Petroleum Generation History

The timing and extent of petroleum generation from the two potential source rocks at the burial history location of the PW-B are listed in Table 9 and summarized in Figures 24-25 by the transformation ratio evolution through time.

As expected for the oil-prone source rocks, the most extensive petroleum generation occurs at Triassic shales which actually experienced deeper burial depths comparing to the Posidonia Beds source rocks. The Vigla shales formation is not detected in this Pseudo-Well. Conversely, the Triassic shale horizons generated oil earlier than Posidonia beds (171 Ma and 13 Ma respectively). However, thrusting buried those horizons, thus cracking the oil to gas. This second face of maturation for the Triassic shales which results to further generation of hydrocarbons, though gas from oil cracking, is expected since it is typical in thrust and fold belts.

Oil generation in Triassic shales followed the normal process and starts at approximately 171 Ma. The timing of oil cracking to gas is observed in the end of the late oil window at about 10.5 Ma and is controlled by the thrusting due to the deeper burial depths. Oil generation in the Posidonia beds began at about 13 Ma. The ages suggest that the thrust emplacement significantly affected the generation of this oil.

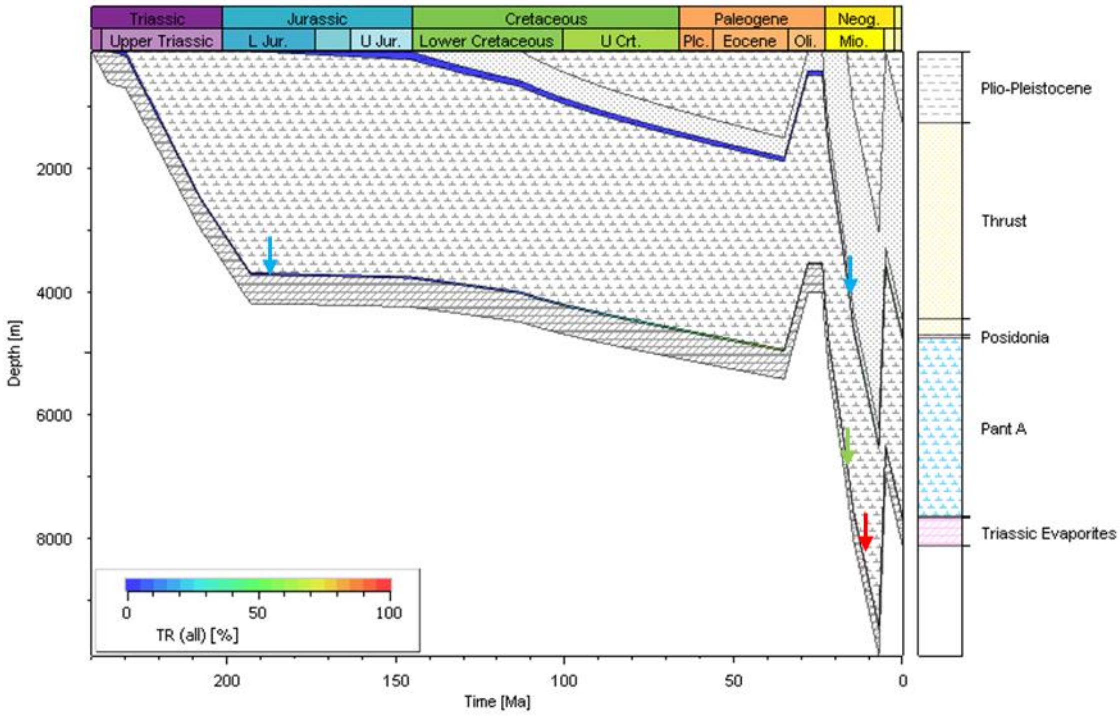

Figure 24: Transformation ratio of organic matter (240 Ma to present) including the two modeled source rocks (Triassic Shales, Posidonia Beds) through geological time. Blue, green and red arrows illustrate the start, peak and end of oil generation for the modeled source rock intervals.

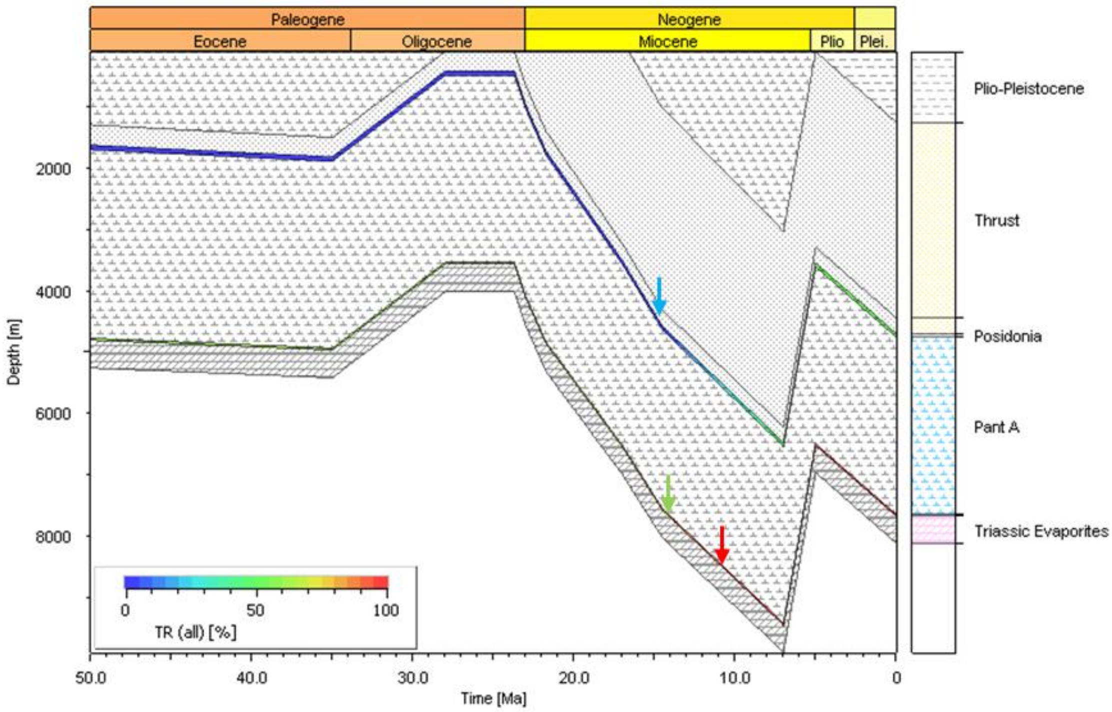

Figure 25: Transformation ratio of organic matter (50 Ma to present) including the two modeled source rocks (Triassic Shales, Posidonia Beds) through geological time. Blue, green and red arrows illustrate the start, peak and end of oil generation for the modeled source rock intervals.

Table 9: Timing of oil generation for the two modeled source rocks and depth of oil generation based on transformation ratio curves. Age values are in Ma. Depth values are in meters. Transformation ratio percentages are in %.

Source Rock	Generation		
	Age	Depth	Transformation ratio
Triassic Shales	171	3900	0.35
Posidonia Shales	13	4500	7.3

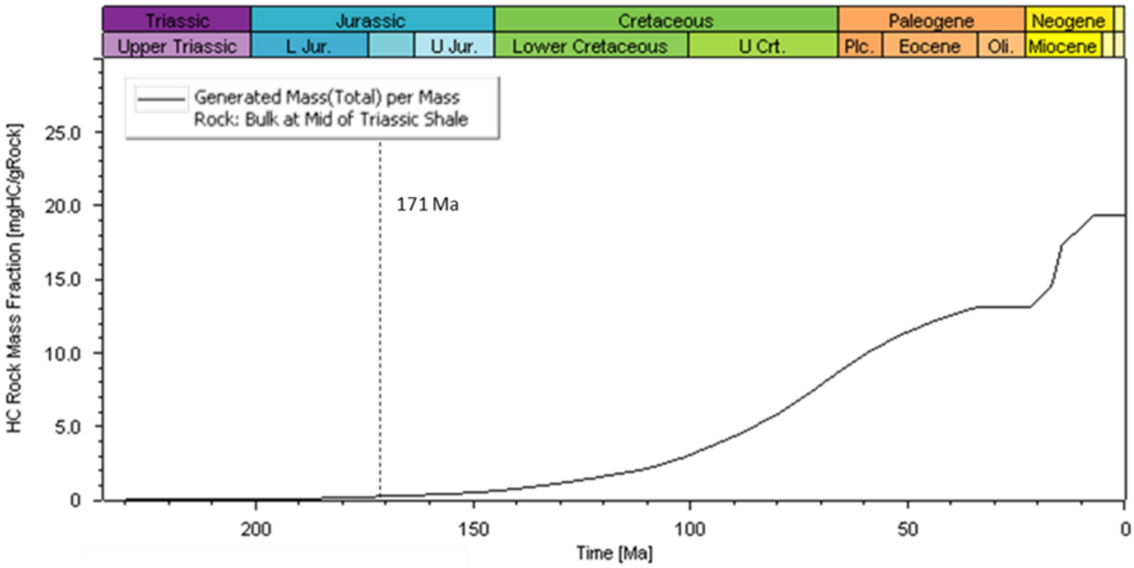

Figure 26: Generation mass curve through geological time for the Triassic shales. Generation mass values are in mg HC/g Rock and time values are in Ma.

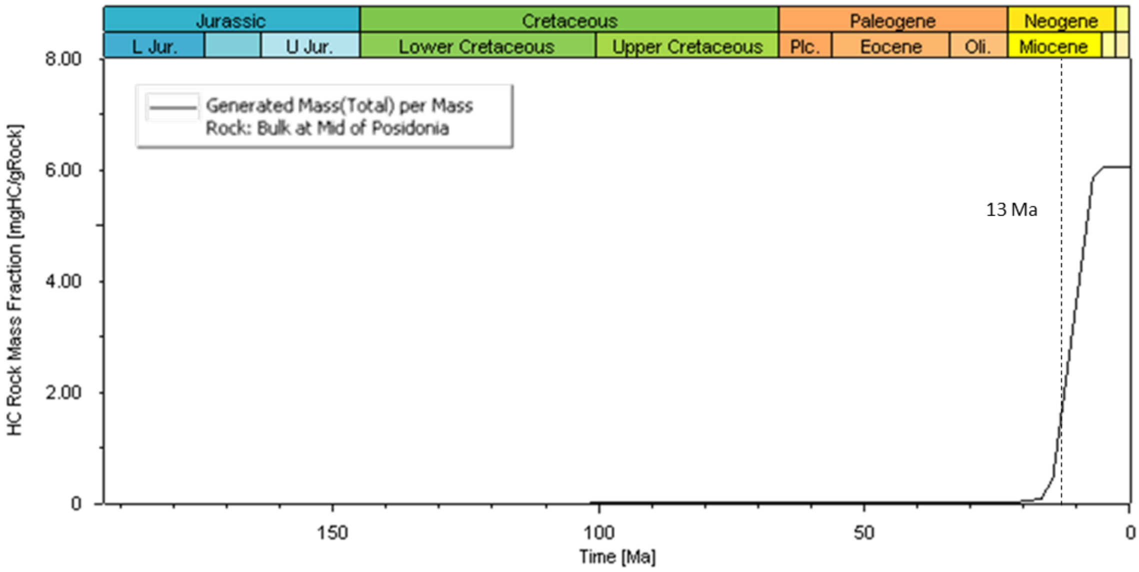

Figure 27: Generation mass curve through geological time for the Posidonia beds. Generation mass values are in mg HC/g Rock and time values are in Ma.

Figure 28: Timing of oil and gas generation for the three modeled source rocks. Dashed line at 23 Ma and at 16.6 Ma represents the thrusting period.

Triassic shales generate 19.29 mg HC/g Rock in total, whereas Posidonia shales generate 6.06 mg HC/g Rock. Hence, Triassic source rocks could be considered as the most important source rock in terms of hydrocarbons generation volumes in the Patraikos Gulf. Generation critical times, generation masses and generation value at expulsion starting time, are summarized in Table 10.

3.4.4 Petroleum Expulsion

The main expulsion for the Triassic shales occurred at 96 Ma following the normal process. Expulsion for Posidonia comes after thrust emplacement at about 11 Ma. Triassic shales finally expel 17.11 mg HC/g Rock. However, Posidonia shales expel 3.8 mg HC/g Rock. Expulsion critical times, expulsion masses are summarized in Table 10.

Table 10: Generation and Expulsion starting times, mass values and generation mass value at expulsion starting time. Time values are in Ma. Mass values are in mg HC/ g Rock.

Source Rock	Generation (Start Ma)	Generation Mass at present-day (mg HC/g Rock)	Expulsion (Start Ma)	Generation Mass at Expulsion Starting Time (mg HC/g Rock)	Expulsion Mass at present-day (mg HC/g Rock)
Triassic Shales	171	19.29	96	3.12	17.11
Posidonia Shales	13	6.06	11	0.45	3.80

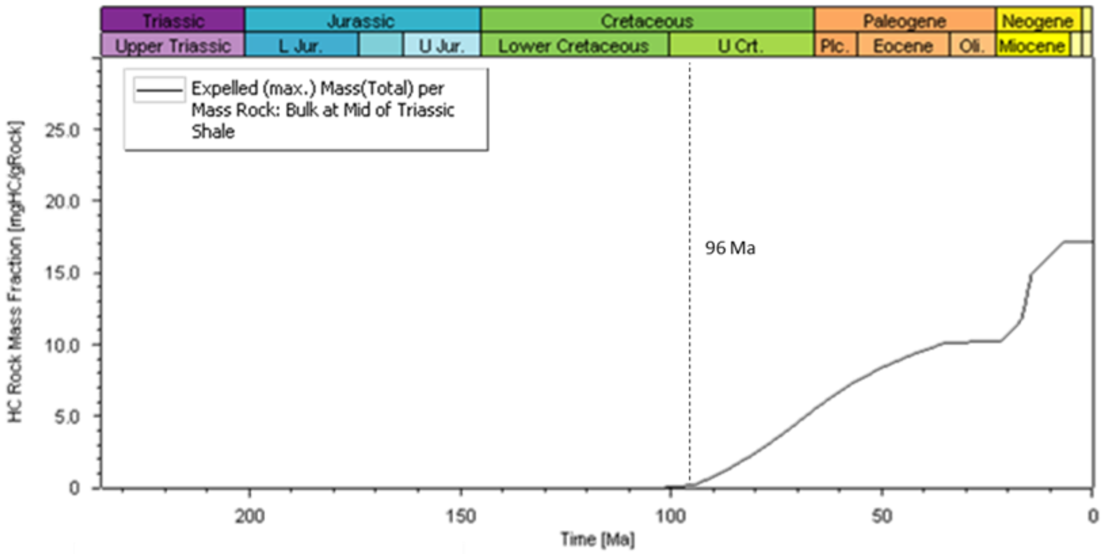

Figure 29: Expulsion mass curve through geological time for the Triassic shales. Expulsion mass values are in mg HC/ g Rock and time values are in Ma.

Figure 30: Generation and expulsion of the two source rocks through geological time in pseudo-well B. The geological time scale is in Ma.

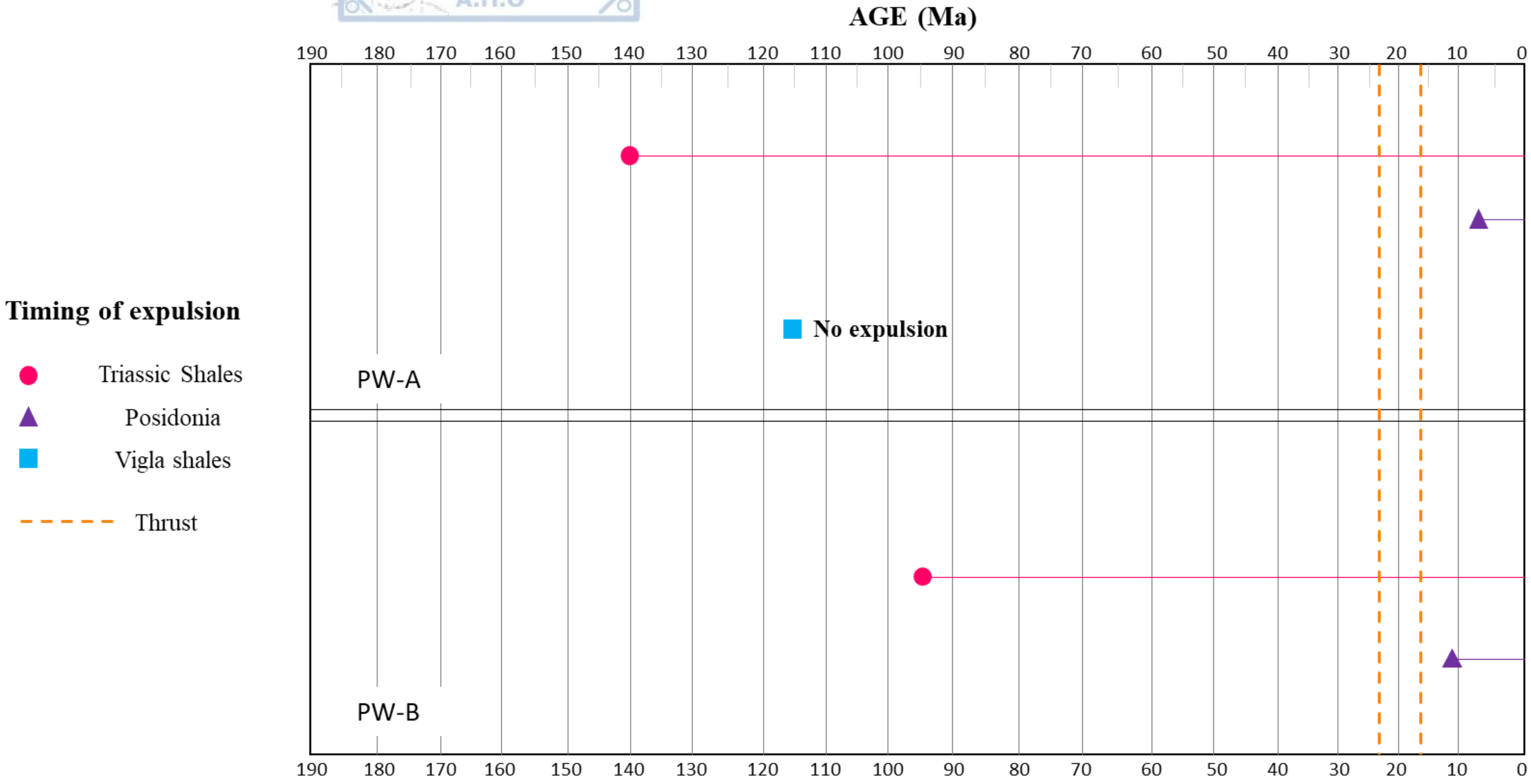

Figure 31: Timing of oil expulsion for the two modeled source rocks. Dashed line at 23 Ma and at 16.6 Ma represents the thrusting period.

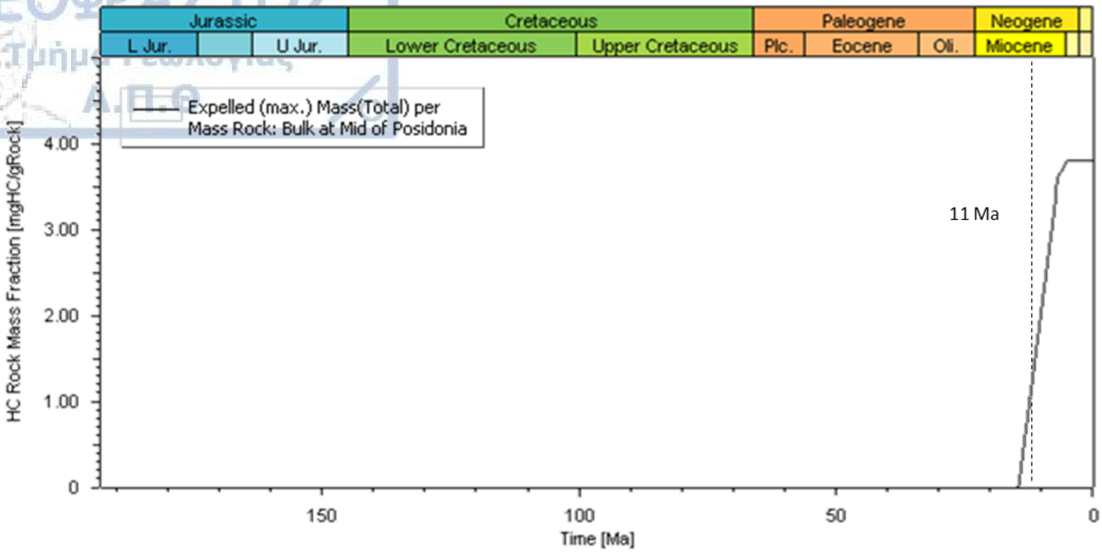

Figure 32: Expulsion mass curve through geological time for the Posidonia beds. Expulsion mass values are in mg HC/g Rock and time values are in Ma.

Concerning the expulsion critical times for the two pseudo-wells, Posidonia shales expelled hydrocarbons earlier (11 Ma) in pseudo-well B, than in pseudo-well A (7 Ma), although Posidonia shales are entered concurrently the oil window (14 Ma) in both pseudo-wells. This is attributed to the sedimentation rate and the erosion and deposition cumulative thicknesses. In PW-A the final thickness for the two erosion/deposition events are 2300 meters, whereas in PW-B the thickness of the two events is almost double (4300 meters). As a result, Posidonia shales were buried deeper in shorter time and thus, the hydrocarbons were earlier expelled in PW-B. Additionally, the ages confirm that the thrust emplacement significantly affected the generation in this source rock.

3.5 Accumulated hydrocarbons

Migration and accumulation view for the three modeled source rocks are shown in Figures 33-34 below. The illustrated 3D models indicate potential migration pathways for the expelled hydrocarbons. The models further suggest which of the mapped traps have access to charge and the possible volumes of expelled hydrocarbons capable of being trapped in the mapped structure. Migration losses are hard to process and thus sensitivity analysis is particularly beneficial. In this dissertation migration losses are not applied. The estimates of trapped volumes which are shown in this dissertation are simplified and based on simple reservoir properties.

Structure size and predicted volume of accumulation are dependent on structure's geometry, reservoir properties and seal effectiveness, all of which are generalized and should be considered as approximations for the purposes of the current study.

The capacity of the cap-rock to seal hydrocarbons depends on its wettability and the size of the pore throats within the interconnected pore system. Sensitivity analysis of seal capacity in the western Patraikos Gulf area has been accomplished by Xanthopoulou (2020). Changes in the seal capacity result in different volumes of expelled and accumulated hydrocarbons.

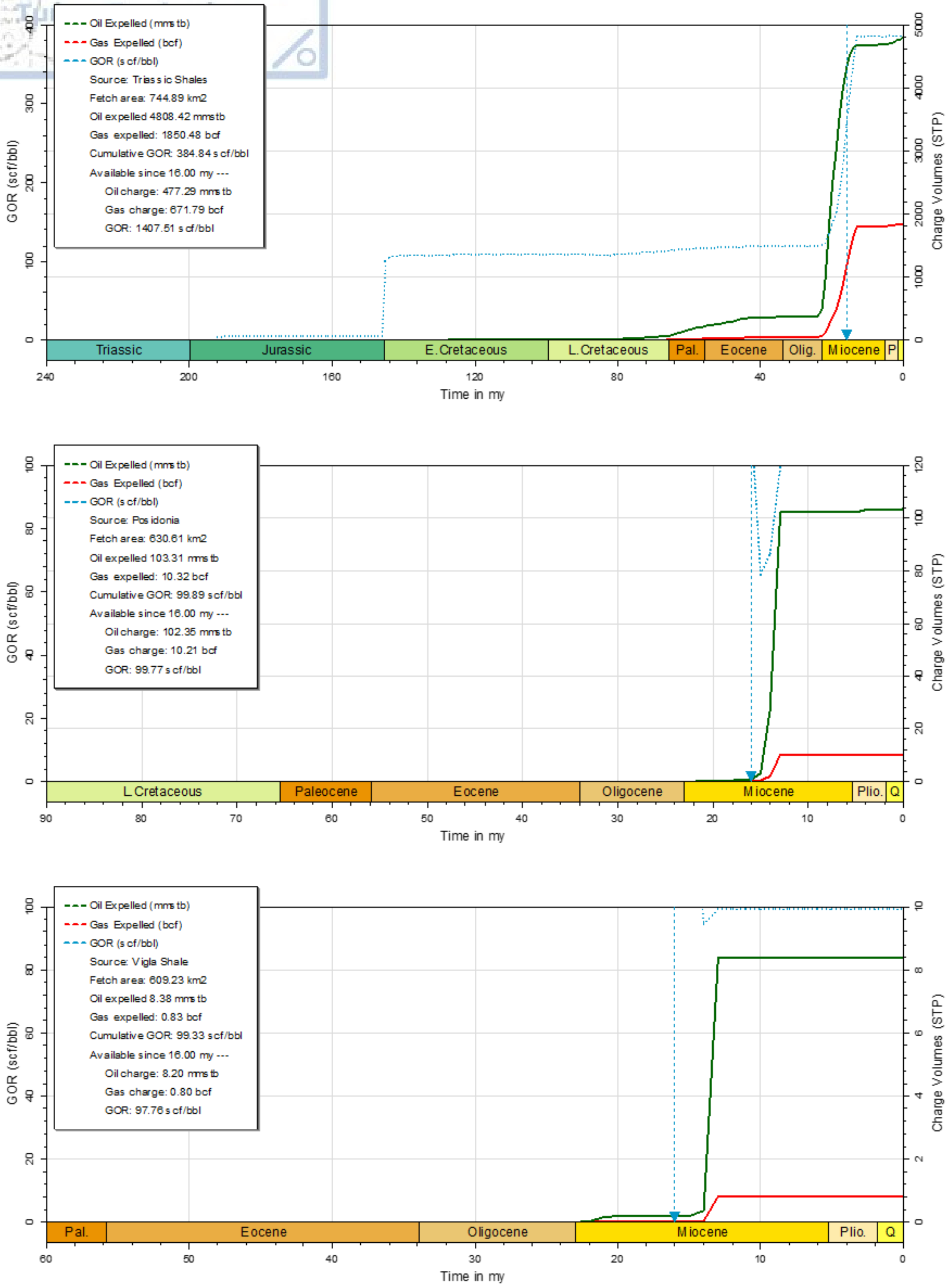

Figure 33: Total expelled oil and gas volumes for the three modeled source rocks. Oil expelled values are in mmstb, gas expelled values are in bcf and GOR in scf/ bbl. The blue arrow represents the petroleum expelled volume which is available after thrusting period (16 Ma).

Charging for Triassic shales starts at Paleocene, while charging for Posidonia and Vigla shales begin at Miocene, after thrusting. As Figure 33 shows, minor expulsion is detected in the pre-thrusting period, whereas during thrusting and post-thrusting period the major expulsion is observed. During Miocene hydrocarbons increase steeply, due to the thrusting emplacement. Additionally, after 14 Ma (end of thrusting emplacement) hydrocarbons' volume remains constant. A slight volume increase in the last 5-6 Ma is noticed.

Expulsion for Triassic shales results in approximately 4810 mmstb totally expelled oil and 1.85 tcf totally expelled gas within 745 km^2 fetch area. However, the potential trap has been created at approximately 16 Ma with the thrusting emplacement. At 16 Ma the available volumes will be 478 mmstb and 0.67 tcf. Expulsion for Posidonia shales results in 103 mmstb and 0.01 tcf totally expelled oil and gas respectively, within almost 631km^2 fetch area, while the available volumes at the possible trap at 16 Ma will be 102 mmstb oil and 0.01tcf gas. Vigla shales have expelled 8.3 mmstb and 0.83 bcf totally expelled oil and gas, within 610 km^2 fetch area. At 16 Ma available volumes will be 8.2 mmstb oil and 0.80 bcf gas. Table 11 summarizes the total expelled volumes and the expelled hydrocarbons at 16 Ma.

Table 11: Total expelled, available hydrocarbons (at 16 Ma) and GOR for the three modeled source rocks. Expelled oil is in mmstb, gas in bcf and GOR in scf/bbl.

Source Rock	Oil (mmstb)		Gas (bcf)		GOR (scf/bbl)	
	Total	16 Ma	Total	16 Ma	Total	16 Ma
Triassic Shales	4808.42	477.29	1850.48	671.79	384.84	1407.51
Posidonia Beds	103.31	102.35	10.32	10.21	99.89	99.77
Vigla Shales	8.38	8.20	0.83	0.80	99.33	97.76

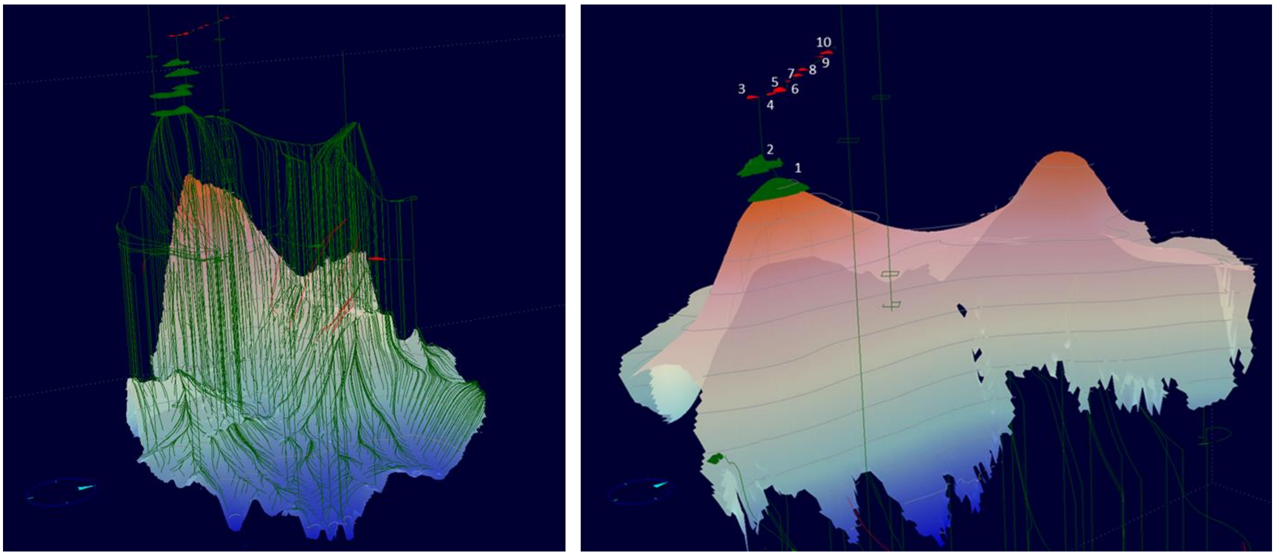

Figure 34: 3D migration model for the expelled hydrocarbons from the Triassic source rock as modeled. Left: flowlines from the Triassic shales to shallower depths as modeled; Right: possible accumulation at Eocene level and shallower.

Triassic shales suffer severe migration losses due to the early generation and expulsion of hydrocarbons. On the other hand, limited or no losses are observed for Posidonia and Vigla shales.

As it is illustrated in Figure 34, the expelled hydrocarbons from the Triassic source rock, is capable to charge the mapped structure and also to create multiple accumulations at various depths. On the other hand, the expelled hydrocarbons from Posidonia source rock are capable to charge a single accumulation in Eocene level. No accumulations are observed that could be attributed to the expelled hydrocarbons from the Vigla source rock.

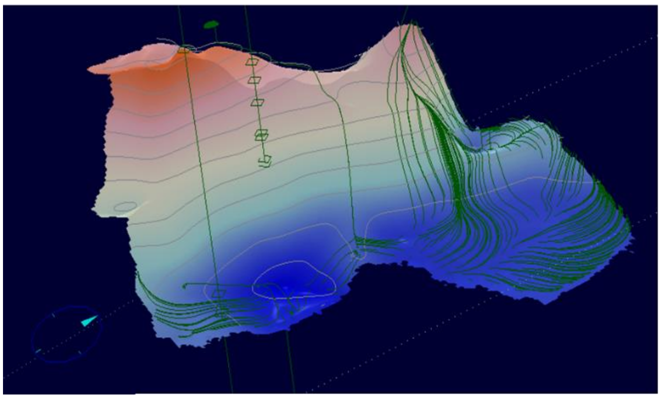

Figure 35: 3D perspective view of migrated hydrocarbons from the Posidonia shales to shallow depths.

The charging of several formations with the migrated hydrocarbons from the Triassic source rock is critical. The cross-section in Figure 36 clearly shows the multilevel reservoir, which includes accumulations in Senonian, Eocene and Miocene levels. The tilted owc is due to limitations during export of the interpreted horizons from the corresponding software.

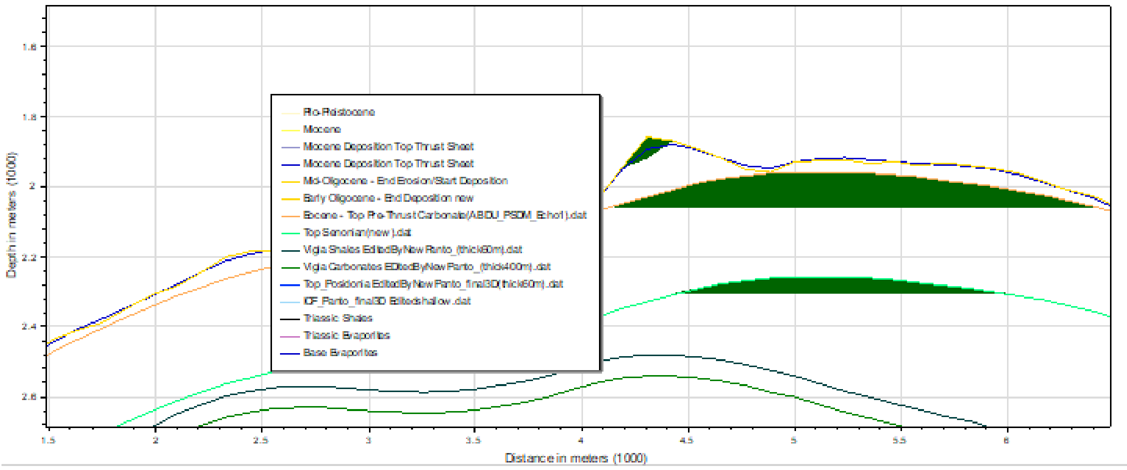

Figure 36: Cross-section of multilevel reservoir from Triassic shales' system. The tilted owc at the top of Miocene formation is due to limitations during export of the interpreted horizons from the corresponding software.

Tables 12 and 13 list information about the possible trapped hydrocarbons in Eocene level which are migrated from Triassic and Posidonia shales, respectively.

Table 12: Possible trapped hydrocarbons from Triassic shales to Eocene level.

	Accumulations									
	1	**2**	**3**	**4**	**5**	**6**	**7**	**8**	**9**	**10**
Column high (m)	100	100	18.42	12.07	22.52	3.48	11.91	12.01	4.48	13.94
Oil (mmbls)	21.8	7.5	0.0	0.0	0.0	0.0	0.0	0.0	0.0	0.0
Sol. Gas (bcf)	11.1	4.2	0.4	0.3	1.0	0.0	0.3	0.3	0.1	0.5
GOR (scf/bbl)	507.7	551.3	--	--	--	--	--	--	--	--

Table 13: Possible trapped hydrocarbons from Posidonia shales to Eocene level.

Accumulation	Column high (m)	Oil (mmbls)	Sol. Gas (bcf)	GOR (scf/bbl)
1	9.65	0.20	0.0	50.7

Chapter 4: Sensitivity analysis

4.1 Introduction

Sensitivity analysis for the three modeled source rocks is summarized in Tables 23 and 24 at the end of the current chapter. There are four parameters such as, Crustal Thickness (CT), Beta-Factor (β), Radioactive Heat (RH) and Rifting Period (RP), which directly affect the thermal regime of a given area, thus the maturity level of the source rocks and hence the critical times of hydrocarbons' expulsion. Separate sensitivity analysis was applied for each of the four above mentioned parameters and two extreme scenarios were applied, which are also on a present-day heat flow basis.
The values which are used for this purpose are based on literature and summarized in Table 14 (published maps are shown in Appendix I). The fixed values for beta-mantle and lithosphere thickness are 3 and 120 km, respectively. Various models and combinations of parameters have been applied for both pseudo-wells in order to establish the two extreme scenarios of the minimum and maximum heat flow values at present day.

Table 14: Possible values of parameters which have been used in the sensitivity scenarios.

Parameters	Values				
Syn-Rift (Ma)	190-145		175-145		170-145
Post-Rift (Ma)			145-0		
Radioactive heat (mW/m^3)	2.5		2.8		3
Beta-factor	1.1	1.3	1.5	2	2.5
Crustal Thickness (km)	20	25	30	32	35

4.2 Data Inputs

Scenarios 2 and 3 refer to the maximum and minimum present-day heat flow values, which have arisen from all the above combinations. Tables 15-18 describe the parameters which have been used in every sensitivity analysis. In order to deeply understand the impact of sensitivity variables on the hydrocarbons' generation and expulsion the value of each single parameter changes, whereas the other parameters remain constant.

Table 15: Parameters which have been used in the sensitivity scenarios 2 and 3. The parameter that changes is the crustal thickness.

	Scenario 2					**Scenario 3**				
Parameters	**Values**									
Syn-Rift (Ma)	190-145					190-145				
Post-Rift (Ma)	145-0					145-0				
Radioactive heat (mW/m^3)	3.0					2.5				
Beta-factor	1.1					2.5				
Crustal Thickness (km)	*20*	*25*	*30*	*32*	*35*	*20*	*25*	*30*	*32*	*35*

Table 16: Parameters which have been used in the sensitivity scenarios 2 and 3. The parameter that changes is the beta factor.

	Scenario 2					Scenario 3				
Parameters	**Values**									
Syn-Rift (Ma)	190-145					190-145				
Post-Rift (Ma)	145-0					145-0				
Radioactive heat (mW/m^3)	3.0					2.5				
Beta-factor	*1.1*	*1.3*	*1.5*	*2.0*	*2.5*	*1.1*	*1.3*	*1.5*	*2.0*	*2.5*
Crustal Thickness (km)	35					35				

Table 17: Parameters which have been used in the sensitivity scenarios 2 and 3. The parameter that changes is the radioactive heat.

	Scenario 2	Scenario 3
Parameters	**Values**	
Syn-Rift (Ma)	190-145	190-145
Post-Rift (Ma)	145-0	145-0
Radioactive heat (mW/m^3)	*3.0*	*2.5*
Beta-factor	1.3	1.3
Crustal Thickness (km)	35	35

Table 18: Parameters which have been used in the sensitivity scenarios 2 and 3. The parameter that changes is the rifting age.

	Scenario 2	Scenario 3
Parameters	**Values**	
Syn-Rift (Ma)	***170-145***	***175-145***
Post-Rift (Ma)	145-0	145-0
Radioactive heat (mW/m^3)	2.8	2.8
Beta-factor	1.3	1.3
Crustal Thickness (km)	35	35

4.3 Results and discussion

In the following paragraphs the impact of the four parameters on heat flow, maturity, petroleum generation and expulsion is extensively discussed.

4.3.1 Crustal thickness variation

4.3.1.1 Heat Flow

For heat flow calculations PetroMod 1D Modeling Software utilizes the McKenzie Heat Flow Model. According to this model, the rifting event is instantaneous. An explanation of this event is based on "instantaneous" finite extension (stretching) of a double-layer lithosphere (Sheplev and Reverdatto, 1998). In the pre-rift period, the model's function is linear, capturing the rapid increase of the crustal heat. In the syn-rift and post-rift period McKenzie's model function becomes exponential, capturing the smooth decrease of the crustal heat.

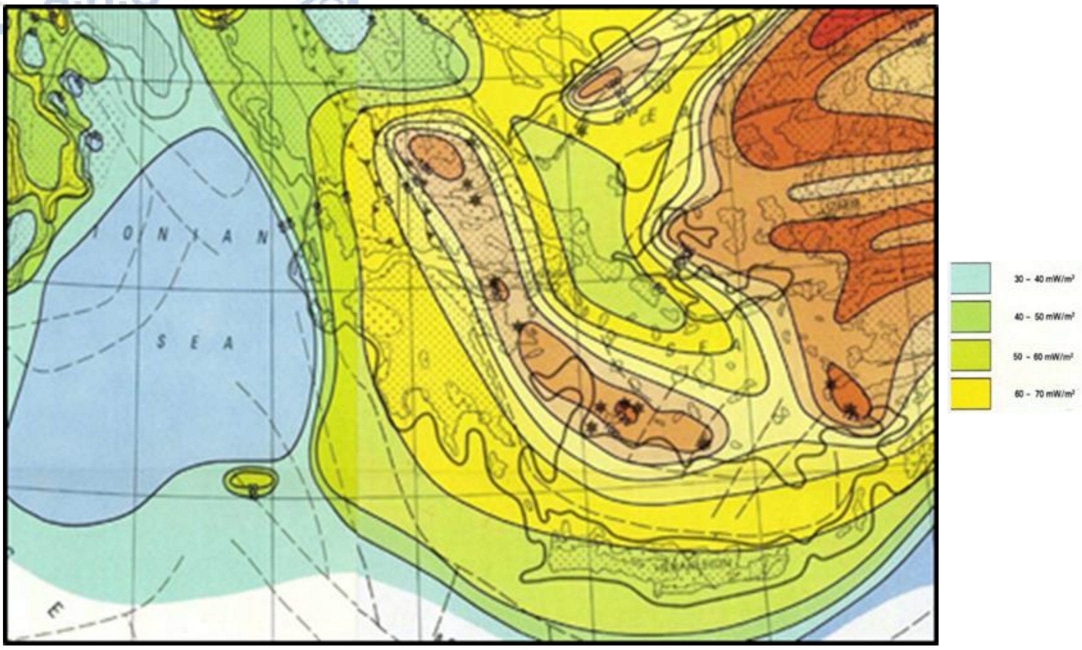

Figure 37: Present day heat flow map for the Western Greece (International Heat Flow Commission.)

Increasing the crustal thickness, a decrease in peak heat flow is observed (Figures 38A and 38B). This could be interpreted due to the intense absorption of heat in a thicker crust than in a thinner crust. The intense increase of heat flow is observed during the syn-rift period (190-145 Ma). However, in the post-rift period (145-0 Ma) a decreasing heat flow curve trend is observed.

The present-day heat flow value is not illustrated in the heat flow plot due to software limitations (Figures 38A and 38B). The latest value represented is at about 7 Ma. In the purpose of better interpretation, an assumption is made, that the curves may continue with the same trend. According to this assumption, the present-day heat flow value will be lower than the latest value at 7 Ma. Table 19 lists the peak and the present-day heat flow values for the scenarios 2 and 3.

Table 19: Peak and present-day heat flow values (in mW/m^3) for the scenarios 2 and 3 in both pseudo-wells.

Scenario	Pseudo-wells	Peak Heat flow	Present-day Heat flow
Scenario 2	**PW-A**	51-56	49
	PW-B	52-56	49
Scenario 3	**PW-A**	57-59	37
	PW-B	56-59	37

The diagrams of heat flow through time (Figures 38A and 38B) clearly suggest that the maximum value of paleo-heat flow is crustal thickness dependent. The thinner the crust the higher the heat flow peak. This is consistent with the widely accepted known factors that control terrestrial heat flow. One of the three factors is the thickness of crust (the other two are the thickness of lithosphere and the radioactive heat generation in the crust). Therefore, the crustal thickness has a significant impact on the thermal distribution through time. This is well illustrated in the diagrams of PW-A and PW-B in Figure 38A, which corresponds to scenario 2. Fewer differences (obvious though) are observed in the two heat flow diagrams of figure 38B, which corresponds to scenario 3.

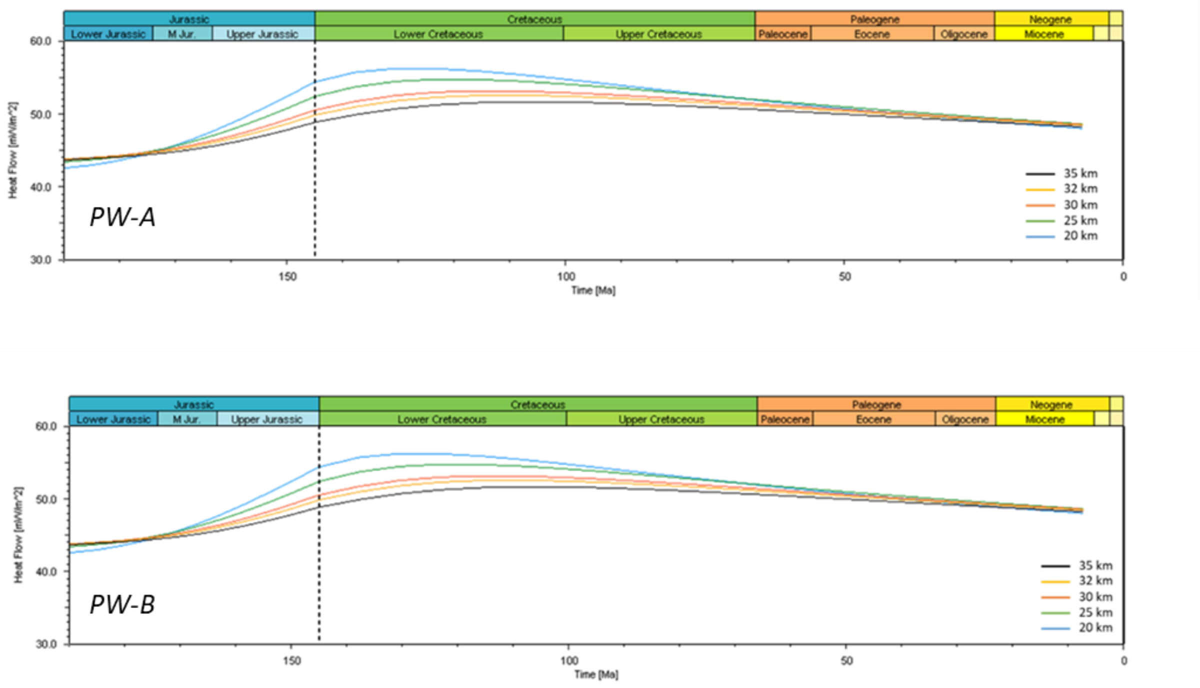

Figure 38A: Heat Flow curves for the Scenario 2 (maximum heat flow values). The colored curves present the crustal thickness variables. The first picture illustrates PW-A and the second PW-B. The parameters were used are presented in the Table 15.

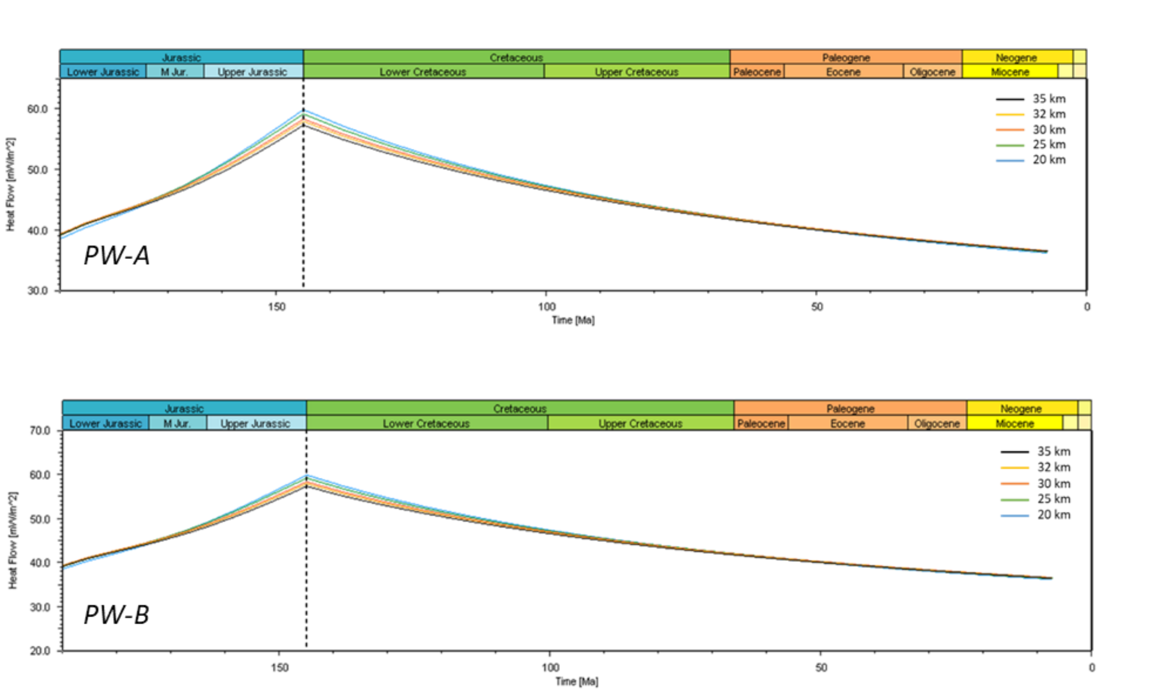

Figure 39B: Heat Flow curves for the Scenario 3 (minimum heat flow values). The colored curves present the crustal thickness variables. The first picture illustrates PW-A and the second PW-B. The parameters are presented in Table 15.

4.3.1.2 Maturity

The burial history superimposed vitrinite reflectance plots (Figures 39 and 40) of the crustal thickness variables (for scenarios 2 and 3) suggest many similarities both for the pseudo-wells A and B. The variation of bulk crustal thickness has a minor impact on the onset of the oil window in terms of timing, for all the three modeled source rocks. However, this observation is limited to the range values that were applied for the study area and does not mean that is generally applied in every case. In those cases, extreme values of crustal thickness are effective, like 8-10 km or 40-45 km, may have important impact on the timing of the onset of the oil window. On the other hand, further division of the crust into upper and lower crust will result in splitting the single bulk crustal thickness into upper and lower crustal thicknesses. Hence, the thickness of upper crust will impact the timing and extend of the oil window. Observations due to the crustal thickness variation in both scenarios are detailed below.

Scenario 2

Triassic source rock is shifted from the late oil window to the wet gas window (at present day) at the given location when crustal thickness increases, as modeled in PW-A. In PW-B Triassic shales are shifted from the late oil window to the dry gas window (at present day). The Jurassic source rock is also shifted from middle oil window to peak oil window in PW-B, whereas a minor shift from early to early-middle oil window in PW-A is observed. Vigla shales are immature to almost mature (early oil window). Burial history plots for both pseudo-wells are shown in the Appendix II (A.II.1-2).
Vitrinite reflectance curves illustrate the evolution of maturity for the modeled source rocks, in both pseudo-wells, through time. As Figure 41A presents, the Triassic shales enter the oil window around 200 Ma, for all the crustal thickness variables. The Triassic shales do not enter the gas window when crustal thickness is 20km, as modeled. In pseudo-well A, Posidonia shales enter the oil window at approximately 15 Ma, whereas Vigla shales marginally enter the oil window at 11 Ma. The maximum vitrinite reflectance values at present day are estimated at around 1.48 %Ro for Triassic shales, about 0.65 %Ro for Posidonia shales and about 0.61 %Ro for Vigla shales (Figure *A.II.3*) at present-day. In pseudo-well B the present-day vitrinite reflectance value is estimated at 1.89 %Ro for the Triassic shales and 0.88 %Ro for Posidonia shales.

Scenario 3

Triassic shales are shifted from the peak to the late oil window (at present day) at the given location when crustal thickness increases, as modeled in PW-A, whereas this source rock is shifted from the late oil window to the dry gas window. The Jurassic source rock is less affected but still shifted from early-middle to middle oil window to peak oil window, as modeled (PW-B). Posidonia shales are in early oil window (PW-A). No maturation for Vigla shales is observed.
Similarly, the Triassic shales enter the oil window, approximately at 190 Ma for all the crustal thickness variables (Figure 41B). Triassic shales do not enter the gas window in PW-A, showing maximum vitrinite reflectance value at around 1.20% Ro in pseudo-well A, at present-day. Posidonia marginally enters the oil window at approximately 8 Ma, whereas Vigla shales are immature (Figure 41D and *A.II.3*). Posidonia's present-day vitrinite reflectance equivalent value is 0.60 %. Present-day vitrinite reflectance value are 1.05% and 0.65 % for Triassic and Posidonia shales in pseudo-well B (Figures A.II.4-Appendix II*)*.

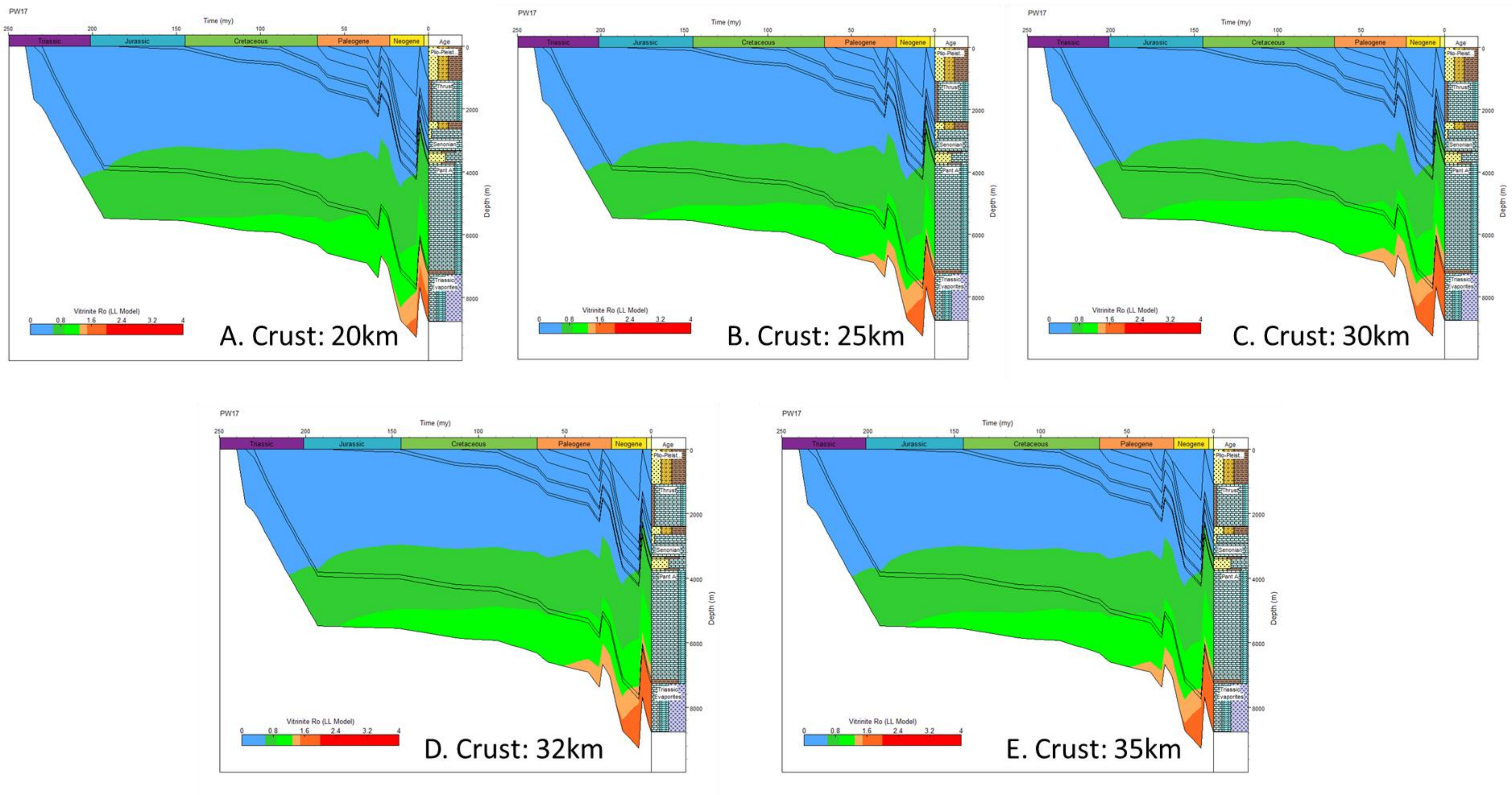

Figure 40: Burial History plots (240 Ma to Present) of pseudo-well A with superimposed colormap of vitrinite reflectance values. These plots describe the scenario 2. The parameters are presented in Table 15. Each plot refers to different crustal thickness.

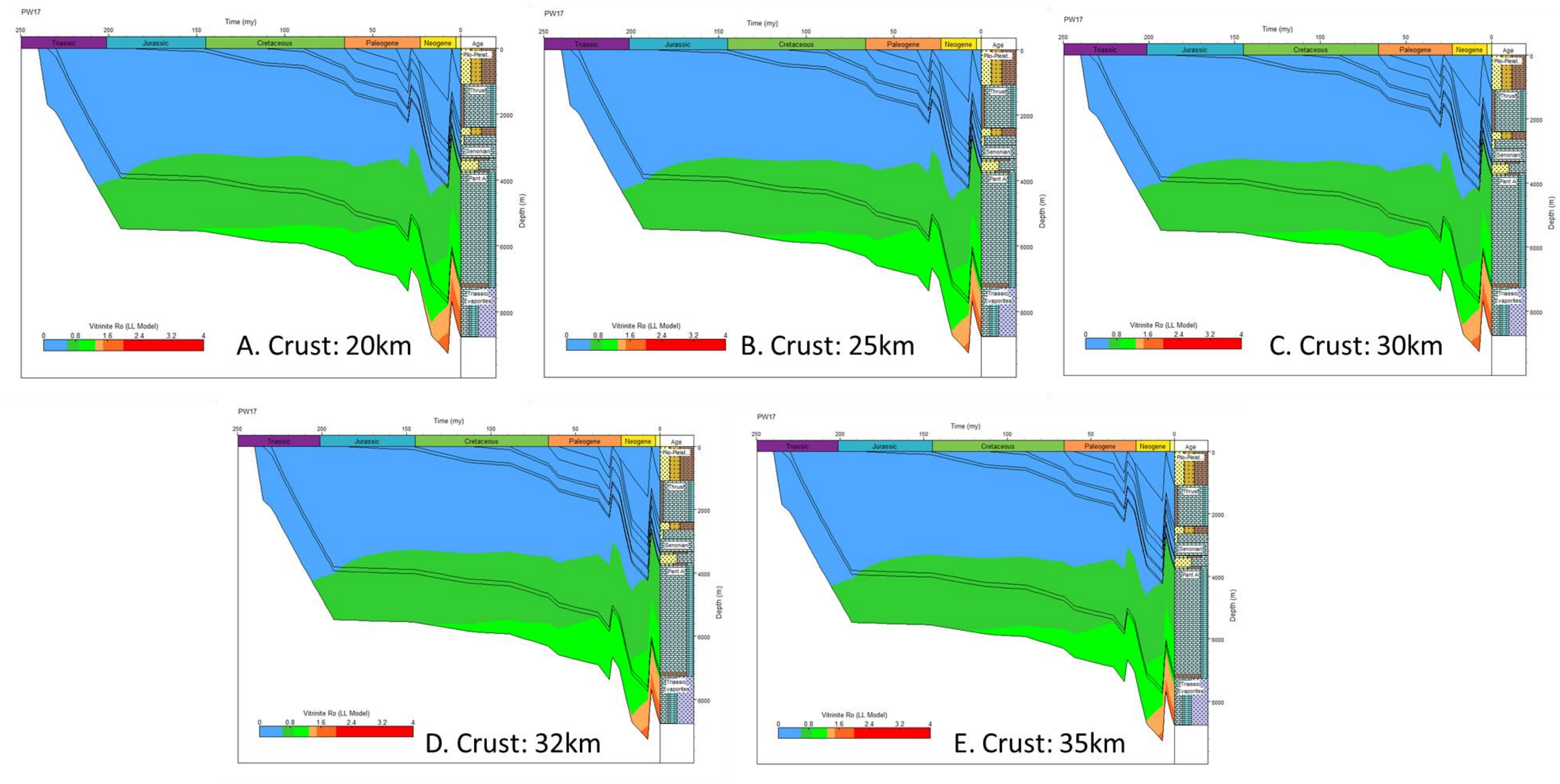

Figure 41: Burial History plots (240 Ma to Present) of pseudo-well A with superimposed colormap of vitrinite reflectance values. These plots describe the scenario 3. The parameters are presented in Table 15. Each plot refers to different crustal thickness.

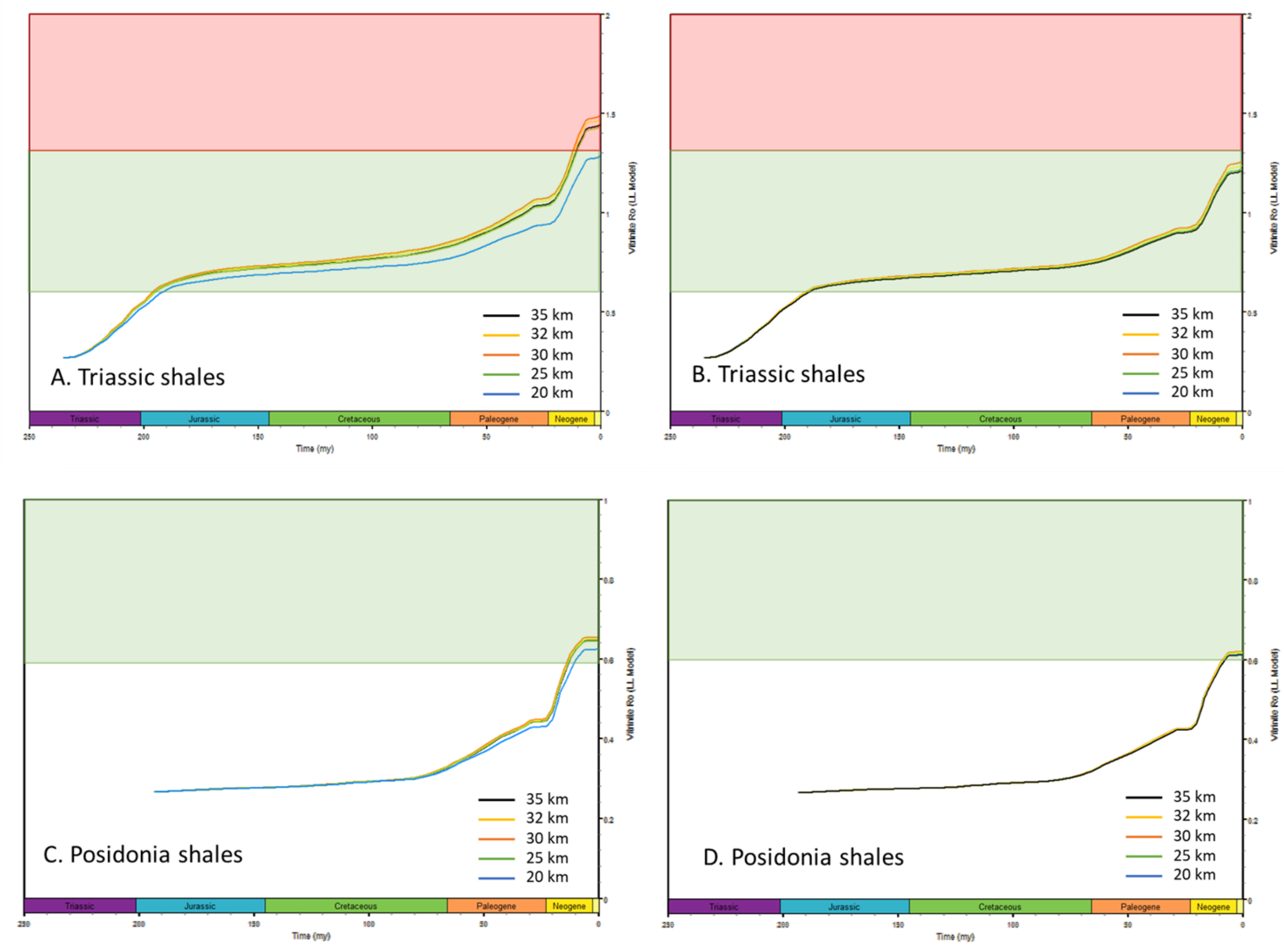

Figure 42: Vitrinite reflectance curve- Time based on Burnham and Sweeney 1990. The colored curves present the crustal thickness variables. Figures 41A and B represent Triassic shales and are based on scenario 2 and 3 respectively. Figures 41C and D illustrate Posidonia shales and based on scenario 2 and 3, respectively. The parameters used for scenarios 2 and 3 are presented in Table 15.

4.3.1.3 Transformation ratio

The variation of crustal thickness has a low to almost no impact in generation critical times for the modeled source rocks.

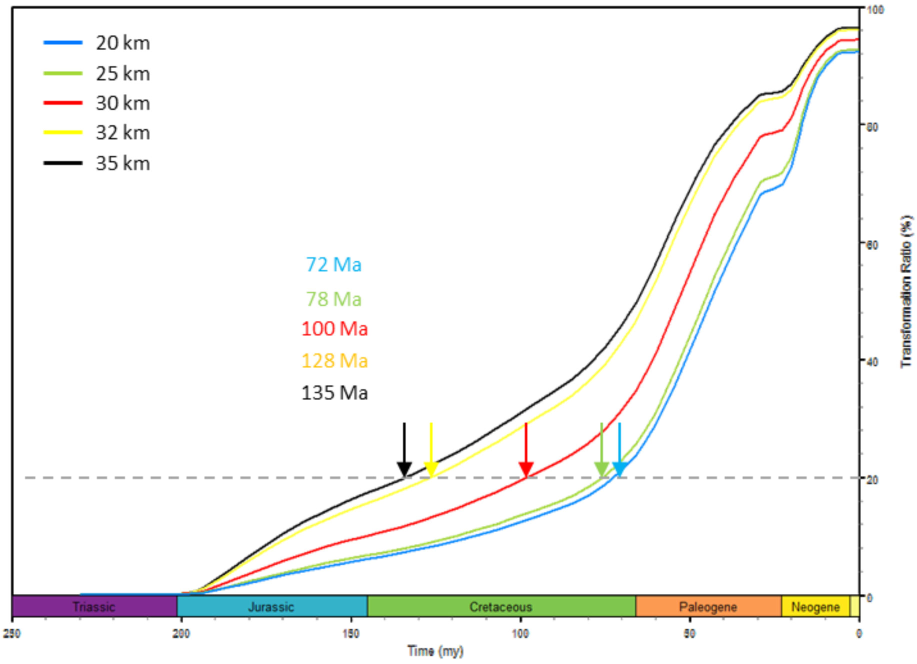

Figure 43: Transformation ratio curves through geological time for the Triassic shales (PW-A). The colored curves present the crustal thickness variables. Transformation ratio values are in % and time values are in Ma. These plots describe the scenario 2. The parameters used are presented in Table 15.

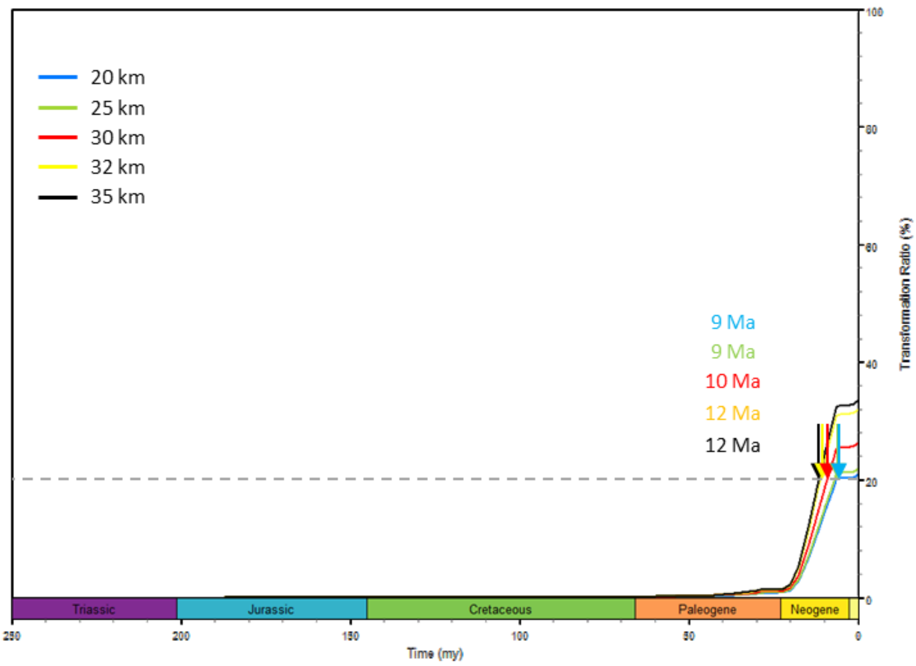

Figure 44: Transformation ratio curves through geological time for the Posidonia shales (PW-A). The colored curves present the crustal thickness variables. Transformation ratio values are in % and time values are in Ma. These plots describe the scenario 2. The parameters used are presented in Table 15.

A reduction of mass fraction, due to the crustal thickness decrease, is clearly observed from the transformation ratio diagrams of the Triassic shales through time (Figure 42). On the other hand, no significant variation in Posidonia (Figure 43) and Vigla shales' mass fractions is observed by crustal thickness variation. The scenarios as modeled suggested that Posidonia shales have different behavior compared with Triassic shales and the changes in crustal thickness cannot affect significantly the generated hydrocarbons. The Vigla shales do not generate hydrocarbons. Generation plot for the Vigla shales is presented in Appendix II (Figure A.II.5A).

Pseudo-well B follows the same trend as in pseudo-well A concerning the expelled volumes of hydrocarbons and the timing of the expulsion window. Generation mass plots for both scenarios are presented in Appendix II (Figures A.II.6.).

4.3.1.4 Petroleum Expulsion

The variation of crustal thickness affects at a point the expulsion critical times for the Triassic shales. Conversely, the variation of crustal thickness does not affect the expulsion critical times for Posidonia and Vigla shales. It is significant to be reported that Vigla shales do not expel hydrocarbons in all sensitivity scenarios, due to immaturity/ borderline maturity. On the other hand, Posidonia shales expel hydrocarbons in some cases (Figures 46 and A.II.7 -Appendix II).

According to expulsion mass plots through geological times, the increase of crustal thickness from 20 to 35 km, with beta factor 1.1, results in the earlier expulsion of hydrocarbons from the Triassic Shales (scenario 2) meaning from Upper Cretaceous (80 Ma) to Lower Cretaceous (140 Ma) respectively. The expulsion mass fraction increases with the increasing thickness of the crust. Figure 44 illustrates the expulsion process for Triassic shales. Minor impact, due to the increasing crustal thickness for Posidonia beds is observed (Figure 46).

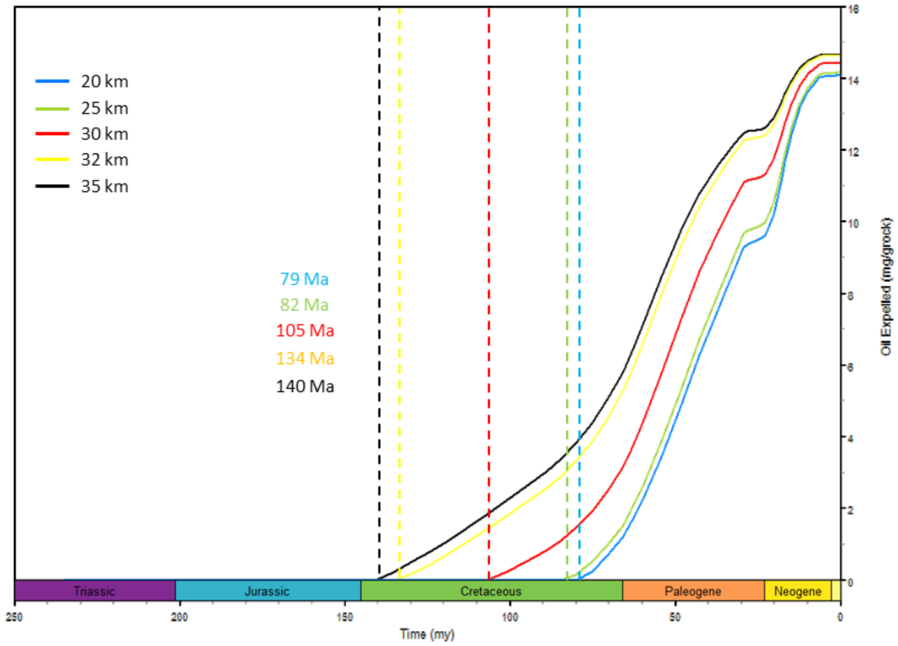

Figure 45: Expulsion Mass curves through geological time for the Triassic shales (PW-A). The colored curves present the crustal thickness variables. Expulsion mass values are in mg HC/g Rock and time values are in Ma. These plots describe scenario 2. The parameters used are presented in Table 15.

Figure 45 illustrates the expulsion process for the Triassic shales and suggests that increasing the crustal thickness results in bigger total expelled hydrocarbons (higher volume during the same time length). Expulsion window shows also mid to major differences; thus, the timing of expelled hydrocarbons varies within Jurassic from 180 Ma to 145 Ma. In the same scenario 3, the Posidonia shales are not capable to expel hydrocarbons. This may attribute to low maturity values.

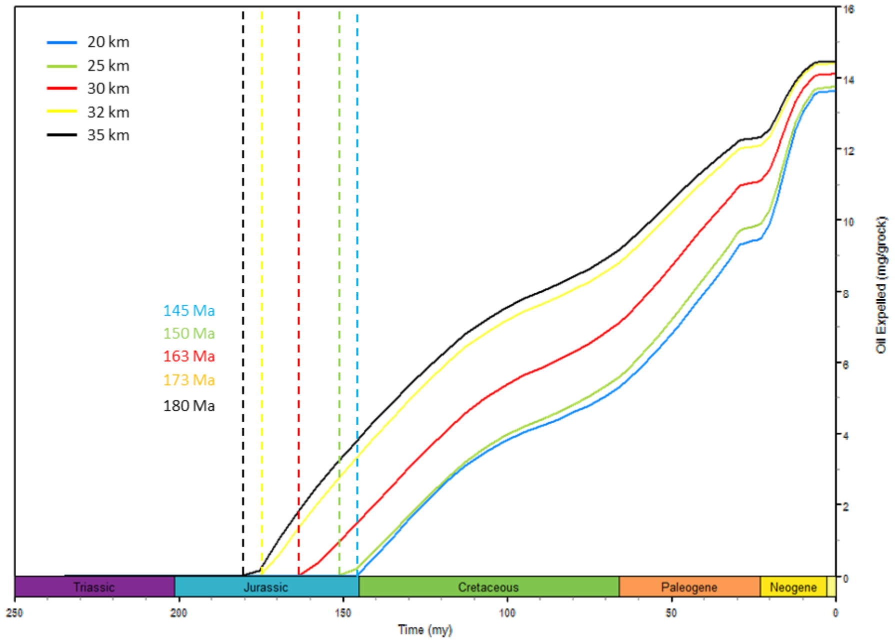

Figure 46: Expulsion Mass curves through geological time for the Triassic shales (PW-A). The colored curves present the crustal thickness variables. Expulsion mass values are in mg HC/g Rock and time values are in Ma. These plots describe scenario 3. The parameters used are presented in Table 15.

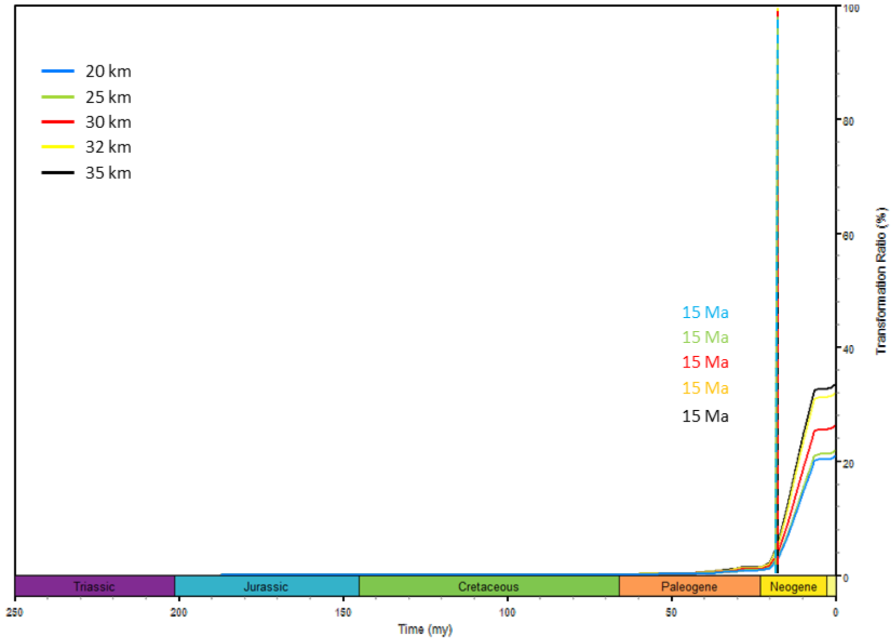

Figure 47: Expulsion Mass curves through geological time for the Posidonia shales (PW-A). The colored curves present the crustal thickness variables. Expulsion mass values are in mg HC/g Rock and time values are in Ma. These plots describe scenario 2. The parameters used are presented in Table 15.

According to the modeled scenarios and the expulsion plots, the final expulsion masses are significantly affected by the variation of crustal thickness in both scenarios. The thicker the crust, the higher the expelled volumes are. The timing of the expulsion window differs also significantly among the modeled scenarios (2 and 3).

Pseudo-well B follows the same trend concerning the expelled volumes of hydrocarbons and the timing of the expulsion window.

4.3.2 Beta Factor

4.3.2.1 Heat flow

By increasing the beta factor, an increase at peak heat flow is observed. The intense increase of heat flow is observed during the syn-rift period (190-145 Ma). However, in the post-rift period (approximately 120-0 Ma) a decreasing heat flow curve trend is noticed. The abrupt increase of the heat flow at the end of Paleogene and also at the end of Neogene are attributed to erosional events at the studied area due to Alpine orogeny and the subsequent uplifting. The diagrams of Figure 47 clearly illustrate that the higher the beta factor the faster the heat flow decreases. This can be attributed to the severe stretching that the crust suffers (as the high beta factor implies) which results in reduced crustal thickness, thus the crust cooling is faster and abrupt.

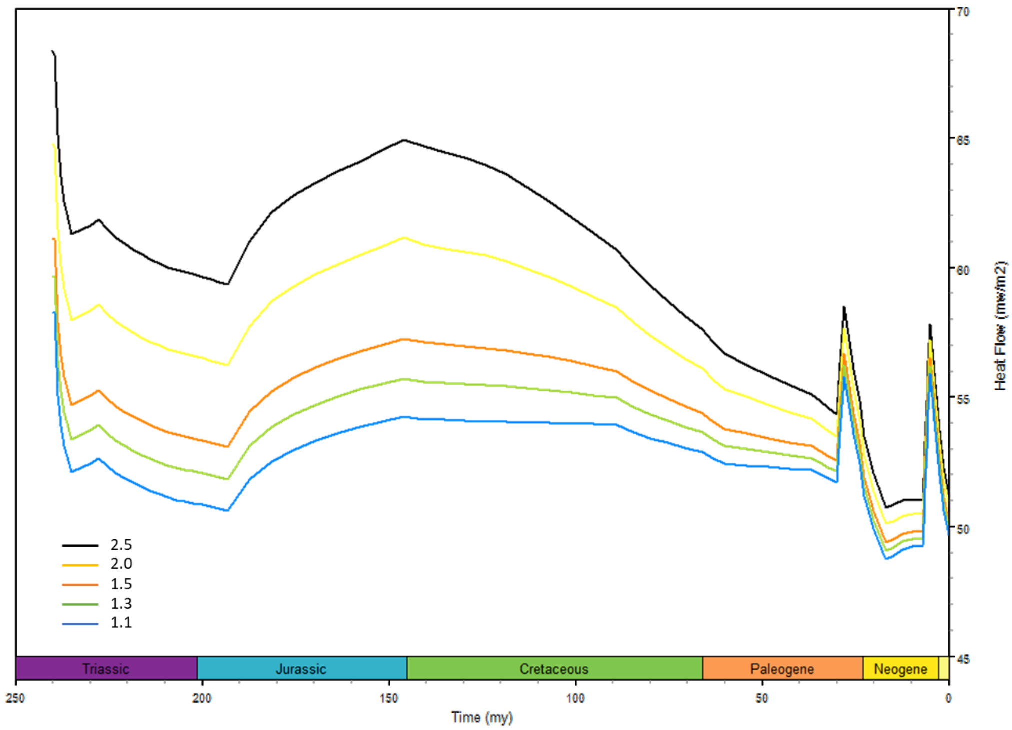

Figure 48: Heat Flow curves for the PW-A. The curves present Scenario 2 (maximum heat flow values). The colored curves present the beta factor variables. The parameters used are presented in Table 16.

In general, the current sensitivity of beta factor suggests that this parameter has strong impact on the heat flow distribution through time, thus extra attention should be paid when modeling, whereas extra discussions with the tectonic and seismic interpreters should be placed.

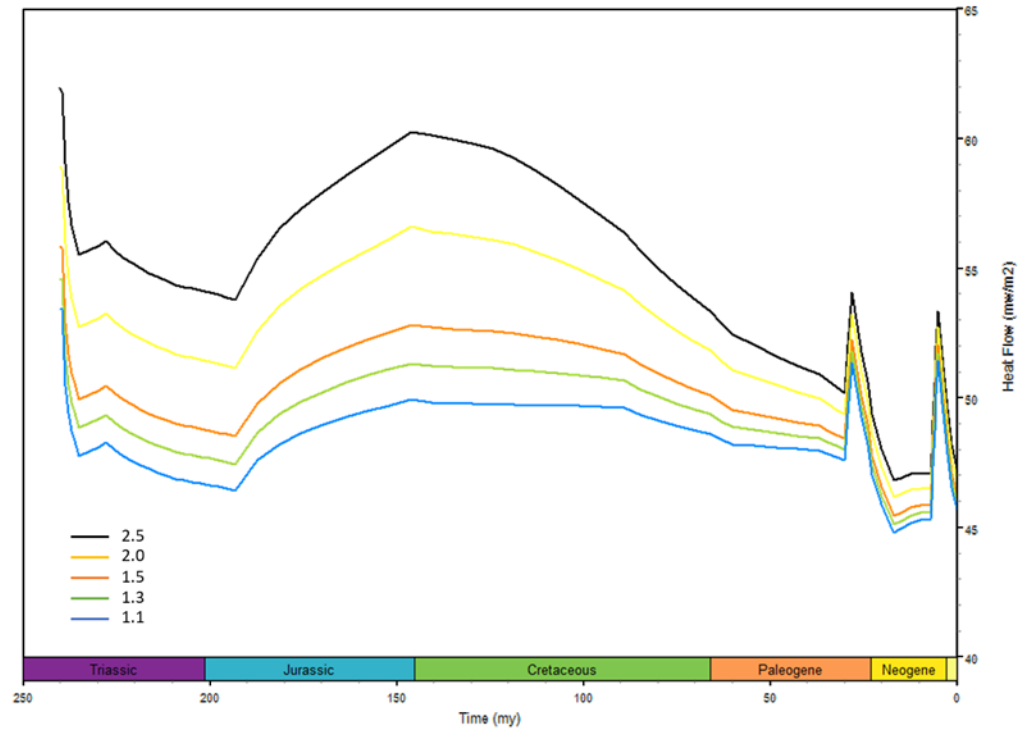

Figure 49: Heat Flow curves for the PW-A. The curves present Scenario 3 (minimum heat flow values). The colored curves present the beta factor variables. The parameters were used are presented in Table 16.

Table 20: Peak and present-day heat flow values (mW/m^3) for the scenarios 2 and 3 in both pseudo-wells.

Scenario	Pseudo-wells	Peak Heat flow	Present-day Heat flow
Scenario 2	**PW-A**	54-65	50-52
	PW-B	54-65	50-52
Scenario 3	**PW-A**	50.5-60	46-48
	PW-B	50.5-60	46-48

4.3.2.2 Maturity

Scenario 2

Triassic source rock is shifted from the wet gas to dry gas (at present day) window at the given location when beta factor increases, as modeled in PW-A (Figures 49, 50). In PW-B Triassic shales remain within the dry gas window showing higher maturity with increasing beta factor (at present day). The Jurassic source rock is shifted from late middle oil window to peak oil window in PW-B, whereas a minor shift from early to early-middle oil window is observed for both Posidonia and Vigla shales in PW-A. Burial history plots for both pseudo-wells are shown in Appendix II (A.II.10-15).

The diagram of vitrinite reflectance versus time for pseudo-well A (Figure 51) indicates that the Triassic shales enter the oil window at around 200 Ma and the gas window at around 15 Ma, for all the beta factor variables. Posidonia shales enter the oil window at approximately 14 Ma, whereas Vigla shales marginally enter the oil window at 11 Ma (Figure 51). Maximum vitrinite reflectance values are estimated at around 1.55 %, 0.68 %, 0.62 % at present-day for the Triassic, Posidonia and Vigla shales of pseudo-well A respectively. In pseudo-well B the present-day vitrinite reflectance value is estimated at 1.90 % for the Triassic shales and 0.95% for the Posidonia shales.

<u>Scenario 3</u>

Triassic shales are shifted from the late oil window to early wet gas window (at present day- PW-A) at the given location when beta factor increases. In PW-B the Triassic source rock is shifted from the wet gas window to the dry gas window, as modeled. The Jurassic source rock in PW-B is less affected but still shifted from early-middle to middle oil window, as modeled. The same source rock (the Jurassic Posidonia shales) in PW-A is shifted from the onset to the early oil window as modeled, whereas the Vigla shales are close to the onset of the oil window when the beta factor is maximum. Based on the vitrinite reflectance versus time diagrams, the Triassic shales enter the oil window, approximately at 205 Ma for all the beta factor variables (Figure A.II.16). Triassic shales as modeled in PW-A, marginally enter the gas window showing maximum vitrinite reflectance value at around 1.32% at present-day. Posidonia enters the oil window at approximately 11 Ma, whereas Vigla shales are immature (Figure A.II.16). The maximum values of vitrinite reflectance at present day for Posidonia and Vigla shales in PW-A are are 0.63% and 0.58%, respectively. Present-day maximum vitrinite reflectance values are 1.60% and 0.85 % for Triassic and Posidonia shales in pseudo-well B (Figure A.II.17).

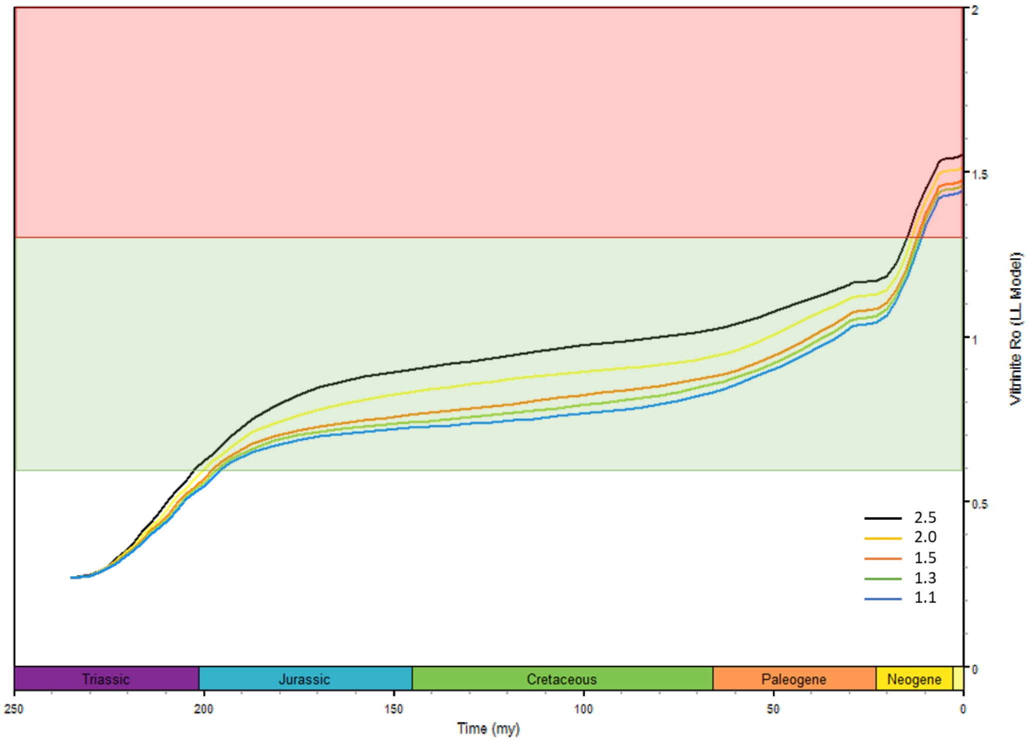

Figure 49: Vitrinite reflectance curve- Time based on Burnham and Sweeney 1990. The colored curves present the beta factor variables. The figure illustrates Triassic shales based on scenario 2 in pseudo-well A.

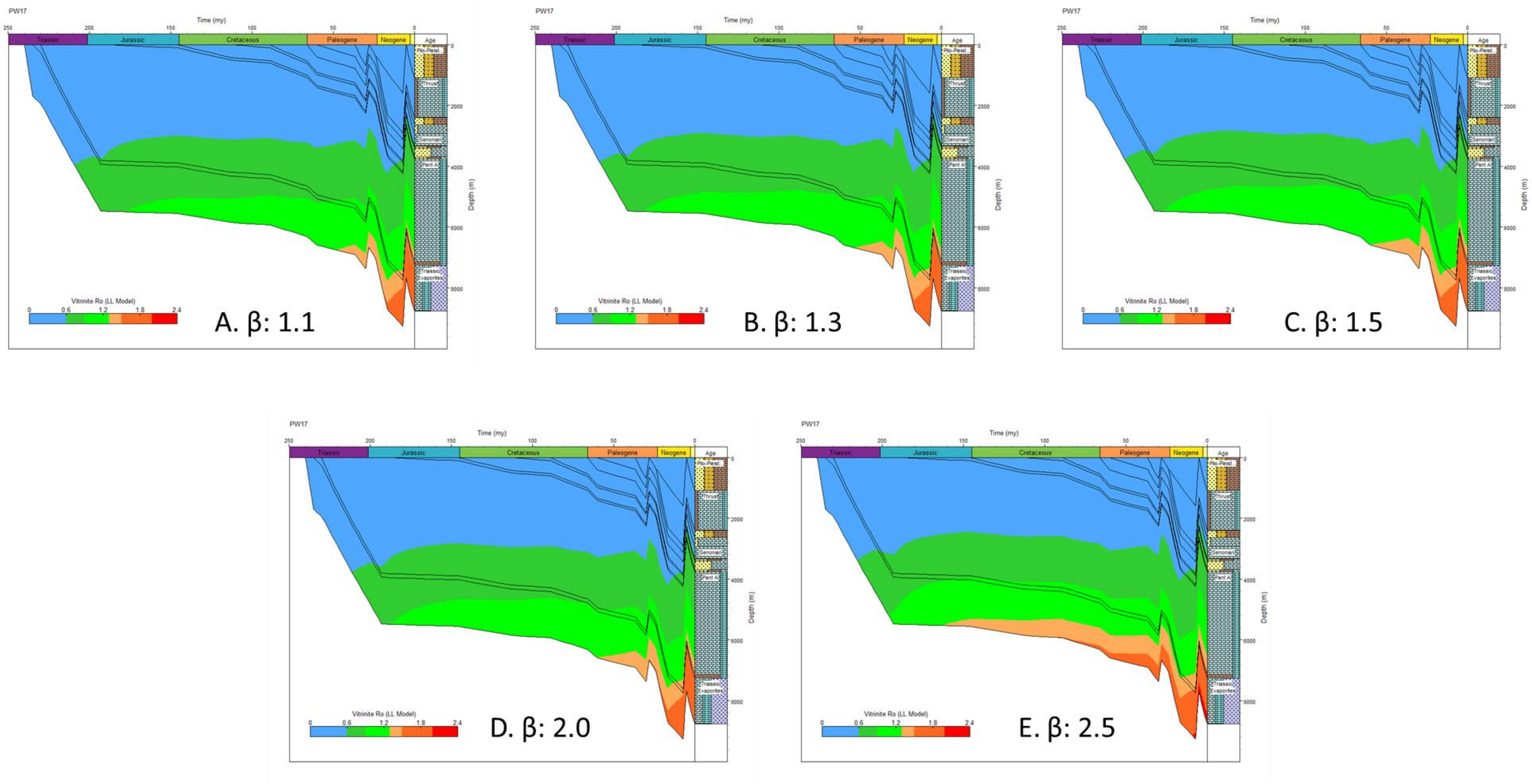

Figure 50: Burial History plots (240 Ma to Present) for the pseudo-well A. These plots describe scenario 2. The parameters are presented in Table 16. Each plot refers to different beta factor.

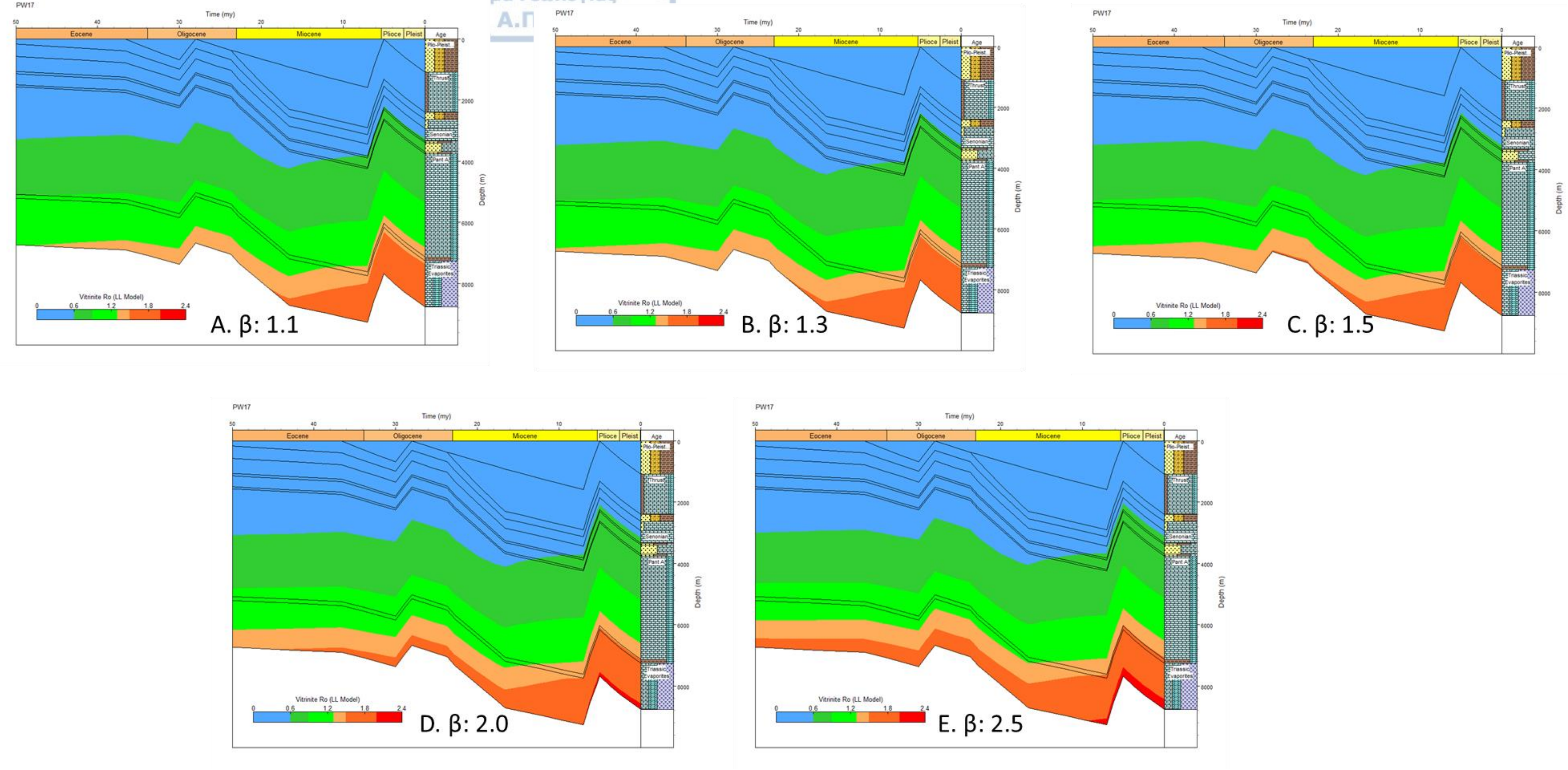

Figure 51: Burial History plots (50 Ma to Present) for the pseudo-well A. These plots describe scenario 2. The parameters are presented in Table 16. Each plot refers to different beta factor

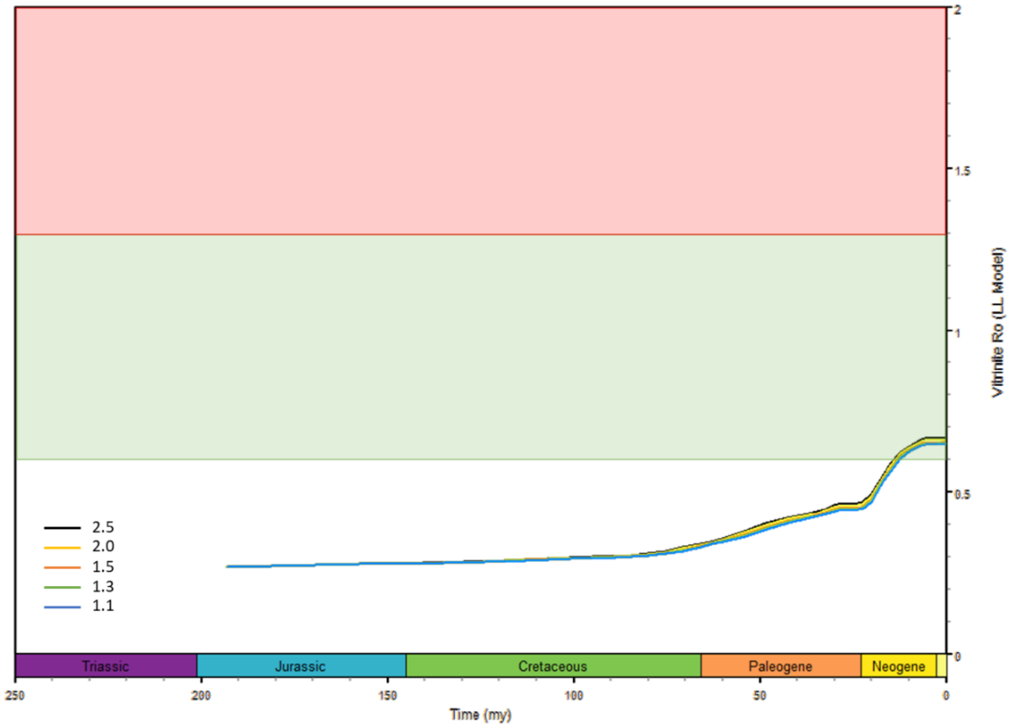

Figure 50: Vitrinite reflectance curve- Time based on Burnham and Sweeney 1990. The colored curves present the beta factor variables. The figure illustrates Posidonia shales based on scenario 2 in pseudo-well A.

4.3.2.3 Transformation ratio

The variation of beta factor results in a significant impact in transformation ratio for the three modeled source rocks. Transformation ratio is a parameter that quantifies the progress of hydrocarbons generation. During Lower Jurassic to Upper Cretaceous there is a range in transformation ratio trend. The higher the beta factor is the earlier the hydrocarbons are generated (Figure 53).

As it is expected in thrust and fold belts, the Triassic shales show two periods with increasing generation mass volume. Figure 53 shows that all the colored curves consist of two periods of increasing transformation ratio (TR). From 135 to 30 Ma (transformation ratio is higher than 20%) and from 20 to 10 Ma an increasing transformation ratio value is noticed. During Paleogene from 30 to 20 Ma and Miocene to present-day (10 to 0 Ma) the TR value remains almost constant.

Moreover, in terms of generation masses the Triassic shales were substantially affected showing also two abrupt phases of generation as expected. Figure 53 shows that black and yellow colored generation curves are characterized by abrupt increasing mass fraction from the starting point of generation to 135 Ma and from 15 to 8 Ma.

On the other hand, the variation of the transformation ratio of the Posidonia (Figure 54) and Vigla shales, due to the increasing beta factor, is observed within a single generation phase at recent times, as expected. However, the various beta factor values result in different transformation ratio values (and as a result, different generation mass volumes) at present-day.

Therefore, the variation of beta factor is considered as critical for the generation of hydrocarbons and thus, significant effort should be put in order to conclude in "a best guess" of this parameter. Seismic interpretation is always a very useful tool for the estimation of the beta factor.

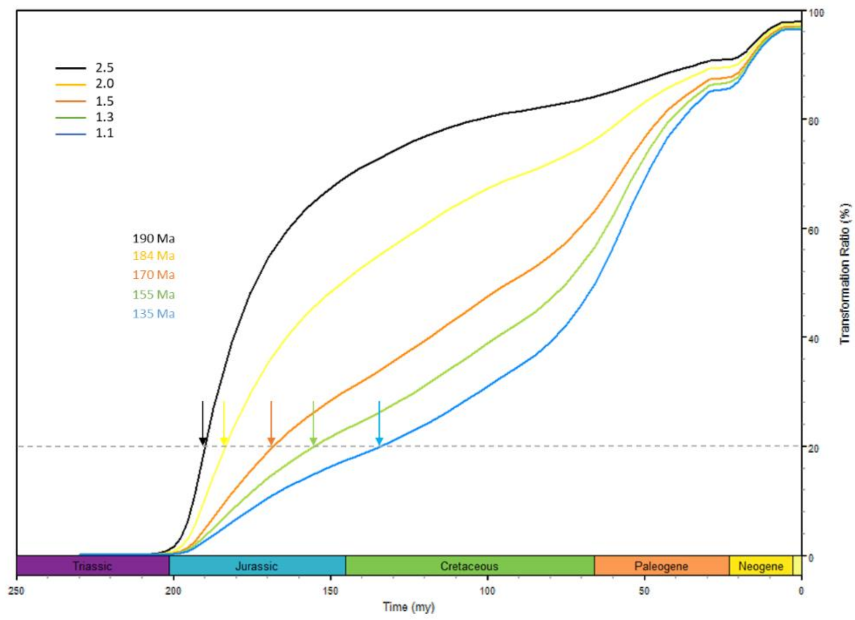

Figure 51: Transformation ratio through geological time for the Triassic shales (PW-A). The colored curves present the beta factor variables. Transformation ratio values are in % and time values are in Ma. These plots describe scenario 2. The parameters used are presented in Table 16.

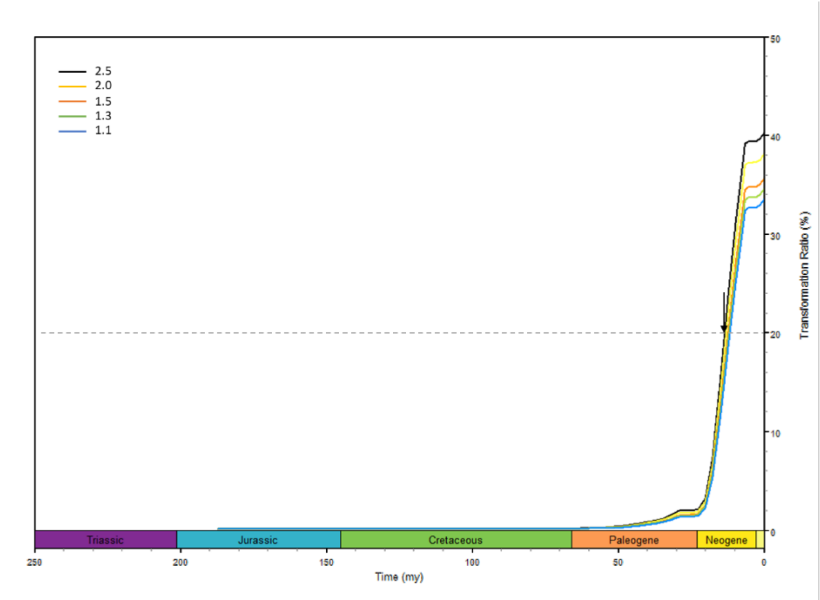

Figure 52: Transformation ratio through geological time for the Posidonia shales (PW-A). The colored curves present the beta factor variables. Transformation ratio values are in % and time values are in Ma. These plots describe scenario 2. The parameters used are presented in Table 16.

The variation of beta factor values in pseudo-well B, has the same impact in both scenarios for the three modeled source rocks, such as in pseudo-well A. Transformation ratio plots for both scenarios are presented in Appendix II (Figure A.II.18-19).

4.3.2.4 Petroleum Expulsion

The Triassic shales are significantly affected by the beta factor variation in terms of expulsion critical times, as modeled. Conversely, the variation of beta factor does not affect the expulsion critical times for Posidonia and Vigla shales, however, variations are suggested for the final volumes of the expelled hydrocarbons.

According to expulsion mass plots through geological times, the variation of beta factor results in the earlier expulsion for the Triassic Shales (scenario 2), which range between 140-192 Ma (pseudo-well A).

From Lower Jurassic to almost end of Paleogene (~30 Ma), the expulsion mass volume increases abruptly, with the increasing beta factor (Figure 55). From 30 to 20 Ma and from 10 Ma to present-day the expulsion mass volume remains constant.

Posidonia shales expel hydrocarbons in scenario 2 with all beta factor variations, showing significant variation on the final expelled volumes (Figure 56). The colored curves increase steeply and the blue curve presents the minimum expelled volume.

The same trends of expulsion curves for Triassic shales are observed when scenario 3 is applied (Figure A.II.20).

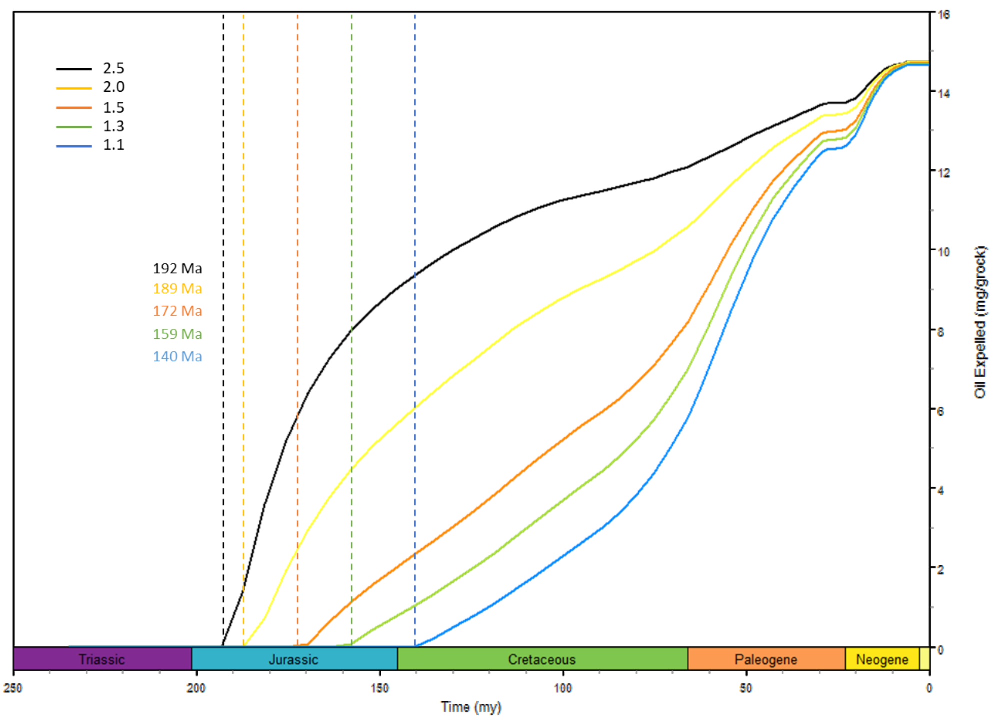

Figure 53: Expulsion Mass curves through geological time for the Triassic shales (PW-A). The colored curves present the beta factor variables. Expulsion mass values are in mg HC/g Rock and time values are in Ma. These plots describe scenario 2. The parameters used are presented in Table 16.

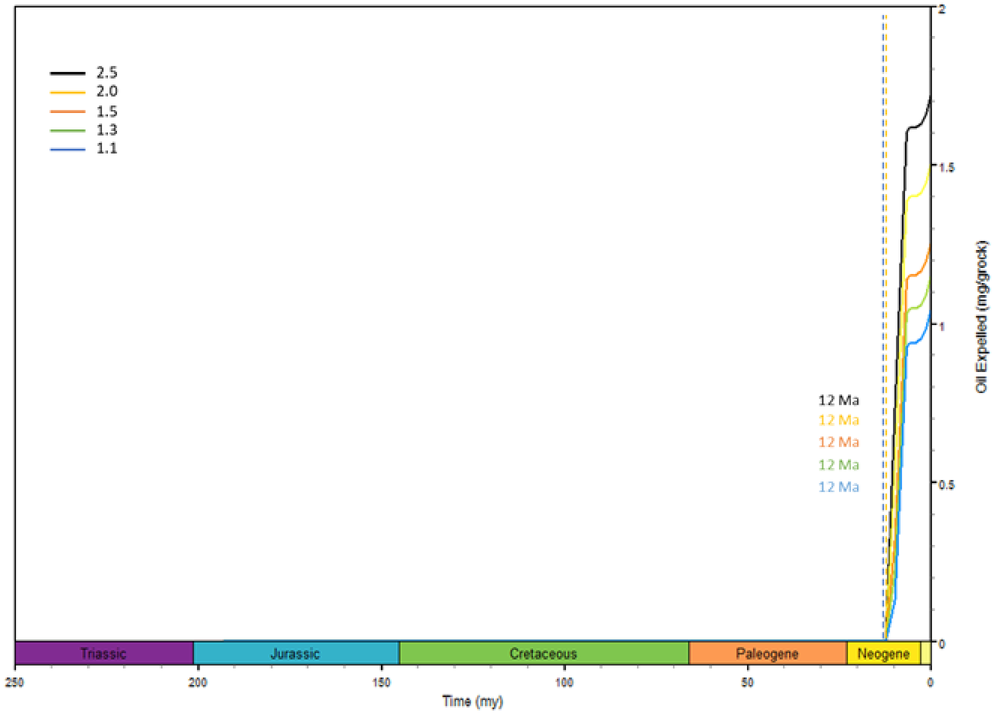

Figure 54: Expulsion Mass curves through geological time for the Posidonia shales (PW-A). The colored curves present the beta factor variables. Expulsion mass values are in mg HC/g Rock and time values are in Ma. These plots describe scenario 2. The parameters used are presented in Table 16.

However, Posidonia shales are not capable to expel hydrocarbons, except when beta factor 2.0 and 2.5 are used (Figure A.II.21). This lag may occur due to low generated values, for example 0.72 mg HC/g Rock. The final expulsion masses increase with the increasing beta factor in both scenarios, as modeled.

Varying the beta factor in pseudo-well B, has the same impact in both scenarios for the three modeled source rocks, such as in pseudo-well A. Expulsion mass plots for both scenarios are presented in Appendix II (Figure A.II.22).

4.3.3 Radioactive Heat

4.3.3.1 Heat flow

Radioactive heat is the heat generated within a medium as a result of absorption of radiation from the decay of radioisotopes in the medium (Hantschel and Kauerauf, 2009). Thus, with the increase of the radioactive heat more heat is absorbed by the crust (the upper crust is more radioactive compared with the lower crust) resulting as an increase of the heat flow. In post-rift period all curves follow a dropping trend. Table 21 lists the peak and the present-day heat flow values for scenarios 2 and 3. Heat flow curves for the pseudo-well B for both scenarios are presented in Appendix II (Figure A.II.23).

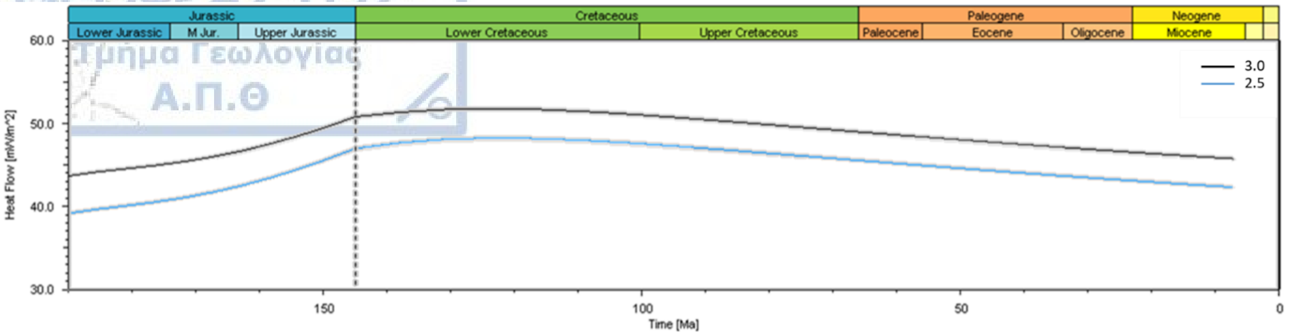

Figure 55: Heat Flow curves for the PW-A. The curves present Scenario 2 (maximum heat flow values) and 3 (minimum heat flow values), respectively. The parameters used are presented in Table 17.

Table 21: Peak and present-day heat flow values (mW/m^3) for scenarios 2 and 3 in both pseudo-wells.

Scenario	Pseudo-wells	Peak Heat flow	Present-day Heat flow
Scenario 2	**PW-A**	51	46
	PW-B	51	46
Scenario 3	**PW-A**	48	43
	PW-B	47	42

4.3.3.2 Maturity

According to burial history VS vitrinite reflectance curves, the variation of radioactive heat has a minor impact on the maturity history for Posidonia and Vigla shales. Posidonia shales enter the oil window at 12 Ma, whereas Vigla shales enter the oil window at 10 Ma (Figure 58C and D). On the other hand, Triassic shales enter the oil window earlier with the increasing radioactive heat. As the Figures 58A and B show, for the pseudo-well A, the depth of the onset of the oil window is shifted from 4200 m to 3700 m and the timing from 195 to 200 Ma.

Correspondingly, for the Triassic shales in pseudo-well B, the depth of the onset of the oil window changes from 3800 m to 3600 m and the timing from 185 to 193 Ma. It is critical to highlight that both the Triassic and the Posidonia shales in PW-A and PW-B are getting more mature when the radioactive heat increases. Burial history curves for the pseudo-well B are presented in Appendix II (Figures A.II.27).

For transformation ratio higher than 20%, hydrocarbon generation is observed. The above observations are consistent with the transformation ratio curves in both pseudo-wells in scenarios 2 and 3.

In numbers, the vitrinite reflectance curves are also consistent with the observations for the burial history curves. Vitrinite reflectance value for the Triassic shales increases from 1.4% to 1.7%, whereas this value changes from 0.65% to 0.70% for the Posidonia shales (pseudo-well A). In the pseudo-well B, the vitrinite reflectance value increases from 1.4% to 1.75% and from 0.74% to 0.82% Ro for the Triassic and the Posidonia shales, respectively. Vitrinite reflectance plots are presented in Appendix II (Figures A.II.24-26).

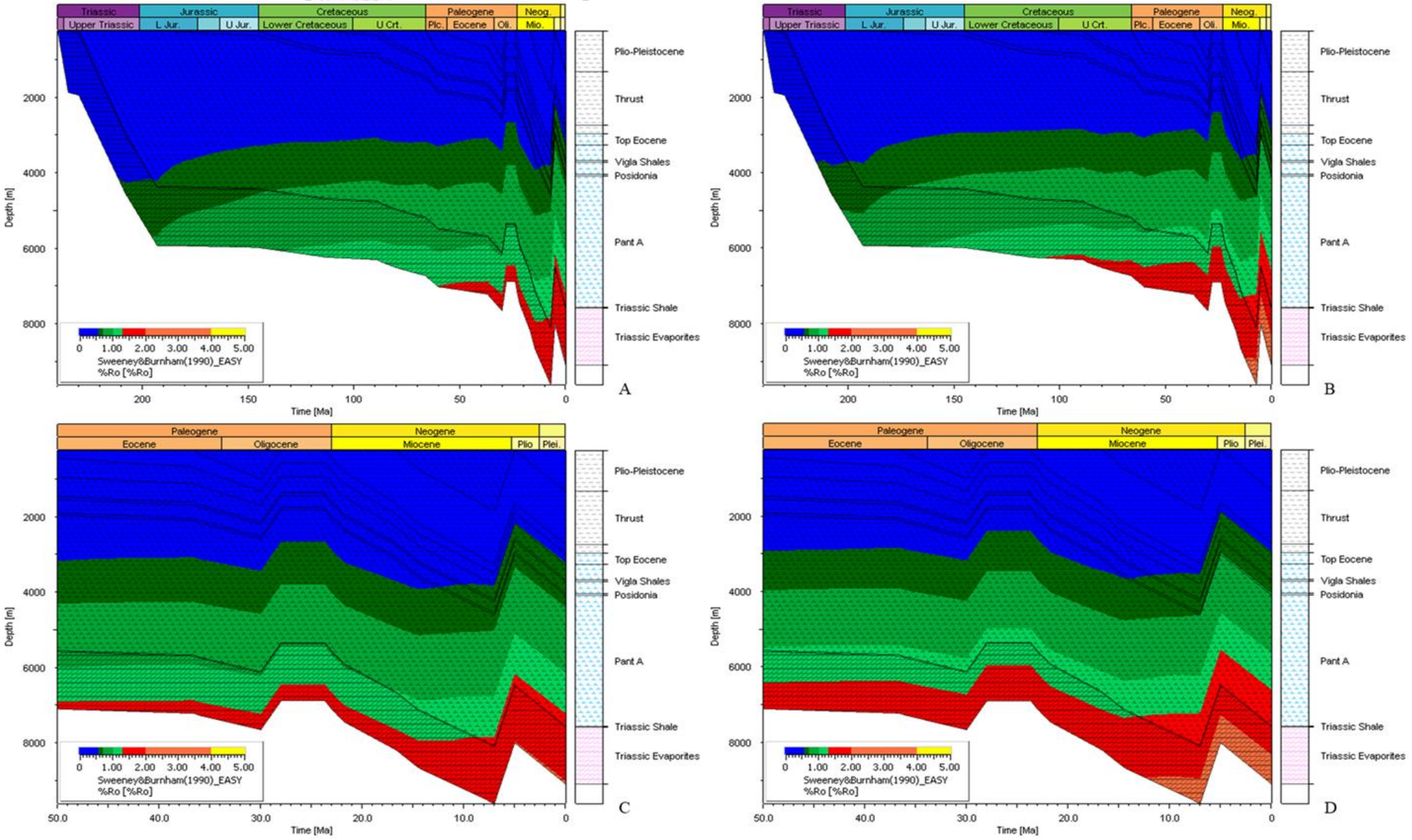

Figure 56: Burial History plots (240 Ma to Present and 50 Ma to Present) for pseudo-well A. The parameters are presented in Table 17.

4.3.3.3 Petroleum Generation

Significant impact of radioactive heat variables on the generation mass fraction is observed for the three modeled source rocks. Figures 59-61 present the generation plots for the Triassic and the Posidonia shales respectively. Timing of hydrocarbons generation is less affected showing tens of million years difference for both the onset of oil and gas window.

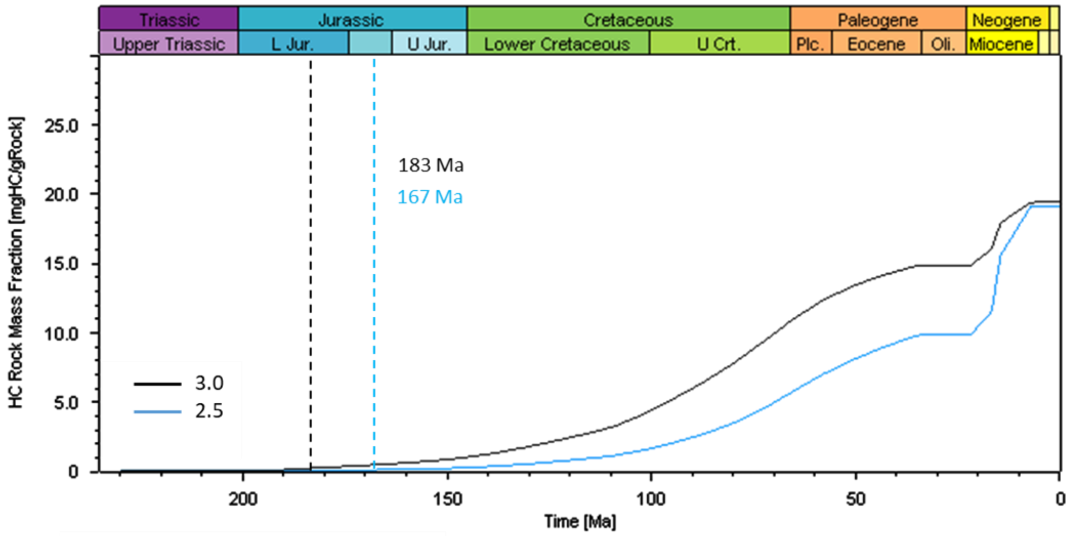

Figure 57: Generation Mass curves through geological time for the Triassic shales (PW-A). The colored curves present the radioactive heat variables. Generation mass values are in mg HC/g Rock and time values are in Ma. The parameters used are presented in Table 17.

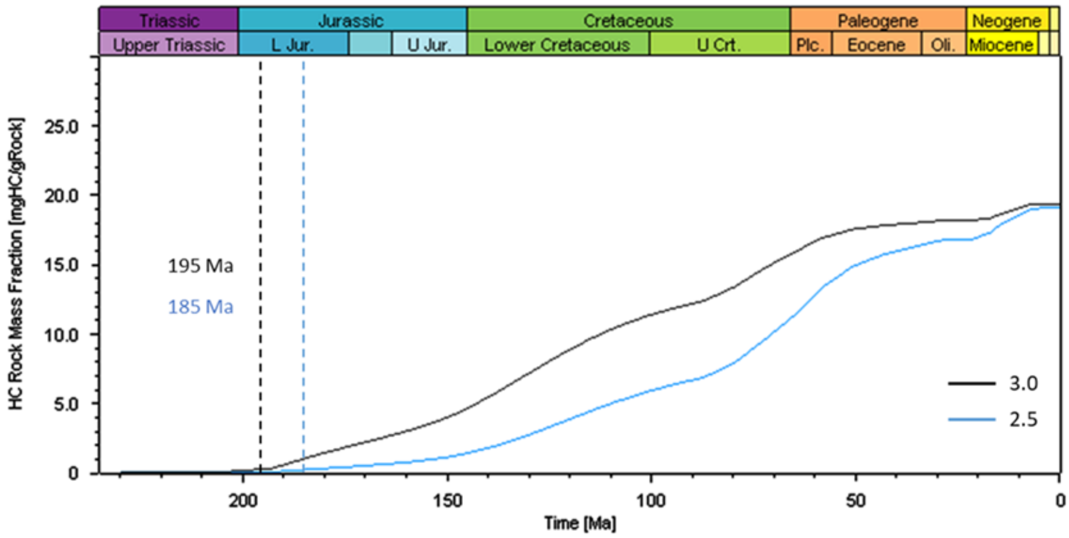

Figure 58: Generation Mass curves through geological time for the Triassic shales (PW-B). The colored curves present the radioactive heat variables. Generation mass values are in mg HC/g Rock and time values are in Ma. The parameters used are presented in Table 17.

Triassic shales are constituted from two periods with increasing generation mass volume in pseudo-well A. As described by Figure 59, from the start of generation to 53 Ma and from 17 to 9 Ma an increasing generation volume is noticed. During Eocene to early Miocene (53 – 17 Ma) and Miocene to present-day (9 to 0 Ma) the mass fraction remains almost constant. Although, there are differences in terms of mass fraction through geological time, final volumes are almost equal for both scenarios. Similarly, the Triassic shales are characterized by two periods of increasing generation mass in pseudo-well B. From the generation starting time to Eocene (35 Ma) and during Miocene of the generation volume increases. It is essential to notice that there is an abrupt increased volume during Miocene (20 to 10 Ma). This is attributed to the thrusting event which increases the buried depths in few million years (23- 16.6 Ma). During Eocene to Oligocene (35 to 22 Ma) and from 8 Ma to present day generation masses remain almost constant (Figure 60).

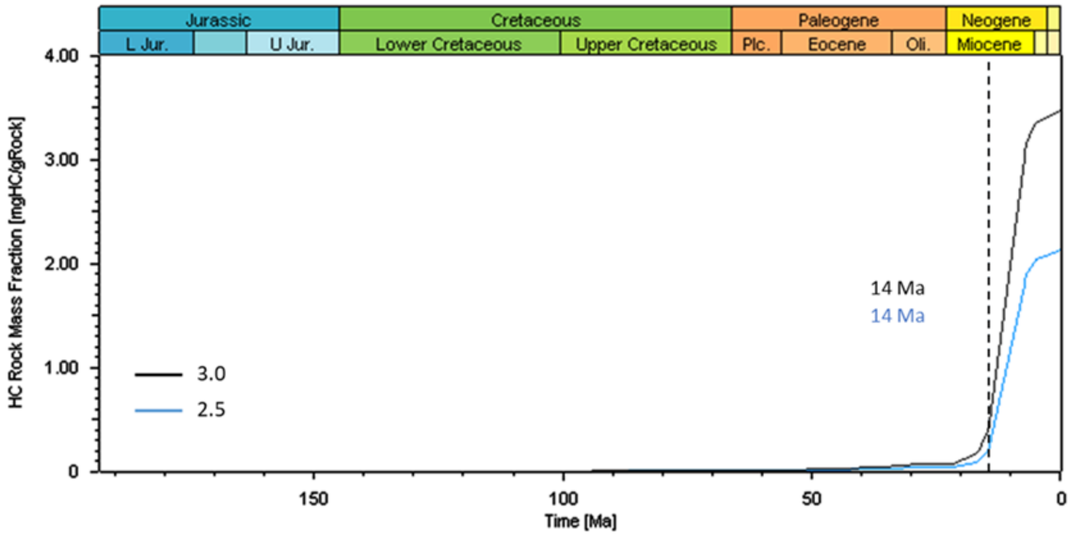

Figure 59: Generation Mass curves through geological time for the Posidonia shales (PW-A). The colored curves present the radioactive heat variables. Generation mass values are in mg HC/g Rock and time values are in Ma. The parameters used are presented in Table 17.

Comparing the final generated masses from the three modeled source rocks, it is clearly indicated that: when the radioactive heat is increased, both the Posidonia (Figure 61) and the Vigla shales double the generated volumes. However, the total generated volumes from the Triassic source rock remain the same. This is attributed to the cracking of oil to gas. Thus, although the liquid hydrocarbon volumes from the Triassic shales remain the same, the gas volumes increase when radioactive heat increases. Generation plots for Vigla shales are presented in the Appendix II (Figure A.II.28).

Similar observations are applied for the Triassic and the Posidonia source rock in PW-B. Generation mass plots for both scenarios are presented in Appendix II (Figure A.II.29).

4.3.3.4 Petroleum Expulsion

The variation of radioactive heat affects the expulsion critical times for the Triassic shales but not for the Posidonia shales (Figures 61, 62 and 63). Valuable changes are also observed in the final expulsion volume for the Posidonia shales, whereas final volumes for the Triassic shales are almost the same. According to the expulsion mass plots through geological time, the variation of radioactive heat results in the earlier expulsion for the Triassic shales, which range between 123-153 Ma in pseudo-well A (Figure 62) and between 80- 110 Ma in pseudo-well B (Figure 63).

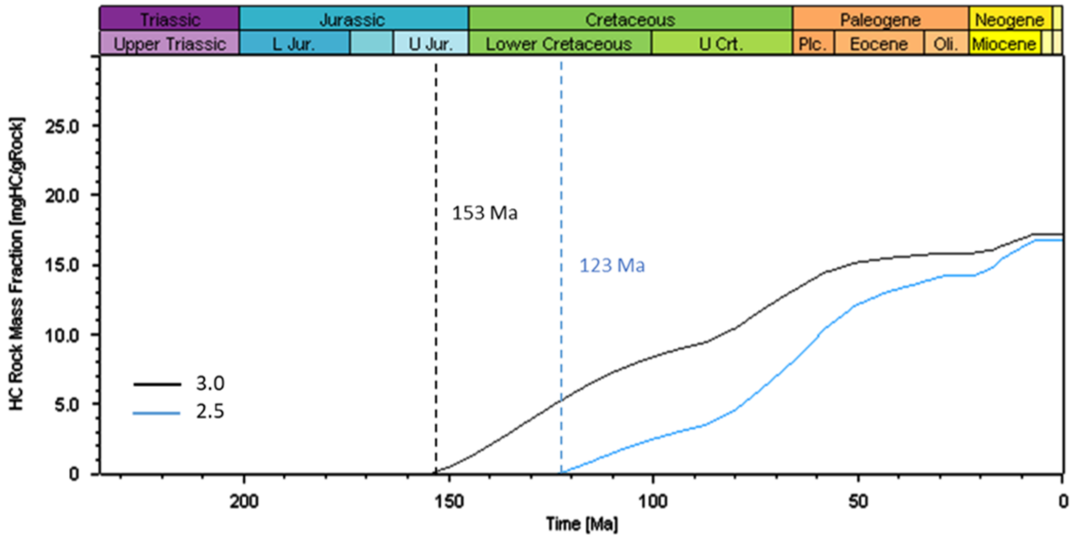

Figure 60: Expulsion Mass curves through geological time for the Triassic shales (PW-A). The colored curves present the radioactive heat variables. Expulsion mass values are in mg HC/g Rock and time values are in Ma. The parameters used are presented in Table 18.

Two phases of increased expulsion volumes are observed in pseudo-well A. From expulsion starting time to Middle Eocene and from 20 to 8 Ma (Miocene) masses increase, whereas during 35 to 20 Ma and 8 Ma to present day expulsion volumes remain constant. Triassic shales are characterized by two periods of increasing expulsion mass in pseudo-well B. From the expulsion starting time to middle Eocene (35 Ma) and during Miocene the expulsion volume increases. It is essential to notice that during Miocene (20 to 10 Ma) expulsion mass curve increases steeply. This is attributed to the thrusting event (23- 16.6 Ma) which results in the second phase of maturation, generation and thus, expulsion of hydrocarbons as expected. During Eocene to Oligocene (38 to 22 Ma) and from 10 Ma to present day expulsion masses remain almost constant.

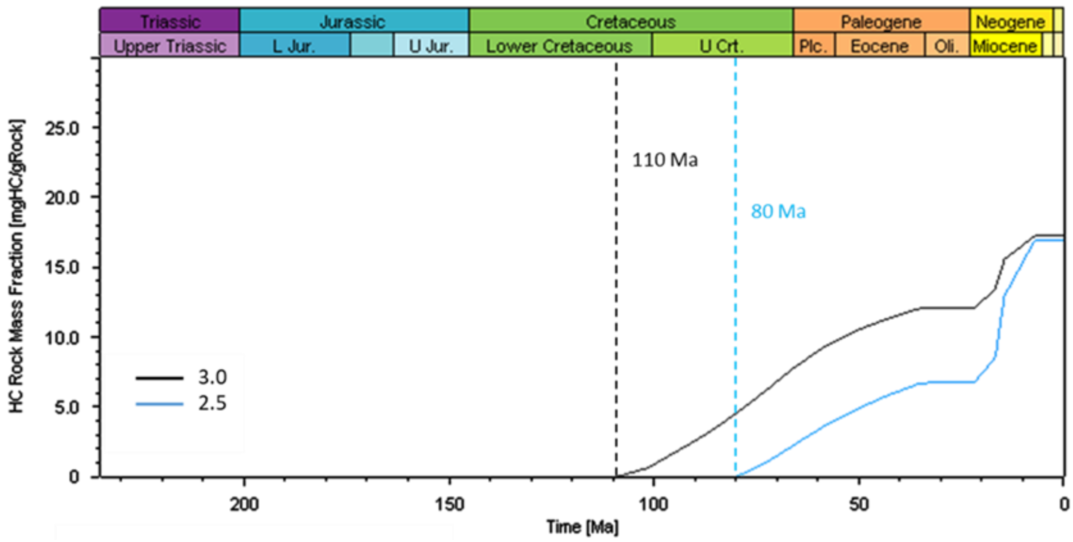

Figure 61: Expulsion Mass curves through geological time for the Triassic shales (PW-B). The colored curves present the radioactive heat variables. Expulsion mass values are in mg HC/g Rock and time values are in Ma. The parameters were used are presented in Table 18.

The Posidonia shales in pseudo-well A expel hydrocarbons only in scenario 2, whereas in pseudo-well B the Posidonia shales expel hydrocarbons in both scenarios. By increasing the radioactive heat in both pseudo-wells the expelled volumes are getting double (Figure 64), suggesting that the radioactive heat variation is critical to thermal and maturity modeling.

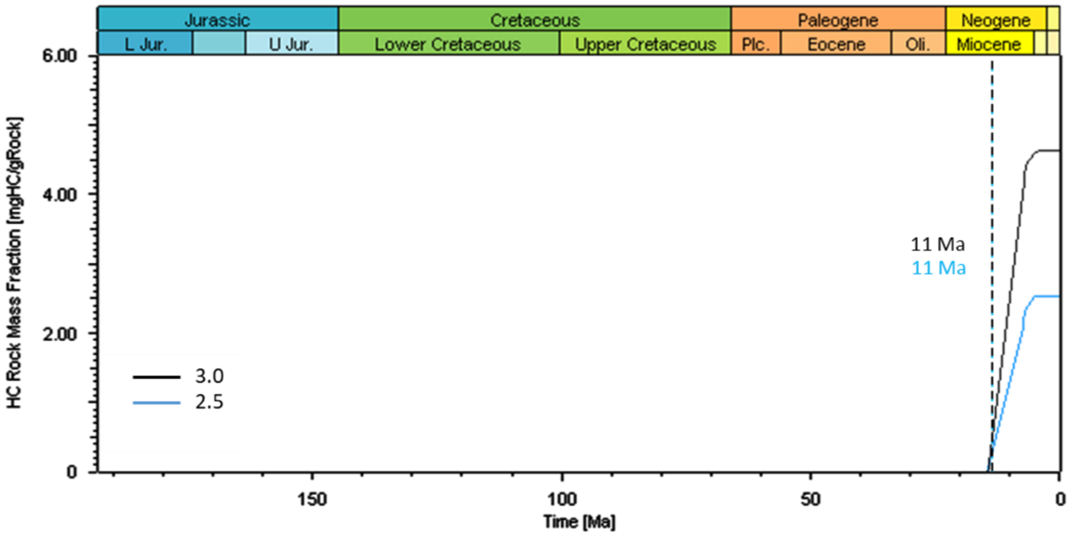

Figure 62: Expulsion Mass curves through geological time for the Posidonia shales (PW-B). The colored curves present the radioactive heat variables. Expulsion mass values are in mg HC/g Rock and time values are in Ma. The parameters used are presented in Table 18.

4.3.4 Rifting age

4.3.4.1 Heat flow

The variation of rifting age has no impact on heat flow curves as modeled and based on the selected variables. Peak and present-day heat flow values are almost equal. Table 22 lists the peak and the present-day heat flow values for scenarios 2 and 3. Heat flow curves for pseudo-well B for both scenarios are also presented in Appendix II (Figures A.II.30).

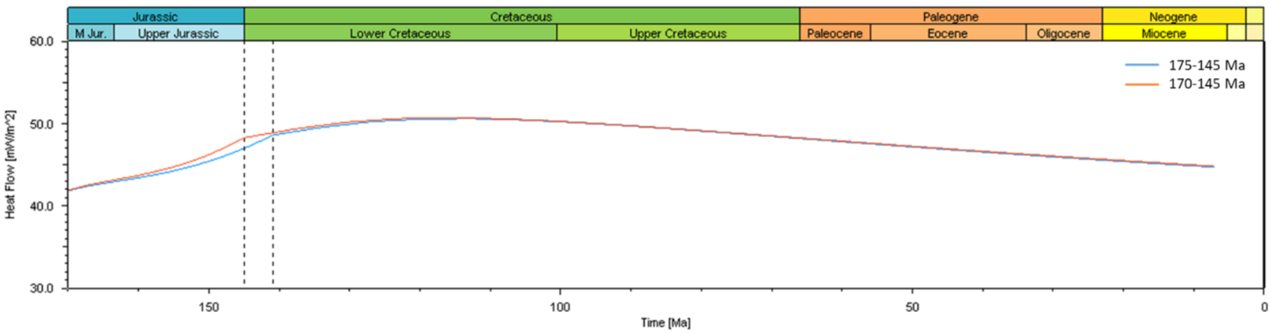

Figure 63: Heat Flow curves for pseudo-well A. The colored curves present the rifting age variables. The parameters used are presented in Table 18.

Table 22: Peak and present-day heat flow values (mW/m^3) for scenarios 2 and 3 in both pseudo-wells.

Scenario	Pseudo-wells	Peak Heat flow	Present-day Heat flow
Scenario 2	**PW-A**	51	45
	PW-B	50.5	44.5
Scenario 3	**PW-A**	51	45
	PW-B	50	44

4.3.4.2 Maturity

No impact was observed on the maturity of the three modeled source rocks when shifting the starting rifting age from 170 Ma to 175 Ma.

For transformation ratio percentage higher than 20%, hydrocarbon generation is observed. The above observations are consistent with the transformation ratio curves for both pseudo-wells.

Vitrinite reflectance curves are also consistent with the above observations. Vitrinite reflectance value is estimated at 1.6 % for Triassic shales, 0.70 % for Posidonia shales and 0.65 % for Vigla shales (pseudo-well A). In the pseudo-well B vitrinite reflectance value is estimated 1.55 % for Triassic shales and 0.78 % for Posidonia. Vitrinite reflectance plots are presented in Appendix II (Figure A.II.31).

4.3.4.3 Petroleum Generation

Similarly, with the case of maturity, when shifting the starting rifting age from 170 Ma to 175 Ma, there is no impact on the generation masses and critical timing for the three modeled source rocks.

The same observations apply to both pseudo-well A and B. Generation mass plots and corresponding tables are shown in Appendix II (Figure A.II.32).

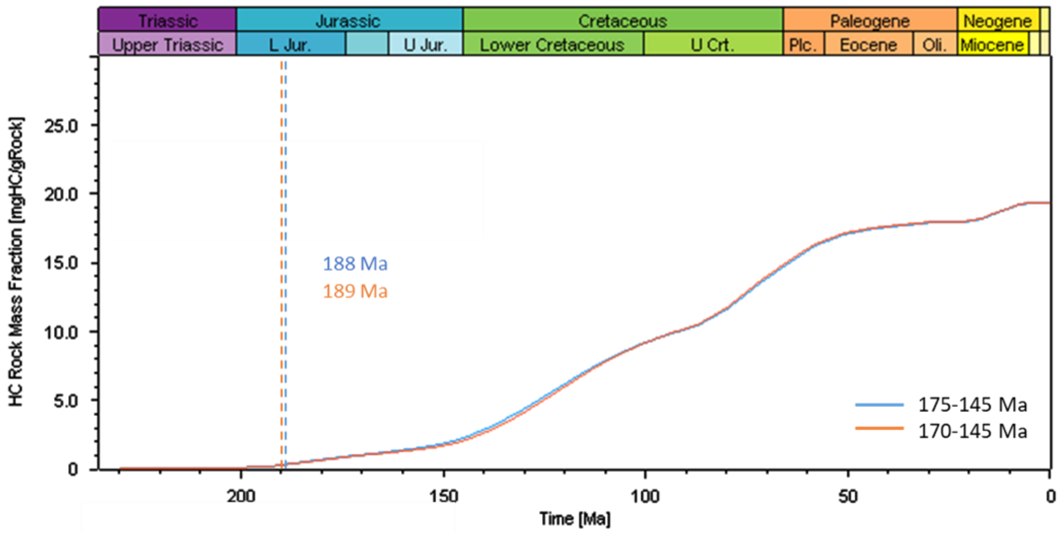

Figure 64: Generation Mass curves through geological time for the Triassic shales (PW-A). The colored curves present the rifting age variables. Generation mass values are in mg HC/g Rock and time values are in Ma. The parameters used are presented in Table 18.

4.3.4.4 Petroleum Expulsion

Observing the expulsion curves of the Triassic and Posidonia source rocks as modeled (Figures 67-69) it is clearly suggested that the slight sift of the rifting age from 170 Ma to 175 Ma has almost no impact on the expelled volumes of hydrocarbons.

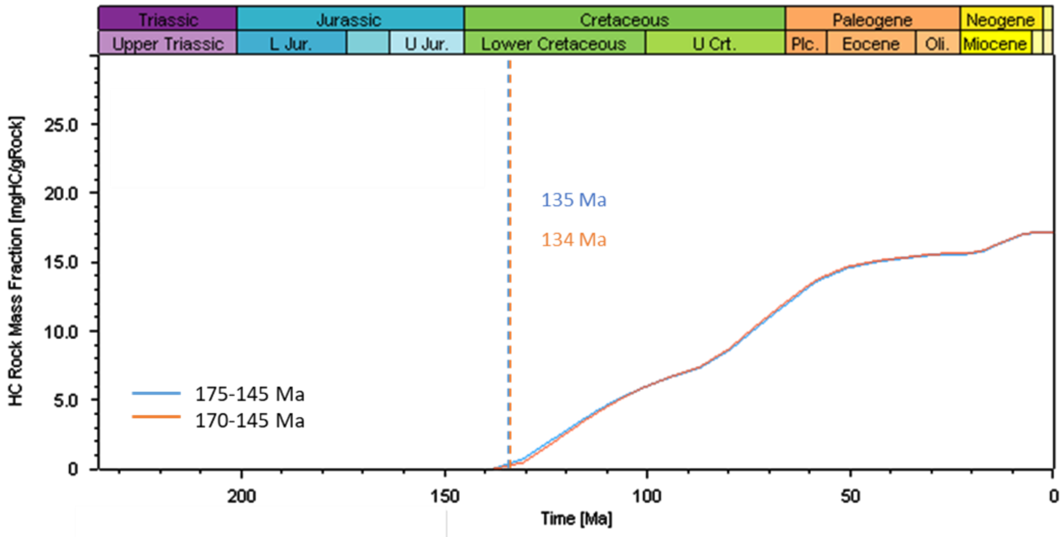

Figure 65: Expulsion Mass curves through geological time for the Triassic shales (PW-A). The colored curves present the rifting age variables. Expulsion mass values are in mg HC/g Rock and time values are in Ma. The parameters used are presented in Table 18.

Expulsion plots for the pseudo-wells A and B are presented in Appendix II.

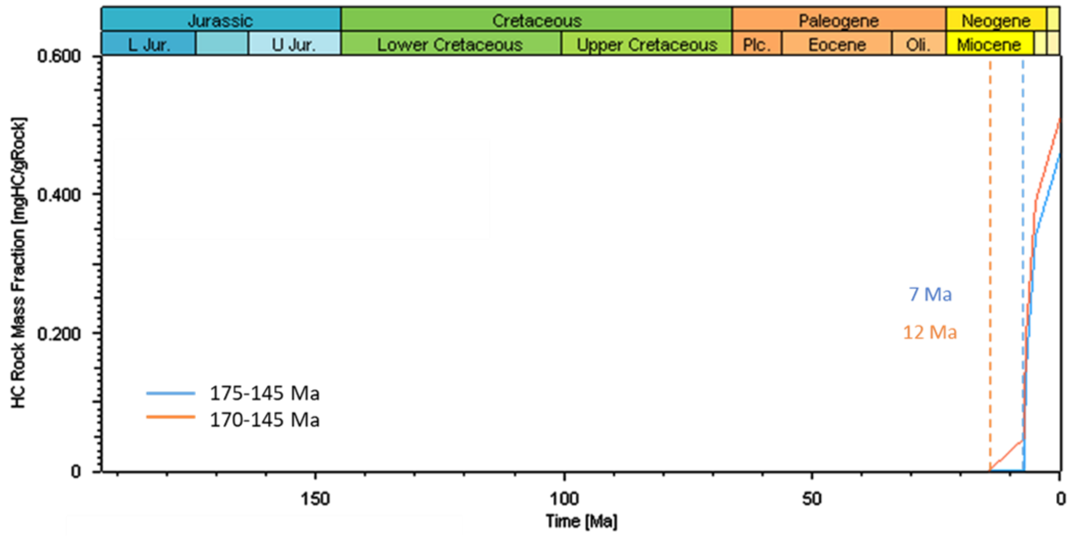

Figure 66: Expulsion Mass curves through geological time for the Posidonia shales (PW-A). The colored curves present the rifting age variables. Expulsion mass values are in mg HC/g Rock and time values in Ma. The parameters used are presented in Table 18.

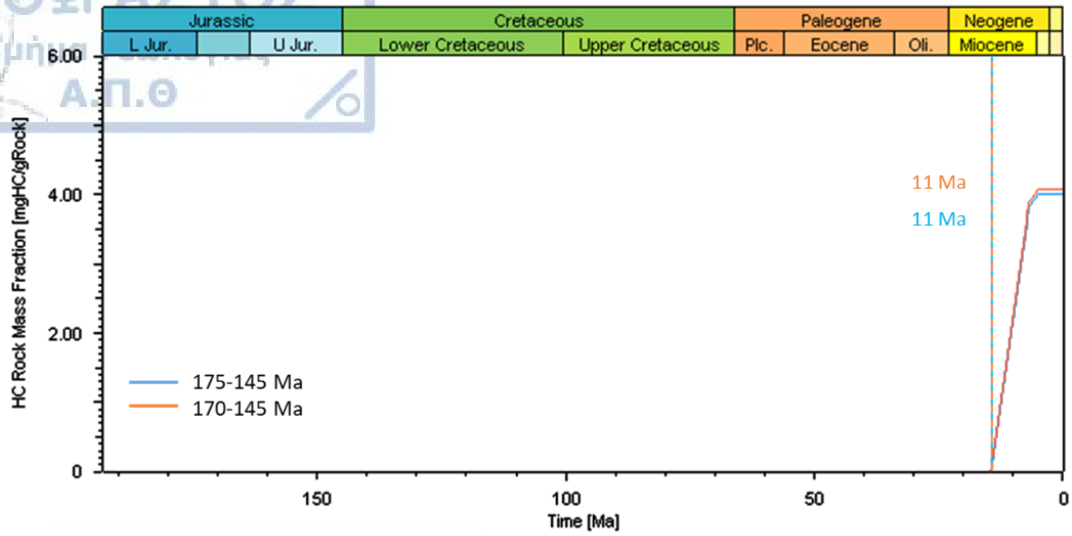

Figure 67: Expulsion Mass curves through geological time for the Posidonia shales (PW-B). The colored curves present the rifting age variables. Expulsion mass values are in mg HC/g Rock and time values are in Ma. The parameters used are presented in Table 18.

4.4 Summary

The results of the sensitivity analysis suggest significant impact of the studied parameters on the thermal regime of the studied area and therefore, on the thermal and maturity modeling. Tables 23 and 24 summarize the impact of the sensitivity variables on numerous parameters which were studied for the western Patraikos Gulf area (western Greece). Also, the Figures 70-74 illustrate the sensitivity analysis of the generation and expulsion processes in terms of timing.

The variation of crustal thickness has a minor impact on present-day heat flow values. However, the maximum value of paleo-heat flow and thermal distribution through time are crustal thickness dependent. Beta-factor variations' have also the same impact on heat flow values. While the radioactive heat and rifting age change, the heat flow curves follow a normal decreasing trend.

A minor impact on the onset of the oil window in terms of timing is also observed, with the crustal thickness variation (this does not mean that is generally applied as it has already mentioned in paragraph 4.3.1.2). Moreover, changes of crustal thickness have a low impact on generation critical times for the three modeled source rocks. A reduction of mass fraction, due to the increasing crustal thickness, is observed. This variation also significantly affects the expulsion critical times for the Triassic shales. The total expulsion masses through time are affected too from the variation on crustal thickness. The thinner the crust is, the higher the expelled volumes are.

Increasing beta factor notices a single generation and expulsion phase at recent times for the Posidonia and Vigla shales (Vigla shales do not expel hydrocarbons) and two periods with increasing generation and expulsion mass volume for the Triassic shales.

The variation of rifting age has a minor impact on generation critical times for the three source rocks. Conversely, the increase of radioactive heat reflects in a rapid change in generation critical times. Expulsion critical times affected by all parameters, except the rifting age. There is a great range in expulsion critical times with the variation of the parameters.

Figure 70 and 71 presents the sensitivity analysis in generation and expulsion processes for the Triassic shales. Generation time ranges between 200-160 Ma (Lower Jurassic to Upper Jurassic). Additionally, expulsion times for the Triassic shales range between 170- 80 Ma (Middle Jurassic to Campanian). However, the variation of expulsion timing is greater comparing to variation of generation timing. Considering the different scenarios, there is a significant distribution in temperatures through geological time. The thermal regime (various peak heat flow values) in both scenarios creates different conditions in the basin. These conditions could affect the expulsion critical times.

Table 23: Sensitivity analysis results for both pseudo-wells. This table summarizes the impact of the increasing parameters on Triassic shales.

	Impact of the sensitivity variables			
Parameters at the study area	**Crustal Thickness**	**Beta Factor**	**Radioactive Heat**	**Rifting Age**
Peak Heat Flow	High	High	Mean	Mean
Present Day Heat Flow	Low	Low	Mean	Mean
Depth of Onset of oil window	Low	High	High	Low
Vitrinite Reflectance	Low	High	High	Low
Generation Critical Time	Low	Low	High	Low
Expulsion Critical Time	High	High	High	Low
Generation Mass Trend	Low	High	High	Low
Expulsion Mass Trend	High	High	High	Low

Table 24: Sensitivity analysis results for both pseudo-wells. This table summarizes the impact of the increasing parameters on Posidonia and Vigla shales.

	Impact of the sensitivity variables			
Study area parameters	**Crustal Thickness**	**Beta Factor**	**Radioactive Heat**	**Rifting Age**
Peak Heat Flow	High	High	Mean	Mean
Present Day Heat Flow	Low	Low	Mean	Mean
Depth of Onset of oil window	Low	Low	Low	Low
Vitrinite Reflectance	Low	Low	Low	Low
Generation Critical Time	Low	Low	Low	Low
Expulsion Critical Time	Low	Low	Low	*High (PW-A)
Generation Final Volume	Low	Low	High	Low
Expulsion Final Volume	High	Low	High	*High (PW-A)

**As it has already mentioned Posidonia shales behave different in pseudo-well A comparing to pseudo-well B with the variation of rifting age.*

Generation time ranges between 15- 11 Ma and 12- 10 Ma for Posidonia and Vigla shales, respectively. Posidonia shales are capable to expel hydrocarbons in some cases, whereas Vigla shales do not expel hydrocarbons. Expulsion time for Posidonia ranges from 14 to 5 Ma. Minor differences in Posidonia's expulsion critical times are observed.

It is worthwhile to mention that Triassic shales generate and expel earlier hydrocarbons in pseudowell-A comparing to pseudowell-B in both scenarios. Similar behavior is observed for Posidonia shales, except in some cases in which the critical times are the same in both pseudowells.

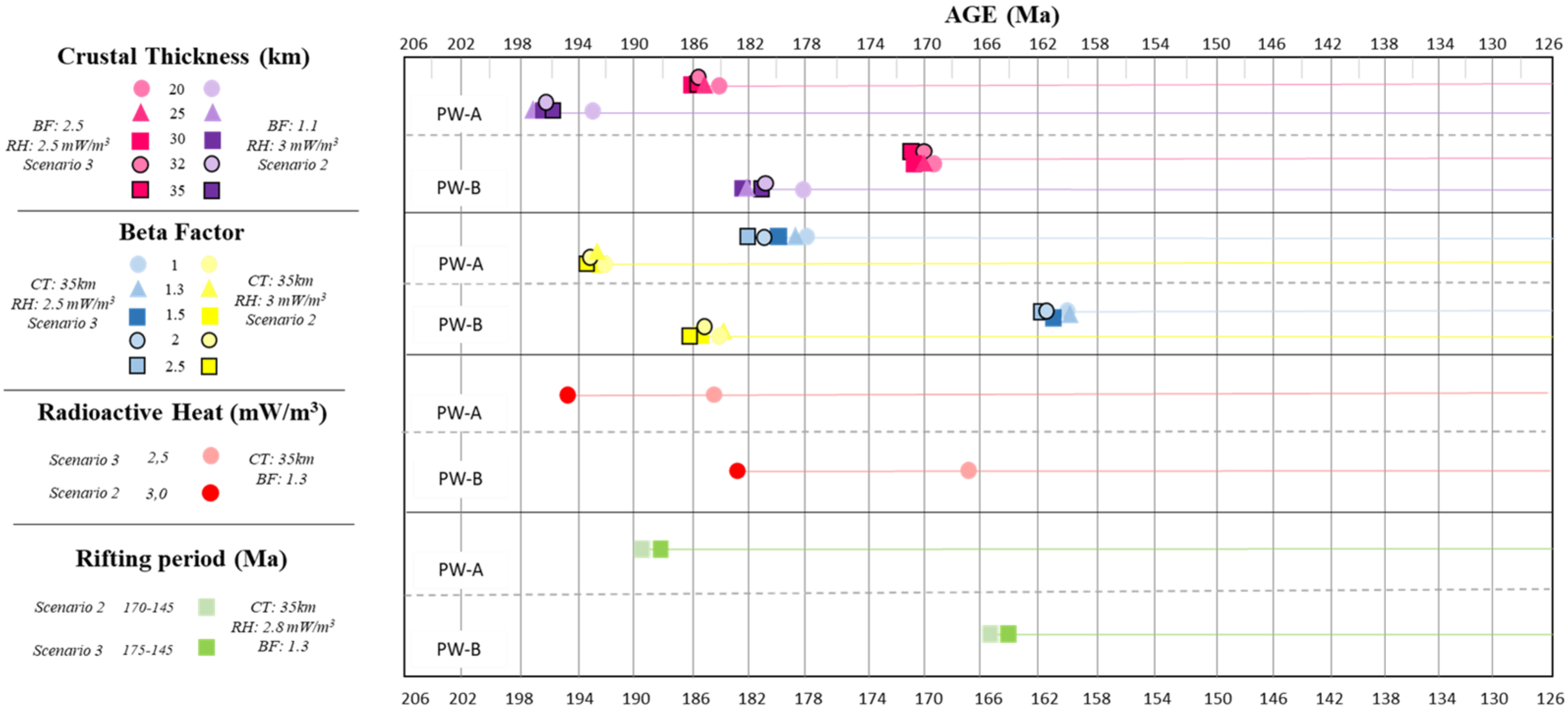

Figure 68: Sensitivity analysis results for Triassic shales generation critical times using PetroMod software. Critical times are in Ma.

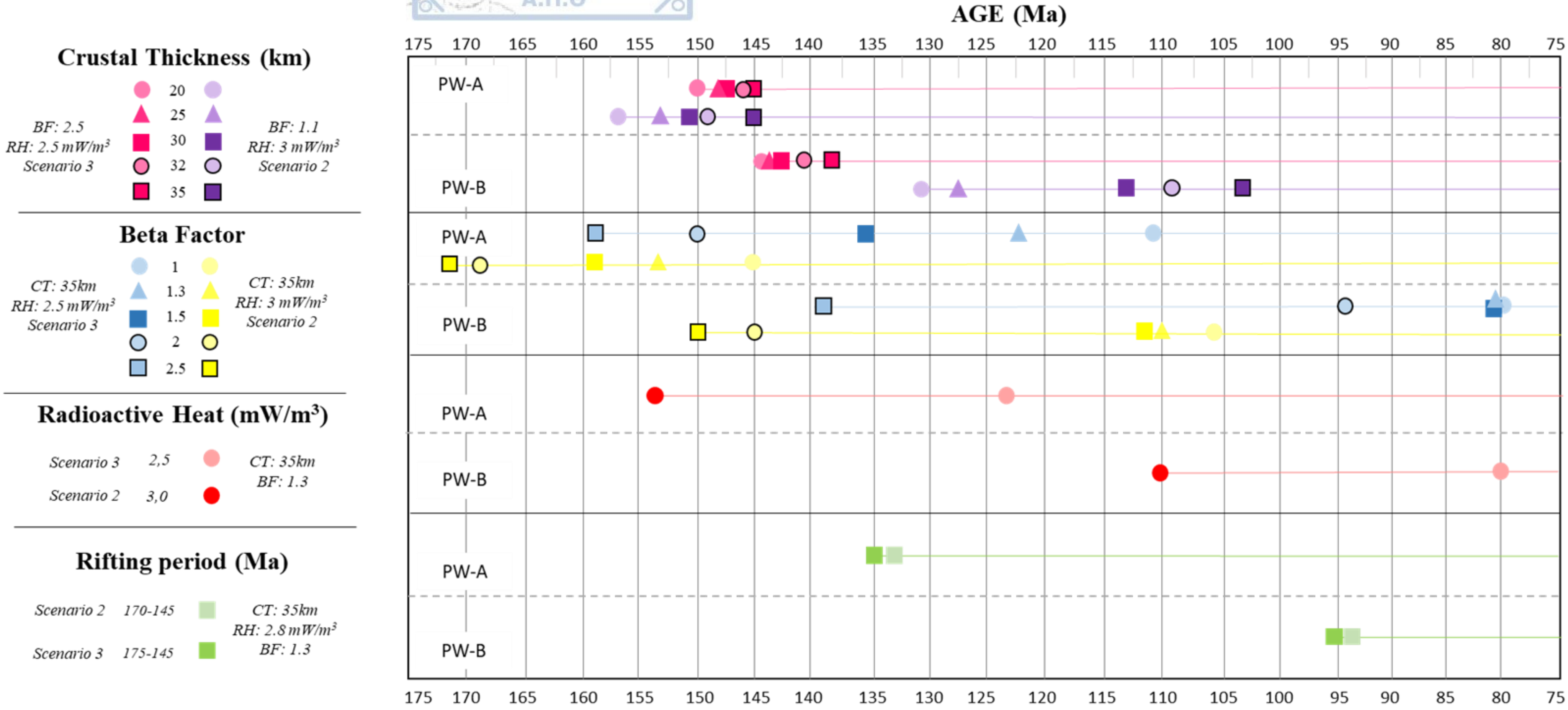

Figure 69: Sensitivity analysis results for Triassic shales expulsion critical times using PetroMod software. Critical times are in Ma.

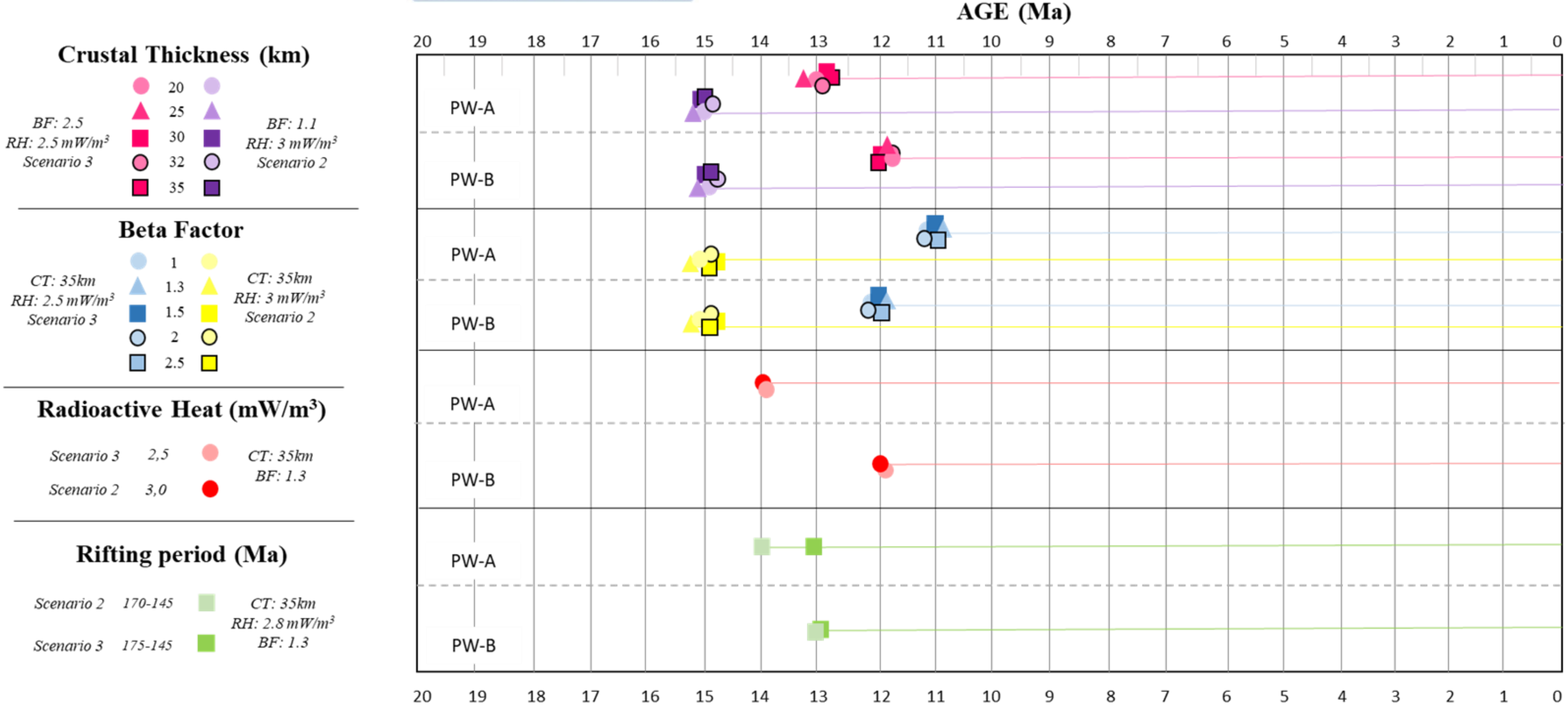

Figure 70: Sensitivity analysis results for Posidonia shales generation critical times using PetroMod software. Critical times are in Ma.

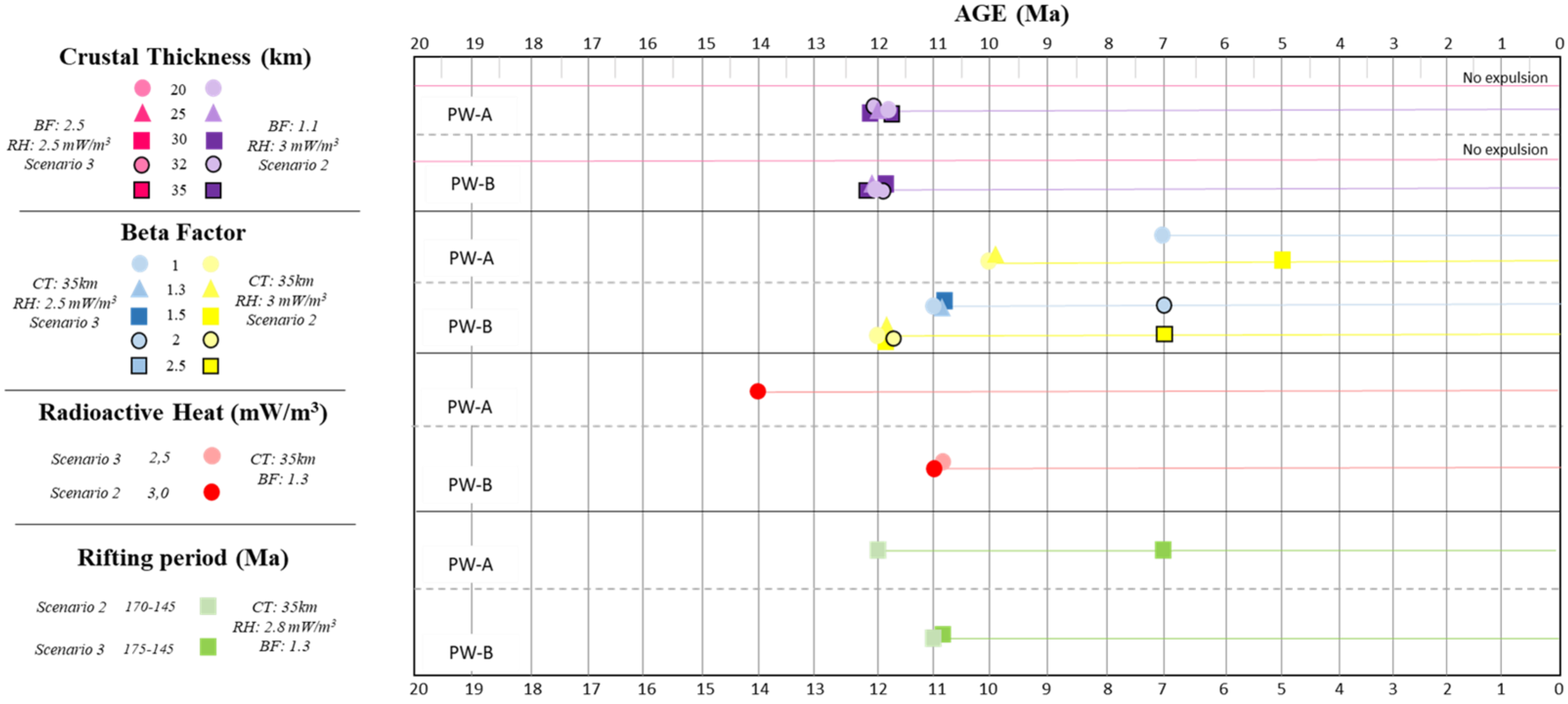

Figure 71: Sensitivity analysis results for Posidonia shales expulsion critical times using PetroMod software. Critical times are in Ma.

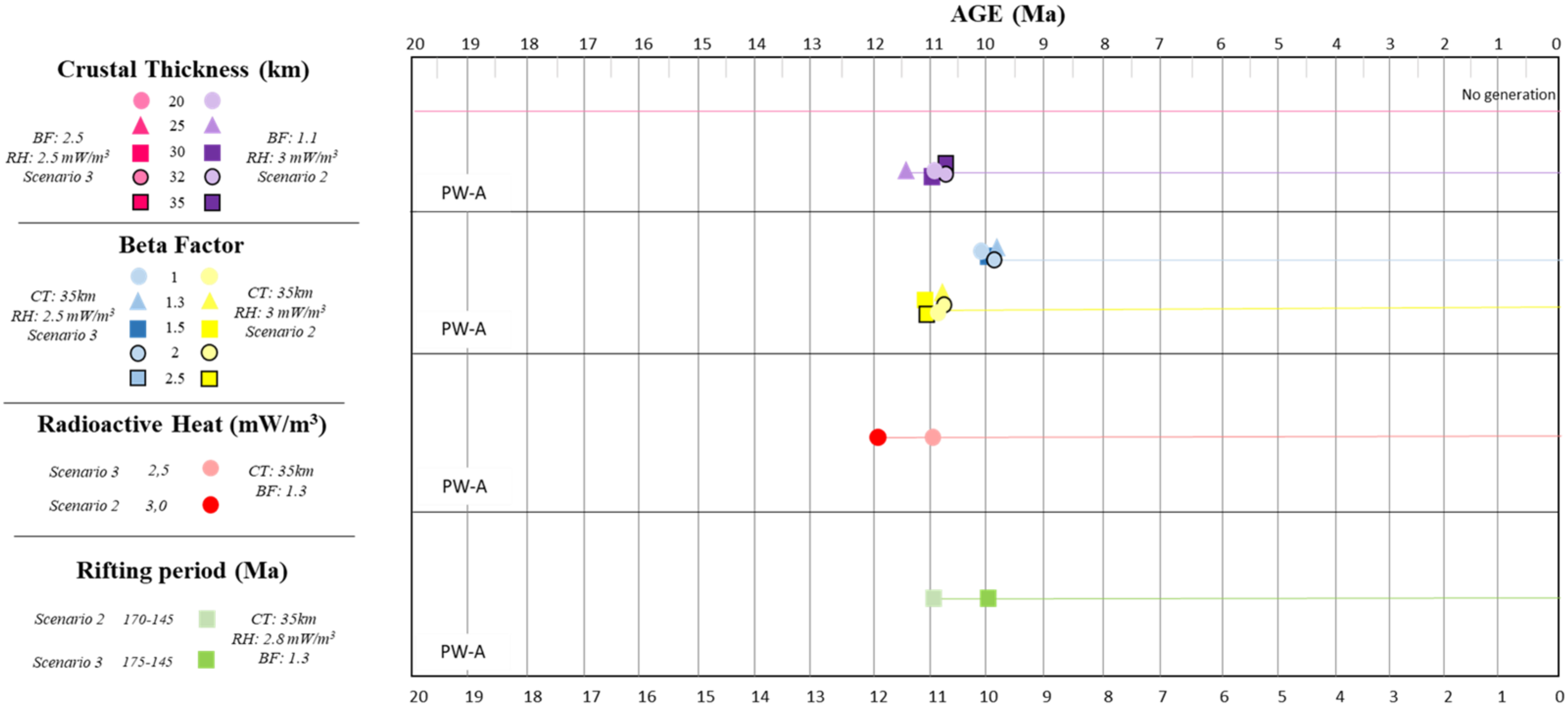

Figure 72: Sensitivity analysis results for Vigla shales generation critical times using PetroMod software. Critical times are in Ma.

Chapter 5: Source rock quality characteristics sensitivity analysis

5.1 Introduction

Source rock quality Sensitivity analysis based on the major quality parameters of the modeled source rocks, named Total Organic Carbon (TOC), Hydrogen Index (HI) and Source Rock Thickness (SRT) was applied. The above-mentioned quality parameters significantly affect the generated volumes of hydrocarbons, whereas these have no impact on the critical timing of the hydrocarbons' maturation, generation and expulsion. Separate sensitivity analysis was applied for each of the studied parameters.

5.2 Data inputs

Tables 25, 26 and 27 present the sensitivity variables for each of the studied parameters (TOC, HI and SRT). The applied values for the modeled source rocks are based on published data (Rigakis, 1999) and HELPE internal reports. The thermal regime remains the same for the three sensitivity variables and is based on the values shown in Table 2 for scenario 1.

Table 25: Values used in the TOC sensitivity analysis.

Source Rock	TOC (%)		
	Minimum	Median	Maximum
Triassic Shales	1.5	3	6
Posidonia Shales	1	2	4
Vigla Shales	1	1.8	3.6

Table 26: Values used in the HI sensitivity analysis.

Source Rock	HI (mg HC/ g TOC)		
	Minimum	Median	Maximum
Triassic Shales	600	650	700
Posidonia Shales	550	600	650
Vigla Shales	450	500	550

Table 27: Values used in the source rock thickness sensitivity analysis.

Source Rock	Source Rock Thickness (m)		
	Minimum	Median	Maximum
Triassic Shales	25	30	60
Posidonia Shales	40	60	100
Vigla Shales	40	60	100

5.3 Results and discussion

5.3.1 Total Organic Carbon (TOC)

TOC value varies from 0 to 100%, however any source rock is unlikely to expel oil if it has a TOC < 0.5%.

5.3.1.1 Petroleum Generation

According to the generation mass plots through geological times (Figure 75), the reduction of the TOC values by half results in the decrease of the generation mass volume almost by half. When the TOC value is doubled, the generation volume is also doubled (Figure 76).

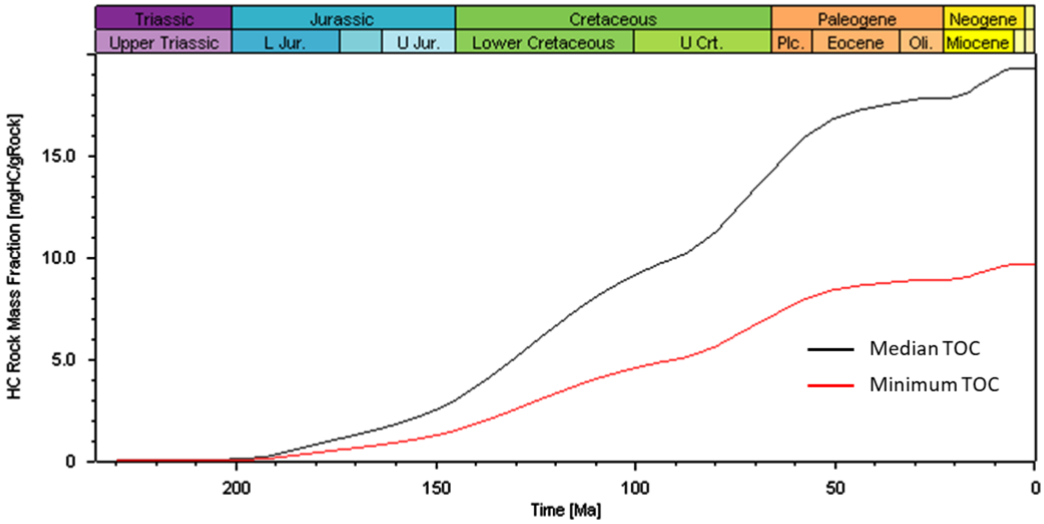

Figure 73: Generation Mass curves through geological time for the Triassic shales (PW-A). The colored curves present the minimum and median TOC. Generation mass values are in mg HC/g Rock.

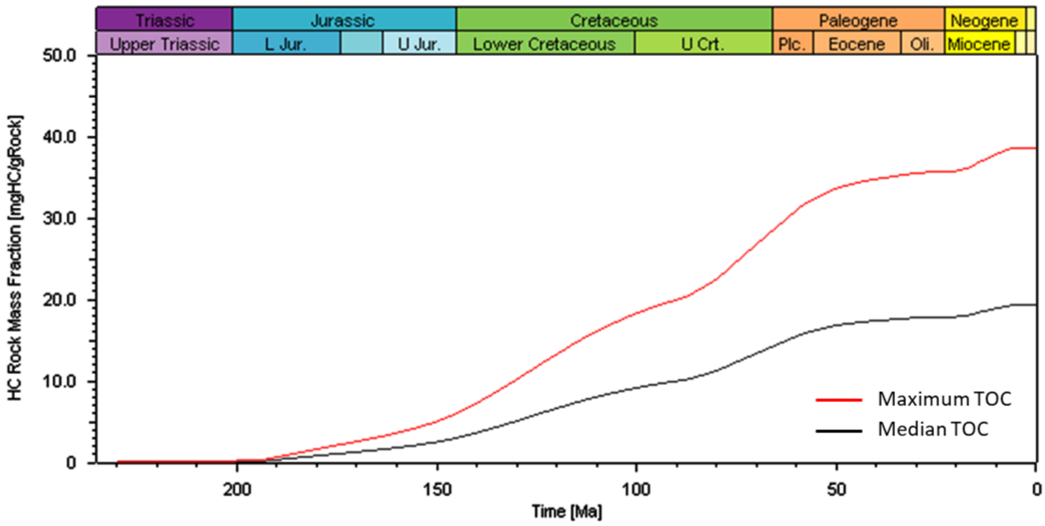

Figure 74: Generation Mass curves through geological time for the Triassic shales (PW-A). The colored curves present the median and maximum TOC. Generation mass values are in mg HC/g Rock.

The variation of the TOC values has the same impact on the generation of hydrocarbon volume for the three modeled source rocks. Table 28 lists information for the generation final masses in pseudo-well A, whereas generation plots for Posidonia and Vigla shales are included in Appendix III (Figure A.III.1). In pseudo-well B the same TOC variations for the three source rocks are observed [generation mass plots are presented in Appendix III (Figures A.III.3)].

Table 28: Generation final masses for the three modeled source rocks using the variables of Table 25. Generation masses at present day are in mg HC/ g Rock.

Results		Minimum	Median	Maximum
Generation Mass at present day (mg HC/g Rock)	**Triassic Shales**	9.62	19.43	38.60
	Posidonia Shales	1.44	2.9	5.77
	Vigla Shales	0.71	1.28	2.55

5.3.1.2 Petroleum Expulsion

The observations for the generated hydrocarbons are also consistent with the expulsion mass plots. The expulsion mass decreases by half when the TOC is reduced by half, whereas there is a double increase in expulsion volume when TOC is double. Figures 77 and 78 illustrate the expulsion mass plots for the Triassic shales. Expulsion mass plots for the Posidonia shales are presented in Appendix III (Figures A.III.2). Vigla shales are not capable to expel hydrocarbons at the given location of the pseudo-wells A and B.

The variation of the TOC values in pseudo-well B, has the same impact for the three source rocks, such as in pseudo-well A. Expulsion plots for pseudo-well B are presented in Appendix III (Figures A.III.4).

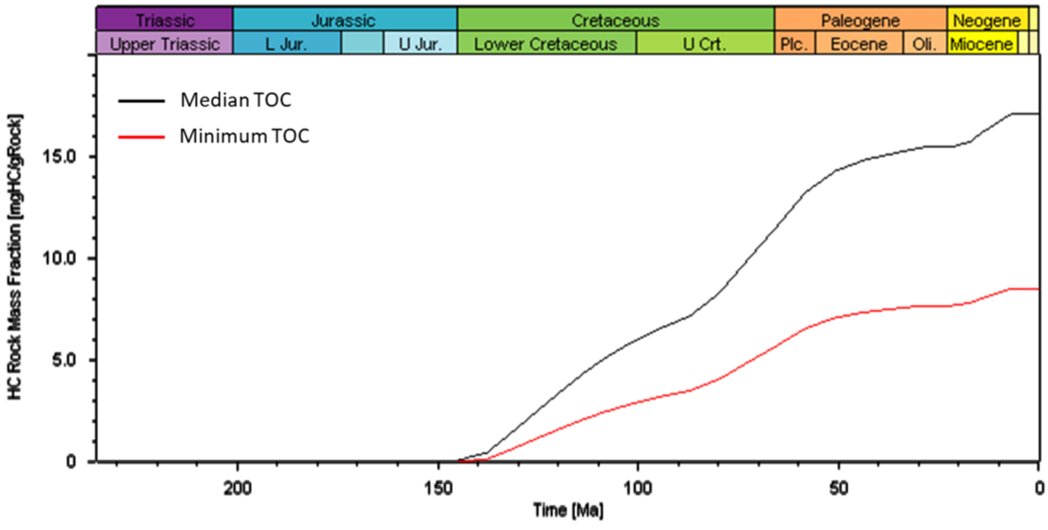

Figure 75: Expulsion Mass curves through geological time for the Triassic shales (PW-A). The colored curves present the minimum and median TOC. Expulsion mass values are in mg HC/g Rock.

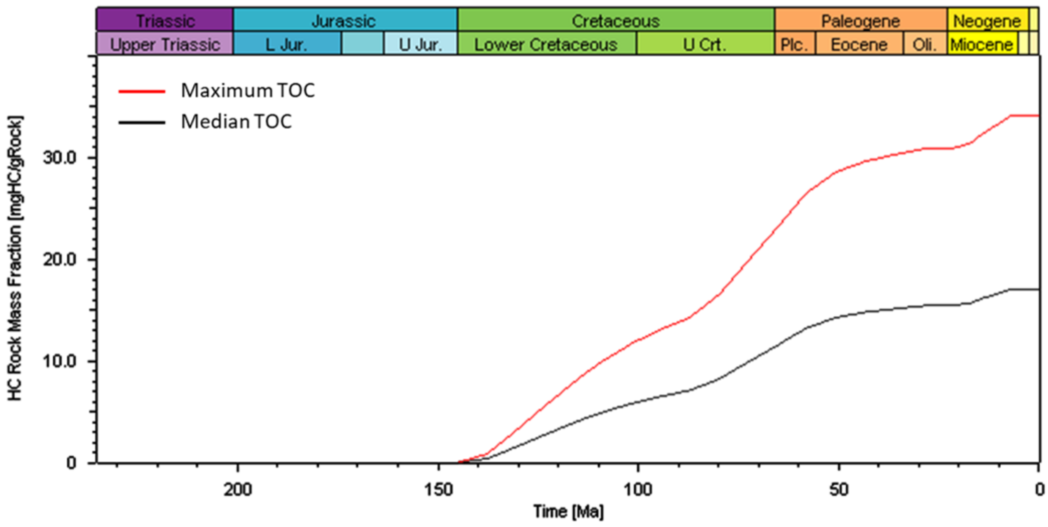

Figure 76: Expulsion Mass curves through geological time for the Triassic shales (PW-A). The colored curves present the median and maximum TOC. Expulsion mass values are in mg HC/g Rock.

Table 29 lists information for the expulsion volume in pseudo-well A, whereas the data for the generation and the expulsion of hydrocarbons for pseudo-well B are included in Appendix III (Tables III.1-2).

Table 29: Expulsion final masses for the three modeled source rocks using the variables of Table 25. Expulsion masses at present day are in mg HC/ g Rock.

Results		Minimum	Median	Maximum
Expulsion Mass at present day (mg HC/g Rock)	Triassic Shales	8.00	17.08	34.81
	Posidonia Shales	0.09	0.31	0.74
	Vigla Shales	-	-	-

5.3.2 Hydrogen Index (HI)

Hydrogen index (HI) is a direct indication of the capability of a source rock to generate hydrocarbons and is calculated from Rock-Eval data.

5.3.2.1 Petroleum Generation

According to the generation mass plots through geological times (Figures 79 and 80), the lower the HI the smaller the generation mass volume and vice versa. For example, when the HI is reduced by 50 units (mg HC/g TOC), then a decrease from 19.43 to 16.85 mg HC/g Rock for Triassic shales is observed (Figure 79).

The variation of HI has also the same impact on the generation mass volume for Posidonia and Vigla shales. Generation plots for Posidonia and Vigla shales are presented in Appendix III (Figure A.III.5), whereas Table 30 lists information for the generation final masses in pseudo-well A.

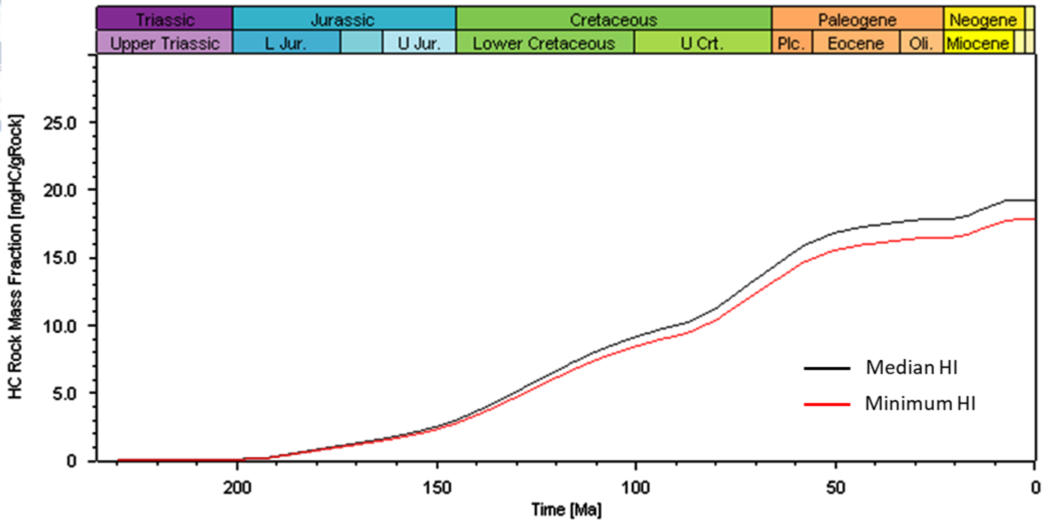

Figure 77: Generation Mass curves through geological time for the Triassic shales (PW-A). The colored curves present the minimum and median HI. Generation mass values are in mg HC/g Rock.

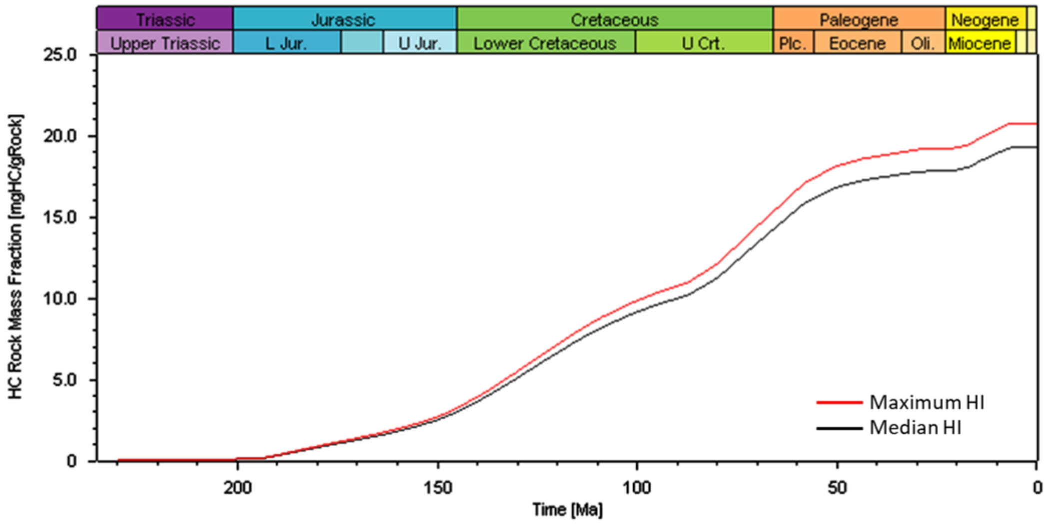

Figure 78: Generation Mass curves through geological time for the Triassic shales (PW-A). The colored curves present the median and maximum HI. Generation mass values are in mg HC/g Rock.

Table 30: Generation final masses for the three modeled source rocks using the variables of Table 26. Generation masses at present day are in mg HC/ g Rock.

Results		Minimum	Median	Maximum
Generation Mass at present day (mg HC/g Rock)	**Triassic Shales**	17.85	19.43	20.83
	Posidonia Shales	2.64	2.9	3.12
	Vigla Shales	1.15	1.28	1.41

In pseudo-well B the same variations for the modeled source rocks are observed. Generation mass plots and tables are presented in Appendix III (Figure A.III.7, Table III.3).

5.3.2.2 Petroleum Expulsion

The observations on the generation masses are also consistent with the expulsion mass plots. The expulsion mass decreases when the HI is reduced (Figure 81), whereas there is an increase in expulsion volume with increasing HI (Figure 82). For instance, the expelled hydrocarbon volume from the Triassic shales decreases from 17.08 to 15.4 mg HC/ g Rock when HI is reduced by 50 units. Expulsion mass plots for the Posidonia shales are presented in the Appendix III (Figure A.III.6).

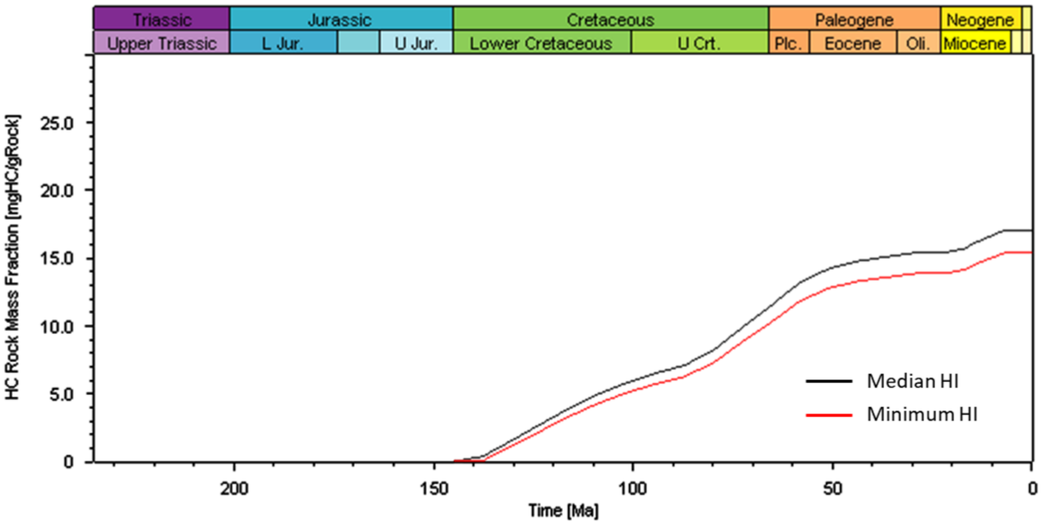

Figure 79: Expulsion Mass curves through geological time for the Triassic shales (PW-A). The colored curves present the minimum and median HI. Expulsion mass values are in mg HC/g Rock.

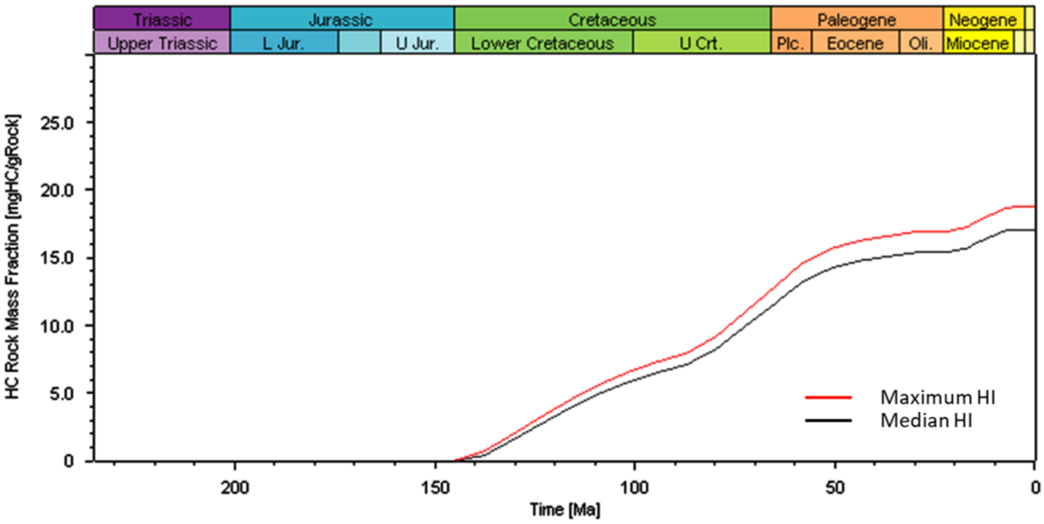

Figure 80: Expulsion Mass curves through geological time for the Triassic shales (PW-A). The colored curves present the median and maximum HI. Expulsion mass values are in mg HC/g Rock.

Table 31 lists information for the expulsion volume in pseudo-well A, whereas the variation of HI in pseudo-well B, has the same impact for the three source rocks, such as in pseudo-well A (expulsion plots and values in table format are included in the Appendix III Figure A.III.8 and Table III.4).

Table 31: Expulsion final masses for the three modeled source rocks using the variables of Table 26. Expulsion masses at present day are in mg HC/ g Rock.

Results		Minimum	Median	Maximum
Expulsion Mass at present day (mg HC/g Rock)	**Triassic Shales**	15.40	17.08	18.79
	Posidonia Shales	0.05	0.31	0.57
	Vigla Shales	-	-	-

5.3.3 Source Rock Thickness (SRT)

5.3.3.1 Petroleum Generation and Expulsion

Changing source rock thickness affects the generation and expulsion of the final volumes of hydrocarbons. This impact is clearly presented in charge diagrams for the three modeled source rocks. As expected, the timing of the generated and expelled final HCs' is not affected by thickness changes. Exceptions are those cases where thickness variation leads to the maturation on/off of the Posidonia SR due to burial depth variation.

The total expelled oil from the Triassic SR increases twice when the thickness is duplicated (from 30m to 60 m), whereas the expelled volumes are smaller when the thickness is reduced from 30 m to 25 m (Figure 83 and table 32). The same trend is also observed for the Posidonia and the Vigla shales (Figures 84 and 85; Table 32).

Table 32: Expelled oil and gas for the three modeled source rocks for the scenarios based on Table 27. Oil expelled values are in mmstb and gas expelled values are in bcf.

Source rock	Oil (mmstb)			Gas (bcf)		
	Minimum	Median	Maximum	Minimum	Median	Maximum
Triassic Shales	4006.86	4808.42	9616.85	1542.07	1850.42	3700.97
Posidonia Shales	68.87	103.31	172.18	6.88	10.32	17.20
Vigla Shales	5.59	8.38	13.97	0.56	0.83	1.38

Although minimum thicknesses for each source rock have been used, sufficient expelled hydrocarbons are observed. In the conservative scenario, Triassic shales are capable to expel almost 4000 mmstb oil and 1.5 tcf gas.

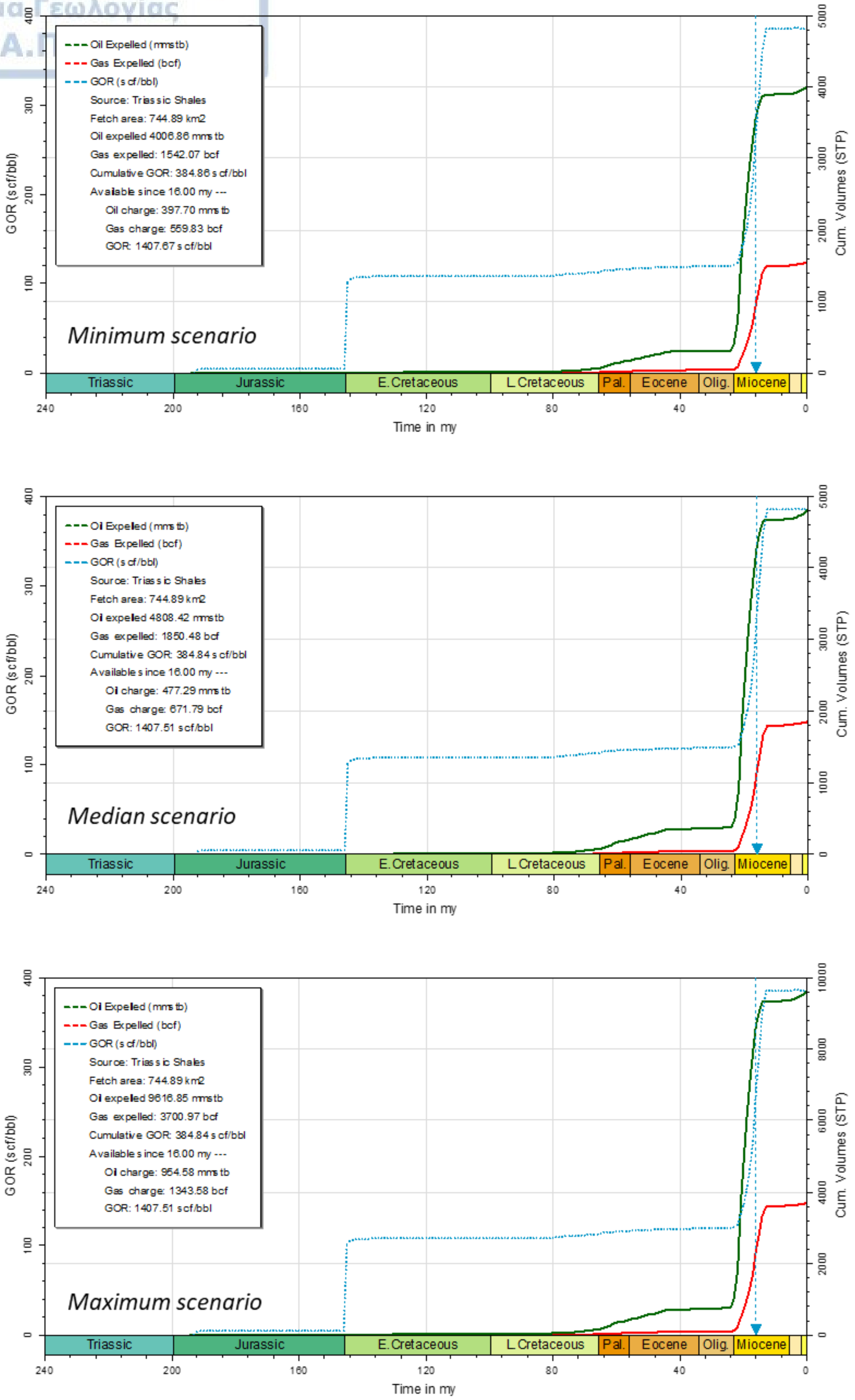

Figure 81: Expelled volume for the Triassic shales through geological time. Oil expelled values are in mmstb and gas expelled values are in bcf. The blue arrow represents the petroleum expelled volume which is available after thrusting period (16 Ma).

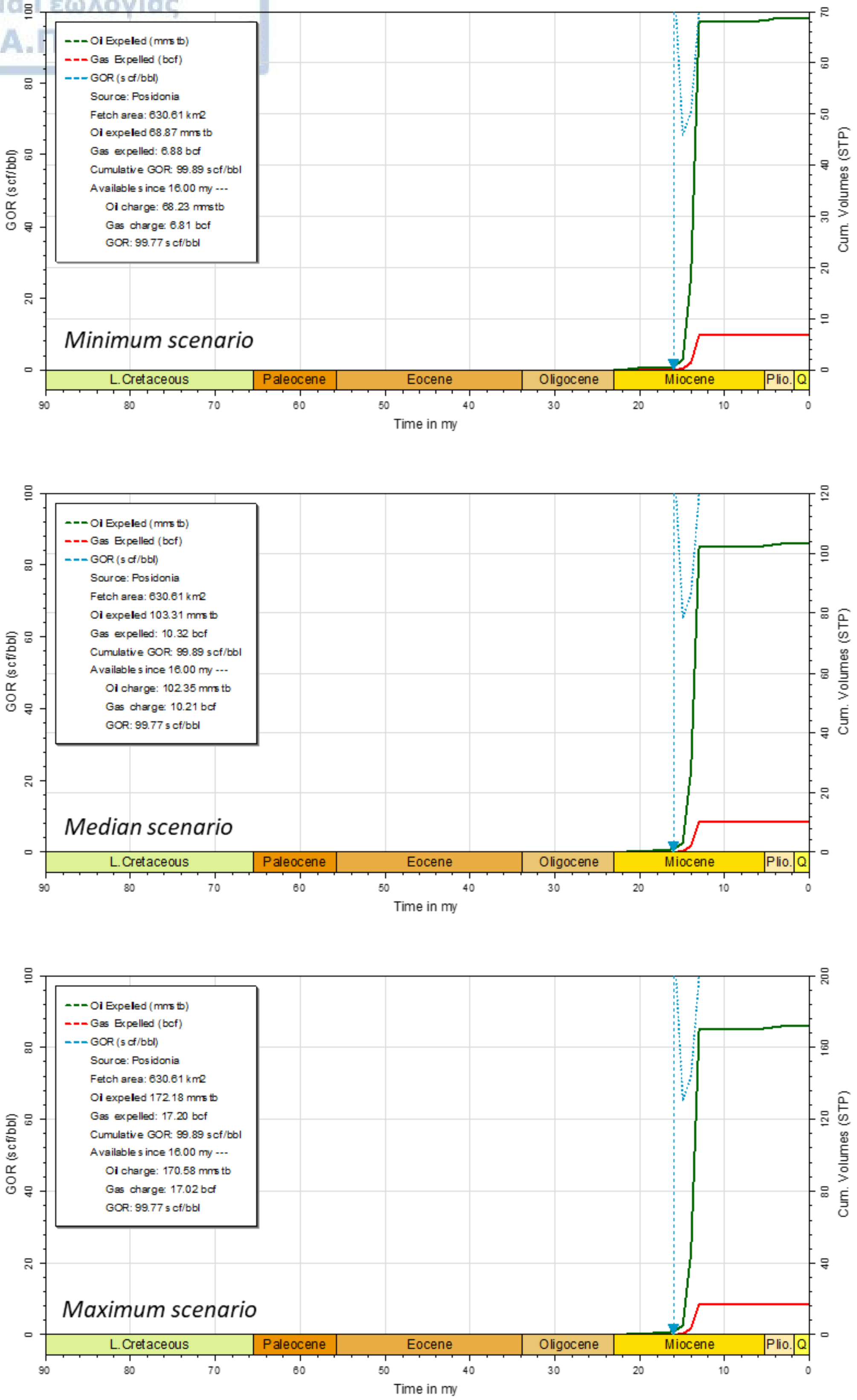

Figure 82: Expelled volume for the Posidonia shales through geological time. Oil expelled values are in mmstb and gas expelled values are in bcf. The blue arrow represents the petroleum expelled volume which is available after thrusting period (16 Ma).

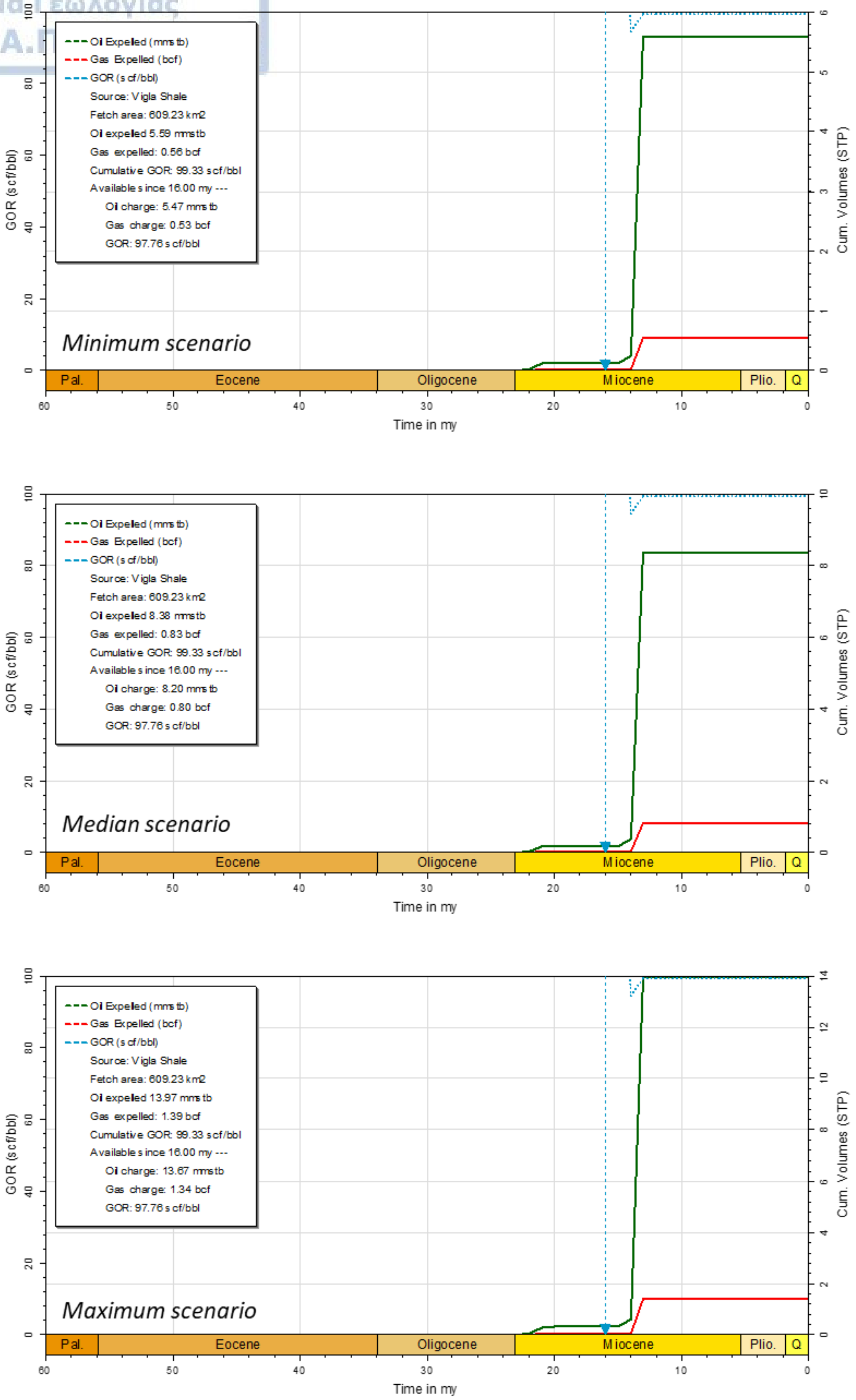

Figure 83: Expelled volume for the Vigla shales through geological time. Oil expelled values are in mmstb and gas expelled values are in bcf. The blue arrow represents the petroleum expelled volume which is available after thrusting period (16 Ma).

It is remarkable that in Agios Georgios-3 well (Western Greece), the Vigla shales are subdivided in two organic rich zones. The first zone amounts to 150 m thick. The second zone is characterized by approximately 200 m of thickness (Rigakis, 1999). Additionally, Posidonia shales show variations of thickness depending on their position in each half- graben. The lower Posidonia beds display a thickness of 150 m and upper Posidonia beds approximately 140 m (Karakitsios, 2013). As a result, if the kitchen location is close to the area, Posidonia and Vigla shales will expel big volumes of hydrocarbons.

5.3.4 Minimum VS Maximum values

The minimum and maximum values of TOC, HI and SRT were studied also in map view, in order to better understand the influence of source rock quality characteristics on the expelled and migrated hydrocarbons from the modeled source rocks. As expected, the maximum values for the TOC, HI and SRT result in larger volumes of hydrocarbons and present larger accumulations. No migration losses are taking into account in the modeled scenarios.

The migration maps of Figure 86 suggest a principal oil accumulation at the interpreted structural high of the modeled area due to the migration of the generated hydrocarbons from the deep kitchen area of the Triassic shales. Smaller accumulations of hydrocarbons are also observed at different stratigraphic levels. The volume of the principal accumulation increases (right map of Figure 86) due to the increasing values of the TOC, HI and source rock thickness. On the other hand, volume changes in the smaller accumulations are not observed. Similar variations are also noticed for the Posidonia and Vigla shales.

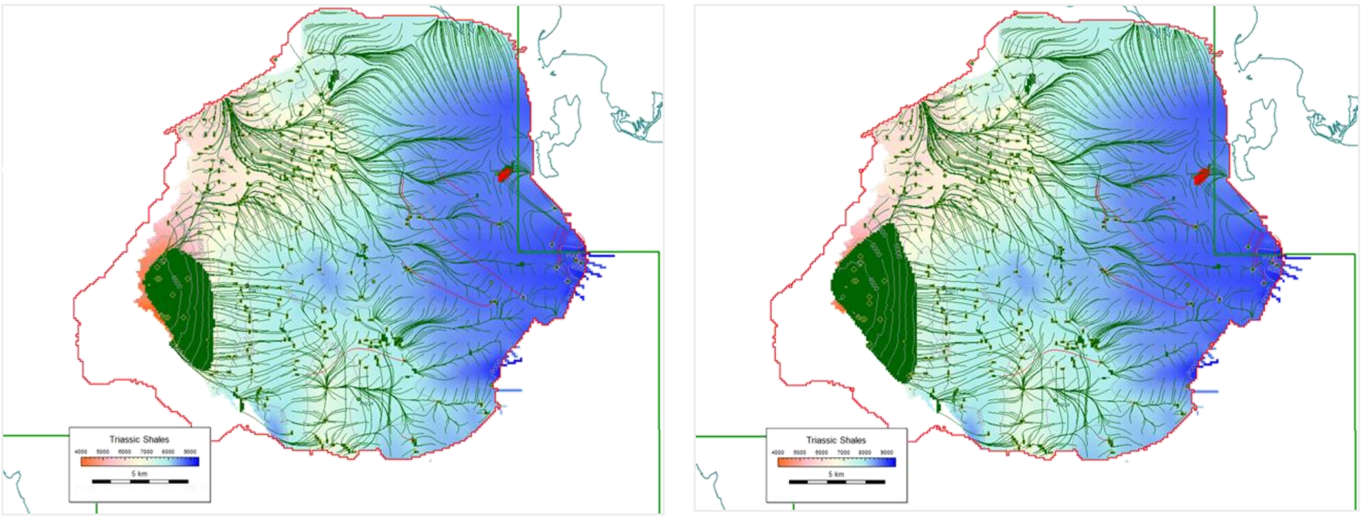

Figure 84: Migration and accumulation maps for Triassic shales. Left and right maps illustrate the minimum and maximum TOC, HI and source rock thickness, respectively.

Figures 87 and 88 illustrate the minimum and the maximum case of the total expelled volumes for the three modeled source rocks. Total oil expelled is estimated up to 751 mmstb and total gas expelled up to 254 bcf for the minimum TOC, HI and SRT values (Figure 87). Conversely, increasing these parameters results in 10642 mmstb and 3000 bcf expelled oil and gas, respectively (Figure 88).

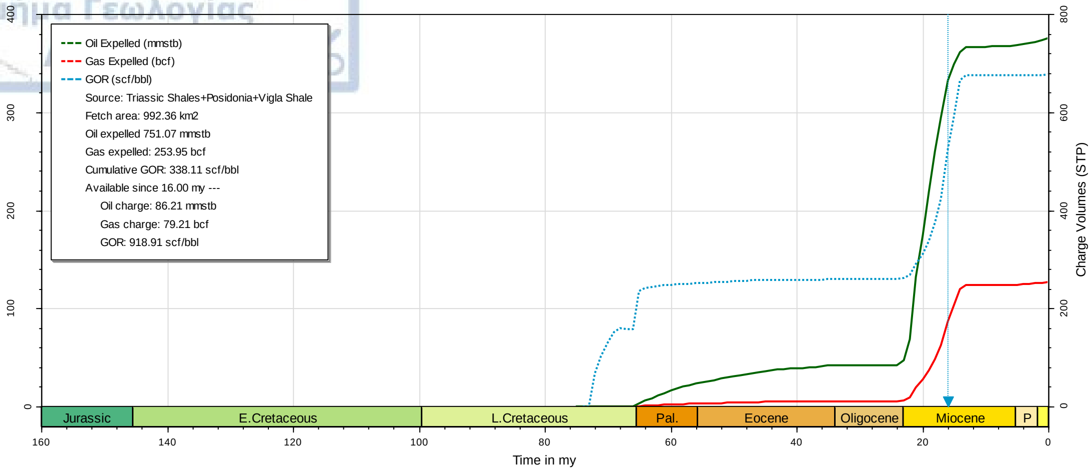

Figure 85: Total expelled volume for the three modeled source rocks through geological time (minimum case). Oil expelled is in mmstb and gas expelled in bcf. The blue arrow represents the petroleum expelled volume which is available after thrusting period (16 Ma).

It is significant that more oil and gas are expelled between 23 Ma and approximately 14 Ma, based on the charge diagrams. This is the main period of thrusting and little period of post thrusting. This observation enhances the idea that thrusting controls the expulsion process as modeled. It is also suggested that the most extensive petroleum generation occurs for the Triassic shales. Therefore, the Triassic shales could be considered as the most important source rock in terms of generation and expulsion volumes in the Patraikos Gulf, as modeled.

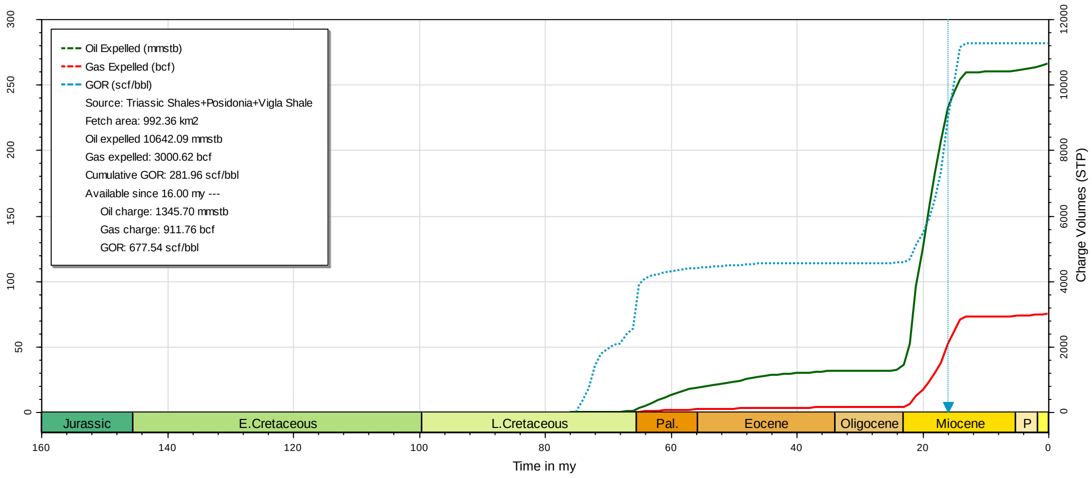

Figure 86: Total expelled volume for the three modeled source rocks through geological time (maximum case). Oil expelled values are in mmstb and gas expelled values in bcf. The blue arrow represents the petroleum expelled volume which is available after thrusting period (16 Ma).

5.4 Summary

Total organic carbon (TOC), hydrogen index (HI) and source rock thickness (SRT)are critical for the hydrocarbons' generated volumes. The variation of TOC values suggests substantial fluctuation in the volume of the generated hydrocarbons. HI and SRT have also great impact on the generated and expelled volume of hydrocarbons. This impact is clearly observed in charge diagrams and corresponding maps. Table 33 summarizes the sensitivity analysis results for the three modeled source rocks.

Table 33: Sensitivity analysis results for both pseudo-wells. This table summarizes the impact of the source rock quality characteristics on generation and expulsion final volumes.

Parameters	Minimum TOC, HI, SRT	Maximum TOC, HI, SRT
Generation Mass	Decrease	Increase
Expulsion Mass	Decrease	Increase

Chapter 6: Conclusions

The area of Patraikos Gulf in Western Greece represents a working petroleum system that consists of:

I. Three Mesozoic potential source rock intervals. The Triassic shales, the Middle-Upper Jurassic Posidonia beds and the Lower Cretaceous Vigla shales. The three potential source rocks differ in their lithology, thickness and geochemical characteristics such as Kerogen type, Total Organic Carbon (TOC) and Hydrogen Index (HI). However, all the three source rocks are considered as oil- prone source rocks.
II. The Eocene limestones as reservoir. Senonian and Pantokrator limestones may be also considered as potential reservoirs at the area.
III. The Oligocene flysch is considered as the primary seal formation of the area. However, Miocene and Pliocene sediments may also act as a seal – the case of Katakolo.

The Triassic shales mainly consist of type I lacustrine organic matter having TOC values from 0.49% to 16.12% and HI 400 - 600 mg HC/ g rock. The Posidonia shales consist of type I-II marine oil-prone organic matter with TOC values from 1.05% to 19.12% and HI values 460- 565 mg HC/ g rock. The Vigla shales are dominated by oil-prone type I – II marine organic matter with TOC values from 0.94 to 5.00% and HI values 475-600 mg HC/ g rock (even higher TOC and HI values for Vigla shales have been reported in Agios Georgios 3 exploration well at the internal Ionian zone). The kitchen area of all the three potential source rocks is modeled towards east of the Patraikos Gulf area.

The timing of hydrocarbons' generation is controlled by the Early Miocene thrusting event for all the potential source rocks, as modeled. Thrusting resulted in duplication of the stratigraphic section thus increasing the burial depth of the potential source rocks and therefore the thermal stress of the organic matter due to the elevated temperature. The result is the maturation of the potential source rocks, the generation of hydrocarbons, their expulsion from the first carrier bed towards the modeled trap through vertical (mainly) and lateral migration.

Posidonia and Vigla shales generate hydrocarbons (oil) from early Miocene to present day, as modeled. The Triassic shales generated oil as early as lower Jurassic (~190 Ma) at given location (PW-A), whereas oil cracking to gas during early/ middle Miocene (~12 Ma).

The timing of the expelled hydrocarbons is also strongly dependent, as modeled, on the crustal thickness and the beta factor (β) parameters. These two parameters are considered as the most critical variables during the sensitivity analysis on the four specific parameters, which significantly affect the thermal regime of the area and thus the maturation of the potential source rocks. The generated volumes of hydrocarbons are affected by the total organic carbon (TOC), the hydrogen index (HI) and the thickness of the modeled source rocks.

The burial history diagrams suggest that the variation of crustal thickness affects the level of thermal maturity of the potential source rocks. The Triassic source rocks are shifted from the late oil window to the dry gas window (at present day) at a given location (PW-A) when crustal thickness increases, as modeled. The Jurassic source rocks are also shifted from middle oil window to peak oil window, as modeled. The timing of the expelled hydrocarbons is also shifted towards recent times when crust thickness decreases.

Increasing beta factor, the transformation ratio of the Triassic shales is accelerating, thus the generation of hydrocarbons occurs earlier, as modeled. Significant differences are also observed in the timing of the expelled hydrocarbons from the Triassic shales with beta factor variation. For Posidonia and Vigla shales, which generate hydrocarbons at late times, these observations are less apparent.

The radioactive heat variation shows positive correlation with the heat flow history and thus, the higher the radioactive heat the higher the paleo-heat flow. Therefore, the increase of the radioactive heat values results in the earlier maturation and thus generation/ expulsion of hydrocarbons from the Triassic source rocks. The expelled volumes of hydrocarbons are also increased, for all modelled source rocks.

The age variation of the Triassic rifting does not show any significant impact on the maturation, generation and expulsion of hydrocarbons from the source rocks.

The quality characteristics of the modeled source rocks do not impact the timing of hydrocarbons' generation; however, the values of TOC, HI and thickness have major impact on the final expelled volumes of hydrocarbons from the modeled source rocks. The duplication of TOC value results in the duplication of the final expelled volumes. The same trend is also followed when HI and thickness are increased.

References

Accordi, G.C. Federico, and J. Pignatti, 1998, Depositional history of a Paleogene carbonate ramp (western Cephalonia, Ionian Islands, Greece): Geologica Romana, v. 34, p. 131– 205.

Artemieva I., Thybo, 2013, Crustal thickness controlled by plate tectonics: A review of crust–mantle interaction processes illustrated by European examples: Tectonophysics 530-531 (2012) 18–49.

Aubouin, J., 1959, Contribution à l'étude géologique de la Grèce septentrionale: les confins de l'Epire et de la Thessalie: Annales Géologiques des Pays Helléniques, v. 9, p. 1– 483.

Beardsmore and Cull, 2001, Crustal Heat Flow. A Guide to Measurement and Modelling. x + 324 pp. Cambridge, New York, Melbourne

Beicip, 2014: New exploration opportunities in offshore western Greece and south Crete – A petroleum assessment report. YPEKA.

Bellas, S. M., 1997, Calcareous nannofossils of the Tertiary flysch (post-Eocene to early Miocene) of the Ionian zone in Epirus, NW Greece: Taxonomy and biostratigraphical correlations: Ph.D. thesis, Selbstverlag Fachbereich Geowissenschaftlichten, Berlin, Germany, p. 1–173.

BP (British Petroleum) Co., Ltd, 1971, The geological results of petroleum exploration in western Greece: Institute for Geology and Subsurface Research (now Institute of Geology and Mineral Exploration) Special Report 10, p. 1–73.

Burnham K. Alan, Sweeney J. Jerry, 1989, A chemical kinetic model of vitrinite maturation and reflectance: Geochimica et Cosmochimica Acta Volume 53, Issue 10, October 1989, Pages 2649-2657

Cavazza et al., 2004: The TRANSMED Atlas. The Mediterranean Region from Crust to Mantle

Dragastan O., Papanikos D. and Papanikos P. (1985). Foraminiferes, algues et microproblematica du Trias de Messopotamos, Epire (Grece continentale). Revue Micropaleontologie, v. 27, No 4, p. 244-24

Fleury J.-J. (1980). Les zones de Gavrovo-Tripolitza et du Pinde-Olonos (Grece continentale et Péloponnèse du Nord). Evolution d' une plate-forme et d' un bassin dans leur carde Alpin. Société Géologique du Nord, publication No 4, p. 1-651.

Getsos K., Pomoni-Papaioannou F., Zelilidis A., 2007. A carbonate ramp evolution in the transition from the Apulia platform to the Ionian basin during Early to Late Cretaceous (NW Greece), Bulletin of the Geological Society of Greece, Vol. 40 (1), 53-63 pp.

Hantschel and Kauerauf, 2009: Fundamentals of Basin and Petroleum Systems Modeling

Herodotus, 484–430 B.C. Histories: Book D, verse 195.

IGRS-IFP (Institut deGéologie et Recherches du Sous-solInstitut Français du Pétrole), 1966, Etude géologique de l'Epire (Grèce nord-occidentale): Technip eds., Paris, 306p.

inférieurs (Trias Supérieur) de la serie calcaire Ionienne en Epire (Grece continentale). Consequences stratigraphiques. Revue de Paleobiologie, v. 9, No I,ρ. 139-147.

Karakitsios V. and Tsaila-Monopolis S. (1990). Données nouvelles sur les niveaux

Karakitsios V., 2007. Structural Geology o Western Greece's fold-and-thrust belt, Challenge our Myths: Energy Conference & Exhibition, AAPG & AAPG European, 48 pp.

Karakitsios V., 2013. Western Greece and Ionian Sea petroleum systems, AAPG Bulletin, V.97, No.9, 1567-1595 pp.

Karakitsios V., Rigakis N., 2007. Evolution and petroleum potential of Western Greece, Journal of Petroleum Geology, Vol.30 (3), 197-218 pp.

Karakitsios, V., 1990, Chronologie et géométrie de l'ouverture d'un bassin et de son inversion tectonique: Le basin ionien (Epire, Grèce): Ph.D. thesis, University of Pierre and Marie Curie, Paris, France, 310 p.

Karakitsios, V., 1992, Ouverture et inversion tectonique du basin Ionien (Epire, Grèce): Annales Géologiques des Pays Helléniques, v. 35, p. 185–318.

Karakitsios, V., and F. Pomoni-Papaioannou, 1998, Sedimentological study of the Triassic solution-collapse breccias of the Ionian zone (NW Greece). Carbonates & Evaporites, v. 13, no. 2, p. 207–218

Karakitsios, V., and L. Koletti, 1992, Critical revision of the age of the basal Vigla limestones (Ionian zone, western Greece), based on nannoplankton and calpionellids, with paleogeographical consequences, in B. Hamrsmid and J. Young, eds., Proceedings of the 4th International Nannoplankton Association Conference, Prague, Czech Republic: Knihovnicka Zemniho Plynu a Nafty, September 1991, v. 14a, p. 165–177.

Kilias et. al., 2016: A geological cross-section through northern Greece from the Pindos to Rhodope Mountains: a field guide across the External and Internal Hellenides

Makris, J., 1977, Geophysical investigations of the Hellenides: Hamburger Geophysikalische Einzelschriften, v. 3

Mavrikas G. (1993). Evolution Cretacee-Eocene d' une plate-forme carbonatee des Hellenides Externes. La plate-forme des Ori Valtou ("massif du Gavrovo").

Mountrakis D., 2010. Geology and geotectonic evolution of Greece, University Studio Press, 373 pp.

Pasquale V., Verdoya M., Chiozzi P., Ranalli G., 1997. Rheology and seismotectonic regime in the northern central Mediterranean, Tectonophysics, 270, 239-257 pp.

Pomoni-Papaioannou F. and Tsaila-Monopolis S. (1983). Petrographical, sedimentological and micropaleontological studies of an evapori te outcrop, West of Ziros lake (Epirus-Greece). Rivista Italiana di Paleontologia e Stratigrafia, Milano, v. 88, No 3, p. 387-400

Pomoni-Papaioannou, F., V. Karakitsios, E. Kamberis, and F. Marnelis, 2004, Chevron-type halite and nodular anhydrite in the Triassic subsurface evaporites of the Ionian zone (western Greece): Bulletin of the Geological Society of Greece, v. 36, no. 1, p. 578–586.

publication No 20, p. 1-240.4, p. 124.

Rigakis N., 1999. Contribution to stratigraphic research on wells and outcrops of the Alpine formations in Western Greece, in relation to the petroleum generations efficiency of their organic matter, Ph.D. Thesis, University of Athens, 255 pp.

Rigakis N., Karakitsios V., 1998. The source rock horizons of the Ionian Basin (NW Greece), Marine and Petroleum Geology, 15, 593-617 pp.

Rigakis N., Karakitsios V., Marnelis F., Sotiropoulos Sp., 2013. Geological solutions concluded by Petroleum geochemical data in Western Greece, Bulletin of the Geological Society of Greece, Vol. XLVII 2013

Rigakis, N., Th. Noussinanos, F. Marnelis, and V. Karakitsios, 2004, Oil potential of pre-Apulian zone (ext. abs.): 10th International Congress of the Geological Society of Greece, Thessaloniki, Greece, April 15–17, 2004, p. 576–577.

Sheplev V.S, Reverdatto V.V., 1998. A Contribution to the Further Investigation of McKenzie's Rifting Model, Geophysics, 34(1-2), 63-76 pp.

Xanthopoulou I., 2020: Hydrocarbon migration and seal properties sensitivity analysis by applying 1D/2D/3D basin modeling, Patraikos Gulf, Western Greece, Master thesis

Appendix I: Literature maps

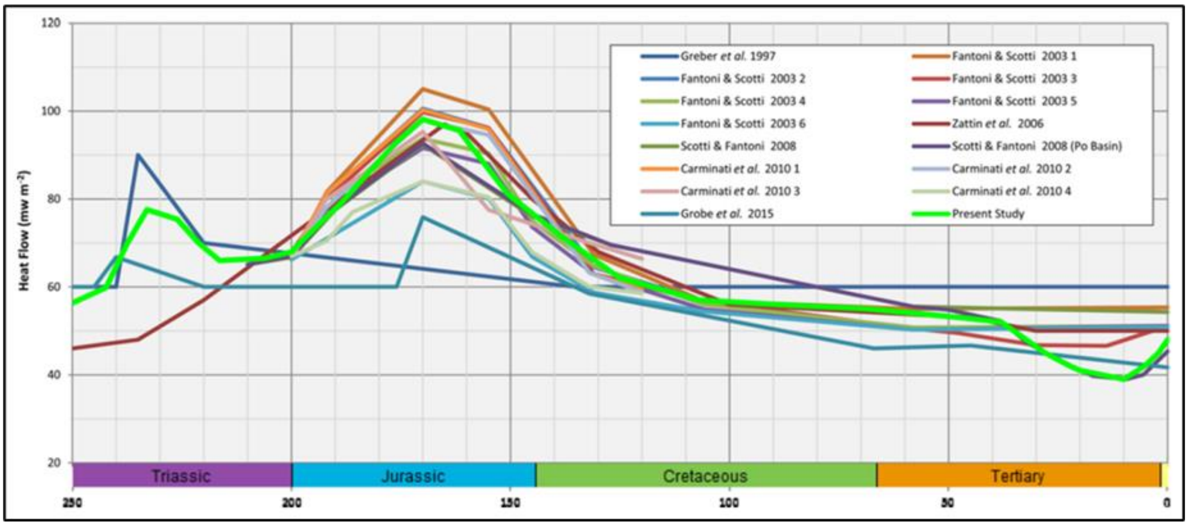

Figure A.I.1: The distribution of heat flow through time based on several studies.

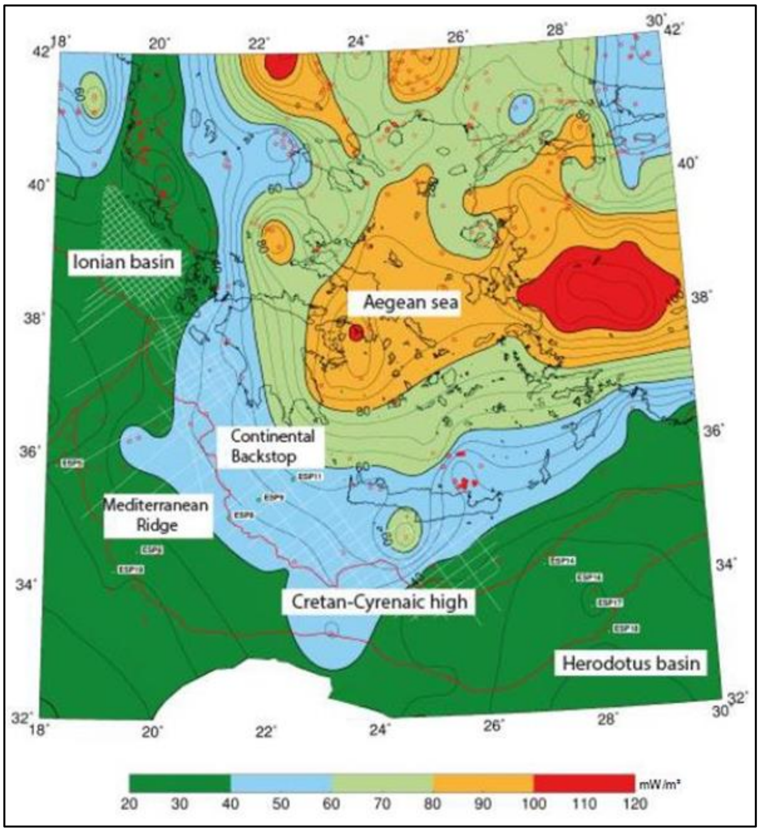

Figure A.I.2: Present day heat flow map for Greece (International Heat Flow Commission, Beicip 2014)

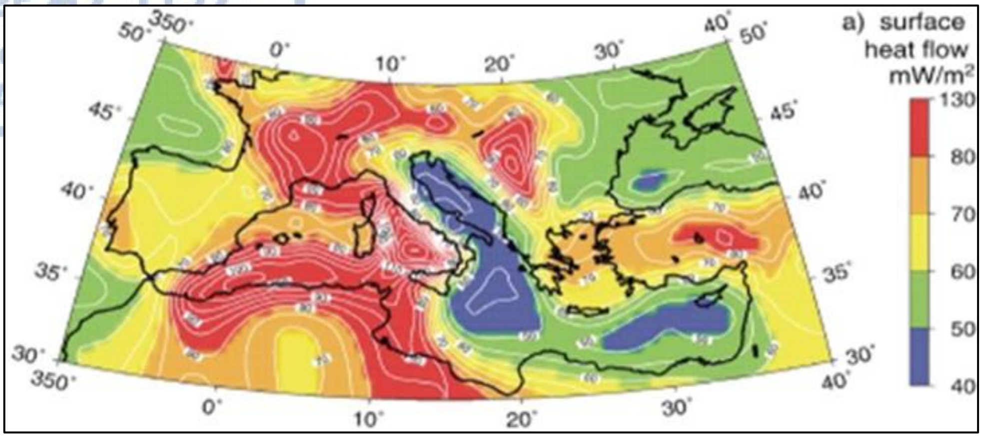

Figure A.I.3: Present day heat flow map (Cavazza et al., 2004).

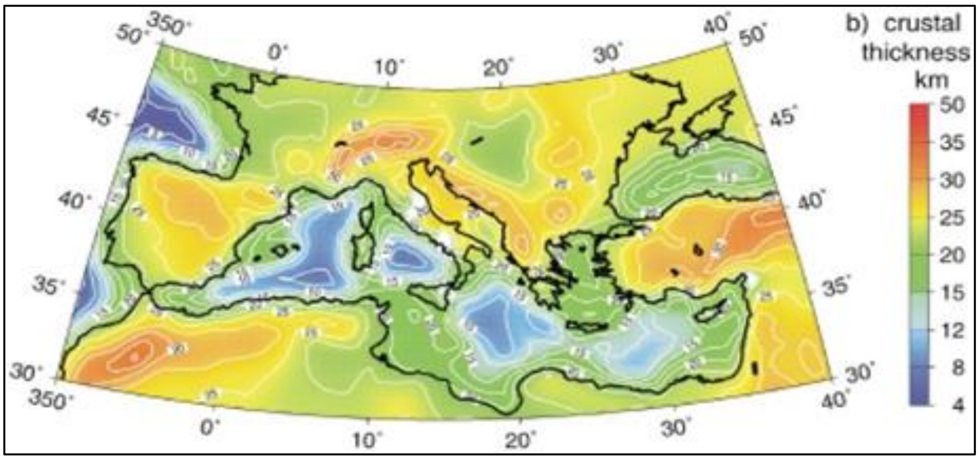

Figure A.I.4: Crustal thickness map (Cavazza et al., 2004).

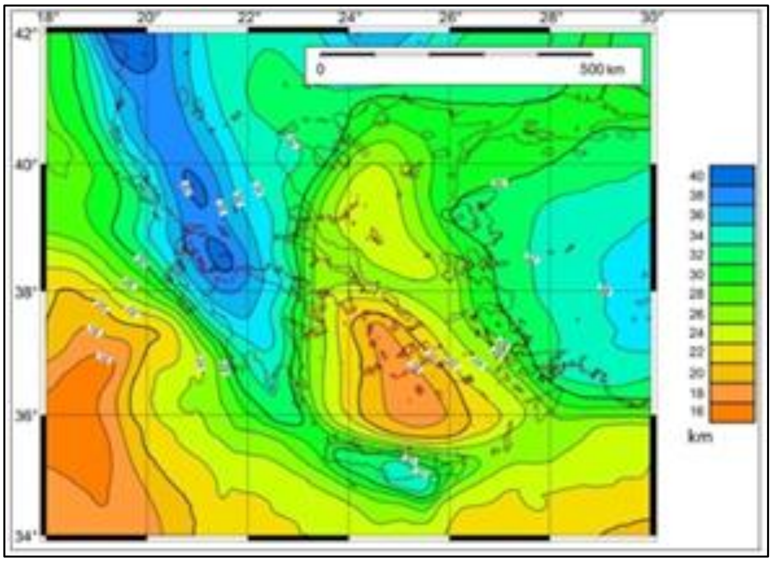

Figure A.I.5: Crustal thickness map (Makris et al., 2013).

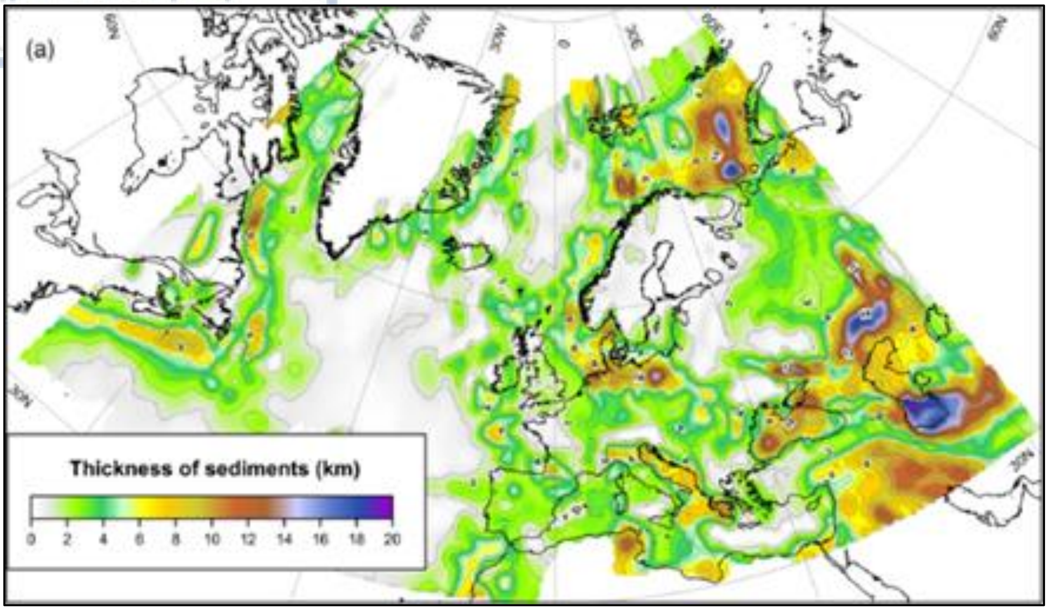

Figure A.I.6: Thickness of sediments (Artemieva and Thybo, 2013).

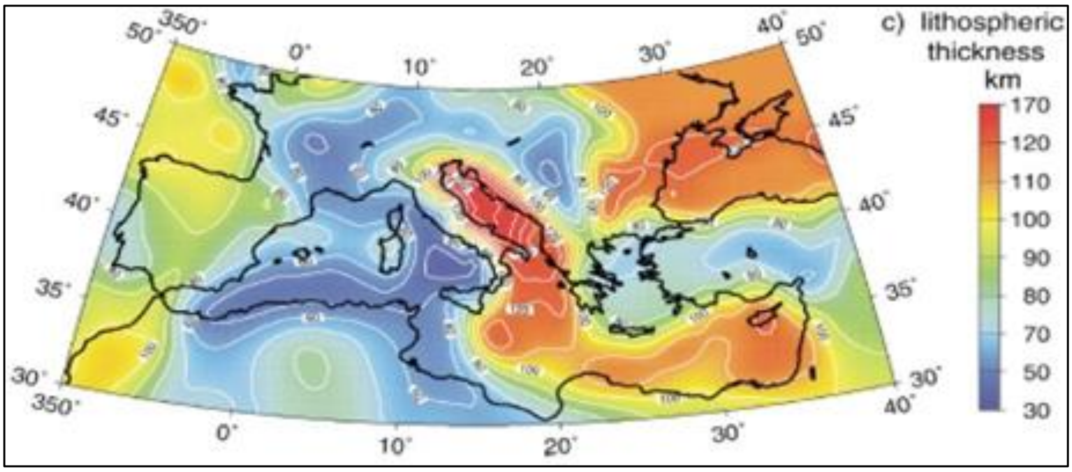

Figure A.I.7: Lithospheric thickness (Cavazza et al., 2004).

Appendix II: Sensitivity analysis plots

Figures:

Parameters	Figures
Crustal Thickness	A.II.1- A.II.8
Beta Factor	A.II.9- A.II.22
Radioactive Heat	A.II.23- A.II.29
Rifting Age	A.II.30-A.II.33

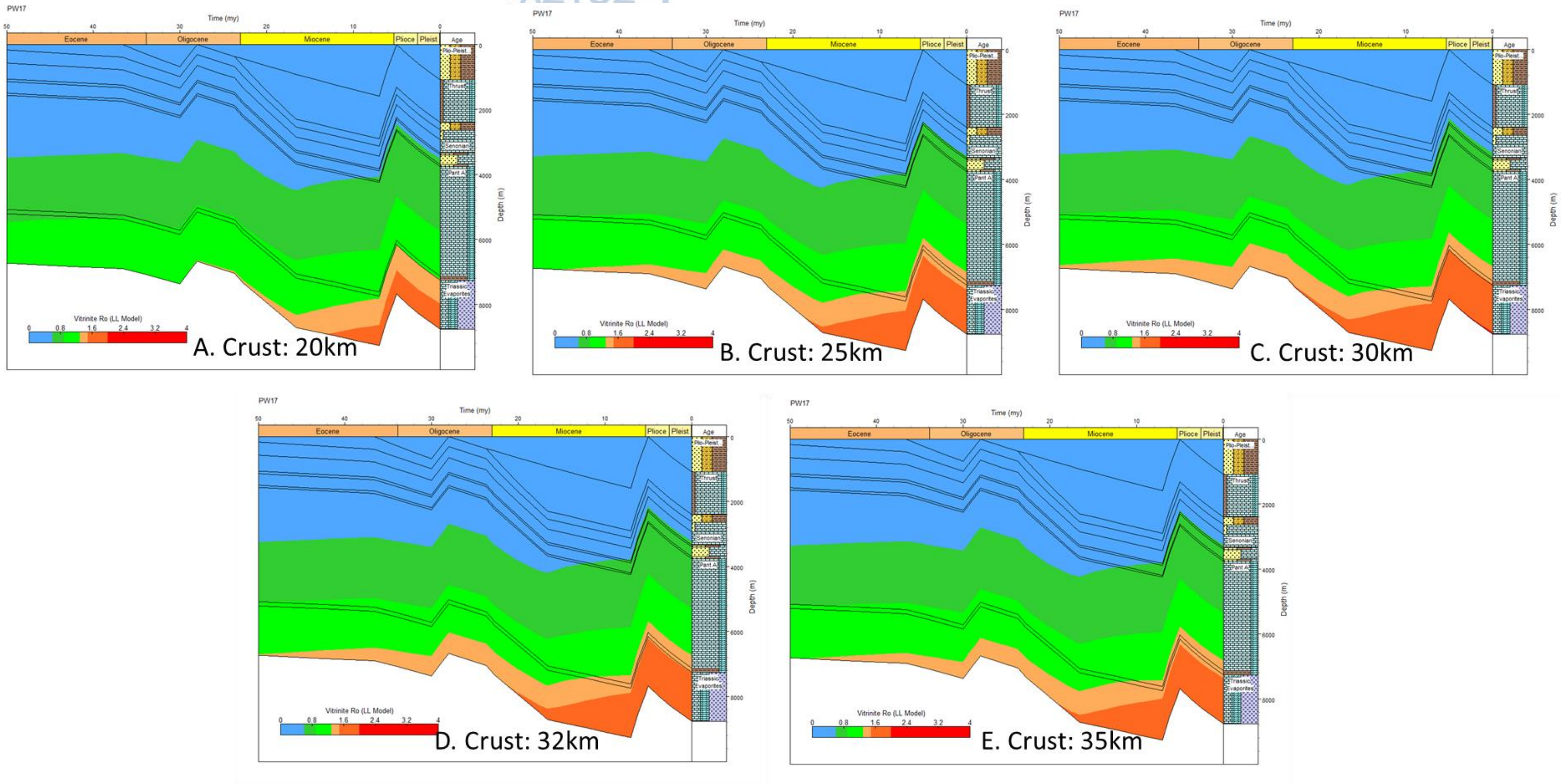

Figure A.II.1a: Burial History plots (50 Ma to Present) of pseudo-well A with superimposed colormap of vitrinite reflectance values. These plots describe scenario 2. The parameters are presented in Table 15. Each plot refers to different crustal thickness.

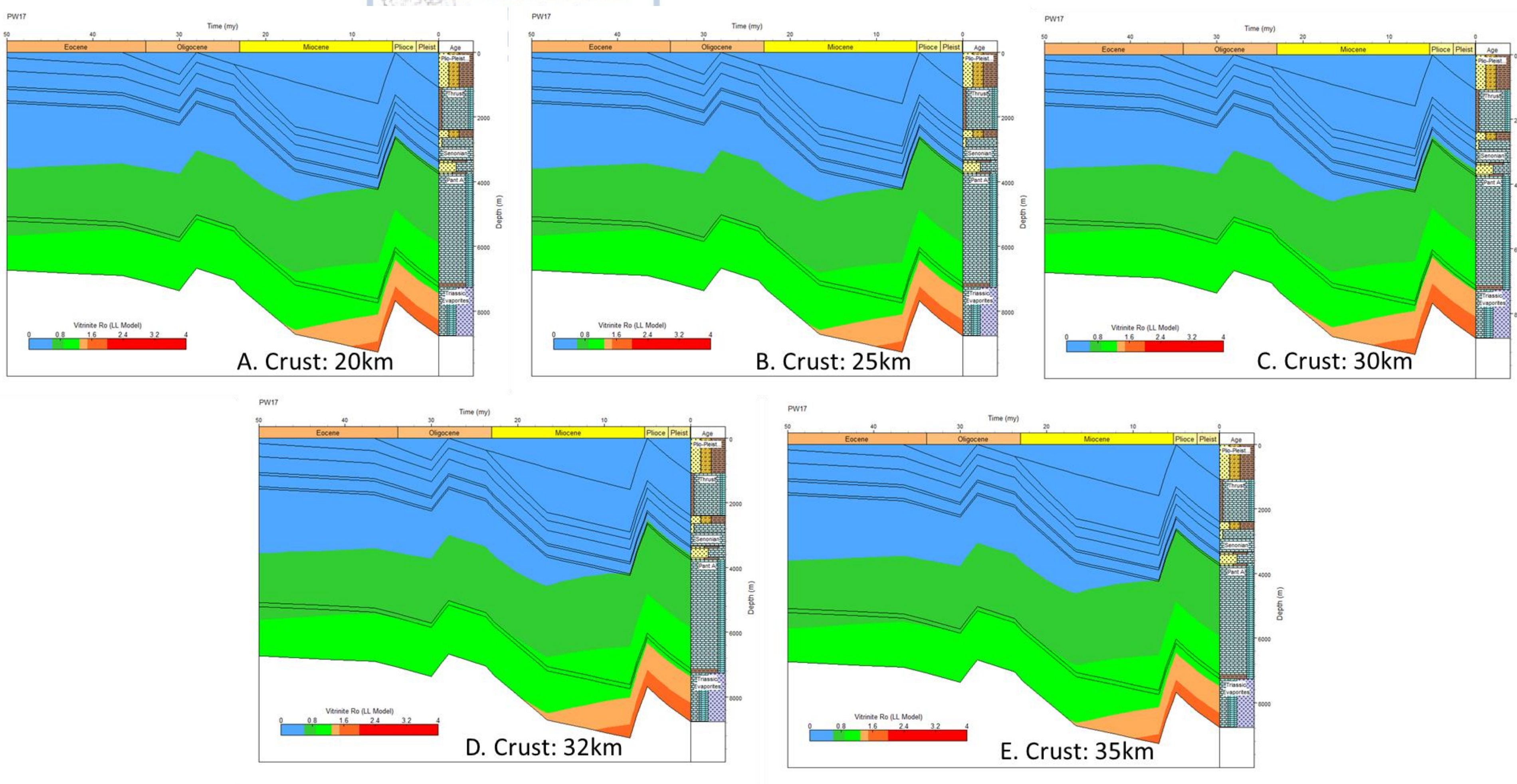

Figure A.II.1b: Burial History plots (50 Ma to Present) of pseudo-well A with superimposed colormap of vitrinite reflectance values. These plots describe scenario 3. The parameters are presented in Table 15. Each plot refers to different crustal thickness.

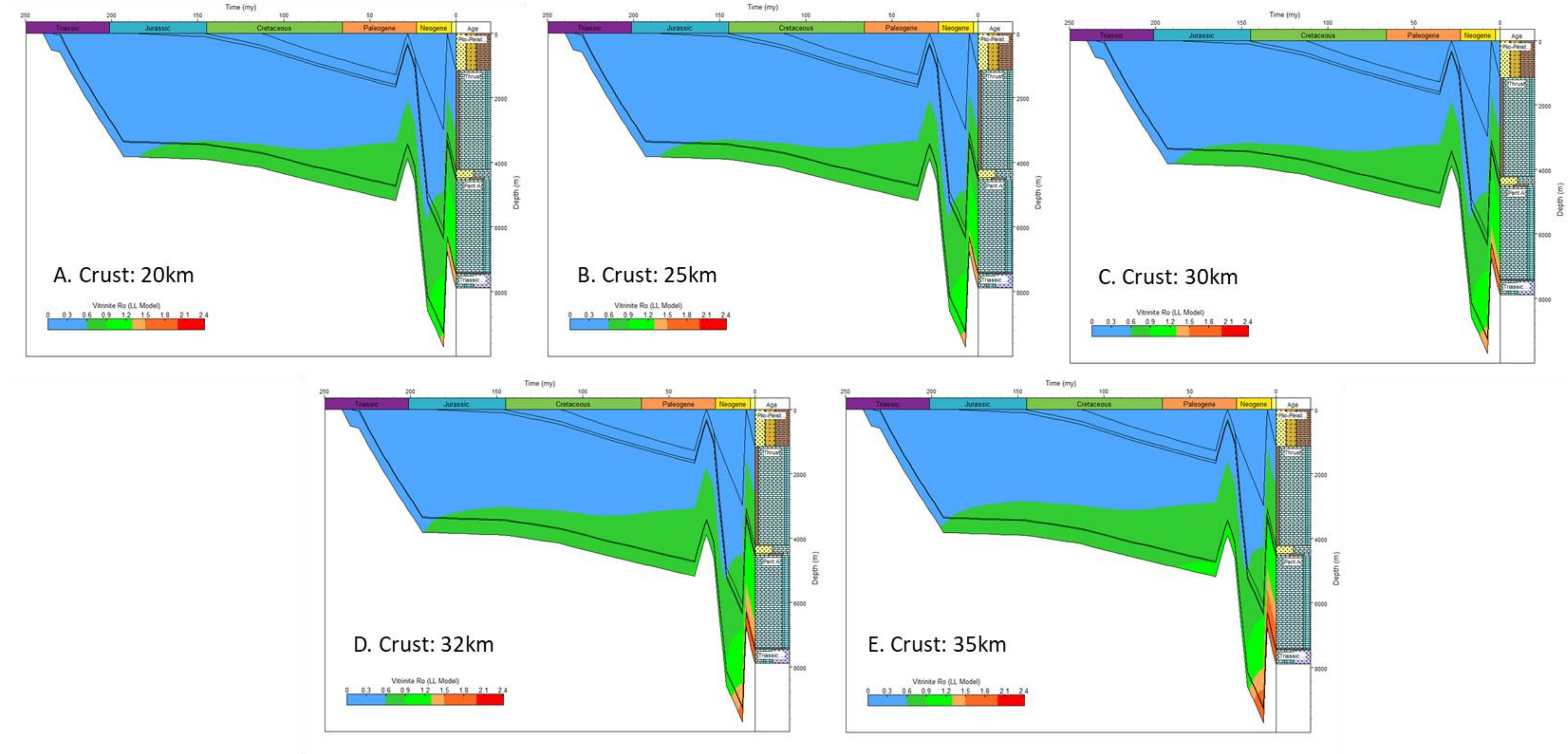

Figure A.II.2a: Burial History plots (250 Ma to Present) of pseudo-well B with superimposed colormap of vitrinite reflectance values. These plots describe scenario 2. The parameters are presented in Table 15. Each plot refers to different crustal thickness.

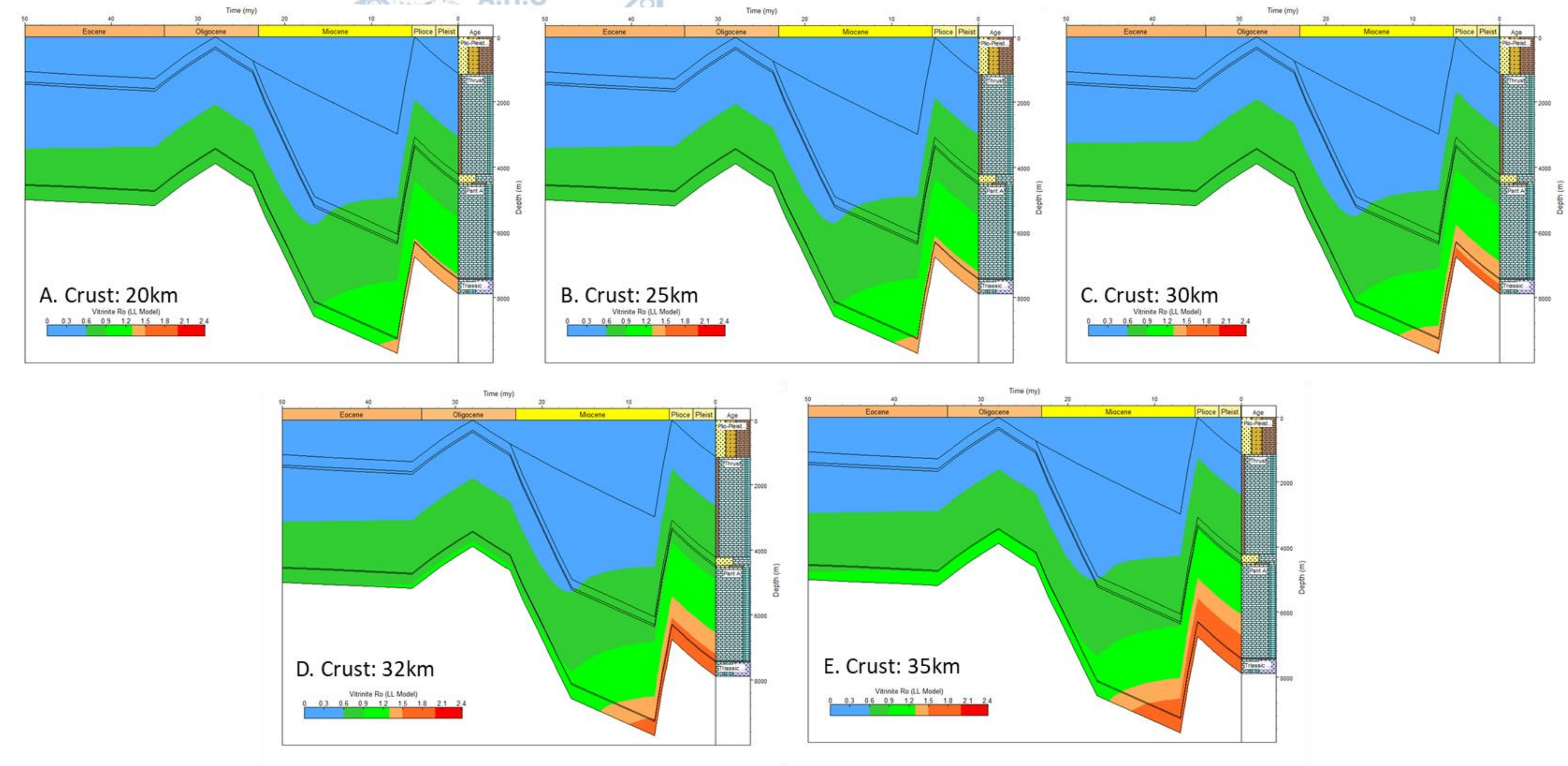

Figure A.II.2b: Burial History plots (50 Ma to Present) of pseudo-well B with superimposed colormap of vitrinite reflectance values. These plots describe scenario 2. The parameters are presented in Table 15. Each plot refers to different crustal thickness.

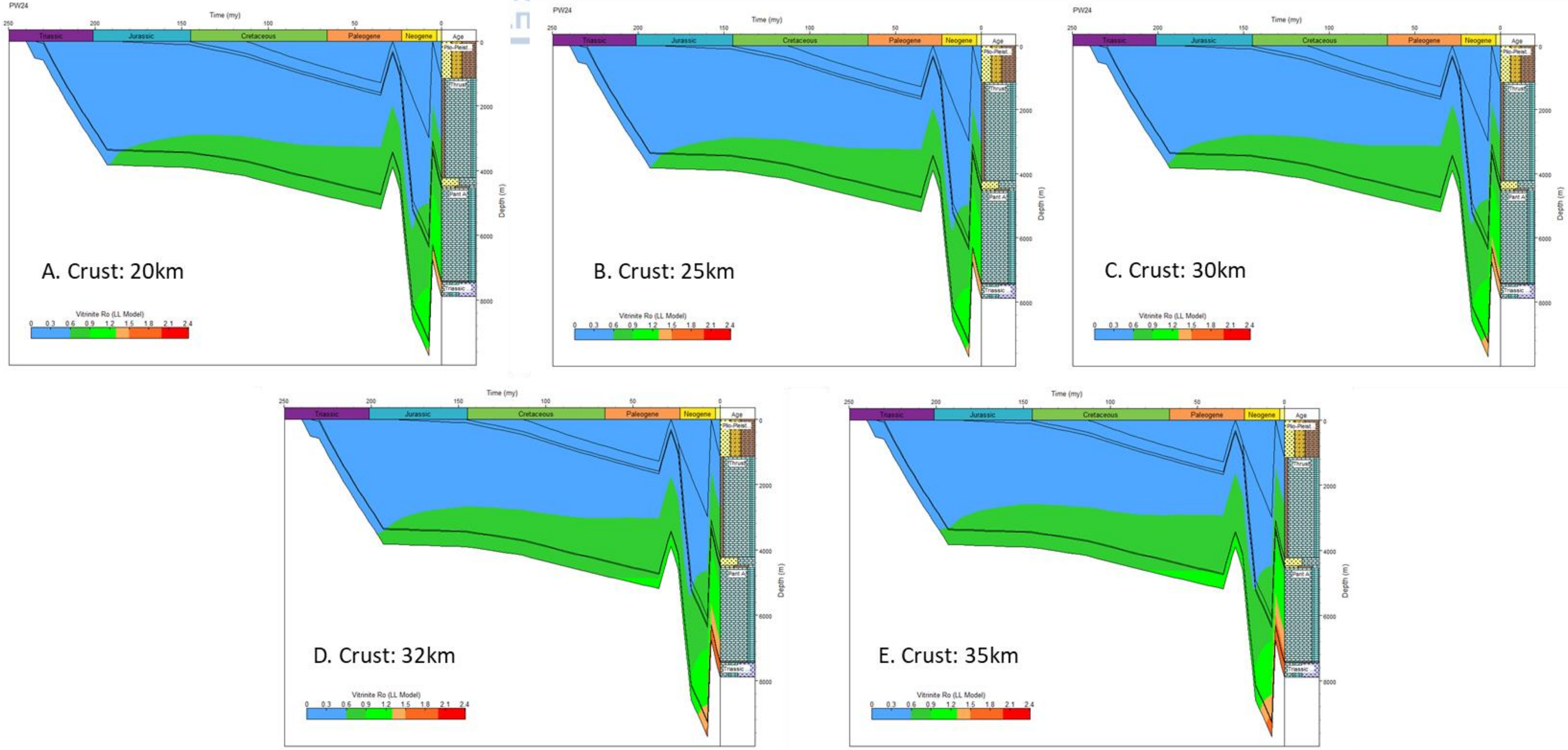

Figure A.II.2c: Burial History plots (250 Ma to Present) of pseudo-well B with superimposed colormap of vitrinite reflectance values. These plots describe scenario 3. The parameters are presented in Table 15. Each plot refers to different crustal thickness.

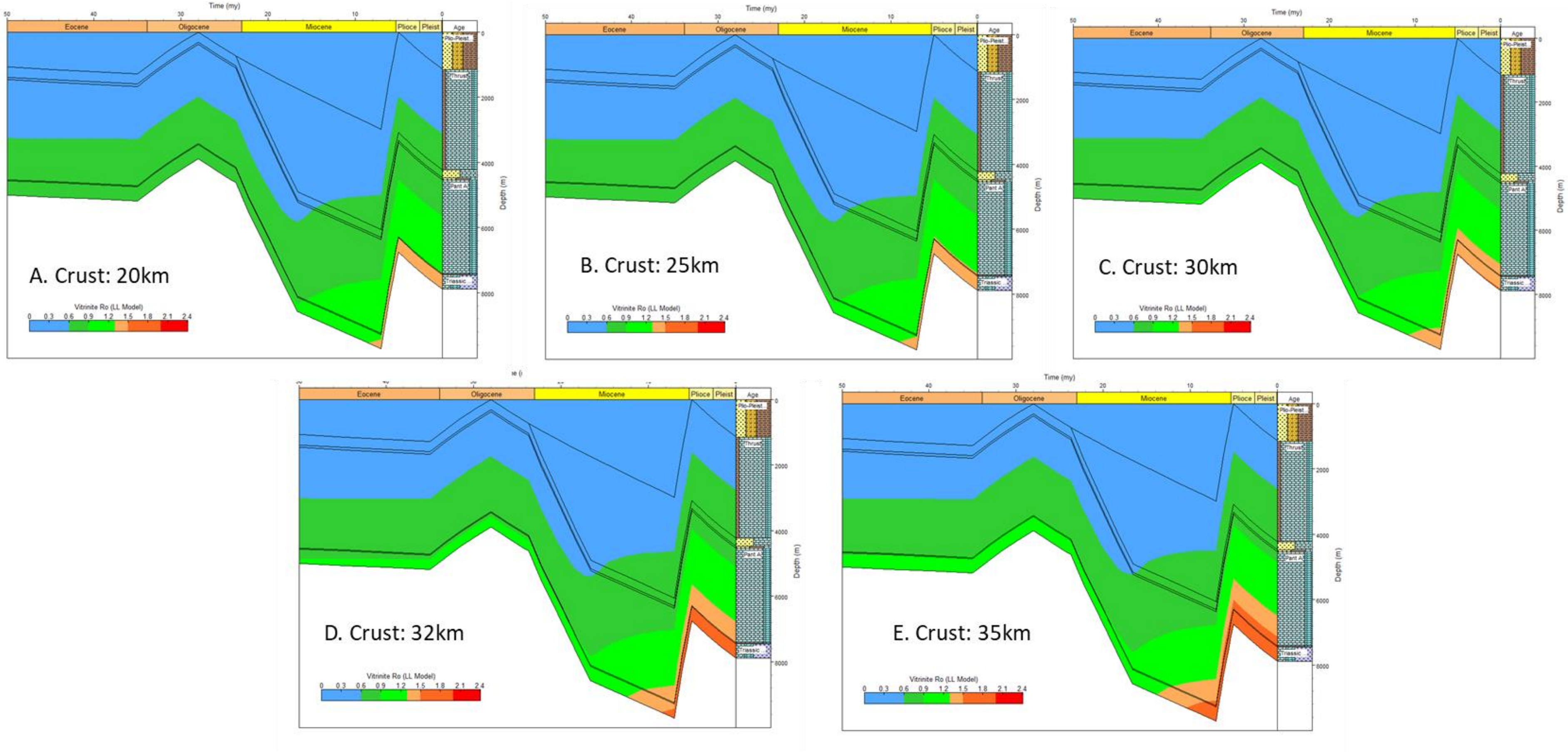

Figure A.II.2d: Burial History plots (50 Ma to Present) of pseudo-well B with superimposed colormap of vitrinite reflectance values. These plots describe scenario 3. The parameters are presented in Table 15. Each plot refers to different crustal thickness.

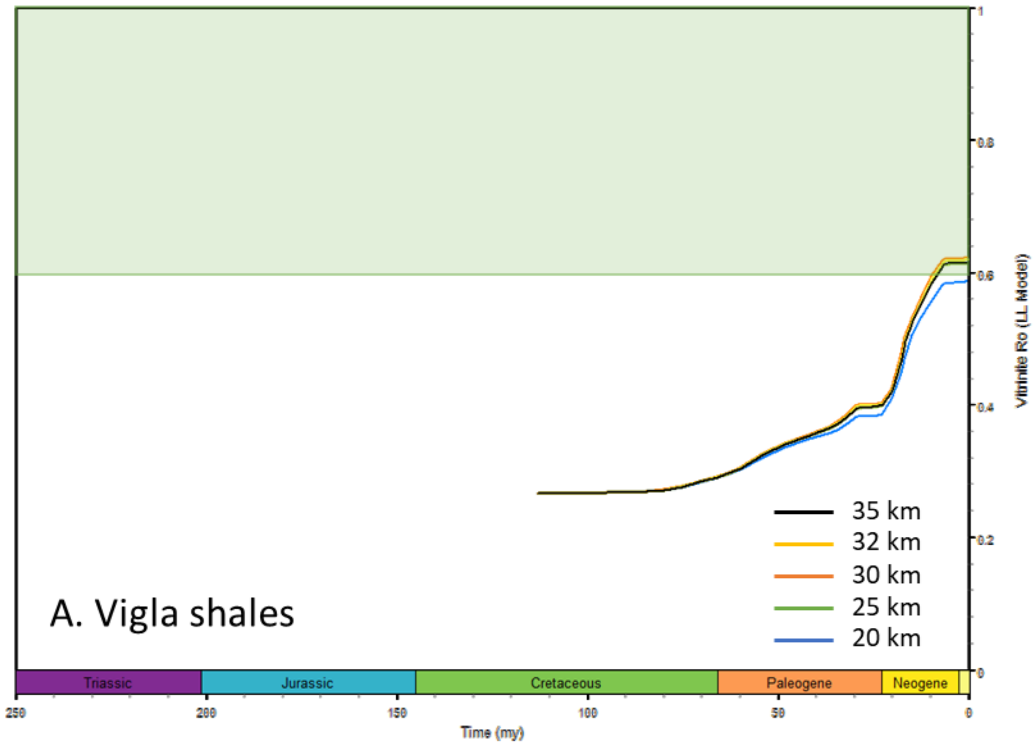

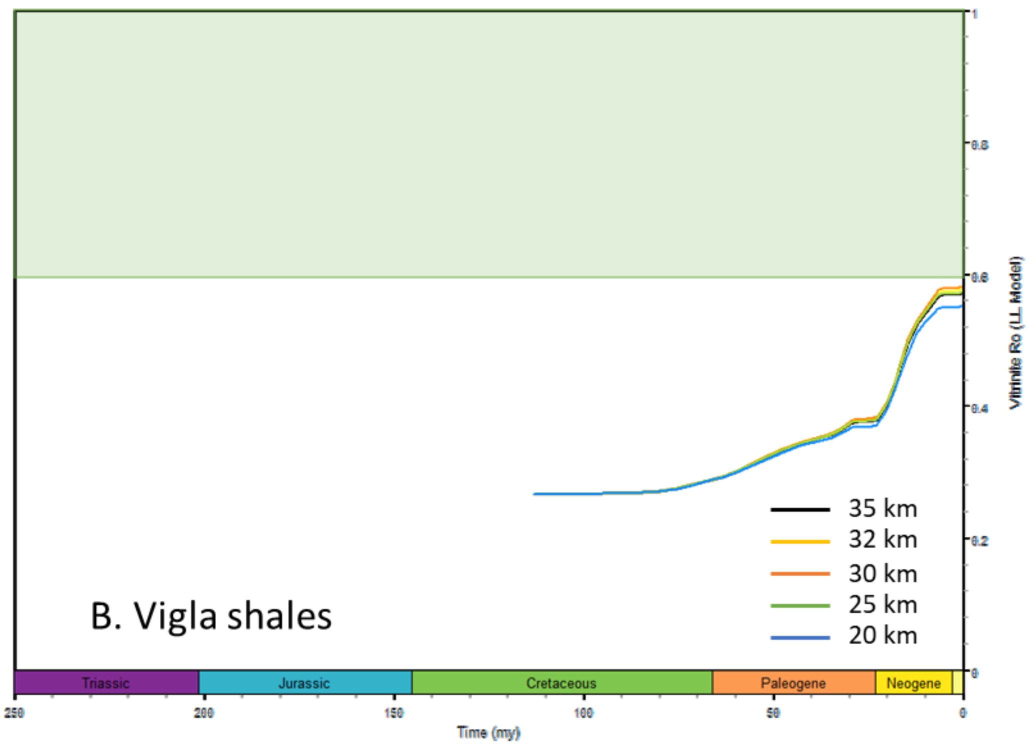

Figure A.II.3: Vitrinite reflectance curve- Time based on Burnham and Sweeney 1990 for Vigla shales. The colored curves present the crustal thickness variables. These curves are based on scenarios 2 and 3, respectively. The parameters used for scenarios 2 and 3 are presented in Table 15.

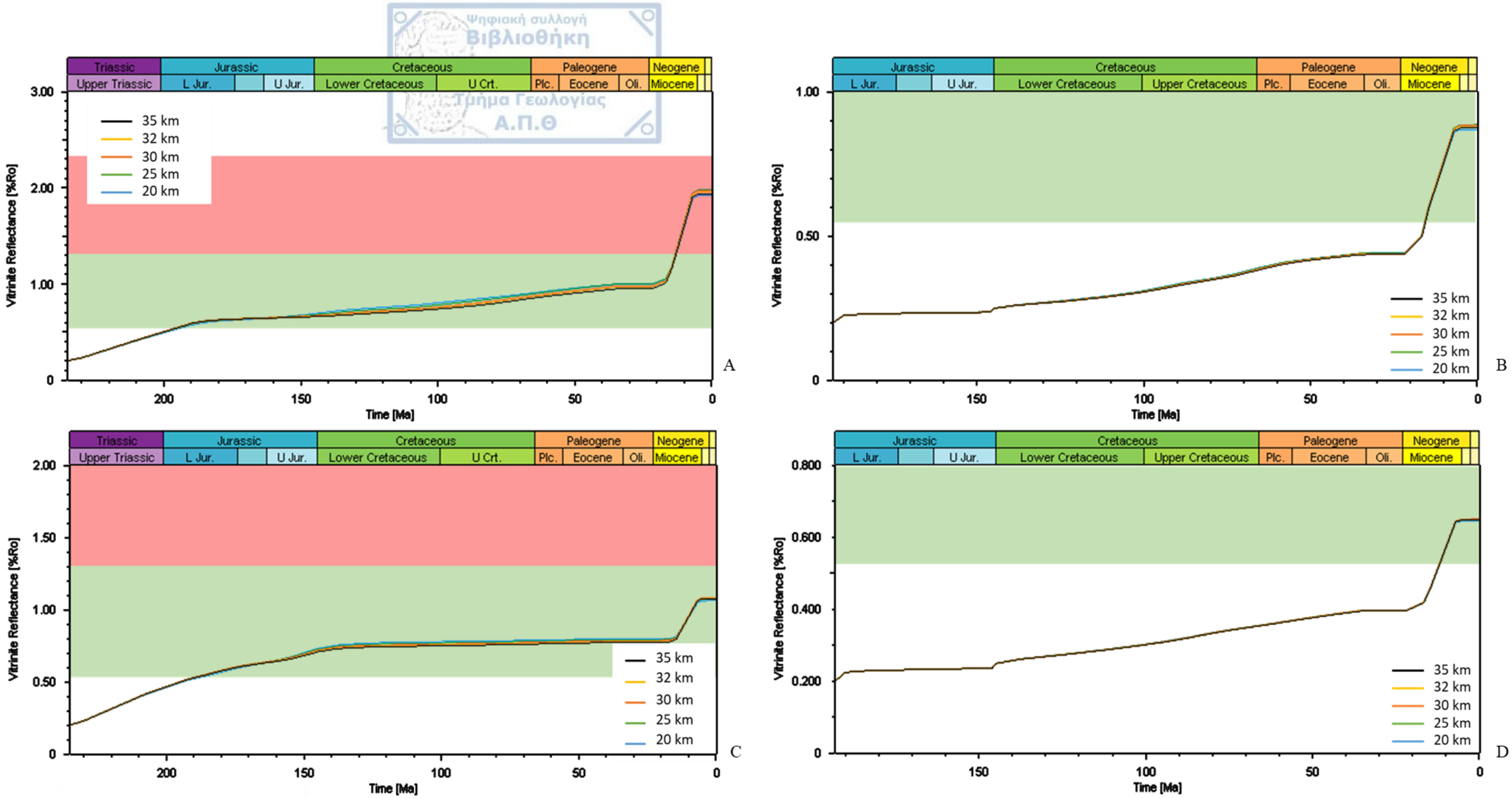

Figure A.II.4: Vitrinite reflectance curve- Time based on Burnham and Sweeney (1990). The colored curves present the crustal thickness variables. Figures A and C represent Triassic shales in pseudo-well B and are based on scenario 2 and 3, respectively. Figures B and D illustrate Posidonia shales in pseudo-well B and are based on scenario 2 and 3, respectively. The parameters used for scenarios 2 and 3 are presented in Table 15.

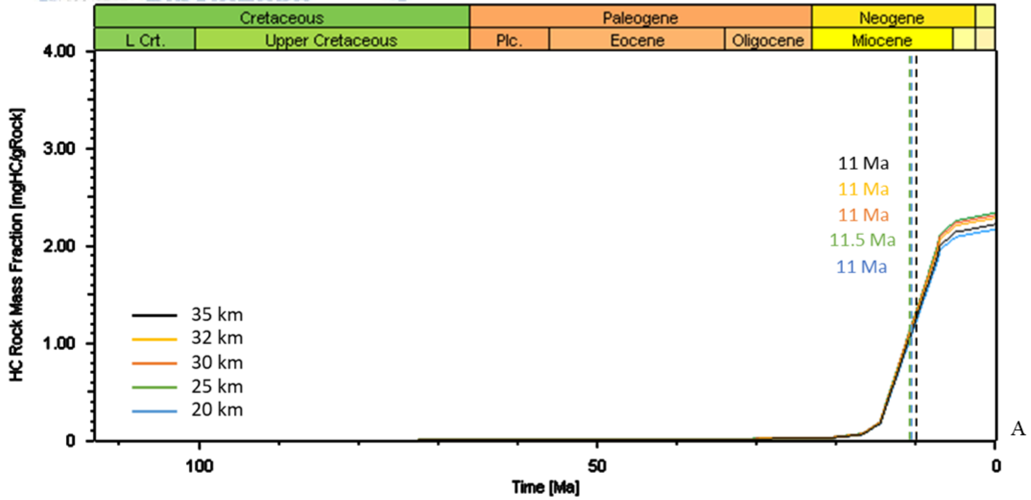

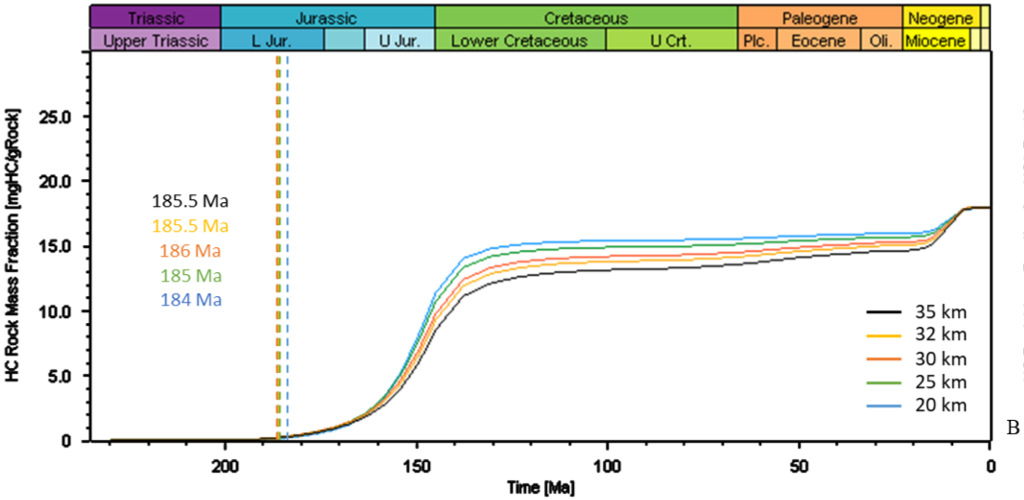

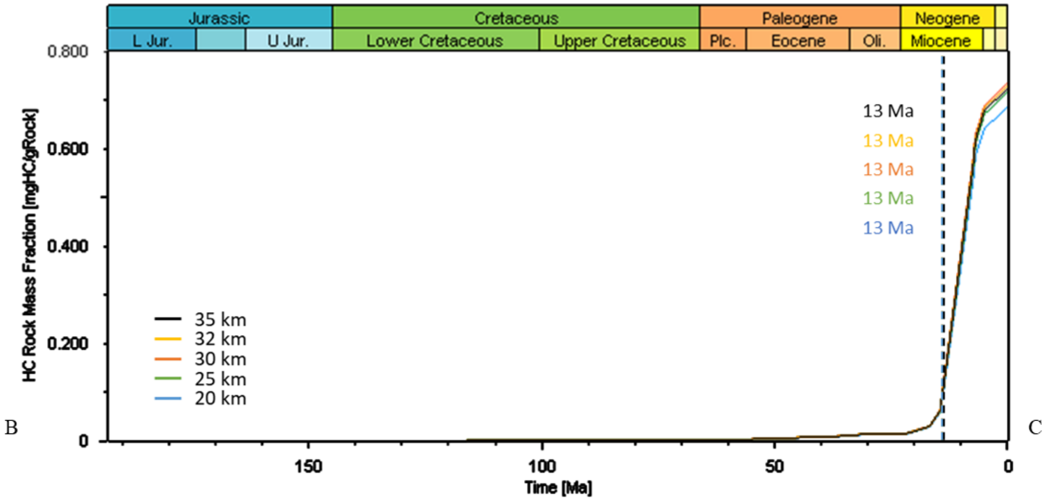

Figure A.II.5: Generation Mass curves through geological time for pseudo-well A. The colored curves present the crustal thickness variables. Generation mass values are in mg HC/g Rock and time values are in Ma. The parameters used are presented in Table 15. Figure 5A illustrates Vigla shales (scenario 2) and Figures 5B and 5C Triassic and Posidonia shales (scenario 3), respectively.

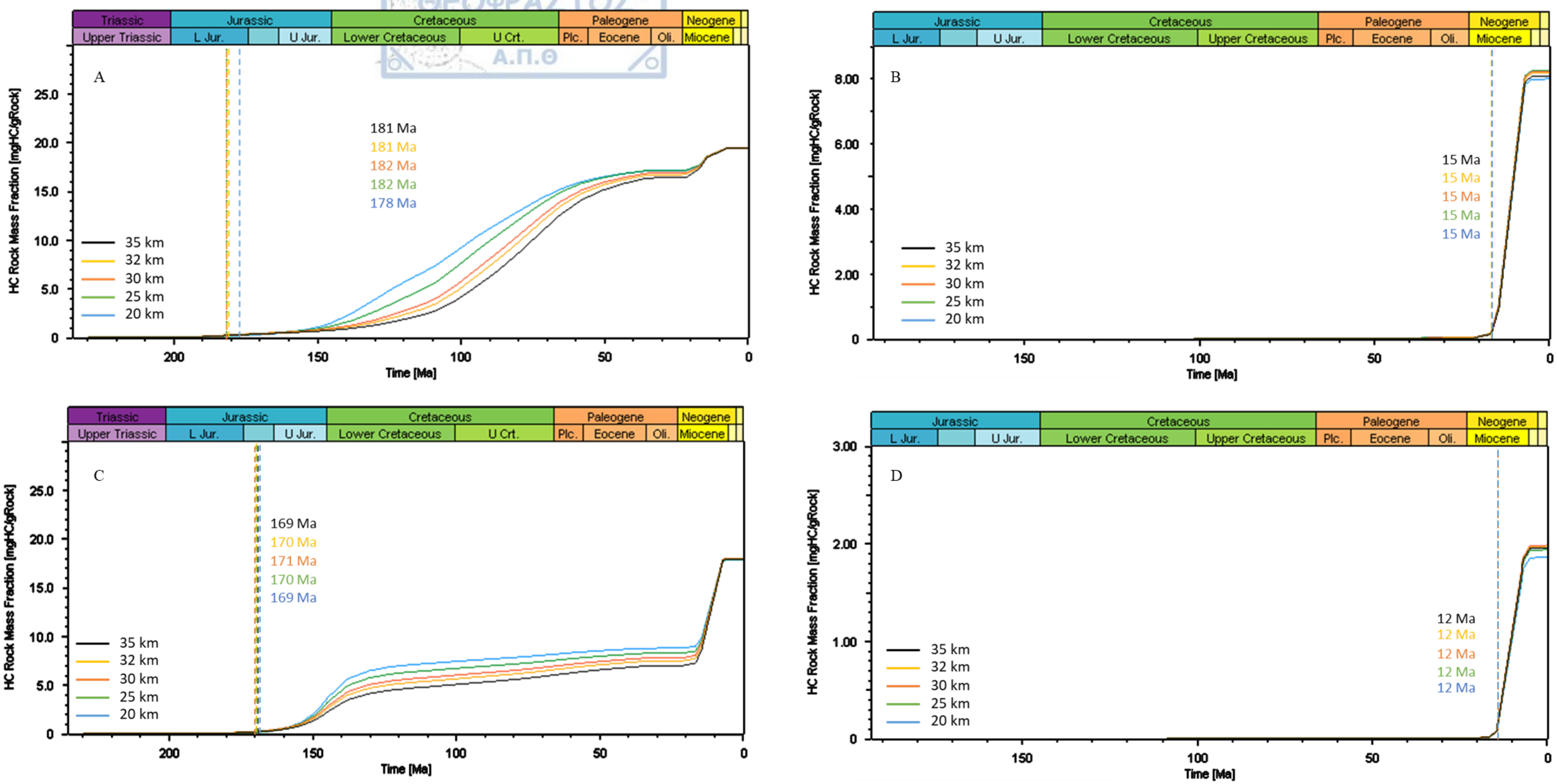

Figure A.II.6: Generation Mass curves through geological time for pseudo-well B. The colored curves present the crustal thickness variables. Generation mass values are in mg HC/g Rock and time values are in Ma. The parameters used are presented in Table 15. Figures 6A and 6C illustrate Triassic shales and Figures 6B and 6D Posidonia shales for scenarios 2 and 3, respectively.

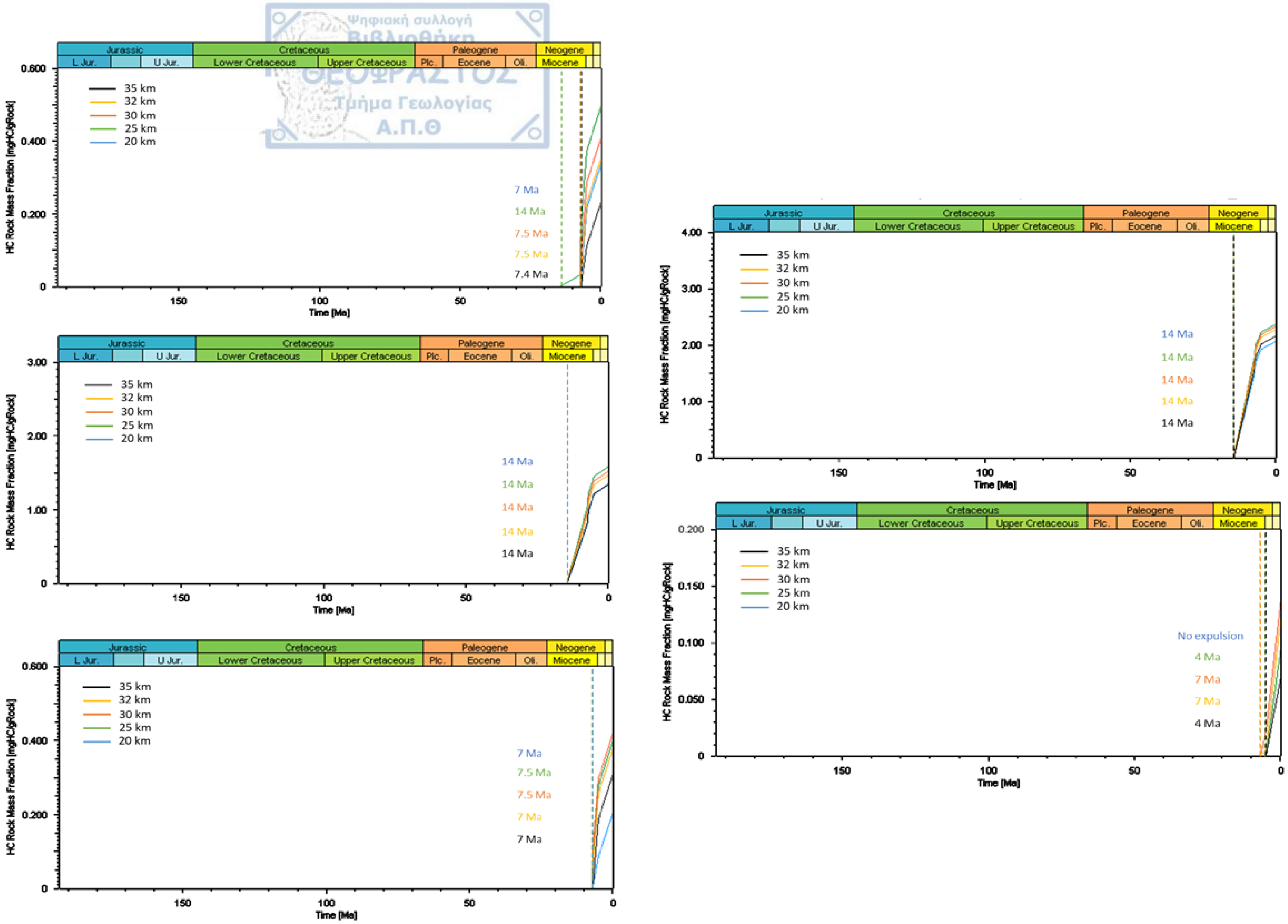

Figure A.II.7: Expulsion Mass curves through geological time for Posidonia shales. The colored curves present the crustal thickness variables when radioactive heat and beta factor are high enough. Expulsion mass values are in mg HC/g Rock and time values are in Ma.

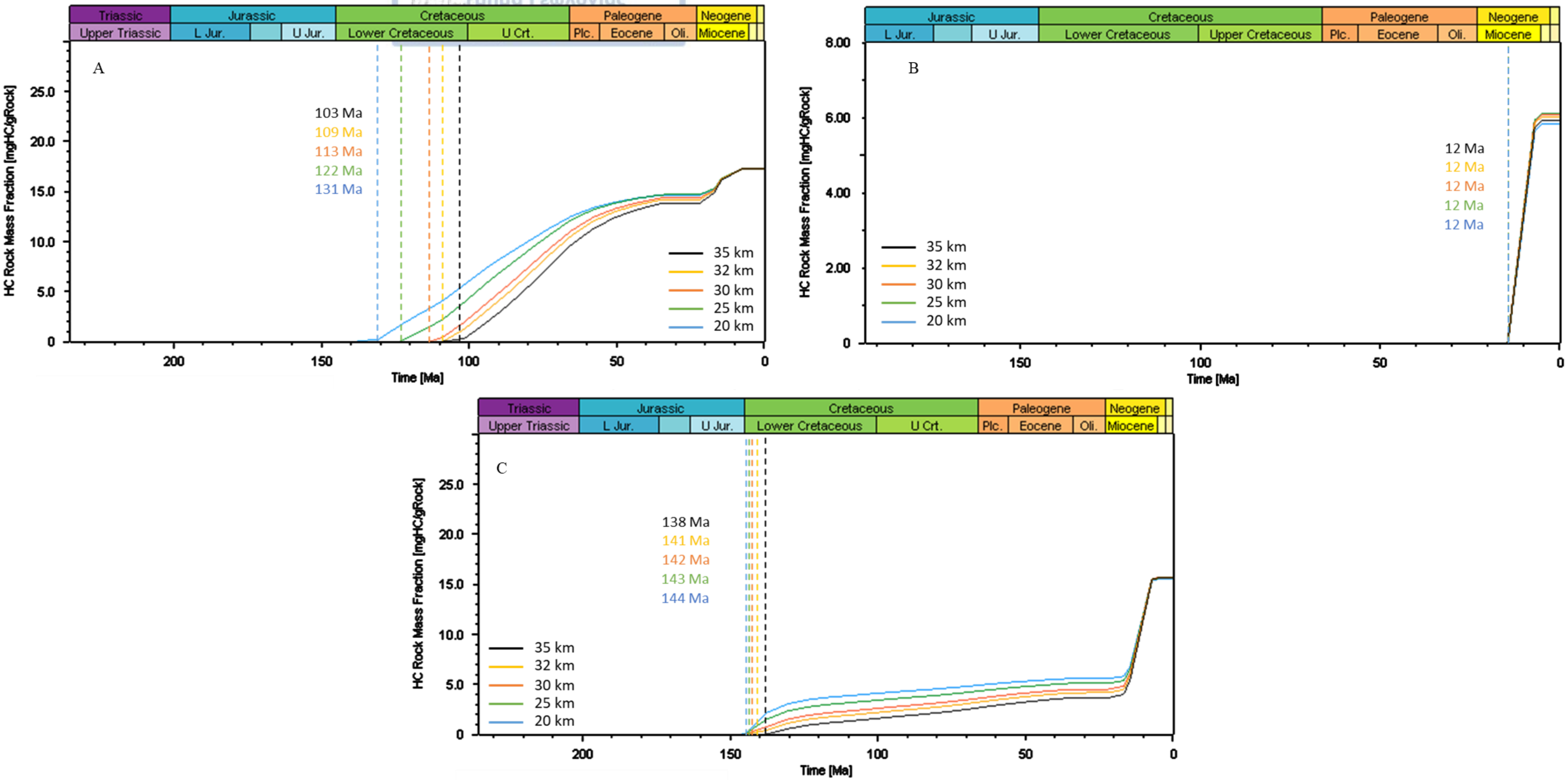

Figure A.II.8: Expulsion Mass curves through geological time for the Triassic and Posidonia shales (pseudo-well B). The colored curves present the crustal thickness variables. Expulsion mass values are in mg HC/g Rock and time values in Ma. The plots A-B and C describe scenarios 2 and 3, respectively. The parameters used are presented in Table 15.

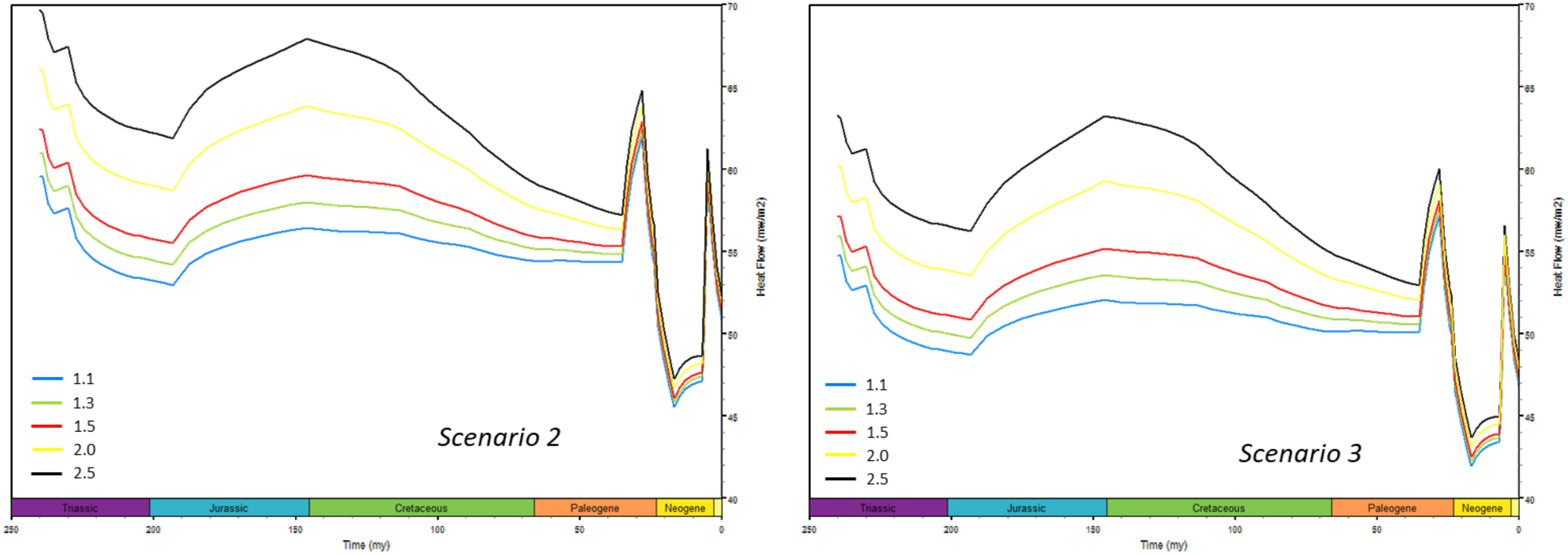

Figure A.II.9: Heat Flow curves for pseudo-well B. The curves present the Scenarios 2 (maximum heat flow values) and 3 (minimum heat flow values), respectively. The colored curves present the beta factor variables. The parameters used are presented in Table 16.

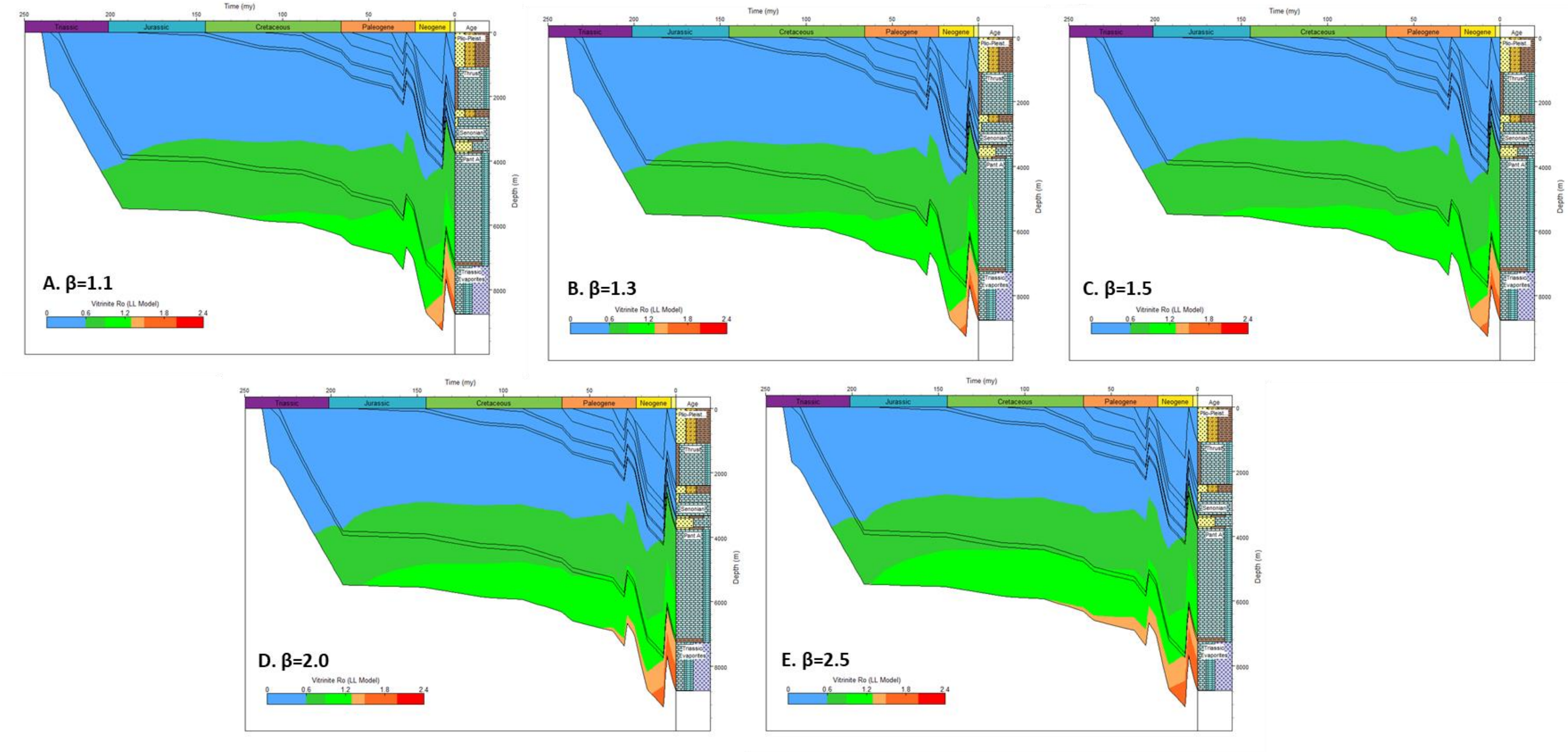

Figure A.II.10: Burial History plots (250 Ma to Present) of pseudo-well A. These plots describe scenario 3. The parameters are presented in Table 16. Each plot refers to different beta factor.

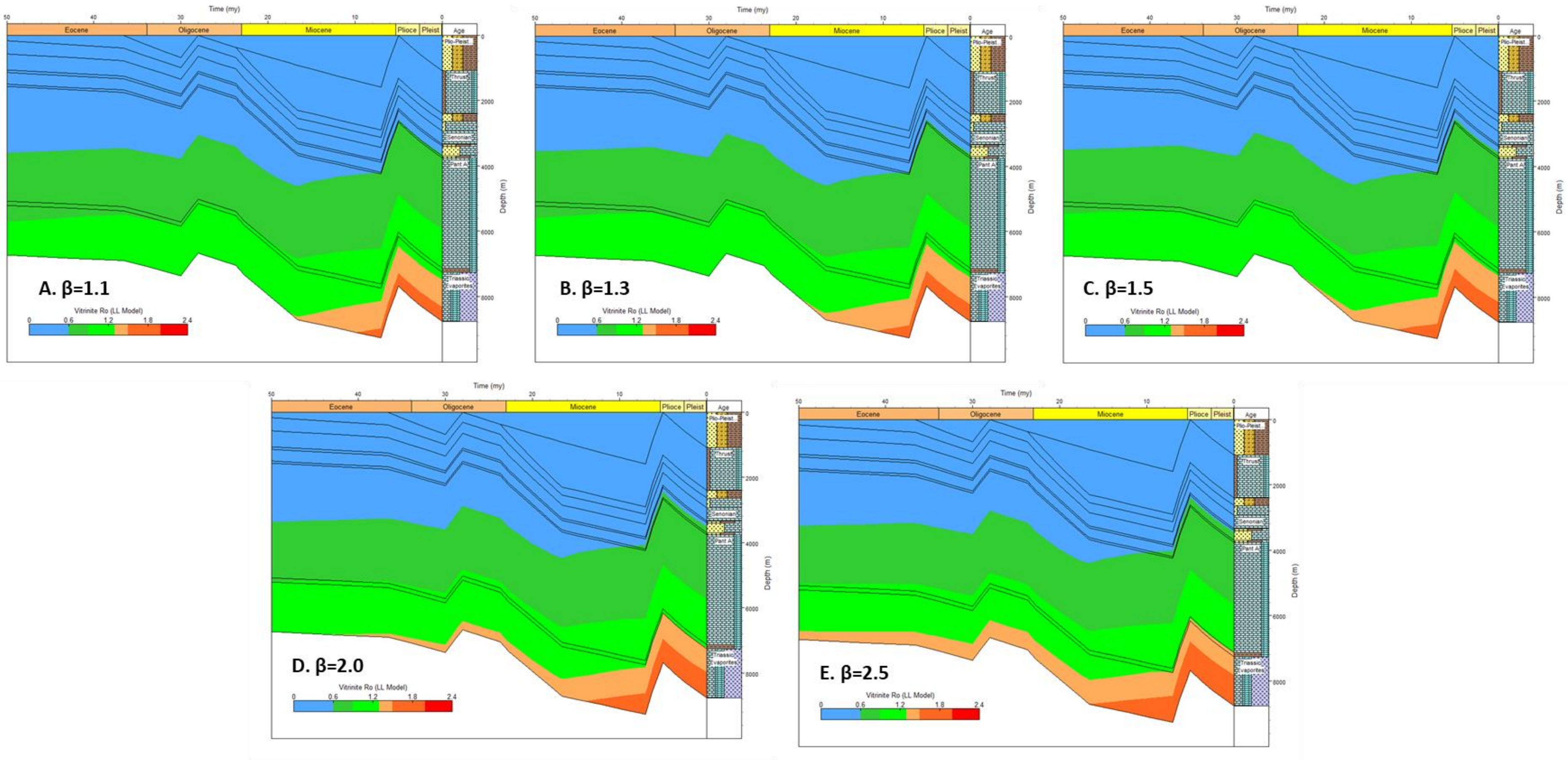

Figure A.II.11: Burial History plots (50 Ma to Present) of pseudo-well A. These plots describe scenario 3. The parameters are presented in Table 16. Each plot refers to different beta factor.

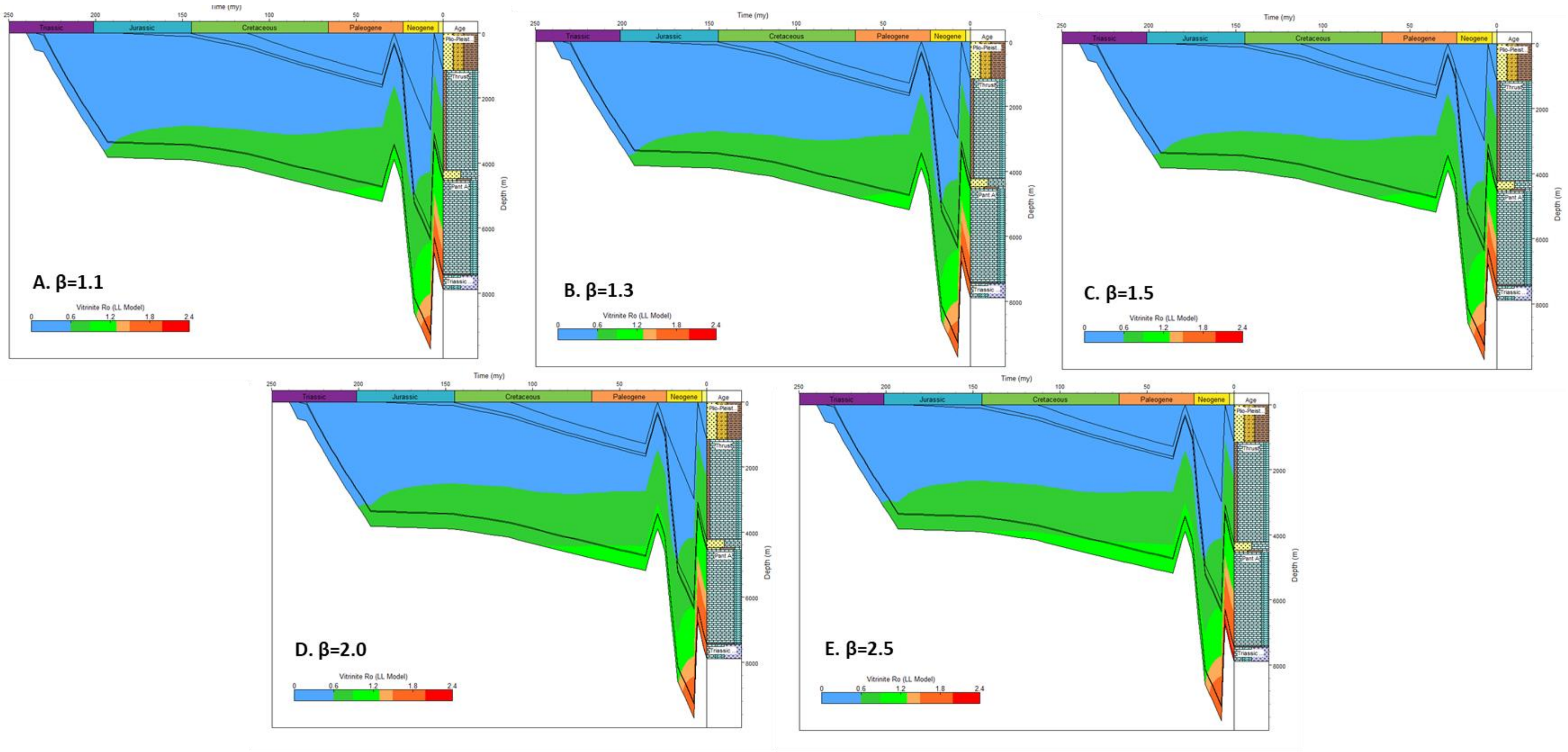

Figure A.II.12: Burial History plots (250 Ma to Present) of pseudo-well B. These plots describe scenario 2. The parameters are presented in Table 16. Each plot refers to different beta factor.

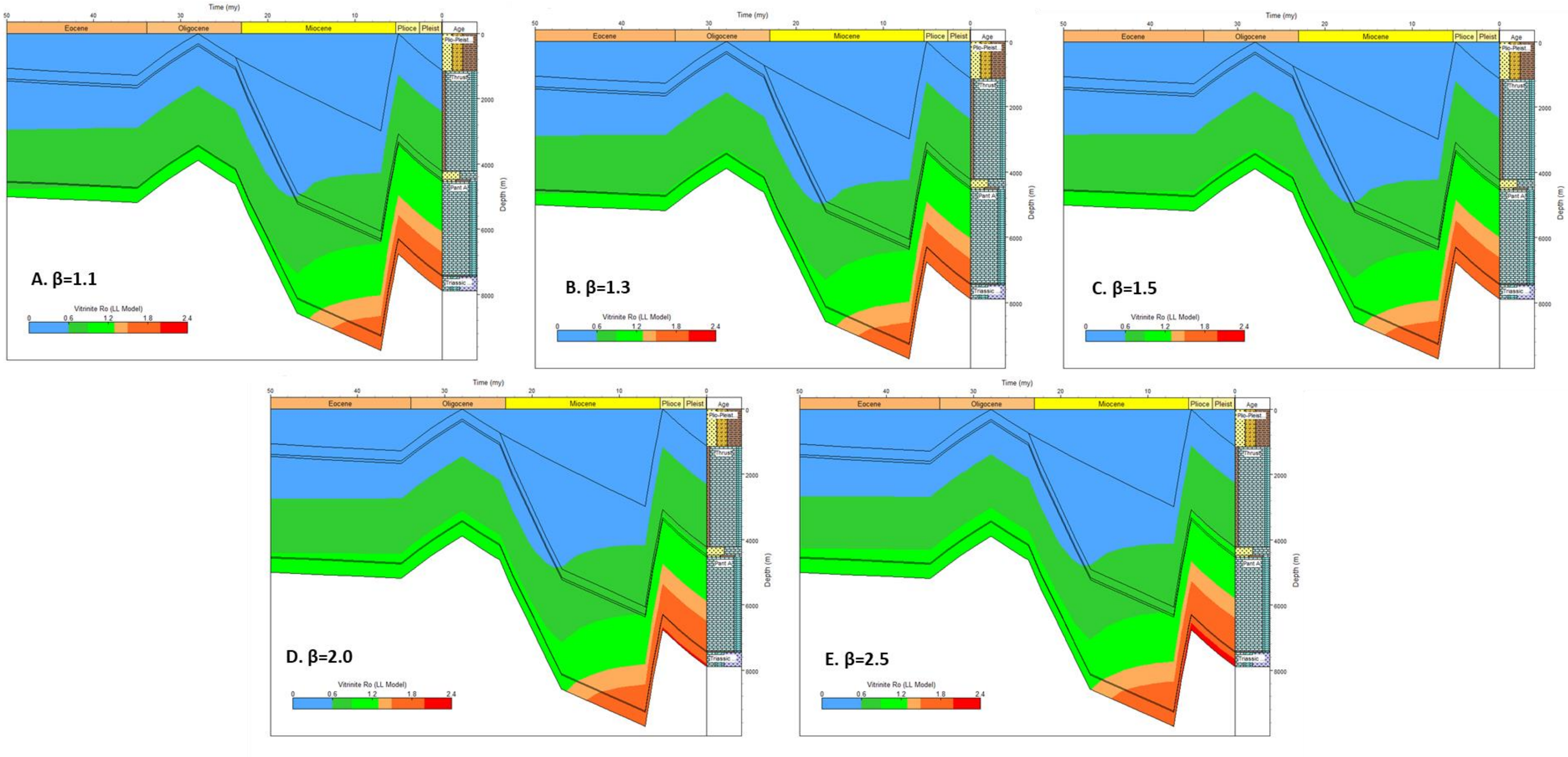

Figure A.II.13: Burial History plots (50 Ma to Present) of pseudo-well B. These plots describe scenario 2. The parameters are presented in Table 16. Each plot refers to different beta factor.

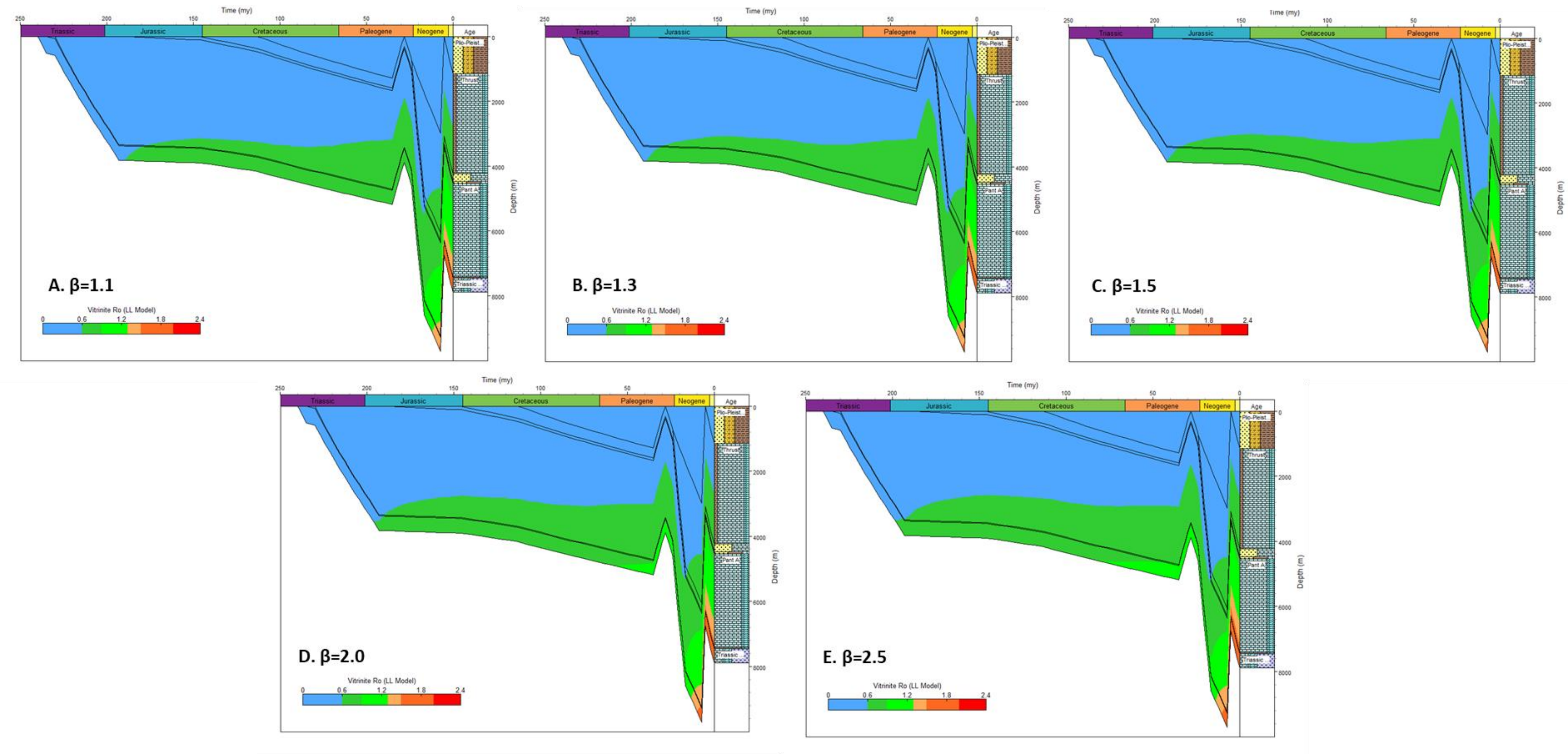

Figure A.II.14: Burial History plots (250 Ma to Present) of pseudo-well B. These plots describe scenario 3. The parameters are presented in Table 16. Each plot refers to different beta factor.

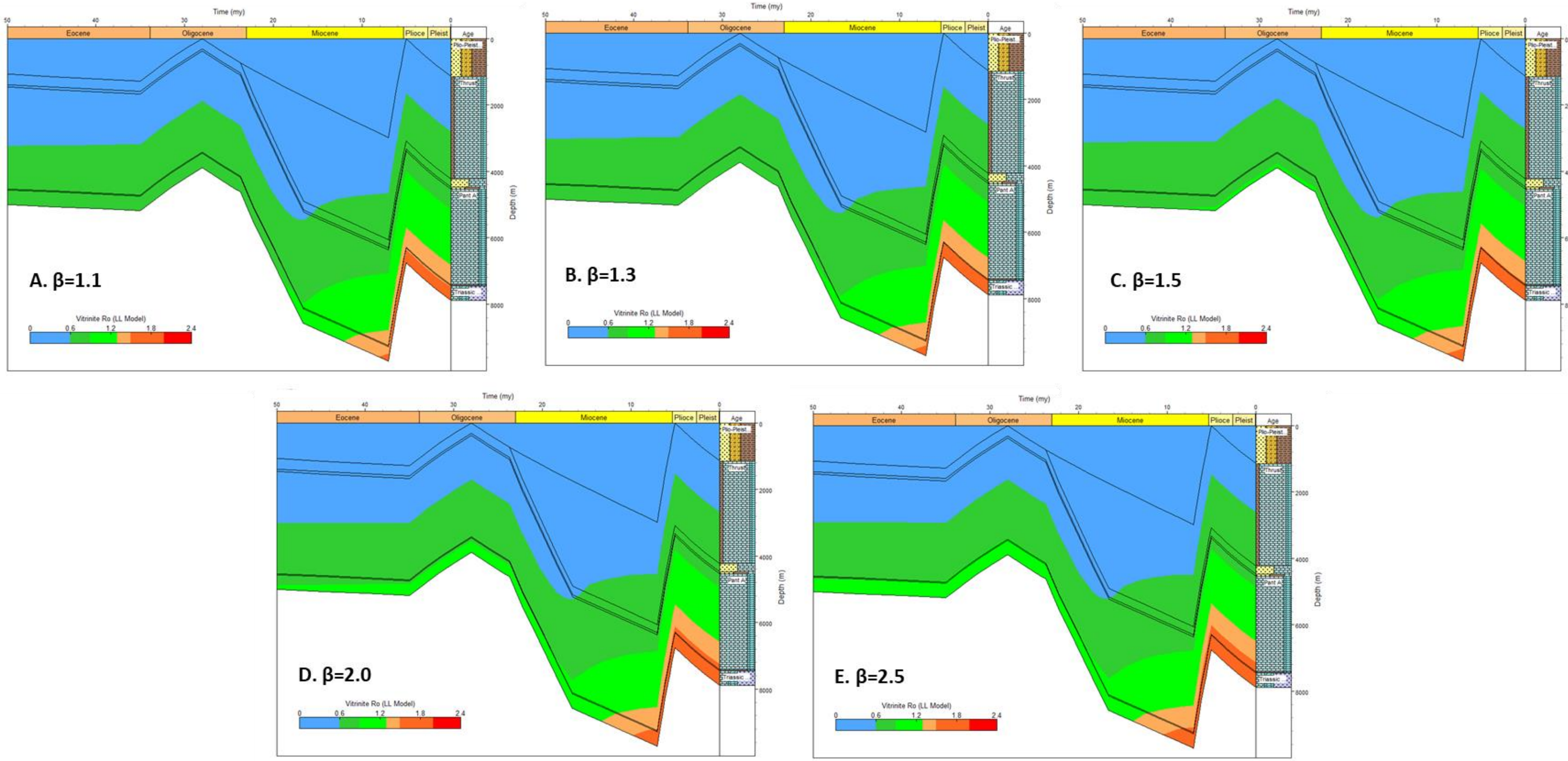

Figure A.II.15: Burial History plots (50 Ma to Present) of pseudo-well B. These plots describe scenario 3. The parameters are presented in Table 16. Each plot refers to different beta factor

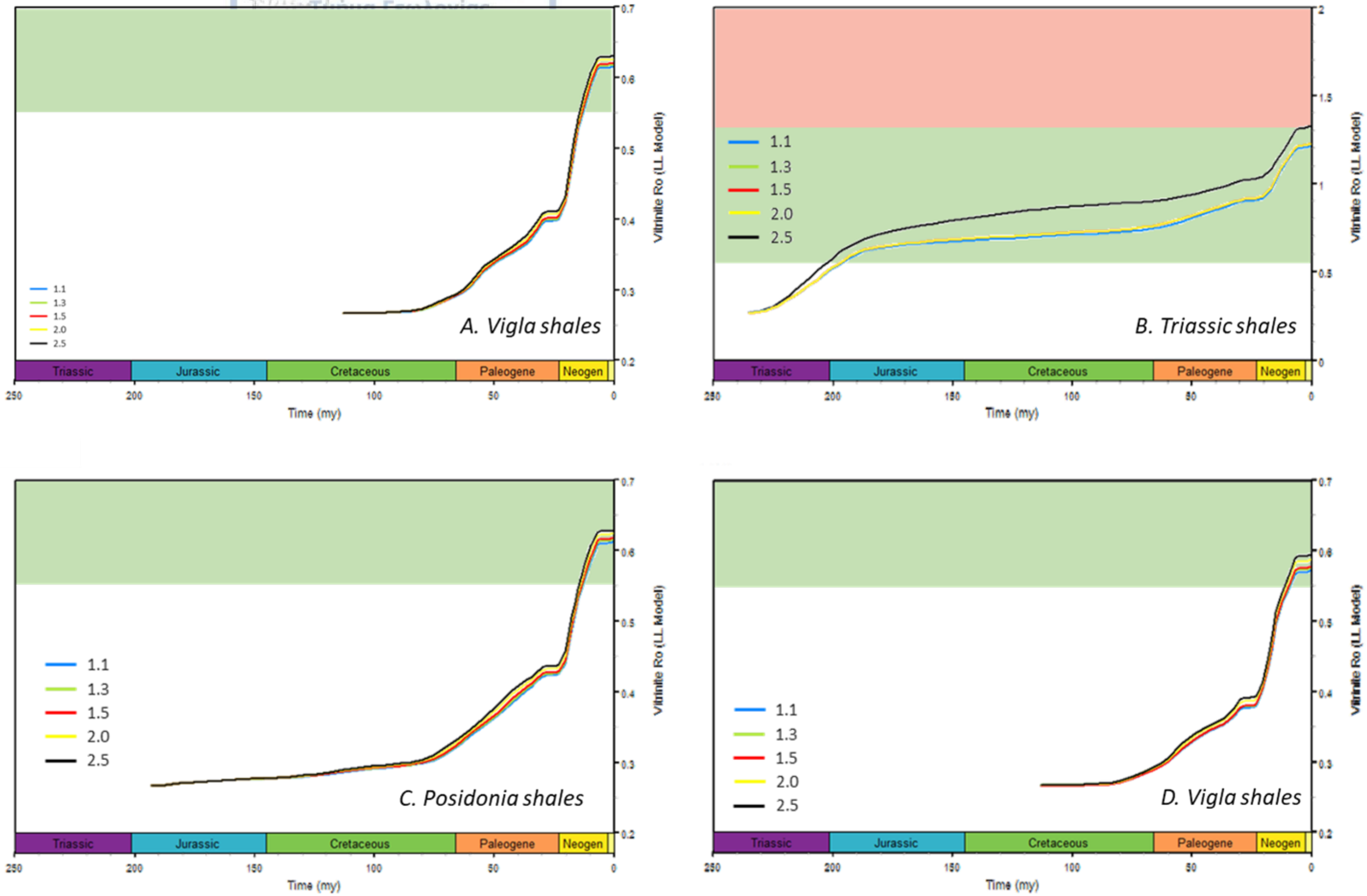

Figure A.II.16: Vitrinite reflectance curve- Time based on Burnham and Sweeney (1990). The colored curves present the beta factor variables. Figure A illustrates Vigla shales based on scenario 2 in pseudo-well A. Figures B, C, D illustrate Triassic, Posidonia and Vigla shales based on scenario 3 in pseudo-well A.

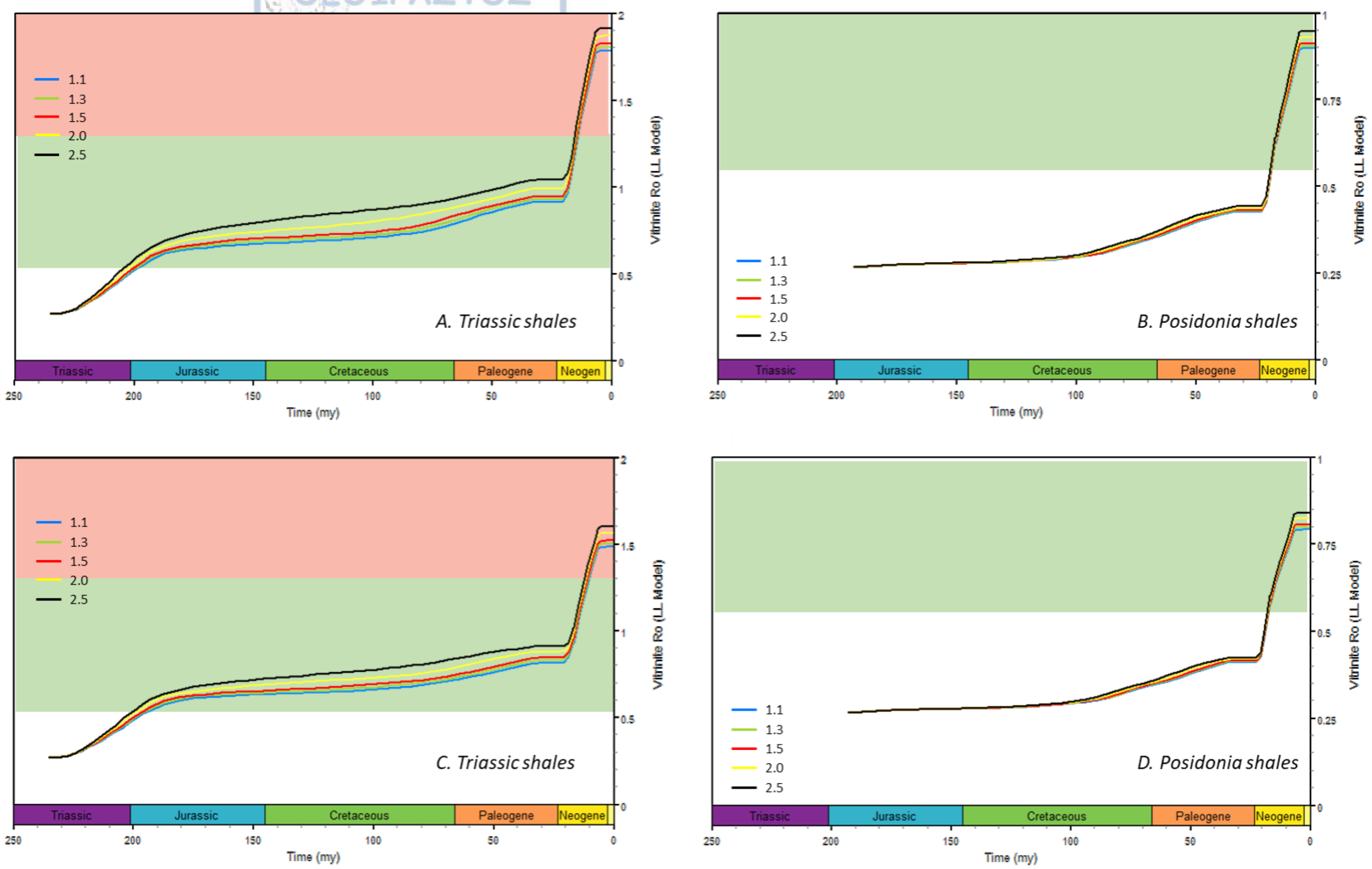

Figure A.II.17: Vitrinite reflectance curve- Time based on Burnham and Sweeney (1990). The colored curves present the beta factor variables. Figures A and B illustrate Triassic and Posidonia shales based on scenario 2 in pseudo-well B. Figures C and D illustrate Triassic and Posidonia shales based on scenario 3 in pseudo-well B.

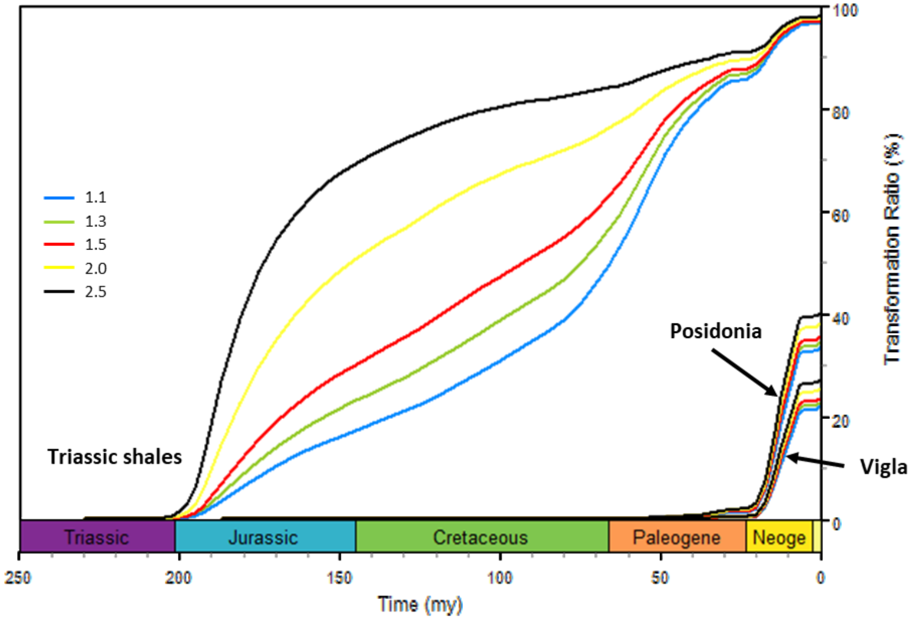

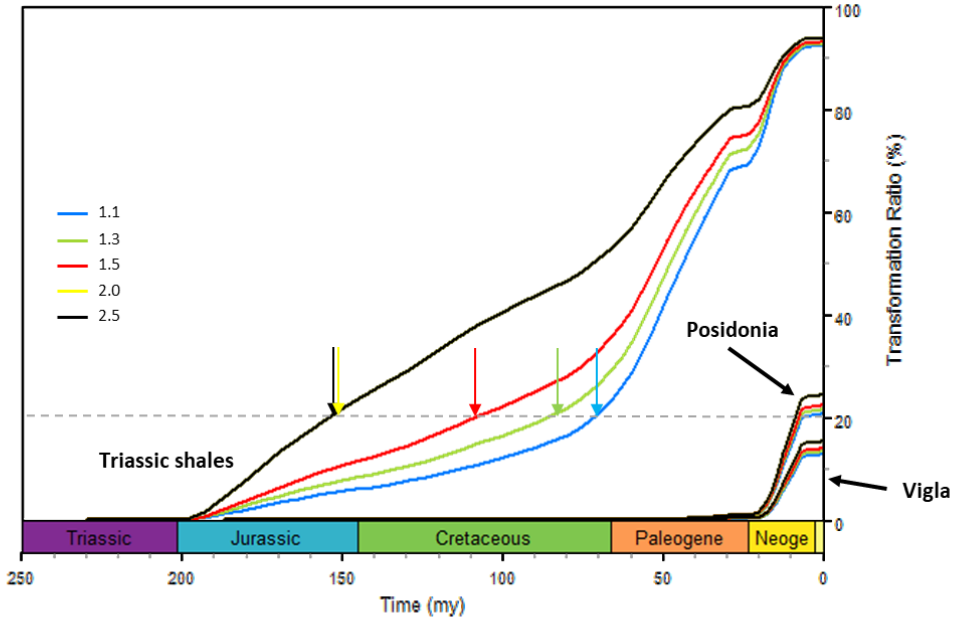

Figure A.II.18: Transformation ratio through geological time for the Triassic shales (PW-A). The colored curves present the beta factor variables Transformation ratio values are in % and time values are in Ma. Left figure illustrates transformation ratio values for the three modeled source rocks based on scenario 2. Right figure illustrates transformation ratio values for the three modeled source rocks based on scenario 3. The parameters used are presented in Table 16.

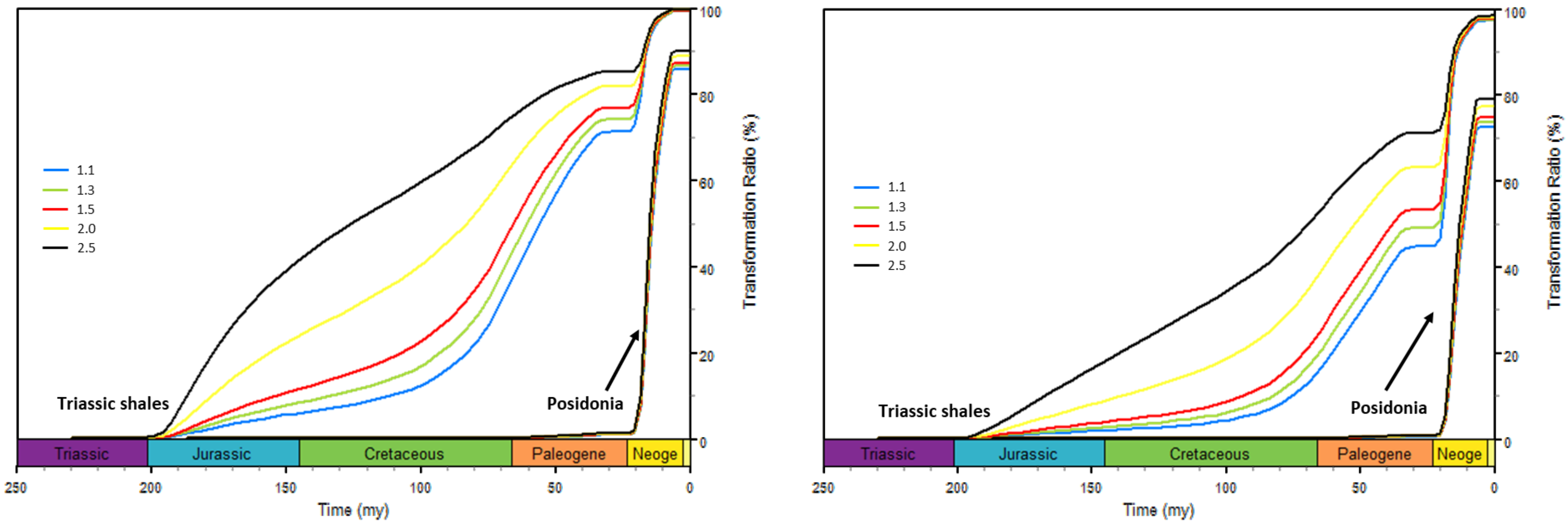

Figure A.II.19: Transformation ratio through geological time for the Triassic shales (PW-B). The colored curves present the beta factor variables Transformation ratio values are in % and time values are in Ma. Left figure illustrates transformation ratio values for the two modeled source rocks based on scenario 2. Right figure illustrates transformation ratio values for the two modeled source rocks based on scenario 3. The parameters used are presented in Table 16.

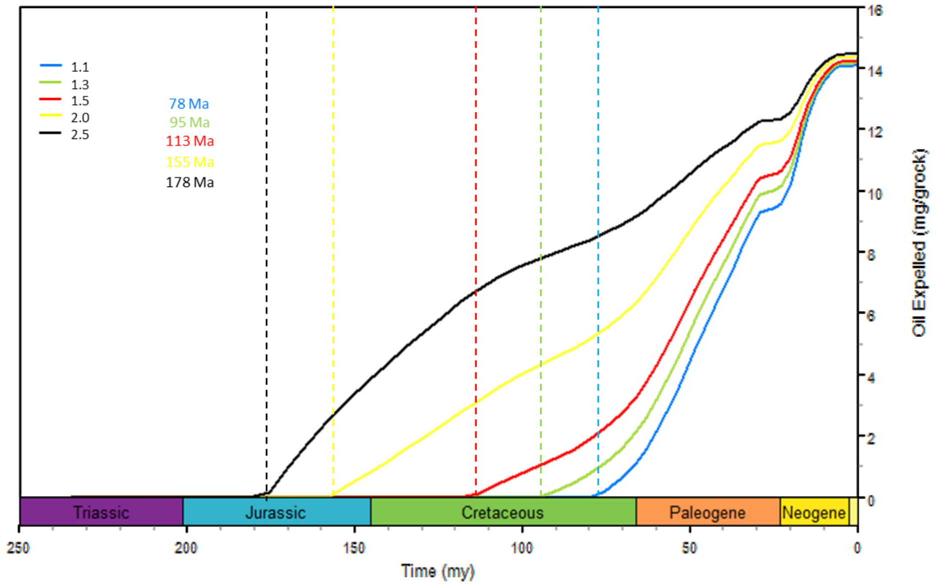

Figure A.II.20: Expulsion Mass curves through geological time for the Triassic shales (PW-A). The colored curves present the beta factor variables. Expulsion mass values are in mg HC/g Rock and time values in Ma. These plots describe scenario 3. The parameters used are presented in Table 16.

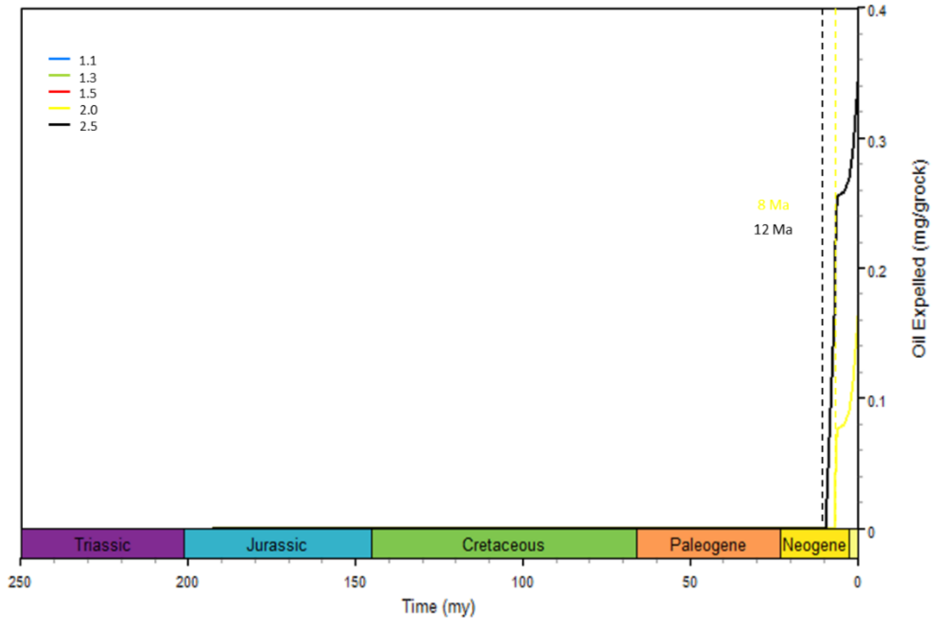

Figure A.II.21: Expulsion Mass curves through geological time for the Posidonia shales (PW-A). The colored curves present the beta factor variables. Expulsion mass values are in mg HC/g Rock and time values are in Ma. These plots describe scenario 3. The parameters used are presented in Table 16.

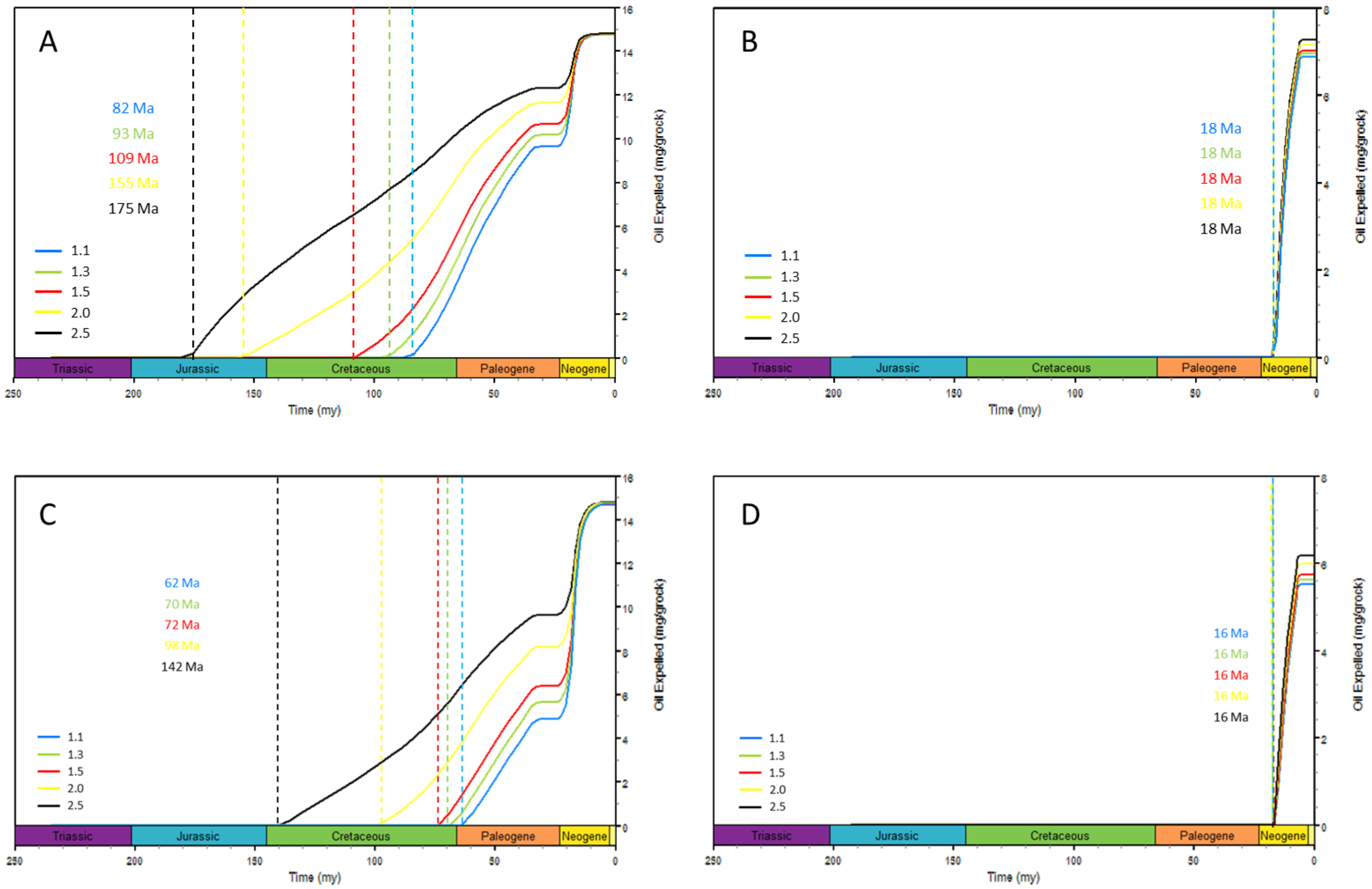

Figure A.II.22: Expulsion Mass curves through geological time for pseudo-well B. The colored curves present the beta factor variables. Expulsion mass values are in mg HC/g Rock and time values in Ma. Figure A and B illustrate Triassic and Posidonia shales based on scenario 2. Figures C and D illustrate Triassic and Posidonia shales based on scenario 3. The parameters used are presented in Table 16.

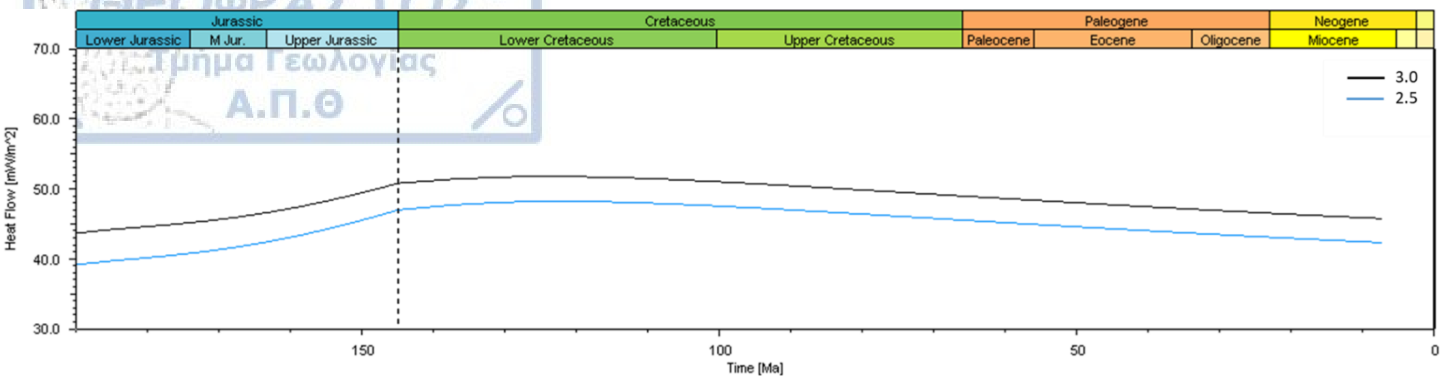

Figure A.II.23: Heat Flow curves for the PW-B. The curves present Scenario 2 (maximum heat flow values) and 3 (minimum heat flow values), respectively. The parameters used are presented in Table 17.

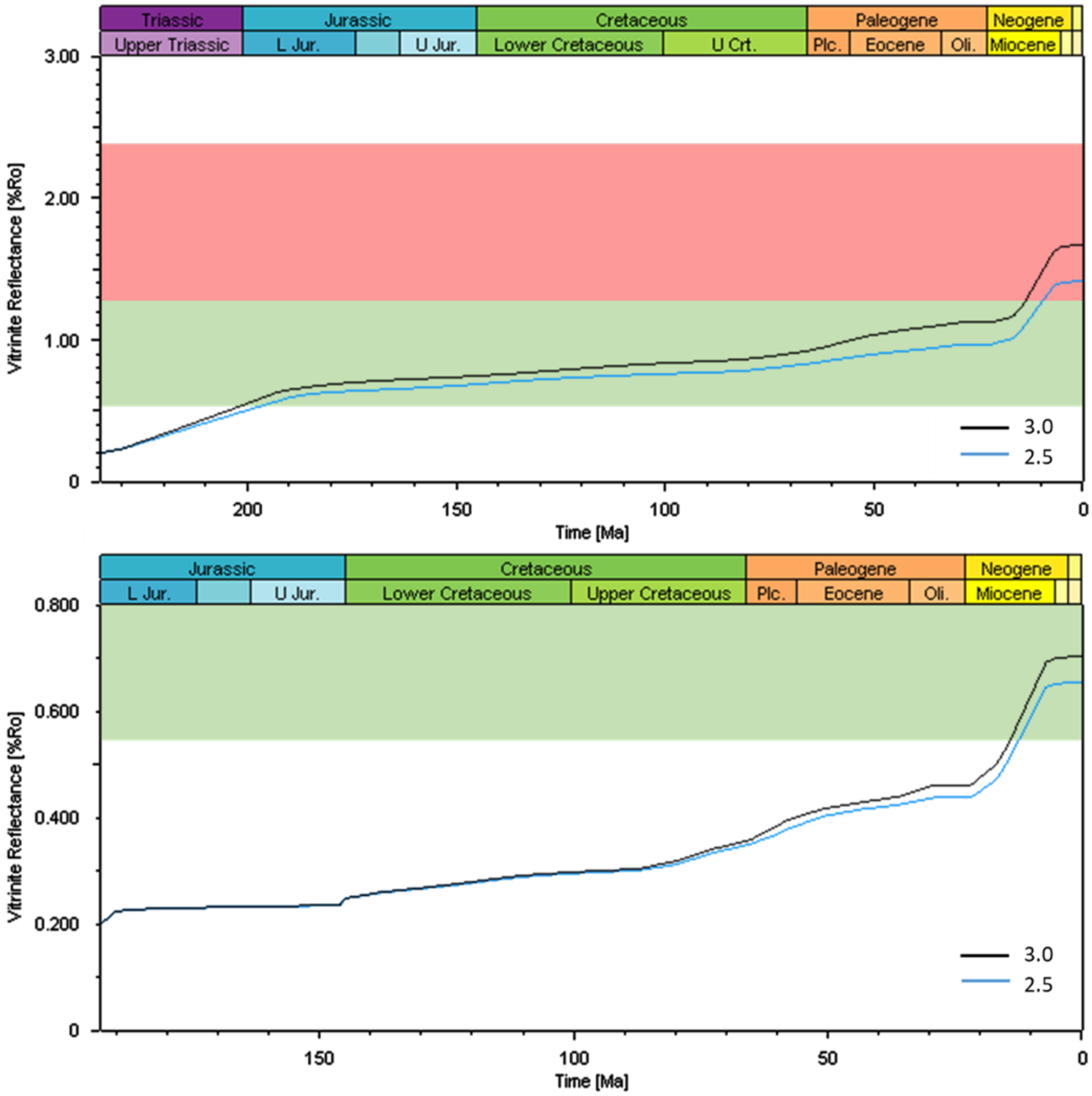

Figure A.II.24: Vitrinite reflectance curve- Time based on Burnham and Sweeney (1990). The colored curves present the radioactive heat variables. Figures illustrate Triassic and Posidonia shales in pseudo-well A, respectively.

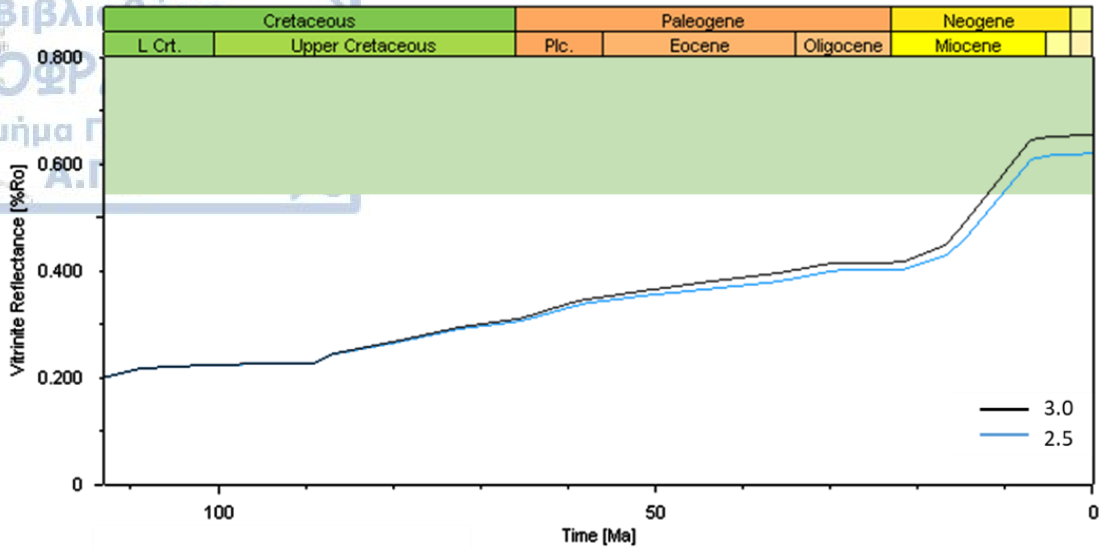

Figure A.II.25: Vitrinite reflectance curve- Time based on Burnham and Sweeney (1990). The colored curves present the radioactive heat variables. Figure illustrates Vigla shales in pseudo-well A.

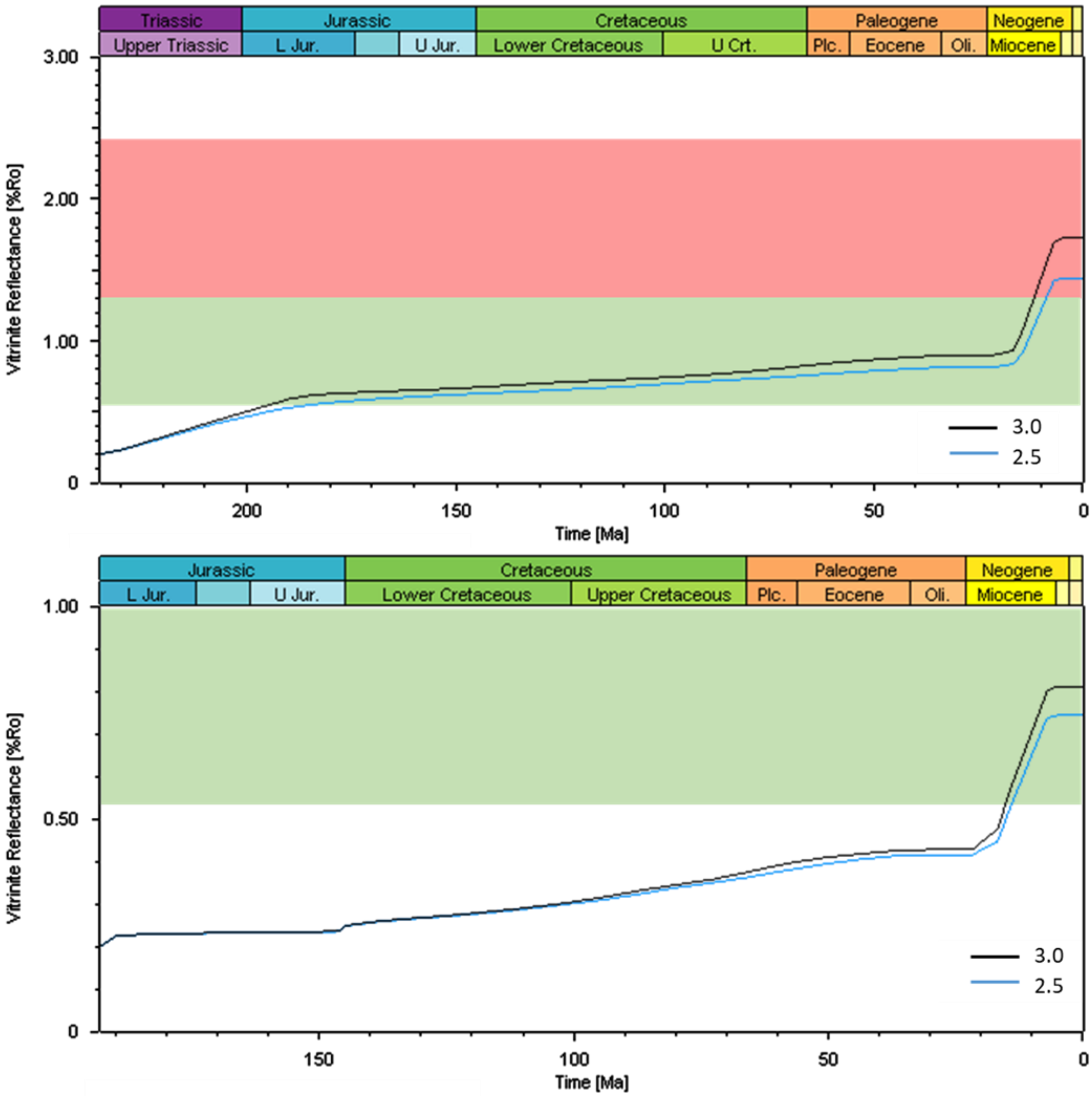

Figure A.II.26: Vitrinite reflectance curve- Time based on Burnham and Sweeney (1990). The colored curves present the radioactive heat variables. Figures illustrate Triassic and Posidonia shales in pseudo-well B, respectively.

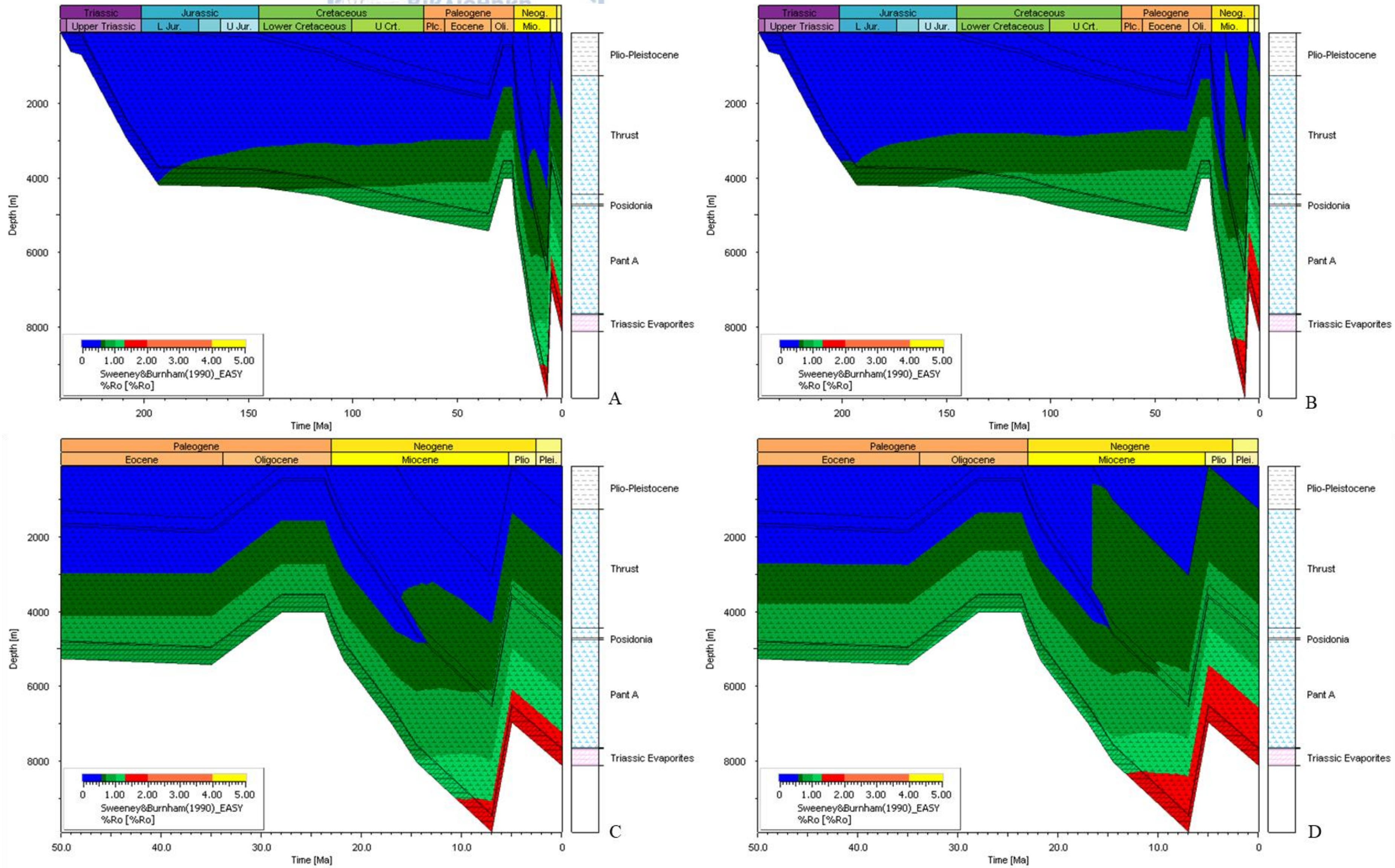

Figure A.II.27: Burial History plots (240 Ma to present and 50 Ma to present) of the pseudo-well B. Plots B-D and A-C describe scenarios 2 and 3, respectively. The parameters are presented in the Table 17.

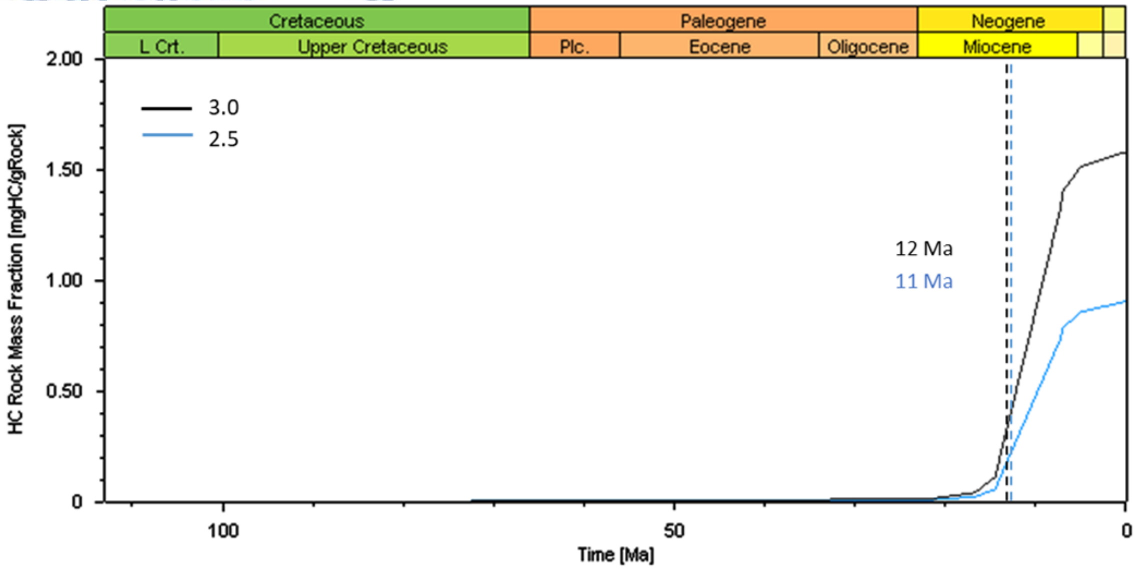

Figure A.II.28: Generation Mass curves through geological time for pseudo-well A. The colored curves present the radioactive heat variables. Generation mass values are in mg HC/g Rock and time values in Ma. The parameters are presented in Table 17. Figure illustrates Vigla shales.

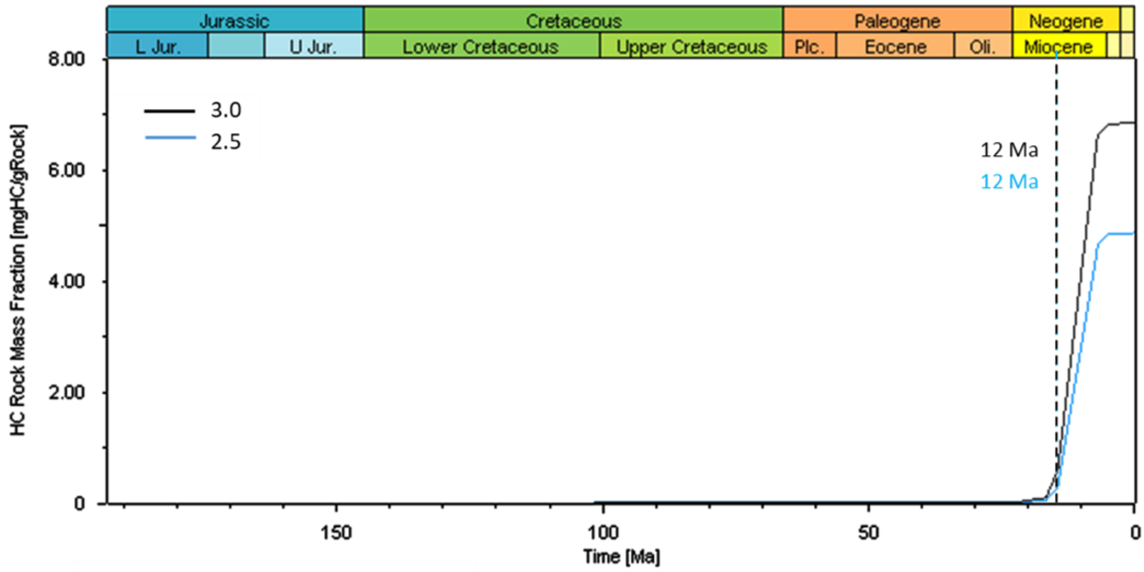

Figure A.II.29: Generation Mass curves through geological time for the pseudo-well B. The colored curves present the radioactive heat variables. Generation mass values are in mg HC/g Rock and time values are in Ma. The parameters were used are presented in Table 17. Figure illustrates Posidonia shales.

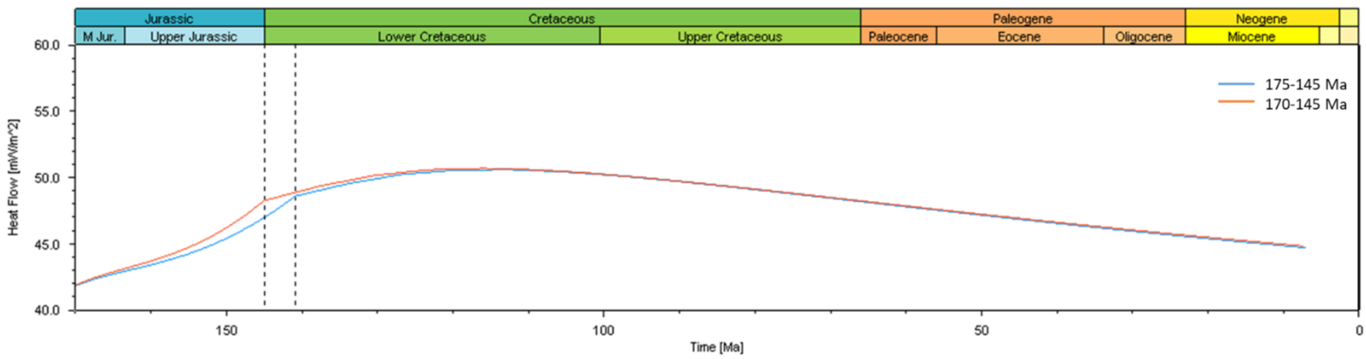

Figure A.II.30: Heat Flow curves for the PW-B. The parameters were used are presented in the Table 18.

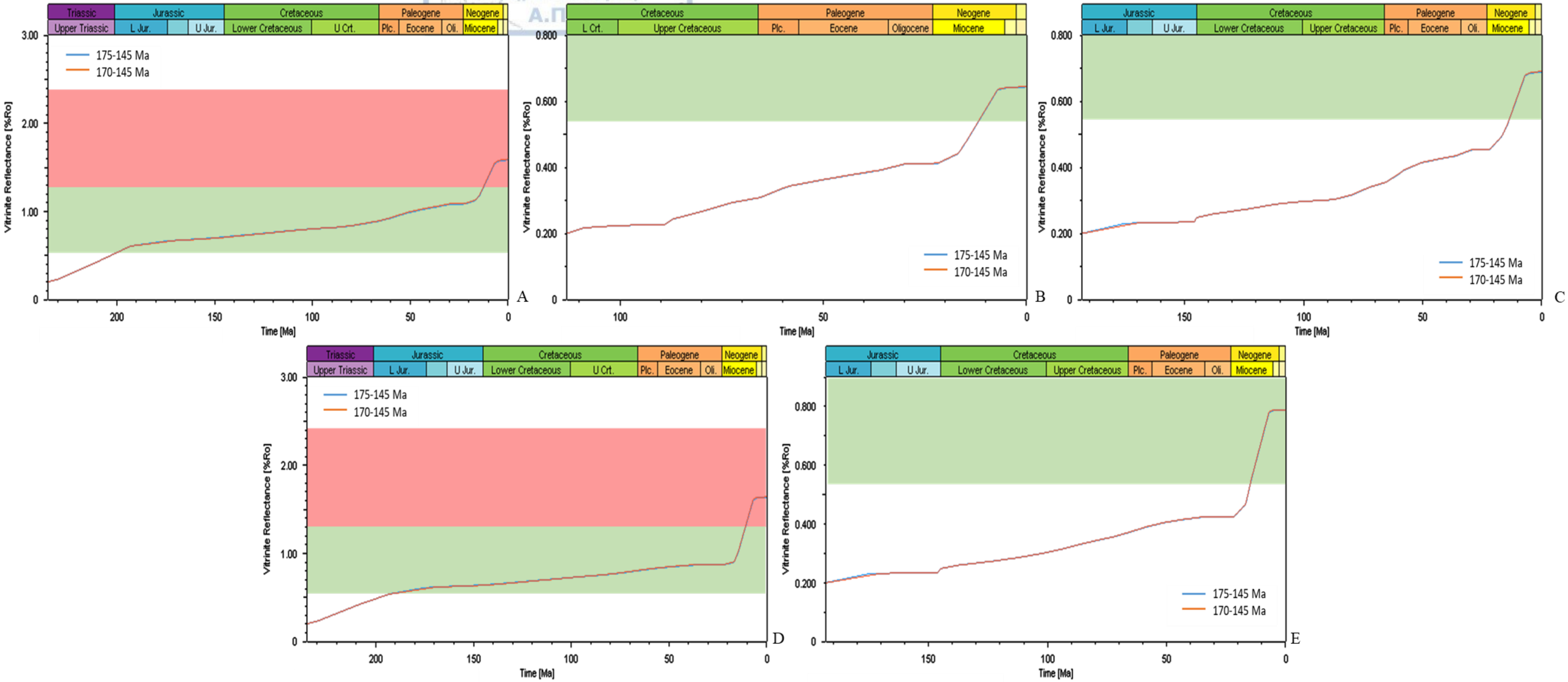

Figure A.II.31: Vitrinite reflectance curve- Time based on Burnham and Sweeney (1990). Figures A, B and C illustrate Triassic, Posidonia and Vigla shales in pseudo-well A, respectively. Figures D and E illustrate Triassic, Posidonia shales, respectively.

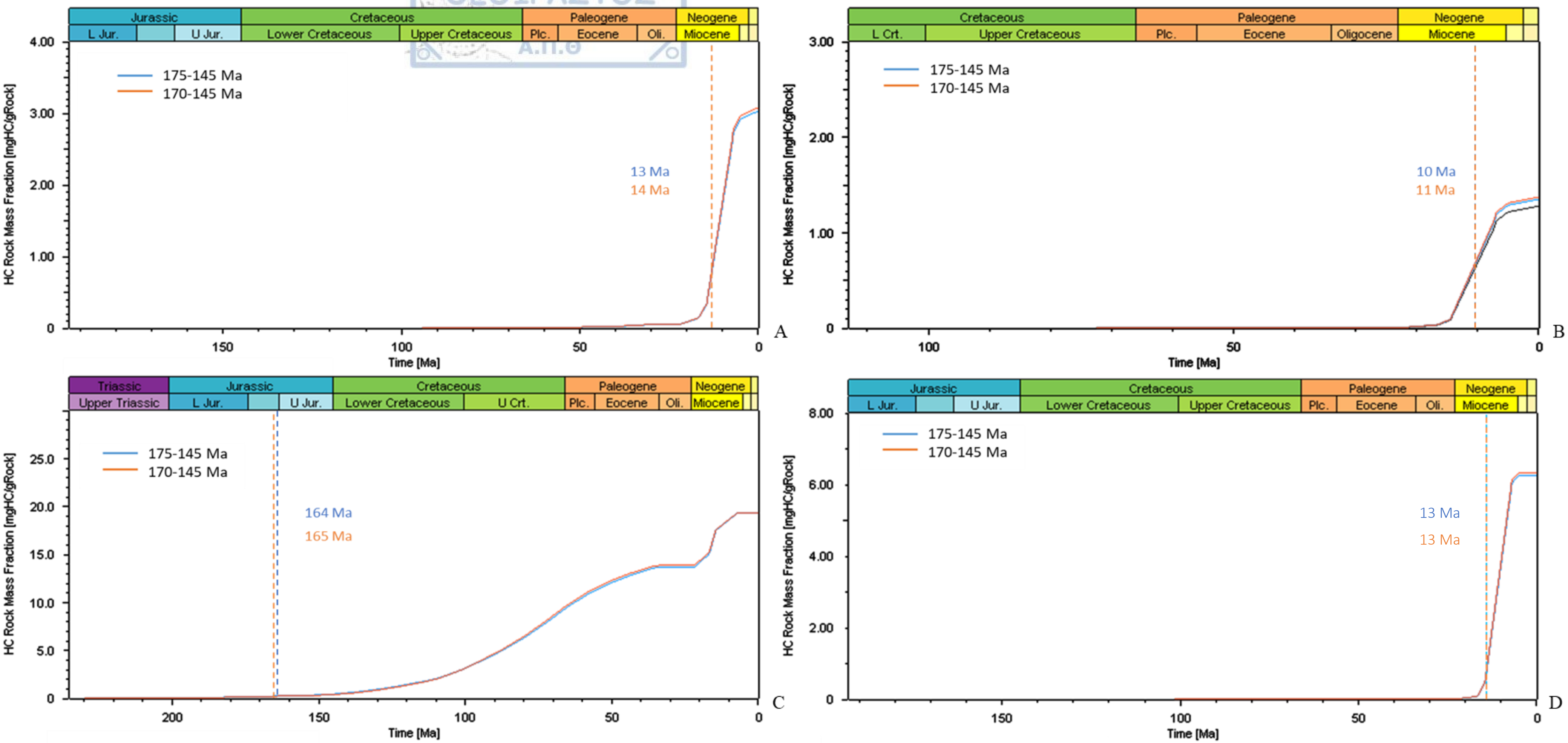

Figure A.II.32: Generation Mass curves through geological time for the pseudo-well A. Generation mass values are in mg HC/g Rock and time values are in Ma. The parameters were used are presented in Table 18. Figures A and B illustrate Posidonia and Vigla shales in pseudo-well A. Figures C and D illustrate Triassic and Posidonia shales in pseudo-well B.

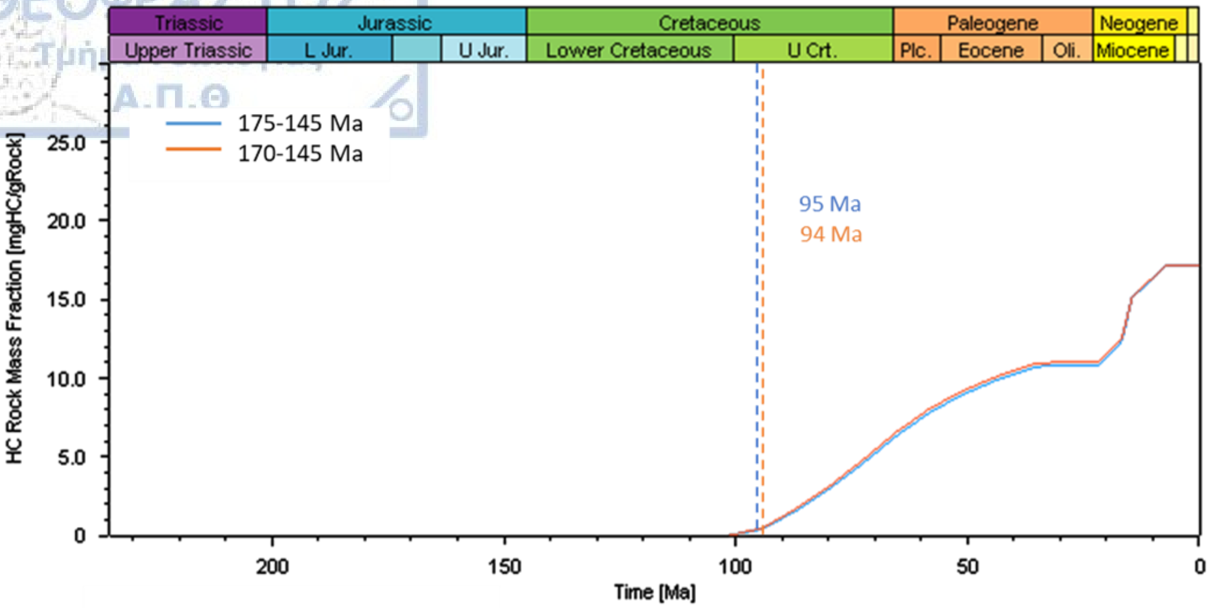

Figure A.II.33: Expulsion Mass curves through geological time for pseudo-well B. Expulsion mass values are in mg HC/g Rock and time values are in Ma. Figure illustrates Triassic shales. The parameters are presented in Table 18.

Appendix III: Source rock quality characteristics sensitivity plots

Figures:

Parameters	Figures
Total Organic Carbon (TOC)	A.III.1- A.III.4
Hydrogen Index (HI)	A.III.5- A.III.8

Tables:

Parameters	Tables
Total Organic Carbon (TOC)	III.1– III.2
Hydrogen Index (HI)	III.3– III.4

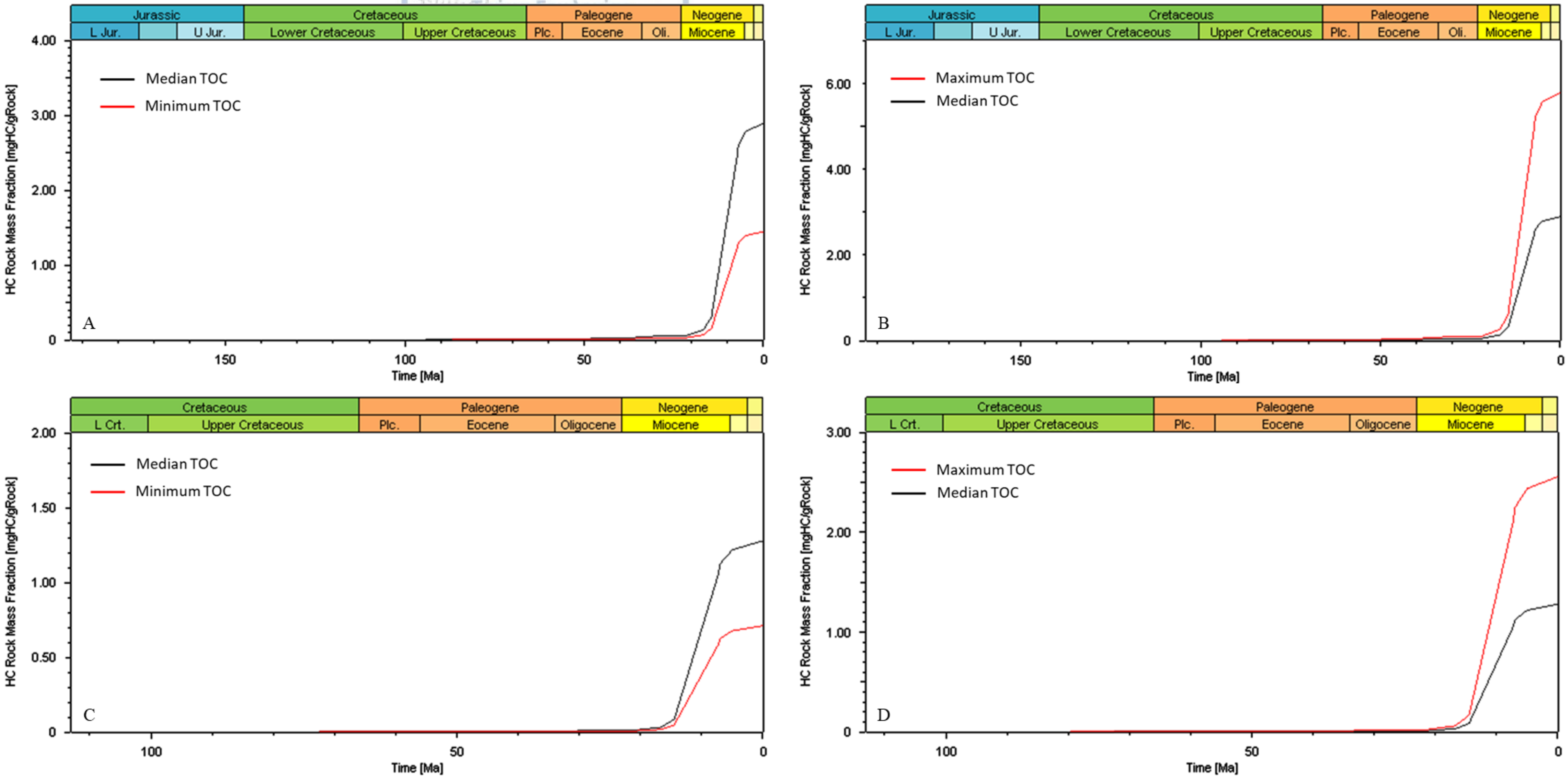

Figure A.III.1: Generation Mass curves through geological time for the Posidonia and Vigla shales (PW-A). The colored curves present the minimum and median TOC (Plots A and C). The colored curves present the median and maximum TOC (Plots B and D). Generation mass values are in mg HC/g Rock.

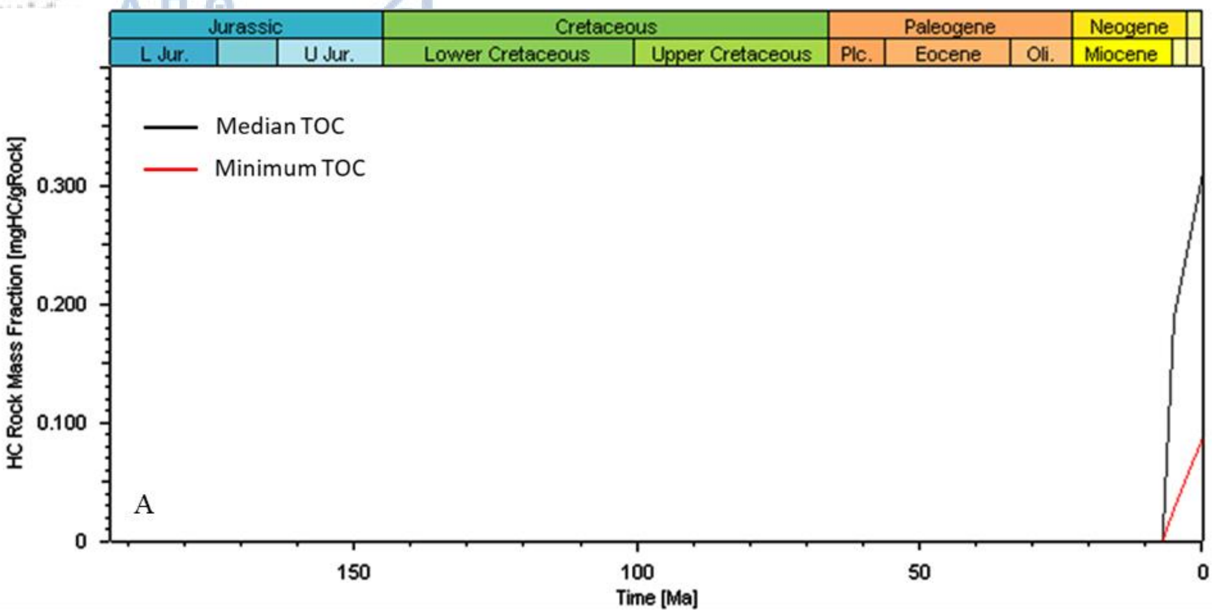

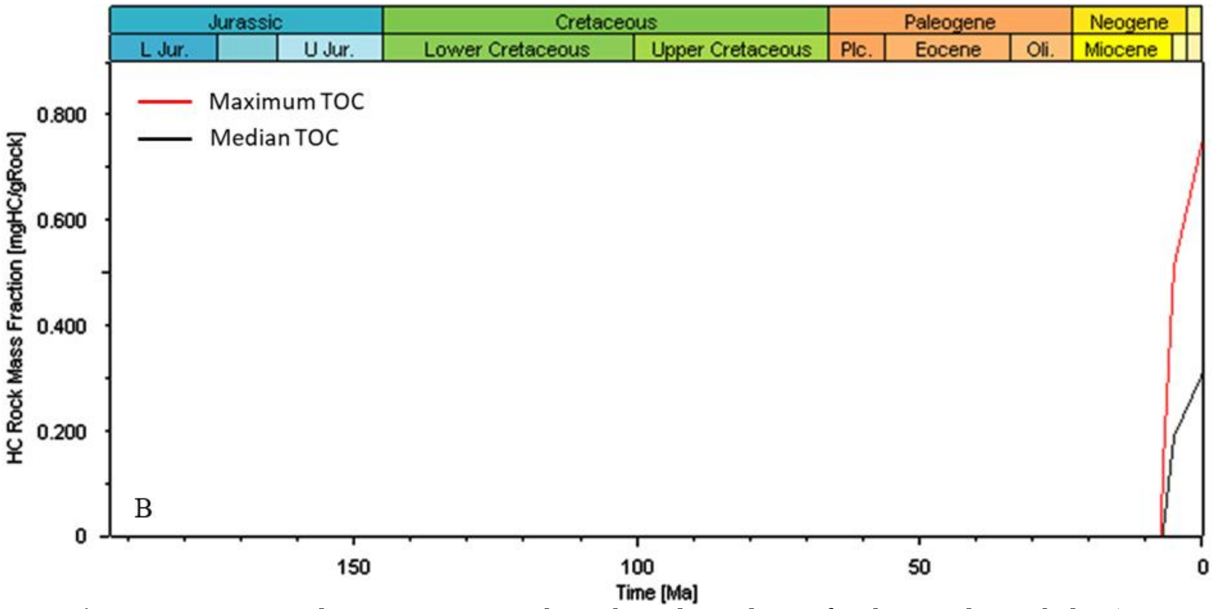

Figure A.III.2: Expulsion Mass curves through geological time for the Posidonia shales (PW-A). The colored curves present the minimum and median TOC (Plot A). The colored curves present the median and maximum TOC (Plot B). Expulsion mass values are in mg HC/g Rock.

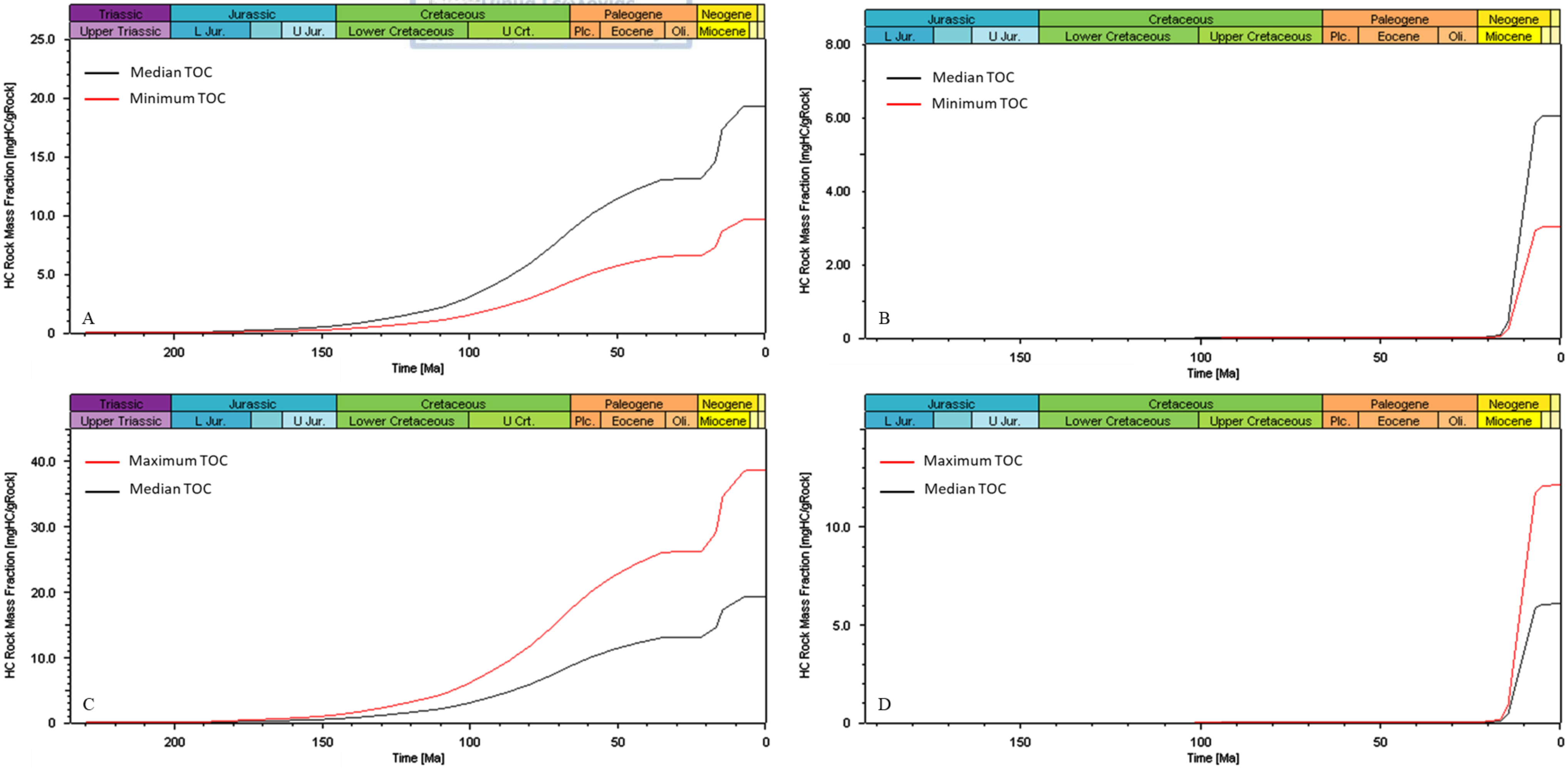

Figure A.III.3: Generation Mass curves through geological time for the Triassic and Posidonia shales (PW-B). The colored curves present the minimum and median TOC (Plots A and B). The colored curves present the median and maximum TOC (Plots C and D). Generation mass values are in mg HC/g Rock.

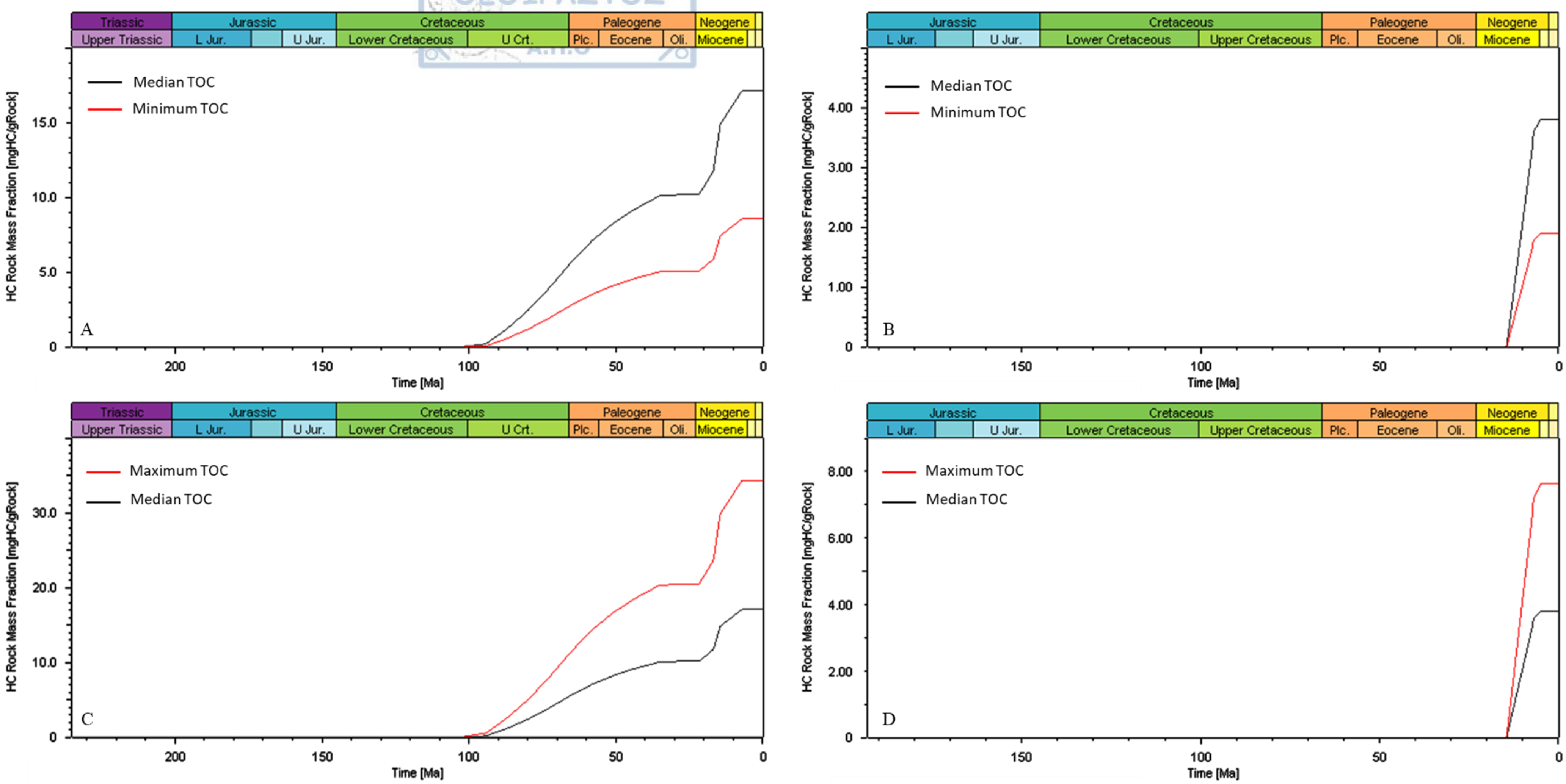

Figure A.III.4: Expulsion Mass curves through geological time for the Triassic and Posidonia shales (PW-B). The colored curves present the minimum and median TOC (Plots A and B). The colored curves present the median and maximum TOC (Plots C and D). Expulsion mass values are in mg HC/g Rock.

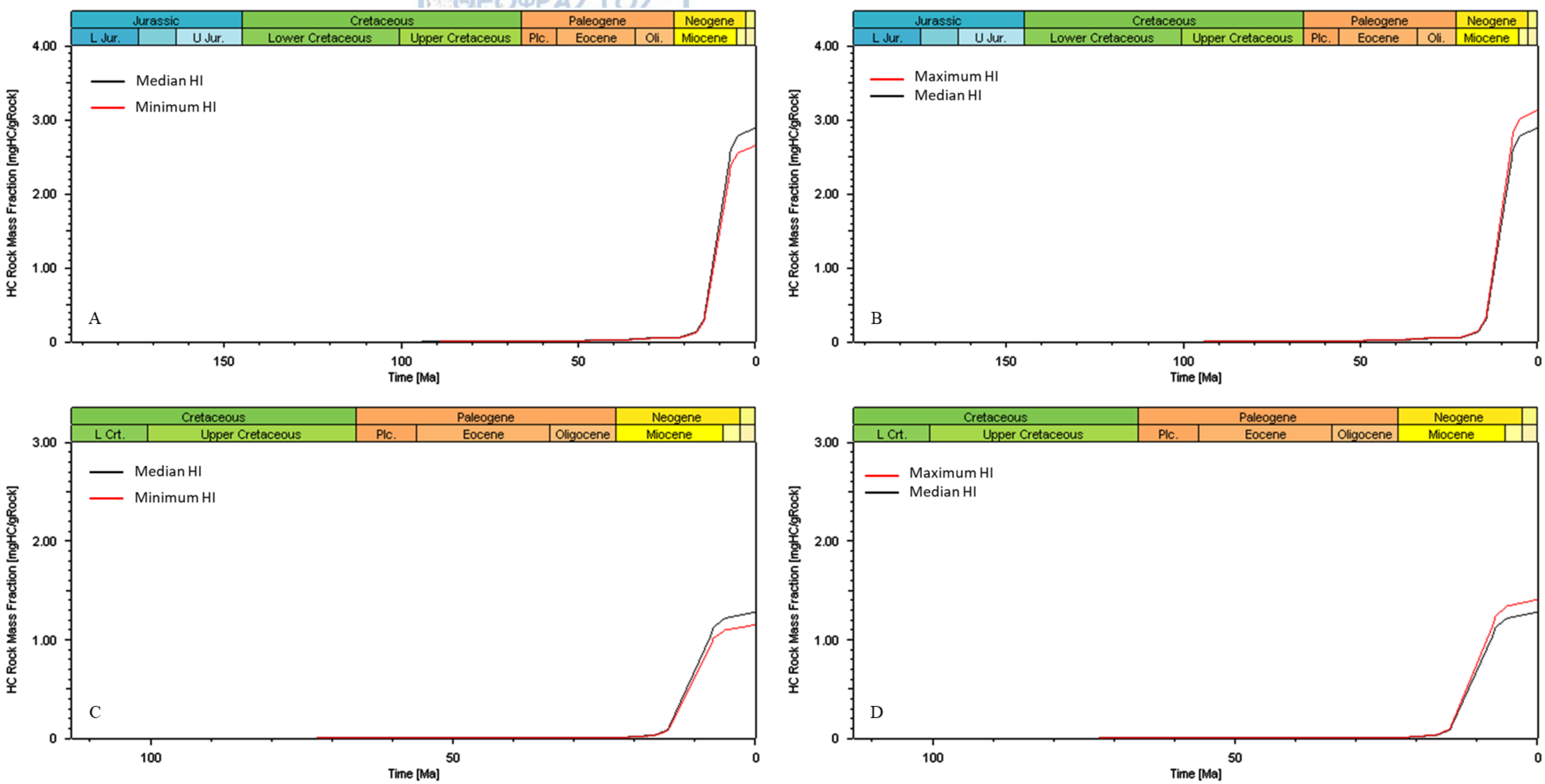

Figure A.III.5: Generation Mass curves through geological time for the Posidonia and Vigla shales (PW-A). The colored curves present the minimum and median HI (Plots A and C). The colored curves present the median and maximum HI (Plots B and D). Generation mass values are in mg HC/g Rock.

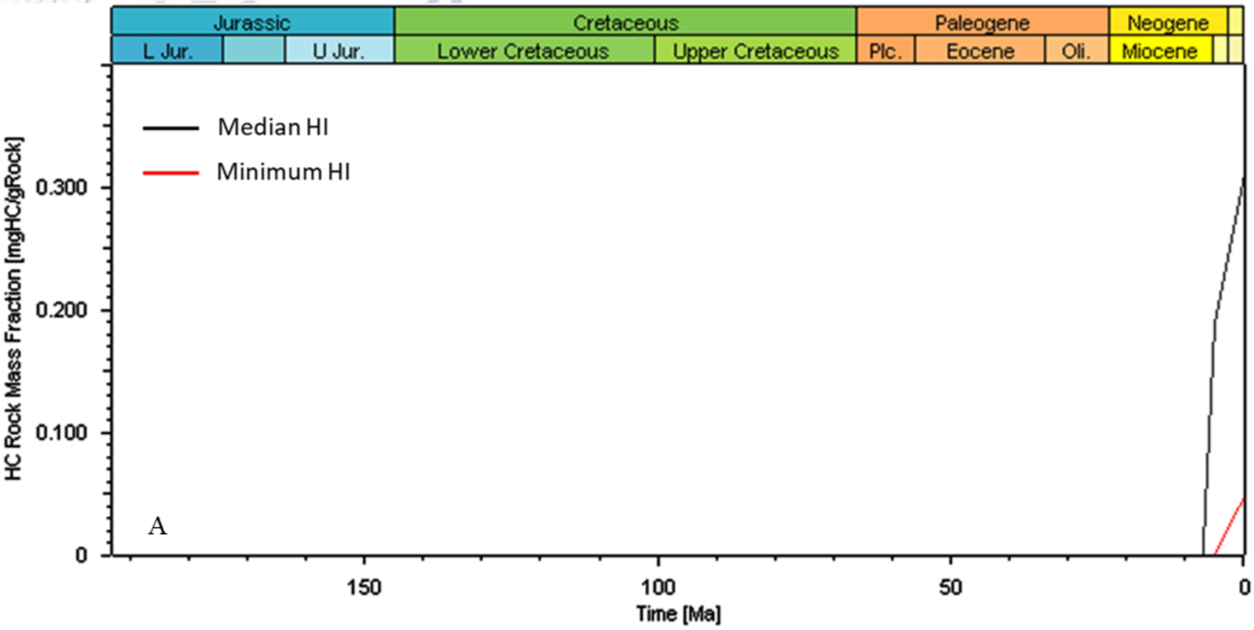

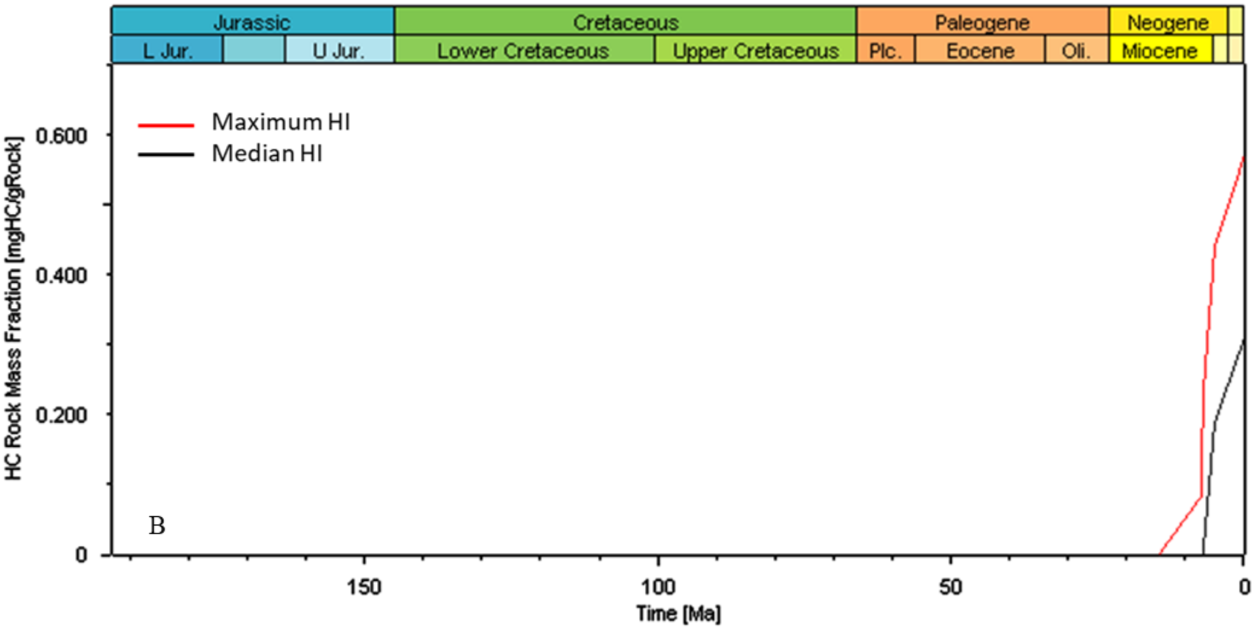

Figure A.III.6: Expulsion Mass curves through geological time for the Posidonia shales (PW-A). The colored curves present the minimum and median HI (Plot A). The colored curves present the median and maximum HI (Plot B). Expulsion mass values are in mg HC/g Rock.

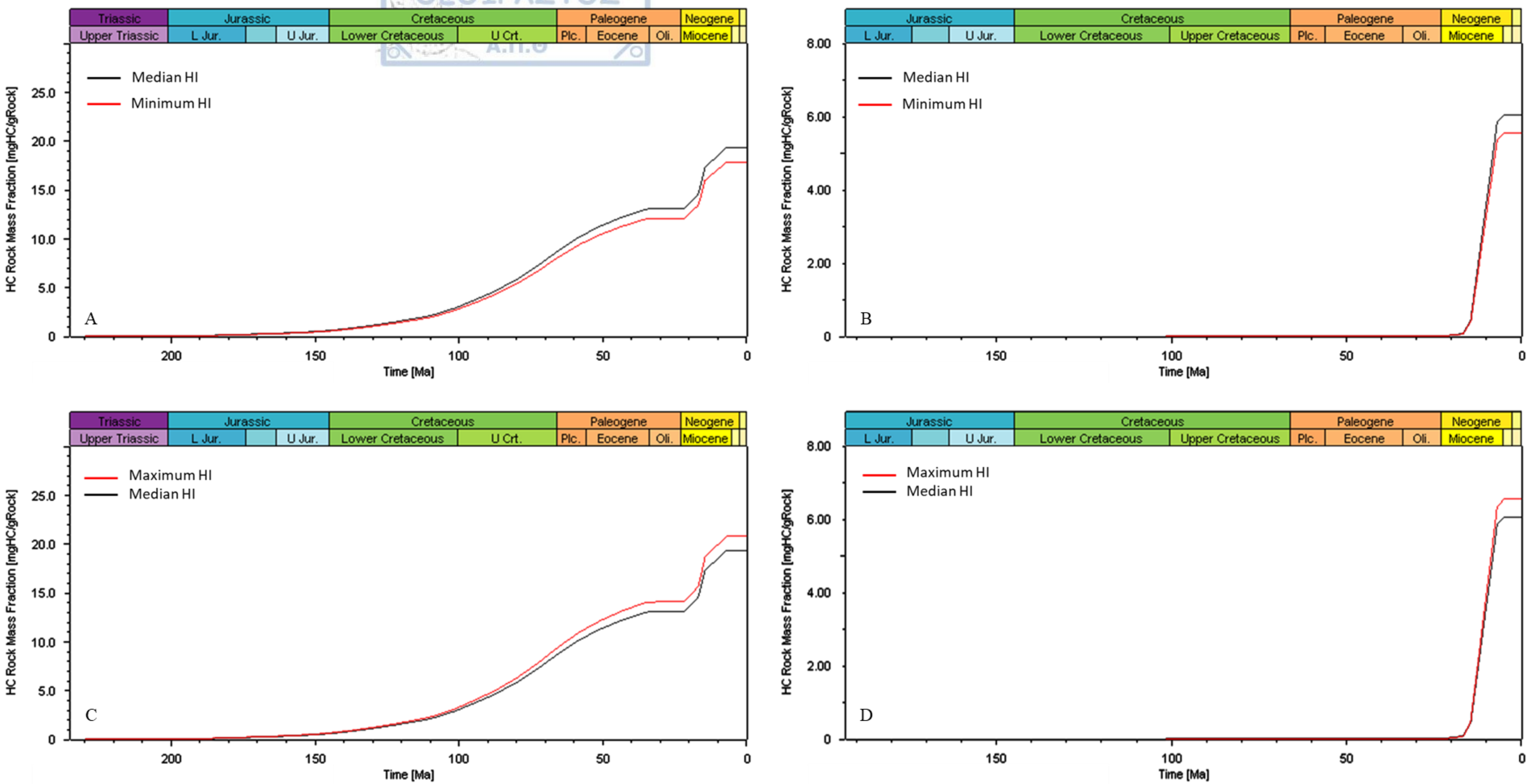

Figure A.III.7: Generation Mass curves through geological time for the Triassic and Posidonia shales (PW-B). The colored curves present the minimum and median HI (Plots A and B). The colored curves present the median and maximum HI (Plots C and D). Generation mass values are in mg HC/g Rock.

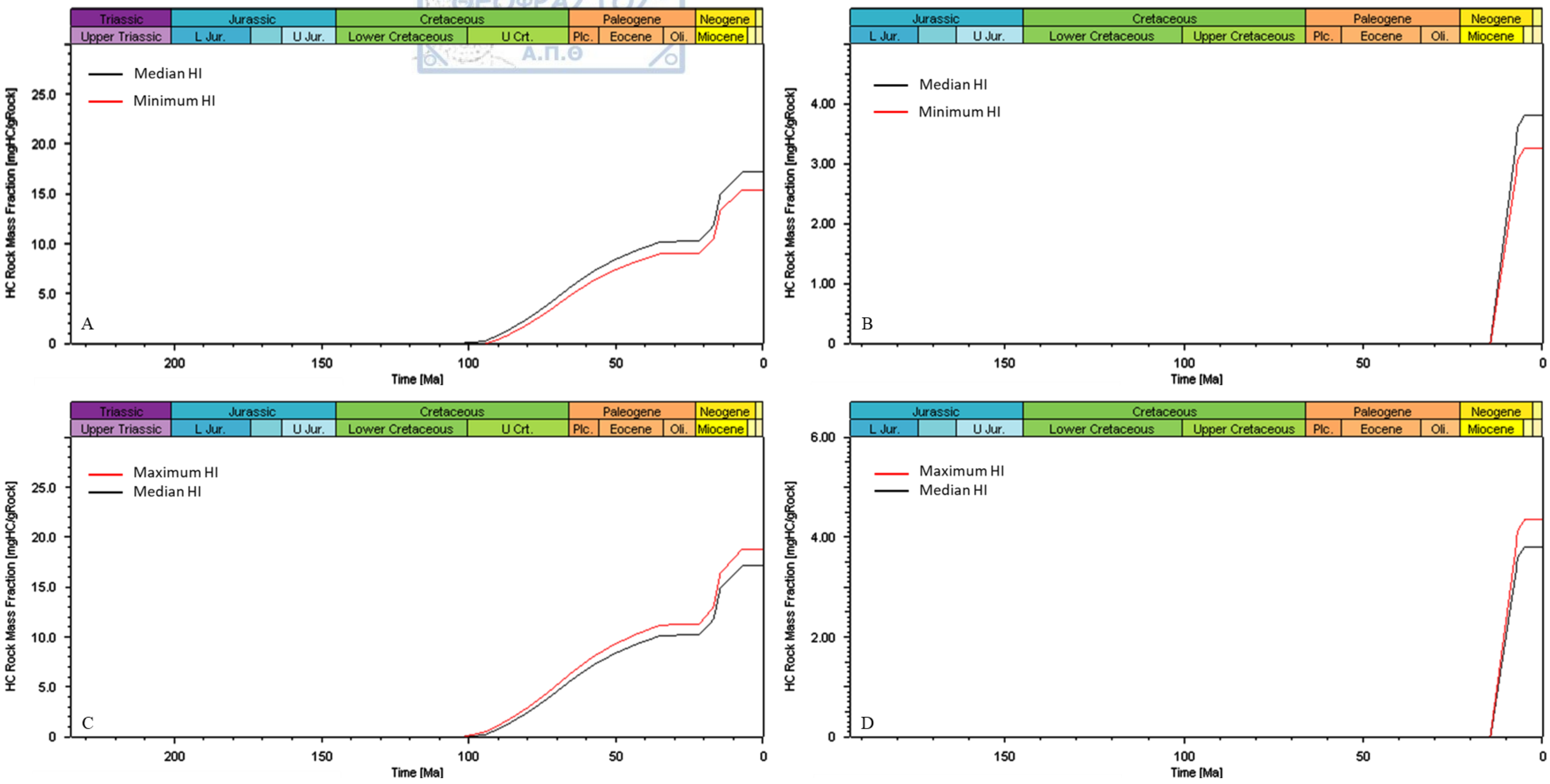

Figure A.III.8: Expulsion Mass curves through geological time for the Triassic and Posidonia shales (PW-B). The colored curves present the minimum and median HI (Plots A and B). The colored curves present the median and maximum HI (Plots C and D). Expulsion mass values are in mg HC/g Rock.

Table III.1: Generation final masses for the scenarios based on Table 25. Generation masses at present day are in mg HC/ g Rock.

Results		Minimum	Median	Maximum
Generation Mass at present day (mg HC/g Rock)	Triassic Shales	9.69	19.29	38.68
	Posidonia Shales	3.04	6.06	12.15

Table III.2: Expulsion final masses for the scenarios based on Table 25. Expulsion masses at present day are in mg HC/ g Rock.

Results		Minimum	Median	Maximum
Expulsion Mass at present day (mg HC/g Rock)	Triassic Shales	8.58	17.11	34.21
	Posidonia Shales	1.89	3.80	7.65

Table III.3: Generation final masses for the scenarios based on Table 26. Generation masses at present day are in mg HC/ g Rock.

Results		Minimum	Median	Maximum
Generation Mass at present day (mg HC/g Rock)	Triassic Shales	17.85	19.29	20.89
	Posidonia Shales	5.55	6.06	6.59

Table III.4: Expulsion final masses for the scenarios based on Table 26. Expulsion masses at present day are in mg HC/ g Rock.

Results		Minimum	Median	Maximum
Expulsion Mass at present day (mg HC/g Rock)	Triassic Shales	15.52	17.11	18.84
	Posidonia Shales	3.26	3.80	4.35